Karlsruhe Institute of Technology

New directions in inelastic Dark Matter

The Role of Parity in Dark Sectors

Zur Erlangung des akademischen Grades eines

DOKTORS DER NATURWISSENSCHAFTEN
(Dr. rer. nat.)

von der KIT-Fakultät für Physik des
Karlsruher Instituts für Technologie (KIT)
genehmigte

DISSERTATION

von

M.Sc. Giovani Dalla Valle Garcia

aus Salto do Lontra - PR (Brasilien)

Tag der mündlichen Prüfung: 31. Oktober 2025

Referent:	Prof. Dr. Thomas Schwetz-Mangold
Korreferent:	Prof. Dr. Felix Kahlhöfer

The work was made possible with the support of a scholarship from the German Academic Exchange Service (DAAD).

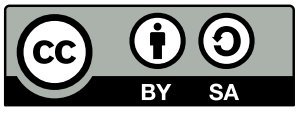

Erklärung

Ich versichere wahrheitsgemäß, die Arbeit selbstständig verfasst, alle benutzten Hilfsmittel vollständig und genau angegeben und alles kenntlich gemacht zu haben, was aus Arbeiten anderer unverändert oder mit Abänderungen entnommen wurde sowie die Satzung des KIT zur Sicherung guter wissenschaftlicher Praxis in der Fassung vom 30. September 2021 beachtet zu haben.

Karlsruhe, den 18. August 2025 _____

Acknowledgements

Firstly, I would like to thank my supervisors and advisors, Prof. Dr. Thomas Schwetz-Mangold and Prof. Dr. Felix Kahlhöfer, for their kind support and invaluable guidance throughout the course of this thesis. I am deeply grateful for their thoughtful suggestions and our regular discussions during the various phases of this work. From the very beginning—when I was still unfamiliar with the field—they provided all the assistance I needed and showed great patience as I took my first steps into this new domain. Toward the end, their help in improving the quality of this manuscript was essential in turning my thesis into a piece of work I am truly proud of. *Vielen Dank!*

I would also like to thank Prof. Dr. Juan Herrero-García, who supervised me during my stay abroad, kindly and patiently introducing me to yet another new topic and encouraging me to explore fresh ideas in our collaboration.

My sincere thanks to Prof. Dr. Ulrich Nierste for helping provide the opportunity to pursue my PhD at the Karlsruhe Institute of Technology. I am also especially grateful to Ms. Martina Schorn, Ms. Raquel Lujan Miravet, and Ms. Anna Friedrich for their generous and consistent support with the many administrative aspects of my PhD. Their prompt assistance helped me navigate the usual (and numerous) formalities that arise over the course of doctoral studies.

I gratefully acknowledge the financial support provided by the German Academic Exchange Service (DAAD) and the Karlsruhe School of Elementary and Astroparticle Physics: Science and Technology (KSETA), which made this research possible. I am also grateful to be part of the Karlsruhe Institute of Technology (KIT) and to have had the opportunity to spend a few months at the Institute for Corpuscular Physics (IFIC) in Valencia. Both institutions have provided a high-level scientific environment and, in the case of Karlsruhe, the opportunity to contribute to teaching both bachelor's and master's students.

A dedicated thank you goes to my collaborators—Maksym Ovchynnikov, Giacomo Landini, Javier Silva-Malpartida, and Joel Jones-Pérez—for helping bring my ideas to life through rigorous scientific work and enriching discussions.

I would also like to thank my colleagues—Sowmiya Balan, Kierthika Chathirathas, Virgile Dandoy, Nicoline Hemme, Tim Robin Kretz, Henda Mansour, Jonas Matuszak, and Kiran Sharma—for the regular meetings that not only enhanced my understanding of how scientific progress is made, but also created many moments of rewarding exchange and camaraderie. I would especially like to mention Xiyuan Gao, with whom I shared ideas and discussed work-related

challenges—often leading to creative and lively conversations.

In the course of the research leading to my publications, I (or, in some cases, my collaborators) benefited from insightful discussions, valuable feedback, or manuscript review by several experts. While I cannot name everyone, I would particularly like to thank Nassim Bozorgnia, Babette Döbrich, Miguel Escudero, Torber Ferber, Benjamin Grinstein, Saniya Heeba, Oleksii Mikulenko, Laura Molina Bueno, Arantza Oyanguren, Javier Reynoso-Cordova, Lesya Shchutska, Vsevolod Syvolap, and Yu-Dai Tsai for their valuable input and exchanges.

I am truly thankful to my partner ($\epsilon\upsilon\chi\alpha\rho\iota\sigma\tau\omega'$) and friends—particularly Daniel, Hemsharan and Ravi—for standing by me through the most stressful times and helping me get through each day, especially during the final stages of writing this manuscript. *Minha profunda e sincera gratidão à minha família pelo amor, apoio e encorajamento incondicionais. Agradeço à minha irmã por sempre estar ao meu lado como uma amiga, e sou eternamente grato aos meus pais pelas oportunidades, pelos valores e pelo apoio incondicional que me ofereceram ao longo da vida. O incentivo deles para que eu seguisse meu próprio caminho e explorasse novas direções foi a base desta jornada.*

Finally, I would like to thank everyone who, in some way, took part in this journey. Whether through scientific discussions, kind encouragement, or simply by being present during important moments, your contribution made a difference. I am sincerely grateful to each and every one of you.

Por fim, gostaria de agradecer a todos que, de alguma forma, fizeram parte desta jornada. Seja por meio de discussões científicas, palavras de incentivo ou simplesmente pela presença em momentos importantes, a contribuição de cada um fez diferença. Sou sinceramente grato a todos vocês.

Abstract

Dark matter remains one of the most pressing and enigmatic challenges in fundamental physics. Despite overwhelming gravitational evidence for its existence, its identity and particle properties remain unknown. Among the most promising frameworks explaining dark matter are *thermal relic scenarios*, in which dark matter was once in equilibrium with the Standard Model plasma. Their attractiveness relies on their predictivity and independence from the initial conditions of the universe. Within this class, *inelastic dark matter* offers a minimal and flexible setup that naturally evades stringent bounds from direct and indirect detection experiments while predicting rich experimental signatures, particularly at particle colliders.

This thesis explores a generalization of inelastic dark matter that lifts the often-unquestioned assumption of parity conservation in the hidden sector. We develop a framework called *not-so-inelastic dark matter*, which smoothly interpolates between inelastic and Majorana dark matter models and involves two mediators: a dark photon and a dark Higgs boson. We show that parity violation in this context enables novel decay channels, allows for large mass splittings, and introduces distinctive di-decay signatures that can be observed at intensity frontier experiments. It further gives rise to a minimal scalar-mediated variant, referred to as *minimal-inelastic dark matter*, offering predictive signals for direct detection experiments.

Through detailed theoretical and phenomenological analysis, we identify viable regions of parameter space that are consistent with thermal freeze-out and current experimental limits. Moreover, large portions of the viable parameter space are expected to be probed by ongoing experiments such as Belle II, NA64, and NA62, as well as by future detectors like DARWIN. Our results suggest that combining multiple collider observables—especially *di-decay signatures*—can enable reconstruction of the coupling structure, or "flavor structure", of dark matter in these models. In particular, our work highlights the complementarity between direct detection, collider searches, and cosmological probes in exploring the not-so-inelastic dark matter framework. This work not only broadens the scope of viable thermal dark matter scenarios but also motivates a re-evaluation of discrete symmetries—particularly *parity*—in the construction of dark sector theories.

Zusammenfassung

Dunkle Materie bleibt eine der drängendsten und rätselhaftesten Herausforderungen der fundamentalen Physik. Trotz überwältigender gravitativer Hinweise auf ihre Existenz sind ihre Identität und Teilcheneigenschaften nach wie vor unbekannt. Zu den vielversprechendsten Erklärungsansätzen gehören *thermische Relikt-Szenarien*, bei denen sich die Dunkle Materie einst im thermischen Gleichgewicht mit dem Standardmodellplasma befand. Ihre Attraktivität beruht auf ihrer Vorhersagekraft und Unabhängigkeit von den Anfangsbedingungen des Universums. Innerhalb dieser Klasse bietet *inelastische Dunkle Materie* einen minimalen und flexiblen Rahmen, der es erlaubt, strenge Beschränkungen durch Experimente direkter und indirekter Detektion zu umgehen, während gleichzeitig vielfältige experimentelle Signaturen, insbesondere an Teilchenbeschleunigern, vorhergesagt werden.

Diese Arbeit untersucht eine Verallgemeinerung der inelastischen Dunklen Materie, bei der die oft nicht kritisch hinterfragte Annahme der Paritätserhaltung im verborgenen Sektor aufgehoben wird. Wir entwickeln ein Modell, das wir *nicht-so-inelastische Dunkle Materie* nennen, das kontinuierlich zwischen inelastischen und Majorana-Modellen der Dunklen Materie interpoliert und zwei Vermittlerfelder beinhaltet: ein dunkles Photon und ein dunkles Higgs-Boson. Wir zeigen, dass die Paritätsverletzung in diesem Zusammenhang neue Zerfallskanäle ermöglicht, große Massendifferenzen erlaubt und charakteristische Di-Zerfall-Signaturen erzeugt, die in Experimenten, die die Intensitätsgrenzen testen, beobachtet werden können. Darüber hinaus ergibt sich eine minimale, skalar-vermittelte Variante, *minimale-inelastische Dunkle Materie* genannt, die vorhersagbare Signale für direkte Detektionsexperimente bietet.

Durch detaillierte theoretische und phänomenologische Analysen identifizieren wir Parameterbereiche, die mit thermischem Freeze-out und aktuellen experimentellen Beschränkungen vereinbar sind. Große Teile des zulässigen Parameterraums dürften zudem durch laufende Experimente wie Belle II, NA64 und NA62 sowie durch zukünftige Detektoren wie DARWIN getestet werden. Unsere Ergebnisse deuten darauf hin, dass die Kombination mehrerer Beobachtungen an Teilchenbeschleunigern (insbesondere *Di-Zerfall-Signaturen*) die Rekonstruktion der Kopplungsstruktur oder „Flavor-Struktur“ der Dunklen Materie in diesen Modellen ermöglichen kann. Insbesondere zeigt unsere Arbeit die komplementäre Stärke von direkter Detektion, Beschleunigern und kosmologischen Beobachtungen bei der Erforschung der nicht-so-inelastischen Dunkle-Materie auf. Diese Arbeit erweitert nicht nur den Gültigkeitsbereich von Szenarien thermischer Dunklen Materie, sondern motiviert auch eine Neubewertung diskreter Symmetrien (insbesondere der *Parität*) bei der Konstruktion verborgener Sektoren.

Publications

Articles that became part of this thesis:

- Giovani Dalla Valle Garcia, Felix Kahlhoefer, Maksym Ovchynnikov and Thomas Schwetz, "Not-so-inelastic Dark Matter" in *JHEP 02 (2025) 127*, [arXiv:2405.08081**[hep-ph]**]

The introduction of the not-so-inelastic Dark Matter framework in chapter 3 (specifically section 3.2) is based on this work. The remainder of chapter 3 is a review of inelastic Dark Matter. Furthermore, the entirety of chapter 4, with the exception of section 4.5, is also derived from this article.

- Giovani Dalla Valle Garcia, "A minimalistic model for inelastic dark matter" in *Phys.Lett.B 862 (2025) 139320*, [arXiv:2411.02147**[hep-ph]**]

The entirety of chapter 5 is based on this work.

- Giovani Dalla Valle Garcia and Maksym Ovchynnikov, "Di-decay signature of new physics particles at intensity frontier experiments" under *review*, [arXiv:2503.01760**[hep-ph]**]

The first part of chapter 7 is based on this reference.

- Giovani Dalla Valle Garcia, Felix Kahlhoefer and Maksym Ovchynnikov, "Multiparticle signatures from inelastic dark matter at colliders" in *progress*

The second and final part of chapter 7 builds upon preliminary results from this work in progress.

- Giovani Dalla Valle Garcia, Felix Kahlhoefer and Thomas Schwetz, "Light dark Higgs in not-so-inelastic Dark Matter" in *progress*

Most of chapter 6 is based on results from this ongoing project. The remainder of that chapter provides a review of inelastic Dark Matter studies that include a dark Higgs boson in the particle spectrum.

Research works that are not presented in this thesis:

- Giovani Dalla Valle Garcia, Felix Kahlhoefer, Maksym Ovchynnikov and Andrii Zaporozhchenko, "Phenomenology of axion-like particles with universal fermion couplings – revisited" in *Phys.Rev.D 109 (2024) 5, 5*, [arXiv: 2310.03524[**hep-ph**]]

- Giovani Dalla Valle Garcia, Juan Herrero-García, Joel Jones-Pérez and Javier Silva-Malpartida, "Expanding the Parameter Space of Exothermic (inelastic) Dark Matter through Parity Violation" in *progress*
- Giovani Dalla Valle Garcia, Thomas Schwetz and Kiran Sharma, "Oscillating inelastic Dark Matter" in *progress*
- Giovani Dalla Valle Garcia, Juan Herrero-García and Giacomo Landini, "Limits on confining dark sectors from dark matter self-interactions" in *progress*

Conference proceedings:

- J. Alimena et al., "Feebly-Interacting Particles: FIPs at LHCb – Workshop Report 2025 Edition" in *progress*,
- G. D. V. Garcia et al., "The European Physical Society Conference on High Energy Physics (EPS-HEP2025)" in *progress*,

Preface

This thesis is based on research conducted during my doctoral studies at the Karlsruhe Institute of Technology, encompassing the work listed in the preceding publication section. Below, I explicitly acknowledge significant contributions from third parties to the work presented in this thesis:

- All simulations involving `SensCalc` [1, 2] or its modified versions were performed by Maksym Ovchynnikov. These include all numerical results for beam dump experiments, as well as Belle II and LHCb predictions for di-decay events in the Higgs-like scalar model. Nevertheless, I independently implemented simulations for Belle II that reproduced `SensCalc` results for the Higgs-like scalar case, and these are the basis for the analyses of the not-so-inelastic Dark Matter scenario presented herein. I also developed semi-analytical recasting techniques for both beam dumps and e^+e^- colliders that closely matched both Maksym Ovchynnikov's simulations and published results from the literature (see appendices for details).
- Our implementation of the `micrOMEGAs` code was based on a model files originally developed by Michael Duerr for the inelastic Dark Matter analysis in Ref. [3].
- The direct detection calculations using `DDCalc` [4, 5] were carried out by Felix Kahlhoefer.
- Generative artificial intelligence tools (in particular, `ChatGPT` and `DeepSeek`) were employed to enhance the grammar and style of the thesis. `ChatGPT` was also used to generate the image in Chapter 8 (*Conclusion*).

Dedicado à minha querida nona.

Contents

Acknowledgements i

Abstract iii

Zusammenfassung iv

Publications v

Preface vii

Contents viii

1 Introduction 1

2 Dark Matter physics 4

2.1 A simple picture of our cosmos 4

2.1.1 A brief (thermal) history of the universe 8

2.1.2 Early universe thermodynamics 11

2.1.3 Freeze-out 14

2.2 The Dark Matter puzzle 16

2.2.1 Evidence for dark matter 17

2.2.2 Possible solutions 19

2.3 The particle Dark Matter 21

2.3.1 Dark Matter properties 22

2.3.2 Examples of candidates 23

2.3.3 Prelude: Boltzmann equations 26

2.3.4 WIMPs: the standard Dark Matter particle 31

2.4 Searches for the Dark Matter particle 32

2.4.1 Indirect detection 34

2.4.2 Direct detection . . . 37
2.4.3 Collider Searches . . . 42
2.5 Dark sectors and Standard Model portals . . . 45
2.5.1 The scalar portal . . . 49
2.5.2 The vector portal . . . 51
2.5.3 The fermionic portal . . . 55

3 The case for (not-so-)inelastic Dark Matter 56
3.1 Inelastic Dark Matter . . . 59
3.1.1 Inelastic scattering . . . 59
3.1.2 Asymmetric dark matter from inelasticity . . . 61
3.1.3 Further implications from inelasticity . . . 63
3.1.4 The case for small mass splittings . . . 64
3.1.5 Pseudo-Dirac Dark Matter . . . 66
3.1.6 The status of pseudo-Dirac and Majorana Dark Matter . . . 67
3.2 Not-so-inelastic Dark Matter . . . 73
3.2.1 The general Lagrangian . . . 76
3.2.2 Reproducing the standard pseudo-Dirac case . . . 81
3.2.3 Optional: The p-wave coannihilation case . . . 83

4 Not-so-inelastic Dark Matter: the vector portal 85
4.1 Excited Dark Matter decays . . . 87
4.2 Relic abundance . . . 89
4.3 (In)Direct detection . . . 92
4.4 Collider searches . . . 94
4.4.1 Proton beam dump experiments . . . 95
4.4.2 NA64 . . . 96
4.4.3 Electron–positron colliders . . . 97
4.4.4 Dark Matter scattering searches . . . 98
4.5 The influence of a light dark Higgs . . . 98
4.6 Results . . . 101
4.7 Concluding remarks . . . 103

5 Not-so-inelastic Dark Matter: the scalar portal 106
5.1 A new minimalistic model . . . 107
5.1.1 The framework . . . 108
5.1.2 Excited Dark Matter decays . . . 111
5.1.3 Perturbative Unitarity . . . 112
5.2 Relic abundance . . . 113
5.3 (In)direct detection . . . 115
5.4 Colliders . . . 116
5.5 Results . . . 116
5.6 Concluding remarks . . . 117

6 Not-so-inelastic Dark Matter with two mediators 120
6.1 Dark Higgs via dark photons . . . 125
6.1.1 Optional: Dark photons via dark Higgs . . . 127
6.2 Dark Higgs production and decays . . . 128
6.2.1 Parameter Space . . . 130
6.3 Dark Matter freeze-out . . . 131
6.3.1 Bound State Formation . . . 133
6.4 Dark Matter searches . . . 134
6.4.1 Direct and Indirect Detection . . . 134
6.4.2 Collider searches . . . 136
6.5 Results . . . 138
6.6 Concluding Remarks . . . 139

7 Not-so-inelastic Dark Matter: exploring new directions 142
7.1 Opportunities from di-decays . . . 143
7.1.1 Optional: Old di-decays signatures (dark Higgs only) . . . 148
7.1.2 New di-decay signatures . . . 151
7.2 A generic picture for not-so-inelastic Dark Matter . . . 155
7.2.1 Probing the not-so-inelastic flavor structure . . . 156
7.2.2 Belle II sensitivity to flavor-probing signatures . . . 161
7.3 Concluding remarks . . . 164

8 Conclusion **169**
8.1 Summary . . . 169
8.2 Outlook . . . 171

Bibliography **175**

A Mathematical details **A-1**
A.1 Details on the mass diagonalization . . . A-1
A.2 Properties of the Interaction Coefficients . . . A-4
A.3 Extra: Oscillating Dark Matter . . . A-5

B `FeynRules` Implementation **B-1**
B.1 Small complex phase . . . B-2

C Analytical recasting of beam dump experiments **C-1**
C.1 Recasting NA64 missing energy searches . . . C-2

D Recasting searches at electron–positron colliders **D-1**
D.1 Simulating the collisions . . . D-1
D.2 A (semi-)analytical approach . . . D-3
D.3 Set-up and cuts for electron–positron colliders . . . D-6
D.3.1 Missing-energy cuts . . . D-7
D.3.2 Displaced-vertex cuts . . . D-9

E Solving Boltzmann Equations **E-1**

F Extra: **News from parity in the exothermic limit** **F-1**

Chapter 1

Introduction

Dark Matter (DM) remains one of the most profound and longstanding mysteries in modern physics [6–9], with its first hints dating back nearly a century [10, 11]. Over the decades, a multitude of astrophysical and cosmological observations—from galaxy rotation curves [12–16] to gravitational lensing [17–20], from large-scale structure formation [21–23] to anisotropies in the cosmic microwave background (CMB) [24–26]—have consistently reinforced the existence of this unseen component of the universe. Yet, despite this overwhelming evidence, we still lack any direct information about its fundamental nature.

There are two principal directions for addressing the DM problem. The first assumes the existence of a new form of matter that interacts very weakly, or not at all, with light—hence the term "dark matter" [27].[1] The second proposes modifications to Einstein's theory of General Relativity, potentially altering our understanding of gravity on galactic and cosmological scales [28]. Although alternative gravity theories are being explored, the new-matter hypothesis has emerged as the leading paradigm. It is incorporated into the current cosmological standard model, ΛCDM [26, 29], and successfully explains DM across all observational scales—from early-universe imprints in the CMB, to structure formation, to galaxy dynamics [30].

Given its explanatory power, much effort has been dedicated to identifying plausible candidates for this new form of matter. Two broad categories remain viable: particle dark matter [7] (new particles beyond the Standard Model) and black holes formed from early-universe dynamics—often referred to as primordial black holes (PBHs) [31, 32].[2] Among these, particle DM remains the more promising candidate, as it arises naturally in many extensions of the Standard Model (SM) [33–43] and offers minimal yet predictive mechanisms for early-universe production [44–57]. In particular, thermal DM [58]—particles that were once in thermal equilibrium with the SM plasma—has become a cornerstone

[1] Strictly speaking, "transparent matter" would be a more accurate term, as it reflects the fact that dark matter does not interact with light, rather than implying it is intrinsically dark.

[2] In order to avoid current constraints, PBHs must have masses within the specific range $10^{-16} M_\odot \lesssim m_{\rm PBH} \lesssim 10^{-12} M_\odot$, with the solar mass denoted by $M_\odot \simeq 2 \times 10^{33}$ g [31].

of model building. The thermal freeze-out production mechanism is especially attractive for its predictivity and independence from initial conditions [59–62].[3]

Over the past decades, thermal DM has been the focus of extensive experimental efforts across multiple frontiers: direct detection [63], indirect detection [64], and collider searches [65]. These searches have placed increasingly stringent limits on canonical candidates, particularly Weakly Interacting Massive Particles (WIMPs) [66, 67], which are now strongly constrained across most regions of parameter space [68]. Nevertheless, the attractive properties of thermal DM continue to motivate refined versions of the WIMP paradigm, known as WIMP-like models [58]. Among these, inelastic dark matter has emerged as a minimal and flexible framework that remains viable and phenomenologically rich.

In its simplest realizations, inelastic Dark Matter (iDM) [69] consists of a stable dark matter particle—referred to as the ground state—and a slightly heavier excited state, with interactions mediated by inelastic transitions between states. This structure alters DM phenomenology in experiments, astrophysical systems and cosmology [70–78]: elastic scattering is strongly suppressed, while inelastic up-scattering can occur only when kinematically allowed. Furthermore, excited states are typically short-lived on cosmological timescales but can be long-lived at particle colliders. These features allow iDM models to accommodate a wide mass range—from sub-GeV to well above the electroweak scale—while remaining compatible with thermal freeze-out production and predicting striking decay signatures at colliders [3, 79–83].

In this thesis, we develop and investigate a generalization of fermionic iDM models with a focus on the role of discrete symmetries—particularly parity—in the dark sector. Many existing models impose parity conservation in an ad hoc manner, despite the fact that parity is known to be maximally violated in the electroweak sector of the SM [84–86]. We argue that parity conservation should not be assumed by default in the construction of dark sector models. In fact, we show that parity breaking is not only consistent, but can also alleviate existing experimental constraints and unlock a variety of novel phenomenological signatures.

Specifically, we demonstrate that parity violation enables:

- the existence of iDM models with large mass splittings;
- a new minimal iDM framework involving only a Dirac fermion and a single scalar mediator;
- excited DM states that decay into dark Higgs bosons;

[3] Some authors also refer to particles in thermal equilibrium within a secluded sector—completely decoupled from the SM bath—as thermal DM. However, such scenarios generally lack the key advantages mentioned above.

- and the appearance of new di-decay signatures at colliders, which—when combined with other, more standard searches—may enable full reconstruction of the coupling structure between DM states and mediators.

The thesis is structured as follows. Chapter 2 reviews the current observational and theoretical status of the DM problem (with an emphasis on thermal DM scenarios), and experimental strategies for probing DM particles. It also includes a brief review of dark sector portals. Chapter 3 explains the basic concepts behind the iDM framework and introduces the most commonly studied iDM realization: the pseudo-Dirac iDM model [70, 87, 88], which typically assumes parity conservation. Motivated by the arbitrary and overly restrictive nature of this assumption, we propose a more general framework—called not-so-inelastic Dark Matter (niDM) [89]—that allows for parity violation and smoothly interpolates between iDM and Majorana DM (mDM) [90] scenarios within a setup featuring both a dark photon and a dark Higgs mediator.

Chapter 4 focuses on the sub-GeV mass regime with only the dark photon portal active [89]. We identify a "not-so-inelastic" regime enabled by parity violation, which mimics iDM signatures at colliders while preserving an mDM-like thermal history. This regime opens viable parameter regions that can be probed by Belle II [91] and NA64 [92]. Chapter 5 turns to the scalar portal and presents a new minimal model for iDM involving only a Dirac fermion and a pseudo-scalar mediator [93]. Although less suited for sub-GeV DM, this model yields concrete predictions for direct detection and becomes an excellent target for future experiments such as DARWIN [94]. Chapter 6 investigates the niDM setup with both mediators active. We show that parity-violating interactions give rise to a novel decay channel—excited DM decaying into a ground state and a dark Higgs boson—which can be probed at Belle II via displaced vertex signatures accompanied by high-energy photons. These regions are shown to be consistent with thermal freeze-out.

Chapter 7 introduces the concept of di-decay signatures at intensity frontier experiments [95]—events in which two dark sector particles decay inside the detector—and highlights their prospects for distinguishing between new physics models. We demonstrate that such signals arise naturally in parity-violating niDM models, and propose a UV-agnostic parametrization to study them. When combined with other more standard signatures, they offer a pathway to reconstructing the DM flavor structure. Finally, chapter 8 concludes the thesis with a summary of key results and a discussion of future theoretical and experimental avenues.

Chapter 2

Dark Matter physics

In this chapter, we introduce the longstanding mystery of Dark Matter (DM): the gravitational evidence for mass not accounted for by the Standard Model (SM) of particle physics. Our goal is to set the stage for the discussion of thermal DM scenarios. More specifically, we lay out the relevant concepts, equations, and reference plots that will be used later in the analysis of inelastic DM and its generalizations.

First, in section 2.1 we briefly review the current standard cosmological model, ΛCDM [29, 96]. Then, in section 2.2 we examine the empirical evidence for DM and survey possible explanations. The particle DM solution is discussed in section 2.3, with particular emphasis on the well-established paradigm of weakly interacting massive particles (WIMPs). We then summarize the main experimental strategies for detecting DM particles in section 2.4. Finally, section 2.5 introduces the concept of dark sectors, setting the stage for the inelastic DM models explored in this thesis.

2.1 A simple picture of our cosmos

Throughout human history, a diverse set of "Cosmological Principles" has been proposed based on philosophical, aesthetic, and physical considerations [97]. After the introduction of Einstein's theory of general relativity [98, 99], Einstein sought solutions to his equations that allow for a static and spatially homogeneous and isotropic space-time [100, 101]. The assumption of an (at least approximately) spatially homogeneous and isotropic universe was later referred to as the "Cosmological Principle" (a term coined by Edward A. Milne [101, 102]) and is the central organizing idea of our current cosmological picture. Although homogeneity cannot be experimentally confirmed [97], the excellent agreement of the standard cosmological model—which assumes the Cosmological Principle—often justifies this working assumption. As for isotropy, measurements of the CMB show that temperature fluctuations on the sky at recombination were at the level of $\Delta T/T \lesssim 10^{-5}$ [26, 103], consistent with an isotropic universe to

high precision. Late-time measurements from galaxy cluster surveys similarly show no statistically significant ($> 3\sigma$) deviation from isotropy [104]. It is worth noting that, because the early-universe presents some degree of anisotropy (rendering the Cosmological Principle an approximate symmetry), today's universe exhibits homogeneity and isotropy only on sufficiently large scales, beyond a few megaparsecs [104, 105].

The Robertson–Walker (RW) metric $g_{\mu\nu}$ is the most general metric satisfying the Cosmological Principle. In spherical coordinates $x^\mu = (t, r, \theta, \phi)$, it can be written in terms of the proper time τ as [9]

$$d\tau^2 = g_{\mu\nu} dx^\mu dx^\nu = dt^2 - a^2(t) \left(\frac{dr^2}{1 - kr^2} + r^2 \left(d\theta^2 + \sin^2\theta \, d\phi^2 \right) \right), \tag{2.1}$$

where $a(t)$ is the scale factor of the Universe and k is the (constant) spatial curvature parameter. The scale factor $a(t)$ characterizes the Universe's expansion, $\dot{a} > 0$, contraction, $\dot{a} < 0$, or static evolution, $\dot{a} = 0$, and encodes the relative size of spatial slices at a cosmological time t.

Einstein's field equations for General Relativity read [106]

$$G_{\mu\nu} = 8\pi G \, T_{\mu\nu} \,, \tag{2.2}$$

where G denotes Newton's constant, $T_{\mu\nu}$ the energy–momentum tensor, and $G_{\mu\nu}$ the Einstein tensor,

$$G_{\mu\nu} = R_{\mu\nu} - \frac{1}{2} R g_{\mu\nu} \,, \tag{2.3}$$

with $R_{\mu\nu}$ and R the Ricci tensor and Ricci scalar, respectively.[1] Plugging the RW metric into eq. (2.2) and adopting the energy–momentum tensor of a perfect fluid with energy density ρ and pressure p in its rest frame (the cosmological frame),[2]

$$T_{\mu\nu} = \begin{pmatrix} \rho & 0 & 0 & 0 \\ 0 & p & 0 & 0 \\ 0 & 0 & p & 0 \\ 0 & 0 & 0 & p \end{pmatrix} = g_{\mu\alpha} g_{\nu\beta} T^{\mu\nu} \,, \tag{2.4}$$

[1] The Ricci tensor and scalar are defined, respectively, by $R_{\mu\nu} = R^\lambda{}_{\mu\lambda\nu}$ and $R = R^\mu{}_\mu = g^{\mu\nu} R_{\mu\nu}$, where the Riemann tensor is

$$R^\rho{}_{\sigma\mu\nu} = \partial_\mu \Gamma^\rho_{\nu\sigma} - \partial_\nu \Gamma^\rho_{\mu\sigma} + \Gamma^\rho_{\mu\lambda} \Gamma^\lambda_{\nu\sigma} - \Gamma^\rho_{\nu\lambda} \Gamma^\lambda_{\mu\sigma} \,.$$

The Christoffel symbols are given by

$$\Gamma^\sigma_{\mu\nu} = \frac{1}{2} g^{\sigma\rho} \left(\partial_\mu g_{\nu\rho} + \partial_\nu g_{\rho\mu} - \partial_\rho g_{\mu\nu} \right) ,$$

with $g^{\alpha\gamma} g_{\gamma\beta} = \delta^\alpha_\beta$.

[2] In a general inertial frame where the fluid moves with a four-velocity U^μ, the stress–energy tensor is [9]

$$T^{\mu\nu} = (P + \rho) \, U^\mu U^\nu - P \, g^{\mu\nu} \,.$$

By the Cosmological Principle, U^μ is spatially constant.

one obtains the Friedmann equations:

$$H^2 \equiv \left(\frac{\dot{a}}{a}\right)^2 = \frac{8\pi G}{3}\rho - \frac{k}{a^2}\,, \tag{2.5}$$

$$\frac{\ddot{a}}{a} = -\frac{4\pi G}{3}(\rho + 3p)\,, \tag{2.6}$$

where $H = \dot{a}/a$ is the Hubble parameter. The conservation of the energy–momentum tensor, $D_\mu T^{\mu\nu} = 0$ (with D_μ the covariant derivative),[3] does not yield an equation independent of eqs. (2.5) and (2.6).

Matter and energy in the universe are well modeled by perfect fluids undergoing adiabatic expansion with a simple equation of state

$$p = w\rho\,, \tag{2.7}$$

where w is constant. Energy–momentum conservation implies

$$\rho \propto a^{-3(1+w)}\,. \tag{2.8}$$

Two important examples are "dust" and radiation. For dust (collisionless non-relativistic matter), $w = 0$ and $\rho_{\rm dust} \propto a^{-3}$ simply tracks the dilution of the number density. For radiation (either photons or relativistic massive species), $w = 1/3$ and $\rho_{\rm rad} \propto a^{-4}$, the additional factor a^{-1} reflecting redshifting of individual quanta. The curvature term in eq. (2.5) is sometimes written as an effective energy density,

$$\rho_k = -\frac{3}{8\pi G}\frac{k}{a^2}\,, \tag{2.9}$$

with $w = -1/3$ so that it does not contribute to eq. (2.6). This notation can be misleading, however, as k is a geometric property of spacetime [107].

From eq. (2.5) together with eq. (2.8), one sees that a homogeneous and isotropic universe cannot be static. Seeking a static solution, Einstein introduced the cosmological constant Λ [100, 101],

$$G_{\mu\nu} + \Lambda g_{\mu\nu} = 8\pi G T_{\mu\nu}\,, \tag{2.10}$$

which effectively adds $\Lambda/3$ on the right-hand side of both Friedmann equations [107]. However, Hubble's 1929 observation that the universe is expanding [108] confirmed the dynamic solution expected for generic matter–radiation contents without fine-tuning.

The cosmological constant is equivalent to a perfect fluid with $w = -1$. This component, which accelerates the expansion, is often called *dark energy* in the

[3] For a rank-2 tensor $V^{\mu\nu}$,

$$D_\sigma V^{\mu\nu} = \partial_\sigma V^{\mu\nu} + \Gamma^\mu_{\sigma\lambda} V^{\lambda\nu} + \Gamma^\nu_{\sigma\lambda} V^{\mu\lambda}\,.$$

context of dynamical explanations for an accelerated Universe's expansion. In the standard cosmological model, Λ is simply taken to be a proper constant, yielding the ΛCDM framework [29, 96]. Recently, tensions with the simplest cosmological-constant picture have been discussed: DESI baryon acoustic oscillation measurements combined with CMB and supernova data show a preference for dynamical dark energy over a pure cosmological constant [109–111].

Current values of cosmological parameters are denoted with a subscript 0. The present Hubble parameter H_0 is the "Hubble constant". It is also useful to define the "critical density" [107]

$$\rho_c \equiv \frac{3H^2}{8\pi G} - \rho_k \,, \tag{2.11}$$

and the dimensionless density parameter for each fluid,

$$\Omega_i = \frac{\rho_i}{\rho_{\rm c}} \,. \tag{2.12}$$

Including the cosmological constant as an energy density,

$$\rho_{\rm tot} = \rho_{\rm fluid} + \rho_\Lambda \,, \qquad \rho_\Lambda = \frac{\Lambda}{8\pi G} \,, \tag{2.13}$$

the first Friedmann equation becomes

$$\frac{k}{a^2} = H^2(\Omega_{\rm tot} - 1) \,, \tag{2.14}$$

where $\Omega_{\rm tot} = \rho_{\rm tot}/\rho_c$. Thus, $\Omega_{\rm tot} > 1$ corresponds to a closed universe ($k > 0$), $\Omega_{\rm tot} < 1$ to an open universe ($k < 0$), and $\Omega_{\rm tot} = 1$ to a spatially flat universe ($k = 0$). Consequently, the overall geometry of the Universe is fixed by the observed total energy budget [107].

In the standard model of cosmology, the universe is well described by four components: matter (a mixture of cold dark matter, CDM, and baryonic matter), radiation (photons and neutrinos), a cosmological constant Λ (which in principle could be an effective dark-energy component with negative pressure), and spatial curvature k. Neutrinos, while weakly interacting like DM, are too light and constitute *hot* DM, thus cannot explain structure formation; the CDM+ Λ combination defines the ΛCDM paradigm [9], our current standard cosmological model.

CMB measurements are in excellent agreement with ΛCDM, and the Planck Collaboration [26] has determined its parameters at the percent level [30]. The inferred cosmological parameters are summarized in table 2.1, where the reduced Hubble parameter h is defined as

$$h = H_0/(100 \text{ km/s/Mpc}) \,, \tag{2.15}$$

Table 2.1: Planck 2018 cosmological parameters [26].

Parameter	Symbol	Value
Hubble constant [km/s/Mpc]	H_0	67.66 ± 0.42
Total matter density	Ω_m	0.3111 ± 0.0056
Cold dark matter density	$\Omega_c h^2$	0.11933 ± 0.00091
Baryonic matter density	$\Omega_b h^2$	0.02242 ± 0.00014
Dark energy density	Ω_Λ	0.6889 ± 0.0056
Spatial curvature density	Ω_k	0.0007 ± 0.0019

and present-day density parameters Ω_i^0 are simply denoted by Ω_i for brevity.

From table 2.1, DM comprises $\sim 84\%$ of the matter density, while baryons account for the remaining $\sim 16\%$. The universe is currently dominated by the cosmological-constant–like component, with $\Omega_\Lambda \simeq 0.69$, whereas matter only contributes with $\Omega_m \simeq 0.31$. The present radiation density is negligible, since $\Omega_r \sim 10^{-4}$ (estimated from $T_{\rm CMB} = 2.7255$ K, $N_{\rm eff} = 3.046$, and $T_\nu = (4/11)^{1/3} T_{\rm CMB}$ with $m_\nu \approx 0$ [6]). The large value of Ω_Λ motivates extensive exploration of dark-energy alternatives to a strict cosmological constant, and recent DESI results hint at an evolving dark energy [109–111]. Finally, the universe is remarkably flat: k is consistent with zero, with $|\Omega_k| < 0.4\%$ at 90% C.L.. This a key motivation for an early period of accelerated expansion (inflation), which dilutes away the curvature and generates the initial anisotropies (perturbations from perfect homogeneity) required for structure formation in the late Universe [112–114].

The large amount of non-baryonic matter is at the heart of the DM problem. This discrepancy—far above the 5σ level—is arguably the clearest indication of new physics beyond the Standard Model of particle physics (or of gravity). The central aim of DM physics is to explain the origin and composition of this component. Alternative approaches modify General Relativity to alter inferences of energy densities. We will discuss these possibilities in the remainder of the chapter. Before that, we briefly summarize the key events in the thermal history of the universe and introduce tools needed later for DM production, in particular early-universe thermodynamics.

2.1.1 A brief (thermal) history of the universe

Conventionally, the beginning of the Universe is set at $t = 0$ with $a(0) = 0$ (the big bang). However, our physical description is not expected to be valid before the Planck time, $t_P = 5.39 \times 10^{-44}$ s, where quantum gravity is required. One therefore typically takes t_P as the effective starting time, with a negligibly small scale factor. As noted, the universe likely underwent an early period of inflation [114]. The end of inflation is model-dependent but occurs at times

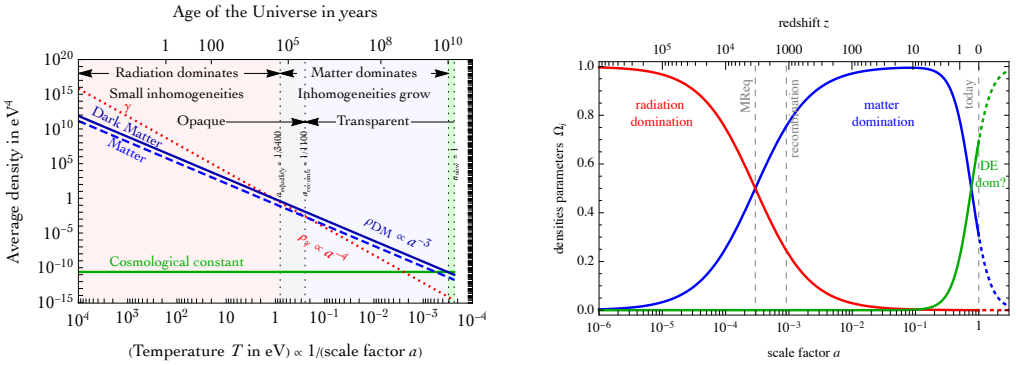

Figure 2.1: Evolution of the different components of a flat Universe as a function of the scale factor a. The corresponding evolution with cosmic time, temperature T, and redshift z is also indicated (see main text for details). Reproduced from Ref. [6].

$\ll 1$ s (temperatures $\gg$ MeV), so it does not affect the broad timing of later cosmological events.

From eq. (2.8), the components of the Universe redshift differently with a, and their relative abundances evolve in time; see fig. 2.1. The redshift is defined as [9]

$$z = \frac{a_0}{a} - 1\,, \tag{2.16}$$

so that today corresponds to $z = 0$ and the earliest times to $z \to \infty$. As $a \to 0$, radiation dominates, and the initial conditions for ΛCDM correspond to a flat, radiation-dominated universe: reheating after inflation deposits energy primarily into radiation. Matter comes to dominate at $t_{\rm eq} \approx 60$ thousand years (matter–radiation equality) [6]. Structure formation proceeds mainly during matter domination [9]. As the universe expands further, both matter and radiation dilute, and at $z \simeq 0.55$ (about 5.3 Gyr ago) the cosmological constant begins to dominate [115].

One can relate the redshift, cosmic time, or the scale factor to the temperature of the Universe by recalling that the radiation energy density scales as $\rho_r \propto T^4$. This implies that the temperature decreases approximately as the inverse of the scale factor, $T \propto a^{-1}$ (see next section for further details). Consequently, the early Universe must have been extremely hot, giving rise to the term *hot Big Bang* cosmology [116].

At times well below a second, several transitions and mechanisms may occur: inflation [114], the electroweak phase transition [117], the QCD (quark–hadron) transition [118], possible DM production and baryogenesis [119], and the breaking from a Grand Unified Theory to the SM gauge group [120]. At the high temperatures of this epoch, all SM species are in thermal (chemical and kinetic) equilibrium, erasing most microphysical information [9]. Gravitational waves,

however, remain out of equilibrium and can probe such early times [121–123].

Two of the earliest SM-era events leaving observable imprints are neutrino decoupling [124] and Big Bang Nucleosynthesis (BBN) [125]. Neutrinos decouple at $t \approx 1$ s ($T \sim 1$ MeV) [126]; thereafter they free-stream, and a possible cosmic neutrino background would carry information about this epoch and their subsequent propagation. Once neutrinos decouple, weak interconversion of neutrons and protons ceases to be efficient. Without nuclear binding, free neutrons would rapidly decay, leaving behind a Universe composed almost entirely of hydrogen.[4] However, during BBN ($t \sim$ minutes) [9], nuclear reactions locked most neutrons into ^{4}He and produced trace abundances of D, ^{3}He, ^{7}Li, and ^{7}Be, in good agreement with observations except for ^{7}Li (the so-called lithium problem) [128]. BBN thus provides the earliest robust test of ΛCDM, bringing together cosmology with particle, nuclear, and statistical physics.

At $t \approx 372{,}000$ years [126], photons decouple, forming the CMB [129]. Above a few eV, electrons and nuclei are ionized, and photons efficiently scatter on these charged particles. Near $T \sim 1$ eV, electrons and nuclei combined into neutral atoms ("recombination"), rendering the Universe neutral and allowing photons to propagate freely for the first time. Later, the formation of stars and galaxies reionized the Universe once again ("reionization") [130], marking the end of the cosmic *dark ages* (i.e., the epoch between recombination and the appearance of the first luminous sources [6]). CMB photons thus probe both early-universe physics and the subsequent expansion history via redshifting (today $T_{\rm CMB} \sim 10^{-4}$ eV), as well as astrophysics of first stars and galaxies [131]. Measurements of these photons form the basis of many of the results reported by the Planck Collaboration [26].

Together with observations of the stochastic gravitational wave background and BBN, the CMB provides one of the earliest cosmic epochs from which constraints on (new) physics models can be derived. Moreover, the exceptional precision of Planck in measuring CMB properties makes the CMB perhaps the most important probe in cosmology.

Figure 2.2 summarizes the cosmic history discussed above. We emphasize that our limited knowledge of physics at extremely high energies ($E \gg$ TeV) and of quantum gravity prevents us from ruling out new phenomena that could alter this picture at very early times ($t \ll 1$ s).

To understand neutrino decoupling, BBN, and CMB decoupling quantitatively, we turn to early-universe thermodynamics in the following sections. We will not detail these events (see Refs. [126, 133, 134] for reviews). Instead, we

[4] At these "low" temperatures, baryon pair creation is inefficient, so no new neutrons are produced. Thus all baryons present today must have been created at earlier times, through baryogenesis and the QCD transition. Moreover, baryon pair creation would also produce antibaryons; the observed absence of large amounts of antimatter implies that baryogenesis must have generated the observed matter–antimatter asymmetry [127].

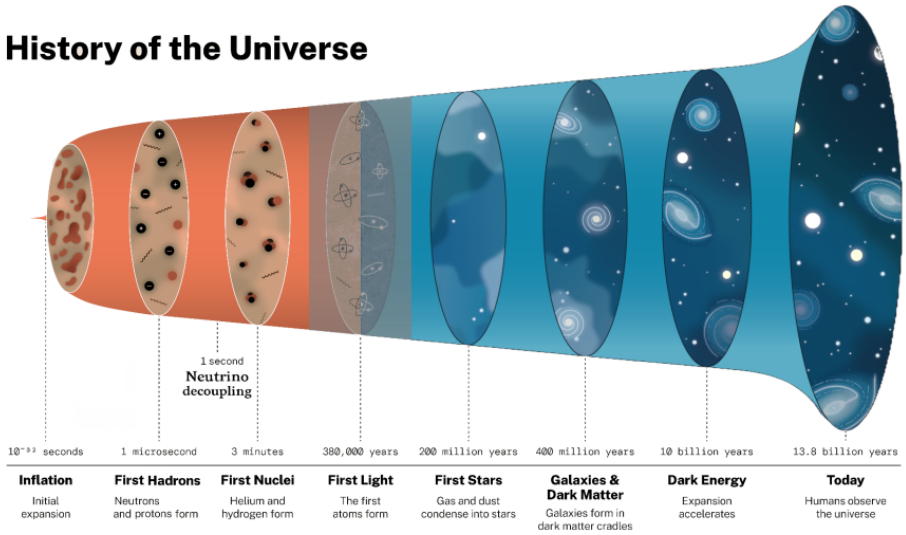

Figure 2.2: Key milestones in the thermal and structural evolution of the universe. Adapted from Ref. [132].

revisit the thermodynamics needed for DM, since the same mechanism that produced the neutrino and photon backgrounds—thermal decoupling (freeze-out)—also provides an elegant production mechanism for DM. We first present a simple approximation to freeze-out (with neutrinos as a standard example) and later return to a refined treatment when discussing particle DM.

2.1.2 Early universe thermodynamics

We introduce basic statistical tools to describe particles in the early plasma. The phase-space distribution $f(\vec{x}, \vec{p}, t)$ gives the occupation number of a particle species such that [105] (we use natural units $c = \hbar = k_B = 1$)

$$f(\vec{x}, \vec{p}, t)\, \frac{d\vec{x}\, d\vec{p}}{(2\pi)^3} \tag{2.17}$$

is the number of particles with positions in the interval $[\vec{x}, \vec{x} + d\vec{x}]$ and momenta within $[\vec{p}, \vec{p} + d\vec{p}]$ at time t. For kinetic equilibrium with a bath at temperature T,

$$f = \frac{1}{e^{(E-\mu)/T} \pm 1}\,, \tag{2.18}$$

where the minus (plus) sign is for bosons (fermions), E is the particle energy, and μ its chemical potential [135].[5]

[5] These Fermi–Dirac and Bose–Einstein distributions apply to dilute, weakly interacting gases, which is generally the case in the early Universe.

Integrating eq. (2.18) over momentum yields the number density n, energy density ρ, and pressure p for a gas with g internal degrees of freedom [135]:

$$n = \frac{g}{(2\pi)^3} \int f(k)\, d^3k\,, \tag{2.19}$$

$$\rho = \frac{g}{(2\pi)^3} \int E(k)\, f(k)\, d^3k\,, \tag{2.20}$$

$$p = \frac{g}{(2\pi)^3} \int \frac{|k|^2}{3E(k)}\, f(k)\, d^3k\,. \tag{2.21}$$

In chemical equilibrium, chemical potentials are conserved: for $i + j \leftrightarrow c + d$, $\mu_i + \mu_j = \mu_c + \mu_d$. Since photon number is not conserved, for example in Bremsstrahlung processes like $ee \leftrightarrow ee\gamma$, one has $\mu_\gamma = 0$. Thus, for species annihilating into photons, particle and antiparticle share the same chemical potential. In a perfectly symmetric plasma with equal particle and antiparticle densities and such massless $\mu = 0$ species, annihilations persisting to $T \to 0$ would completely eliminate massive particles (as in e^+e^- in a static universe [136]). Thus, a particle–antiparticle asymmetry implies a nonzero chemical potential. Nonzero μ may also arise when a species departs chemical equilibrium from the bath containing particles with $\mu = 0$, since particle and antiparticle are then no longer constrained to share the same μ. Consequently, if DM is its own antiparticle or carries no initial asymmetry, thermal equilibrium (i.e., kinetic and chemical equilibrium together) with the SM ensures that its chemical potential vanishes. For this reason, we neglect chemical potentials in what follows. In section 2.3 we return to DM decoupling and number-density evolution with a treatment that also avoids explicit use of μ.

For $T \gg m$ (relativistic), one finds that the integrations in eq. (2.19) simplify to [137]

$$n = \frac{g_{\rm eff}}{\pi^2} \zeta(3) T^3\,, \tag{2.22}$$

with $g_{\rm eff} = g$ (bosons) and $g_{\rm eff} = \frac{3}{4} g$ (fermions), and

$$\rho = \frac{\pi^2}{30} g_{\rm eff*} T^4\,, \tag{2.23}$$

where $g_{\rm eff*} = g$ (bosons) and $g_{\rm eff*} = \frac{7}{8} g$ (fermions). Since $|\vec{k}| \simeq E$, the pressure satisfies $p \simeq \rho/3$ ($w = 1/3$).

While for $m \gg T$ (non-relativistic), one finds [137]

$$n = g \left(\frac{mT}{2\pi} \right)^{3/2} e^{-m/T}\,, \tag{2.24}$$

$$\rho = mn + \frac{3}{2} nT \approx mn\,, \tag{2.25}$$

$$p = nT\,. \tag{2.26}$$

Since $p \ll \rho$, their ratio $w \ll 1$, so in practice non-relativistic species behave as matter ($w = 0$), as expected.

DM production typically occurs during radiation domination, before BBN and CMB, to avoid spoiling the remarkable agreement of ΛCDM with observations from those epochs. In a radiation-dominated Universe, the Hubble parameter from eq. (2.5) reads

$$H \simeq 1.66 \sqrt{g_*} \frac{T^2}{M_P}, \tag{2.27}$$

where $M_P = 1.22 \times 10^{19}$ GeV [138], and

$$g_* = \sum_{\text{bosons}} g \left(\frac{T_i}{T}\right)^4 + \frac{7}{8} \sum_{\text{fermions}} g \left(\frac{T_i}{T}\right)^4 , \tag{2.28}$$

with T the SM plasma temperature and T_i the effective temperature of each relativistic species [135].

The entropy S in a volume V can be defined as $S = sV$ using the entropy density of a particle bath [137]

$$s = \sum_i \frac{\rho_i + p_i - \mu_i n_i}{T_i} . \tag{2.29}$$

Contributions from non-relativistic species are generally negligible, thus the entropy density reads (neglecting μ)[6]

$$s \simeq \frac{2\pi^2}{45} g_{*s} T^3 , \tag{2.31}$$

with

$$g_{*s} = \sum_{\text{bosons}} g \left(\frac{T_i}{T}\right)^3 + \frac{7}{8} \sum_{\text{fermions}} g \left(\frac{T_i}{T}\right)^3 . \tag{2.32}$$

The entropy of all relativistic species is conserved while they follow a thermal distribution, so assuming adiabatic expansion for our Universe is an excellent approximation. Consequently, the total entropy inside a comoving (i.e. cosmologically expanding) volume $V = V_0 a^3/a_0^3$ is conserved, implying

$$\frac{dS}{dt} = \frac{d(sV)}{dt} = \frac{V_0}{a_0^3} \frac{d(sa^3)}{dt} = 0 . \tag{2.33}$$

[6]Note that for a non-relativistic particle species X (with antiparticle $\bar{X}$) in thermal equilibrium with the SM bath and having no significant asymmetry with respect to photons, i.e.,

$$1 \gg \frac{n_X - n_{\bar{X}}}{n_\gamma} \propto \frac{\mu}{T} , \tag{2.30}$$

its chemical potential μ is negligible for the entropy calculation [139].

This relation allows the bath temperature to be tracked throughout cosmic expansion. As mentioned earlier, $T \propto a^{-1}$, except when g_{*s} decreases (e.g., when a particle species becomes non-relativistic), in which case the cooling slows down [137].

It is customary to normalize particle number to entropy,

$$Y = \frac{n}{s}\,, \tag{2.34}$$

which factors out the expansion ($\propto a^3$). In the absence of number-changing processes, Y is thus constant. This will be convenient when discussing the Boltzmann equations, which describe in detail the evolution of number densities, in section 2.3. Using the results above and eq. (2.31), the equilibrium yield for relativistic species is [135]

$$Y_{\rm eq} = \frac{45}{2\pi^4}\zeta(3)\frac{g_{\rm eff}}{g_{*s}} \approx 0.278\frac{g_{\rm eff}}{g_{*s}}\,, \tag{2.35}$$

and for non-relativistic species,

$$Y_{\rm eq} = \frac{45}{2\pi^4}\left(\frac{\pi}{8}\right)^{1/2}\frac{g}{g_{*s}}\left(\frac{m}{T}\right)^{3/2} e^{-m/T}\,. \tag{2.36}$$

In both expressions we assumed the species shares the bath temperature T; for decoupled sectors with different temperatures, T should be replaced accordingly.

2.1.3 Freeze-out

So far we have described species in thermal equilibrium without addressing why equilibrium holds. A simple criterion compares the characteristic timescale for particle collisions t_c with that of the expansion of the Universe, $t_H \sim H^{-1}$. If $t_c \ll t_H$, interactions are rapid and drive the plasma to equilibrium. If $t_c \gg t_H$, expansion outpaces collisions and equilibrium is lost. Thus, a species initially in equilibrium will decouple when $t_c \sim t_H$, i.e. when its interaction rate $\Gamma \sim t_c^{-1}$ drops below the Hubble rate H as the universe expands and cools. This decoupling is called *freeze-out* and, if no particle–antiparticle asymmetry exists, it erases memory of any initial abundance.[7]

For a process with cross section σ, target density n, and relative velocity v, the reaction rate is [7]

$$\Gamma = n\sigma v\,. \tag{2.37}$$

Freeze-out occurs approximately when

$$\Gamma(T_f) = H(T_f)\,, \tag{2.38}$$

[7] Out-of-equilibrium interactions may also erase an existing asymmetry; in that case, freeze-out is completely independent of initial conditions [140]. However, such scenarios require rather complex models. Typically, one simply assumes a small or vanishing initial asymmetry.

defining the freeze-out temperature T_f. A detailed treatment via the Boltzmann equation will be given in section 2.3.

Hot dark matter freeze-out: As an illustration, consider neutrinos. Using the above equations, we can estimate their decoupling temperature $T_\nu^{\rm dec}$ from the SM bath and verify that they are produced with relativistic speeds ($T_\nu^{\rm dec} \gg m_\nu$), corresponding to hot DM species during most of the Universe's history.[8]

At temperatures well below the weak boson masses, $T \ll m_Z$, but still much larger than the neutrino masses, $T \gg \sum m_\nu \sim 0.1$ eV [144], the cross section for weak interactions scales as [8]

$$\sigma \simeq \frac{\pi}{16} G_F^2 T^2 \,, \tag{2.39}$$

where $G_F \approx 1.16 \times 10^{-5}$ GeV^{-2} is the Fermi constant [145]. Since $T \gg m_\nu$, neutrinos are relativistic ($v \simeq 1$), and their number density is given by eq. (2.22). In a radiation-dominated Universe (the case for $T \gg$ eV), we can use eq. (2.27) to write the freeze-out condition as

$$\frac{\Gamma}{H} \simeq \frac{1}{32\pi} \frac{g_\nu}{\sqrt{g_*}} G_F^2 T^3 M_P \approx \left(\frac{T}{5 \text{ MeV}} \right)^3 , \tag{2.40}$$

where in the last step we used $g_{*s} = 10.75$ (valid below $T \lesssim 100$ MeV, when the relativistic bath contains e^-, e^+, ν, $\bar{\nu}$, and γ) and $g_\nu = 2$ (left-handed neutrino plus right-handed antineutrino). We thus obtain $T_\nu^{\rm dec} \sim \mathcal{O}(\text{MeV})$, confirming that neutrinos freeze out while still relativistic. The decoupling scale lies safely between the 100 MeV and the eV regime, ensuring the consistency of our analysis.

After $T_\nu^{\rm dec}$, neutrinos decouple from the SM bath and, within the SM framework, have no strong self-interactions. Hence no number-changing processes take place, and their yield remains constant. Using the relativistic equilibrium yield in eq. (2.35), one finds

$$Y_\nu \simeq 0.2 \frac{g_\nu}{g_{*s}} \,, \tag{2.41}$$

which leads to a present-day abundance [135]

$$\Omega_\nu h^2 = \frac{Y_\nu s_0 \sum_i m_{\nu_i}}{\rho_c} h^2 \simeq \frac{\sum_i m_{\nu_i}}{91 \text{ eV}} \,. \tag{2.42}$$

For $\sum m_\nu \sim 0.1$ eV, this gives $\Omega_\nu h^2 \sim 10^{-3}$, i.e. neutrinos contribute about 1% of the total DM density today.

[8] We say "most" because, although neutrinos are produced as relativistic species with an initial temperature $T_\nu \sim$ MeV $\gg m_\nu$ (given $\sum m_\nu \lesssim 0.1$ eV from cosmological observations [26] and $\sum m_\nu \lesssim 1.35$ eV from KATRIN [141, 142]), today, after redshifting, their temperature is $T_\nu \sim 10^{-4}$ eV [143]. This is expected to be below the masses of at least two of the three neutrino mass eigenstates, according to oscillation data [144], so those states now behave as a (subdominant) cold DM component.

2.2 The Dark Matter puzzle

As previously discussed, measurements of the CMB find that most of the matter in the Universe (about 84%) does not correspond to SM particles,[9] pointing to the presence of a dark matter component. In fact, evidence for a large amount of unknown matter dates back nearly a century, when Fritz Zwicky [10, 148] studied the peculiar motion of galaxies in the Coma cluster [149]. The term "dark matter" is often attributed to Zwicky's 1933 work [10], but its usage was already common in the contemporary scientific literature, where "dark" described unknown astronomical objects such as dark stars, dark planets, or dark "nebulae" [11].

Interestingly, long before Zwicky, astronomers had already faced DM crises: in the 1840s, the proper motion of stars and the orbits of planets in the Solar System were not consistent with the visible mass at the time. In particular, the stars Sirius and Procyon, as well as the planets Uranus and Mercury, showed anomalous motion. The mathematician Friedrich W. Bessel was possibly the first to predict the existence of a new source of matter based solely on gravitational influence [11]. In a letter published in 1844 [150], he explained the observed proper motion of Sirius and Procyon through faint companion stars, later discovered as Sirius B in 1862 [151] and Procyon B in 1896 [152]. For the Solar System, prediction and discovery followed within a month (at least for Uranus): on 31 August 1846, Urbain Le Verrier predicted a new planet perturbing Uranus's orbit, and on 23 September 1846 Neptune was found [105]. John Couch Adams independently predicted Neptune using essentially the same perturbation theory techniques [153]. Similarly, to explain Mercury's orbit, Le Verrier proposed an inner planet—named Vulcan. In this case, no extra matter was found; instead, the anomaly was resolved by a new theory of gravity, Einstein's General Relativity (GR), which superseded the otherwise extremely successful Newtonian dynamics [154].

It is important to remark that in the above cases, one first attempted to solve unrelated problems at very different scales with the same type of solution: a new astrophysical object. Near the Sun, at Vulcan's hypothetical orbit, the gravitational potential ϕ_N is much larger than at Neptune's location or between stars. Thus, corrections to ϕ_N^n with $n \geq 2$, coming from modifications to gravity (such as in GR), can be safely ignored in the latter cases [105]. In contrast, the dark matter problem is not a collection of unrelated anomalies but a coherent set of observations across a wide range of scales, all pointing to compatible amounts of missing mass. This coherence makes the hypothesis of a new, undetected form of matter particularly compelling. In the remainder of this section, we summarize the evidence for DM, showing its robust experimental foundation. We also highlight some possible solutions.

[9] Possibly with the exception of a hypothetical six-quark state [146, 147].

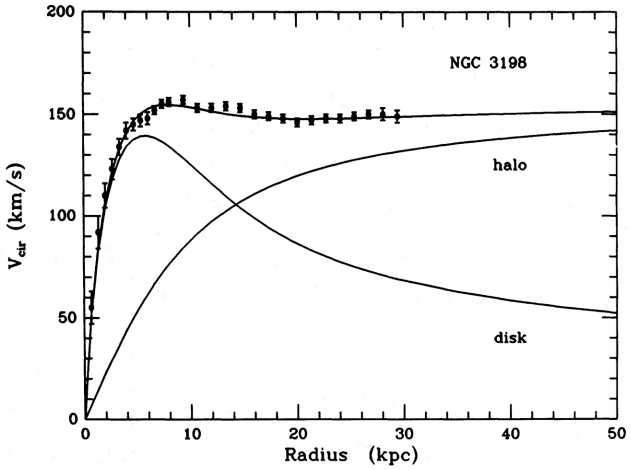

Figure 2.3: Fit of an exponential luminous disk and a spherical halo to the observed rotation curve of the spiral galaxy NGC 3198. Reproduced from Ref. [15].

2.2.1 Evidence for dark matter

At the somewhat "small" scales $\ell \lesssim 100$ kpc [105], we have evidence for DM from rotation curves of spiral galaxies. Assuming a spherical concentration of mass for simplicity $M(r)$, the rotation velocity of objects around this mass satisfies

$$v = \sqrt{\frac{GM(r)}{r}}\,. \tag{2.43}$$

The clearest example is in the Solar System, where essentially all mass is at the center (the Sun), yielding a $1/\sqrt{r}$ law, well verified by data [105]. In the outskirts of galaxies, where $M(r)$ should saturate, one would therefore expect a similar $1/\sqrt{r}$ decay. However, Vera Rubin's observations of galaxy rotation curves [12, 13] showed a surprisingly slow decrease of velocity with galactic radius. Later, Bosma [14] and van Albada and Sancisi [15] demonstrated that this behavior could not be explained by simply adjusting the relative contributions of bulge, disc, and gas [135]. Thus, a new component was required with a different spatial distribution: the DM halo (see fig. 2.3). Such a flat rotation curve is obtained if $M_{\rm halo}(r) \propto r$, precisely the relation expected for a self-gravitating gas of non-interacting particles [135].

At larger scales, $\ell \sim 10$ Mpc, those of galaxy clusters, one can follow Zwicky's approach [10, 148] and use the virial theorem to relate the average velocity of objects with the gravitational potential—i.e., the total mass of the system—assuming the cluster to be an isolated system. As with rotation curves, this method is sensitive only to total mass, DM plus visible matter, and can be contrasted with luminosity-based estimates to infer extremely large mass-to-light ratios, indicating the presence of DM. Modern techniques exploit the fact that in

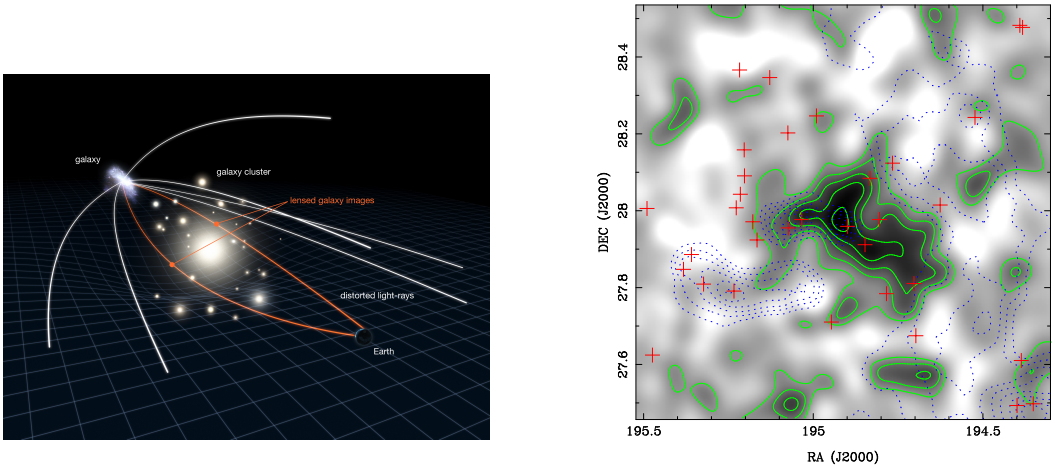

Figure 2.4: Left: Schematic illustration of light from a distant galaxy lensed by the gravitational potential of a galaxy cluster in the line of sight. Illustration by NASA/ESA (L. Calçada) [155]. **Right:** Matter in the Coma cluster inferred from weak lensing. The red crosses represent luminous matter, while the green contours show the mass distribution responsible for the gravitational field. Reproduced from Ref. [20].

GR, light trajectories are also bent by gravitational potentials; thus weak lensing methods [19, 20] provide precise gravitational determinations of cluster masses (see fig. 2.4). In either case, the results are consistent, indicating the presence of large amounts of missing mass.

An even more striking case for DM at cluster scales involves dynamical systems. The Bullet Cluster (1E0657–558) is a paradigmatic example of two galaxy clusters that underwent a collision [18]. The most accepted interpretation of the remarkable separation between the visible and DM distributions (see fig. 2.5) is that the gas of the two clusters interacted efficiently through SM cross sections and was left behind, while the DM components passed through without significant interaction [135]. This yields an upper bound on the self-interaction strength of DM particles—and on their interaction with the SM, although the latter are not competitive with terrestrial or other astrophysical constraints.

At the largest observable scales, the CMB provides evidence of DM in the early Universe. The CMB power spectrum (the spherical Fourier transform of the photon temperature field) displays distinct peaks from acoustic oscillations of the baryon-photon plasma. The positions of these acoustic peaks depend on the DM density (more DM implies an earlier radiation–matter equality), while their amplitudes depend on the ratio of DM to baryons (since DM does not undergo such oscillations), see fig. 2.6. This yields the most precise measurement of the DM density Ω_{DM}, already discussed in section 2.1.

There are additional lines of evidence for DM not mentioned above, such

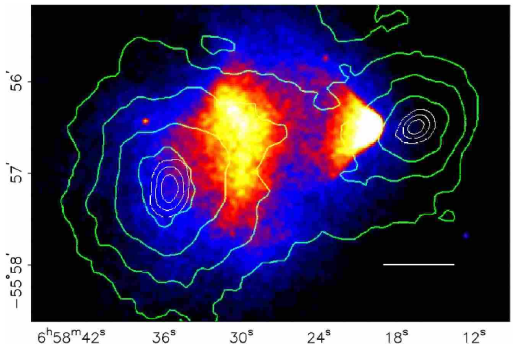

Figure 2.5: Green contours of the weak lensing reconstruction of the mass distribution superposed on the X-ray imaging of the visible matter of the two galaxy clusters composing the Bullet Cluster (1E0657–558). Reproduced from Ref. [18].

as at even smaller scales from dwarf galaxies, or across multiple scales related to structure formation. Detailed simulations [156] show the emergence of filamentary structures, which have recently been detected observationally as dark filaments (matter distributions lacking visible counterparts) connecting, for example, two clusters in the Abell 222/223 supercluster [157], as well as other nearly dark filaments between superclusters [158, 159]. Moreover, statistical results from these simulations agree well with astronomical data from the late Universe [160]. It is also worth noting that BBN constrains the baryonic matter density to be much smaller than the total matter density inferred from other probes, $\Omega_b < \Omega_{\rm DM}$. In particular, CMB and BBN estimates of Ω_b are in excellent agreement, $\Omega_b^{\rm BBN} \simeq \Omega_b^{\rm CMB}$ [138, 161]. For further discussion of these and other evidences, see Ref. [6] and references therein.

2.2.2 Possible solutions

It is important to emphasize that all evidence for DM so far is gravitational in nature. This makes the DM problem somewhat analogous to the gravitational anomalies of the 19th century. At that time, two distinct approaches were pursued: invoking new matter (planets or stars), and modifying gravity (Einstein's GR). Consequently, two broad classes of solutions exist for the DM problem: 1. a hidden mass component of matter not yet identified (possibly multiple components), pointing to new physics in particle physics or early-Universe cosmology; 2. a breakdown of the laws of gravity on the relevant scales.

A recent discussion of these two approaches can be found in Ref. [162].[10] A

[10] One could imagine extreme possibilities: that the vast body of experimental data is merely a statistical fluctuation, that systematic errors pervade all measurements, or even that the laws of physics somehow conspire to mislead us. Such scenarios, however, are not scientifically productive. We therefore restrict to the viable options discussed in the main text.

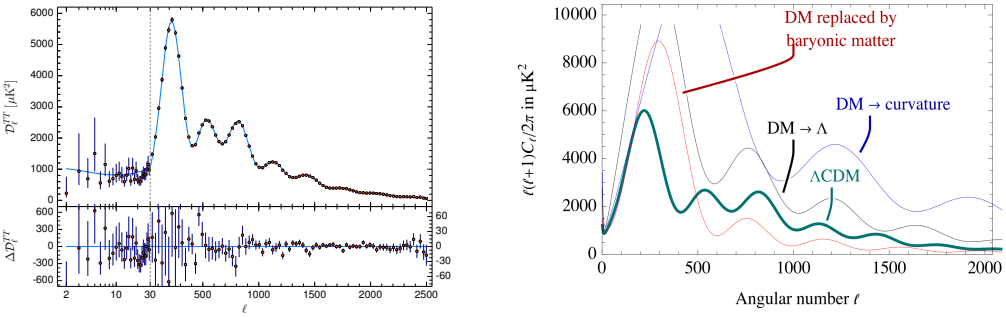

Figure 2.6: Left: CMB temperature power spectrum measured by Planck. The ΛCDM theoretical best fit is shown in light blue. Image from Ref. [26]. **Right:** The best-fit ΛCDM spectrum compared to alternative models without DM. Reproduced from Ref. [6].

third option combines both approaches [163–165], though such solutions are less minimal, given that neither direction alone has yet been completely ruled out.

The regularity of rotation curves, asymptotically converging to a constant circular velocity v_∞, and the absence of non-gravitational evidence for DM, motivated M. Milgrom in 1983 to propose a modification of Newtonian dynamics at low accelerations [28]. This framework, known as Modified Newtonian Dynamics (MOND), has been remarkably successful in describing galaxy rotation curves and in explaining the Baryonic Tully–Fisher relation, $v_\infty \propto \mathcal{M}_b^{1/4}$, which connects asymptotic velocity v_∞ with baryonic mass $\mathcal{M}_b$, and matches observations from dwarf galaxies up to clusters [6, 166].

However, the simplicity of MOND fades when addressing the full DM problem across all scales and phenomena, and when remembering that Newtonian gravity is merely an approximation to GR—this means that MOND must be embedded into a covariant framework to preserve GR's successes. On the phenomenological side, MOND struggles with several key observations: structure formation and baryon acoustic oscillations [7, 167], the CMB acoustic peaks [168], and merging clusters such as the Bullet Cluster (1E0657–558) [169]. On the theoretical side, covariant extensions of MOND, such as the TeVeS (Tensor–Vector–Scalar) theory proposed by Bekenstein in 2004 [170, 171], introduce multiple new fields, reducing its minimality. Furthermore, multimessenger observations from GW170817 [172] constrain the relative speed of gravitational and electromagnetic waves, excluding a significant class of GR modifications [173]. For more on MOND, see Refs. [6, 174] and references therein.

Solutions involving a new dark component of matter also face challenges, but all current evidence can be accommodated within the CDM framework, given the uncertainties in data and modeling [30]. A DM component is also the most minimal and natural explanation, since we already know of astrophysical

objects that behave exactly like CDM (e.g., black holes [31, 32]), and because new particles generically arise in extensions of the SM addressing other fundamental problems. Historically, several astrophysical objects were considered as DM candidates, such as large planets, small dead stars, and stray black holes (all non-luminous). These were collectively termed Massive Compact Halo Objects (MACHOs) [175, 176]. However, BBN and CMB constraints exclude baryonic DM, ruling out MACHOs [6]. The sole exception is black holes produced before BBN, known as primordial black holes (PBHs) [177, 178].

On the particle side, DM candidates arise naturally in many SM extensions. Examples include solutions to the hierarchy problem such as supersymmetry [33, 39, 43], technicolor [35, 36], and composite Higgs models [40]; solutions to the strong CP problem (axions) [34]; and candidates from unifying frameworks like GUTs [37, 42] and string theory [38, 41]. The variety of DM production mechanisms in the early Universe is equally broad [44–57], with thermal freeze-out [60] standing out as a particularly natural and predictive scenario. This breadth strongly favors particle DM as the most promising solution.

PBHs as DM, on the other hand, require somewhat contrived early-Universe dynamics to avoid disrupting the successes of the standard cosmological model, and are subject to stringent bounds on their possible masses, $10^{-16} M_\odot \lesssim m_{\rm PBH} \lesssim 10^{-12} M_\odot$ [31]. Realizing such PBHs typically demands complex inflationary models [179, 180] or other non-minimal cosmological scenarios [181], making them less minimal and appealing.[11]

In the remainder of this thesis, we will restrict our attention to particle DM scenarios.

2.3 The particle Dark Matter

The idea of new particles beyond our current understanding is not driven solely by Dark Matter physics. In fact, several outstanding questions of the SM point to new degrees of freedom: the origin of neutrino masses [186], the matter–antimatter asymmetry [119], electric charge quantization [187, 188], the strong CP problem [189], and the hierarchy problem [190]. Assuming DM is composed of new particles, what properties must these particles have to be compatible with the broad phenomenology discussed so far?

Remarkably, the diverse body of DM evidence—from dwarfs to clusters, from the CMB to structure formation—can be addressed by a single new particle that is sufficiently massive to be non-relativistic, stable on cosmological timescales, effectively collisionless (at least on cluster scales), feebly interacting with the

[11] PBHs have regained attention recently due to possible connections with gravitational-wave observations [182–185].

SM, and non-baryonic [105]. Of course, multi-component DM remains a viable possibility.

2.3.1 Dark Matter properties

Let us briefly examine these properties in turn.

Cold (non-relativistic): Numerical simulations of structure formation require that DM behaves as a pressureless fluid ($w \approx 0$) to seed the growth of small perturbations visible in the CMB. Massless (or relativistic) DM would instead behave as radiation ($w = 1/3$) and erase small-scale structure via free streaming. Thus DM must be "cold" (small typical velocities) to accumulate in galactic halos. By contrast, hot (relativistic) DM has a large free-streaming length and conflicts with observations—one of the reasons neutrinos cannot account for all DM.

At the smallest galactic scales, vanilla CDM simulations predict more subhalos than observed [191]. Warm DM, with intermediate velocities, would partially suppress small-scale structure and may alleviate these tensions [192]. However, a definitive conclusion requires detailed simulations including baryonic feedback.

Stable: DM must be present already at recombination, facilitate structure formation, and still manifest in galaxies and clusters today. If it decays, its lifetime must exceed the age of the Universe; stronger bounds arise channel by channel from indirect searches. Stability is often guaranteed by a symmetry, making DM the lightest state carrying a new conserved quantum number. In scenarios with decays, extremely small couplings and/or small mass splittings are required to achieve cosmologically long lifetimes.

Collisionless: Dynamical systems such as merging clusters indicate that DM is predominantly collisionless, passing through with little drag while the baryonic gas is shocked and slowed. The near-sphericity of halo profiles also disfavors strong dissipation. A range of astrophysical probes—most notably the absence of significant drag (deceleration) of the DM component in the Bullet Cluster—constrain the DM self-interaction cross section per unit mass to [193]

$$\frac{\sigma}{m_{\rm DM}} \lesssim 0.7 \text{ cm}^2/\text{g}\,. \tag{2.44}$$

Intriguingly, self-interactions in the range $0.1 \lesssim \sigma/m_{\rm DM} \lesssim 1$ cm^2/g at galaxies and dwarf scales may help with small-scale puzzles [193].

Dark (feebly interacting): By definition, DM must be very weakly coupled to the SM. Its interactions with the baryon–photon plasma must be sufficiently small to avoid spoiling the CMB, and small enough to evade the many null results from direct, indirect, and collider searches. The canonical example is the Weakly *Interacting* Massive Particle (WIMP), historically motivated by weak-scale cross sections and masses.

In particular, DM must be effectively neutral: even a tiny electromagnetic charge ϵe is strongly constrained by recombination-era observations and direct detection [6, 194]. For $m_{\rm DM} \sim$ TeV, one typically needs $\epsilon \lesssim 10^{-9}$ [6].

Non-baryonic: BBN and CMB tightly constrain the baryon fraction, $\Omega_b \simeq 0.16\,\Omega_m$, implying that most matter is non-baryonic. This motivates particle DM over MACHO-like solutions (with the exception of PBHs). Setting aside still-debated exotic baryonic states such as $uuddss$ hexa-quarks [195, 196], the inequality $\Omega_m > \Omega_b$ is a clear sign of physics beyond the SM.

2.3.2 Examples of candidates

The DM phenomenology can be reproduced by an enormous variety of models. Since we do not yet know anything about its fundamental properties—its mass, spin, charges, or even whether it is a particle at all—we must remain agnostic and explore as many directions as possible until a positive signal arises [197].

Indeed, the possible DM mass impressively spans over 90 orders of magnitude. On the light side, bosonic candidates can be as light as [198]

$$m_{\rm DM} \gtrsim 10^{-21}\ \text{eV} \sim 10^{-49} M_P\,. \tag{2.45}$$

Such ultralight DM presents extremely large number densities that it can be treated as a classical field, much like photons or electromagnetic fields. Lighter bosons are excluded, since their de Broglie wavelengths would exceed the size of dwarf galaxies. Fermions face even stricter constraints, $m_{\rm DM} \gtrsim 0.1$ keV [199], due to the Pauli exclusion principle, which forbids too many fermions from occupying a confined region such as a dwarf galaxy [200].

On the heavy side, DM masses can in principle exceed the Planck mass M_P, provided DM is a composite object, possibly reaching up to the gravitational limit where they collapse into black holes. At that point DM would no longer be composed of quantum particles but macroscopic objects. A generic upper bound can once again be derived from dwarf galaxies: since they contain large amounts of DM, the DM particle mass must be smaller than the total mass of such systems, giving [6]

$$m_{\rm DM} \lesssim 10^{37}\ \text{kg} \sim 10^{44} M_P\,. \tag{2.46}$$

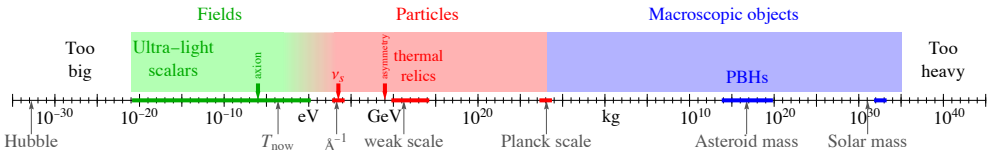

Figure 2.7: Possible range for the DM mass highlighting the three qualitatively distinct regimes: fields, particles, and macroscopic objects. Some well-known DM candidates are also shown. Reproduced from Ref. [6].

In the intermediate mass regimes, DM is expected to behave more like an ordinary particle interacting with individual atoms, since in this case its de Broglie wavelength is much smaller than atomic scales.

Although the possible DM mass range is gigantic, we can, as discussed above, conceptually split it into three qualitatively distinct regimes: fields, particles, and macroscopic objects. While the particle–field duality of quantum field theory formally unifies the first two, their phenomenological behaviors are so different that this pragmatic separation is useful. The three regimes are summarized in fig. 2.7.

Similarly, the DM coupling to the SM, g, can span many orders of magnitude, from the purely gravitational limit $g \sim m_{\rm DM}/M_P$ up to strong-interaction-like couplings $g \sim 4\pi$ [6].

Clearly, it is impossible to cover the full landscape of DM candidates in this thesis. Instead, we will present a short and admittedly biased selection, focusing on those models that have become most prominent in the literature or in experimental searches.

The most intensively studied candidate of the past decades has been the Weakly Interacting Massive Particle (WIMP), motivated by its natural connection to electroweak physics and the hierarchy problem [201]. WIMPs are a broad class of models, but notable examples include supersymmetric neutralinos, Little Higgs models, and Kaluza–Klein theories with extra dimensions. In each case, stability is typically ensured by a discrete symmetry such as R-parity in supersymmetry [202], T-parity in Little Higgs models [203], or KK-parity in extra-dimensional scenarios [204].

A second, and increasingly popular, candidate is the axion [205], originally introduced to solve the strong CP problem. Axions correspond to decaying DM, but with lifetimes so long that their decays are effectively suppressed by very high mass scales. Other notable decaying DM candidates include gravitinos [206, 207], whose decays are suppressed by gravity, and sterile neutrinos ν_s, whose decays are suppressed by their tiny mixing with SM neutrinos [208].

Other well-known examples include simplified models such as Asymmetric DM [209], strongly interacting massive particles (SIMPs) [49], self-interacting

DM (SIDM) [193], and Fuzzy DM [210].

Finally, there exist candidates whose only free parameter is their mass, since they correspond to new SM multiplets and interact simply through the known SM forces. These are collectively known as Minimal DM [211].

Production mechanisms: Many production modes are possible. Here we briefly outline some of the most widely studied in the literature before focusing on the particularly predictive thermal freeze-out, already foreshadowed in section 2.1.

Perhaps the most popular mechanism to produce relatively heavy ($\gtrsim$ MeV) DM is *thermal freeze-out*, precisely because of its independence from the initial conditions of the Universe thanks to DM achieving thermal equilibrium with the SM plasma. The DM annihilation processes, typically driving the equilibrium, automatically ensure that DM inherits the adiabatic inhomogeneities of the SM [212], as required by CMB observations [25, 26].

For ultra-heavy masses, *non-thermal production* becomes more natural. One possibility is the direct generation of super-heavy WIMPZILLAS from gravity during inflation [45], with masses up to the inflationary scale. Other non-thermal mechanisms include production from decays or annihilations of other bath particles, collectively known as the *freeze-in mechanism* [213]. In freeze-in, any initial DM abundance is assumed to be negligible, and the requirement of avoiding thermal equilibrium forces extremely small couplings to the SM.[12] Such candidates are often called Feebly Interacting Massive Particles (FIMPs) [213]—or superWIMPs [46] when their dominant production comes from decays. Freeze-in is particularly well suited for sub-MeV DM, which cannot thermalize without conflicting with BBN constraints.

Closely related is the *Dodelson–Widrow mechanism*, where sterile neutrinos are produced from oscillations of active neutrinos in thermal equilibrium with the SM bath [215].

At even lighter masses, where DM behaves as a coherent field, production can arise from the dynamics of *cosmological topological defects*, such as cosmic strings [216] or domain walls [217], often tied to phase transitions. In the specific case of *axions*, another important mechanism is *vacuum misalignment* [218]. If the Peccei–Quinn $U(1)_{\rm PQ}$ symmetry (associated with the axion field) breaks after inflation, the axion field is initialized with random phases in causally disconnected patches. Since any pre-inflationary abundance is erased, the axion effectively starts with zero abundance, and the subsequent misalignment of these phases—together with contributions from topological defects—can generate the observed DM relic density. This renders axion DM both predictive and largely

[12] Assuming a very low inflationary reheating temperature can instead allow such couplings to reach freeze-out values [214].

independent of initial conditions.

However, axion production is subject to large systematic uncertainties arising from the complex dynamics of cosmological topological defects. In addition, axions may emerge either from simple UV-complete field theories or from more elaborate constructions involving extra dimensions or string theory. The UV origin of axions can determine, for example, the domain wall number and whether cosmic strings are formed at all, both of which are intrinsically linked to the predictions for the axions coupling with the SM [219]. In any case, axions remain among the leading DM candidates.

Finally, phase transitions in the early Universe have recently become a rapidly growing field, largely due to their connection with gravitational waves [220]. They also open up alternative DM production channels, such as those associated with bubble collisions [221–223], which are attracting increasing attention.

Other examples of production mechanisms can be found in Refs. [6, 224] and references therein.

In the remainder of this section, we will zoom in on the thermal freeze-out scenario and, in particular, on the case of WIMPs. Before doing so, we present in fig. 2.8 a schematic overview of the main possible directions for solving the DM problem.

2.3.3 Prelude: Boltzmann equations

In this prelude, we derive the Boltzmann equation governing the evolution of the number density of particles in kinetic equilibrium with a thermal bath (or, more generally, with a thermal phase-space distribution). This equation will later be applied to the freeze-out mechanism (and could be applied to freeze-in as well).

The evolution of the phase-space distribution $f(\vec{x}, \vec{p}, t)$ is described by the Liouville equation [60]:

$$\hat{L}[f(\vec{x}, \vec{p}, t)] = \hat{C}[f(\vec{x}, \vec{p}, t)] \,, \tag{2.47}$$

where $\hat{L}$ is the Liouville operator, and $\hat{C}$ is the collision operator, encoding processes that change the number of particles with momentum $\vec{p}$ at position $\vec{x}$ (e.g. annihilations, decays, or scatterings).

In covariant form, for $x^\mu = (t, \vec{x})$ and $p^\mu = (E, \vec{p})$, the Liouville operator reads [135]:

$$\hat{L} = p^\mu \frac{\partial}{\partial x^\mu} - \Gamma^\mu_{\sigma\rho} p^\sigma p^\rho \frac{\partial}{\partial p^\mu} \,, \tag{2.48}$$

where gravitational effects enter through the Christoffel symbols $\Gamma^\mu_{\sigma\rho}$.

Figure 2.8: A schematic summary of possible solutions to the DM problem. Reproduced from Ref. [197].

The Liouville equation can be recast as a total time derivative of f, making it manifest as the conservation of particles in phase space [105]:

$$\frac{Df(\vec{x},\vec{p},t)}{dt} = (\text{gain of } \vec{p}\text{-particles at } \vec{x} \text{ per unit time}) - (\text{loss of } \vec{p}\text{-particles at } \vec{x} \text{ per unit time})\,. \quad (2.49)$$

In a homogeneous and isotropic Universe, described by the Robertson–Walker metric (2.1) and the Friedmann equations (2.5)–(2.6), the Liouville operator simplifies to

$$\hat{L} = E\frac{\partial}{\partial t} - H|\vec{p}|^2\frac{\partial}{\partial E}\,. \quad (2.50)$$

We can integrate Liouville's equation over the covariant phase-space measure,

$$d\Pi = \frac{g}{(2\pi)^3}\frac{d^3\vec{p}}{2E}\,, \quad (2.51)$$

to obtain an equation for the number density n. The Liouville side becomes

$$2\int d\Pi\,\hat{L} = \frac{dn}{dt} + 3Hn\,, \quad (2.52)$$

while the integrated $\hat{C}$ represents the net creation and annihilation of particles.

—

For concreteness, let us focus on annihilation processes in which two DM particles $(\chi,\bar{\chi})$ annihilate into two SM particles $(X,\bar{X})$, and vice versa, $\chi\bar{\chi} \leftrightarrow X\bar{X}$. Annihilations with two incoming particles generally dominate over processes with $n \geq 3$ initial particles, as the likelihood of multiple particles encountering each other in the bath is strongly suppressed. Larger numbers of final states are typically disfavored by phase-space suppression, while increasing the number of particles either in the initial or final states (or both) usually entails an extra suppression from higher powers of the couplings. Decays could in principle be more efficient, since they do not require particle encounters, but DM is assumed to be stable (or at least extremely long-lived), while SM particles generally have negligible branching fractions into DM (due to constraints on their properties or simply kinematics). Consequently, the dominant contribution usually arises from $2 \leftrightarrow 2$ annihilations, and we may restrict to the process

$$\chi\bar{\chi} \leftrightarrow X\bar{X}\,. \quad (2.53)$$

In this case, the collision operator (governing f_χ) takes the form

$$2\int d\Pi_\chi\,\hat{C} = -\int d\Pi_\chi d\Pi_{\bar{\chi}} d\Pi_X d\Pi_{\bar{X}}\,(2\pi)^4\delta^{(4)}(p_\chi + p_{\bar{\chi}} - p_X - p_{\bar{X}}) \times \Big[|M_{\chi\bar{\chi}\to X\bar{X}}|^2 f_\chi f_{\bar{\chi}}(1\pm f_X)(1\pm f_{\bar{X}}) - |M_{X\bar{X}\to\chi\bar{\chi}}|^2 f_X f_{\bar{X}}(1\pm f_\chi)(1\pm f_{\bar{\chi}})\Big]\,. \quad (2.54)$$

The delta function ensures four-momentum conservation. In particular, energy conservation, together with the assumption that all particles are non-relativistic ($m_i \gg T$),[13] implies

$$f_X f_{\bar{X}} = f_X^{\rm eq} f_{\bar{X}}^{\rm eq} = e^{-(E_X+E_{\bar{X}})/T} = e^{-(E_\chi+E_{\bar{\chi}})/T} = f_\chi^{\rm eq} f_{\bar{\chi}}^{\rm eq}\,, \tag{2.55}$$

where $f_i^{\rm eq}$ describes particles in thermal (i.e., kinetic and chemical) equilibrium with the SM bath of temperature T (hence $\mu_i = -\mu_{\bar{i}}$) and, in the first equality, we use the fact that SM particles are in equilibrium (which is generally true at high temperatures).

The factors $(1 \pm f_i)$ account for Pauli blocking (fermions, minus) or Bose enhancement (bosons, plus). For non-relativistic species, $f_i \ll 1$, and thus $(1 \pm f_i) \simeq 1$.[14]

Assuming $\mathcal{CP}$ conservation (and hence $\mathcal{T}$ invariance from the $\mathcal{CPT}$ theorem [227]), both spin averaged amplitudes squared can be related as

$$|M_{\chi\bar{\chi}\to X\bar{X}}|^2 = |M_{X\bar{X}\to\chi\bar{\chi}}|^2 \equiv |M|^2\,. \tag{2.56}$$

If DM remains in kinetic equilibrium with the SM bath,[15] then $f_\chi/f_\chi^{\rm eq} = n_\chi/n_\chi^{\rm eq}$. In this case, the integrated collision term reduces to

$$2\int d\Pi_\chi\, \hat{C} = -\langle\sigma v\rangle(n^2 - n_{\rm eq}^2)\,, \tag{2.57}$$

with the thermally averaged cross section

$$\langle\sigma v\rangle \equiv \frac{1}{n_{\rm eq}^2}\int d\Pi_\chi d\Pi_{\bar{\chi}} d\Pi_X d\Pi_{\bar{X}}\,(2\pi)^4\delta^{(4)}(p_\chi+p_{\bar{\chi}}-p_X-p_{\bar{X}})\,|M|^2 f_\chi^{\rm eq} f_{\bar{\chi}}^{\rm eq}\,. \tag{2.58}$$

This leads to the well-known Boltzmann equation for the number density:

$$\frac{dn}{dt} + 3Hn = -\langle\sigma v\rangle(n^2 - n_{\rm eq}^2)\,. \tag{2.59}$$

When $\Gamma_{\rm ann} = \langle\sigma v\rangle n \gg H$, the right-hand side dominates over the Hubble term, the number density is driven towards equilibrium, erasing any initial over-

[13] This assumption is generally valid in the absence of degenerate Fermi species ($\mu_i \gtrsim T$) or Bose condensates [225]. More generally, within the CDM paradigm, DM must be non-relativistic. If, on the other hand, the SM particle is relativistic, only the high-energy tail of its distribution contributes to annihilations into DM, since $T \ll m_\chi$. In this regime, all three distribution functions (classical, Bose–Einstein, and Fermi–Dirac) are very similar at large momenta, making the non-relativistic assumption a good approximation. Alternatively, one may bypass this discussion entirely by invoking the Principle of Detailed Balance [226] to derive the Boltzmann equation, see Ref. [60].

[14] More generally, $\langle E\rangle \sim m + 3T/2$, and the approximation $(1 \pm f_i) \approx 1$ is accurate at the $\sim 10\%$ level [6].

[15] Maintained through elastic scatterings $\chi X \leftrightarrow \chi X$, which are typically much faster than annihilations since $n_X \gg n_\chi$ for $m_\chi \gg m_X$.

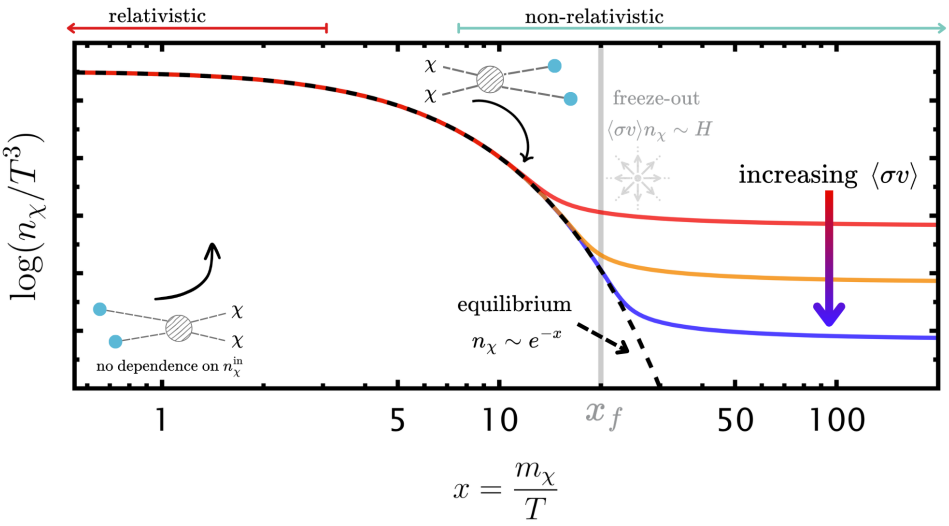

Figure 2.9: Illustrative solution of the Boltzmann equation for different values of $\langle\sigma v\rangle$ (with constant g_{*s}). Larger cross sections yield smaller relic abundances $\Omega_\chi \propto m_\chi n_\chi$. For a given m_χ, only one value of $\langle\sigma v\rangle$ reproduces the observed abundance $\Omega_\chi = \Omega_{\rm DM}$, provided DM thermalized with the SM ($\Gamma = \langle\sigma v\rangle \max(n_\chi, n_\chi^{\rm eq}) > H$). If $\Gamma \ll H$, $n \propto a^{-3}$ and DM is simply diluted by expansion.

or under-abundance of DM. Eventually, however, the Hubble rate takes over, since $n_{\rm eq} \propto e^{-m_\chi/T}$ decreases exponentially while $H \propto T^2$ falls only as a power law. In this regime, the right-hand side becomes negligible and the differential equation $dn/n = -3\,da/a$ implies $n \propto a^{-3}$. Physically, this corresponds to DM particles no longer annihilating or being produced, so that their number density decreases solely due to the expansion of the Universe. In other words, this is precisely the freeze-out mechanism previously discussed.

It is convenient to introduce dimensionless variables, in particular the yield Y (see Eq. (2.34)) and $x = m_\chi/T$. Entropy conservation then gives

$$\frac{dY}{dx} = -\frac{\lambda\langle\sigma v\rangle}{x^2}\left(Y^2 - Y_{\rm eq}^2\right)\,, \tag{2.60}$$

with

$$\lambda \equiv \frac{sx^3}{H(T = m_\chi)} \approx 0.26\,\frac{g_{*s}}{\sqrt{g_*}}\,\frac{M_{\rm Pl}}{m_\chi}\,, \tag{2.61}$$

where we used Eq. (2.31) and the Hubble rate in a radiation-dominated Universe (2.27). Eq. (2.60) is a Riccati equation, which generally requires numerical solution [135], though approximate analytic solutions are sometimes possible. See Fig. 2.9 for a schematic numerical example.

—

In particular, for a DM model with two free parameters—the DM mass m_χ and its coupling to the SM g—one can determine g as a function of m_χ by computing the thermally averaged cross section $\langle\sigma v\rangle$ and requiring it to reproduce the observed relic abundance, $\Omega_\chi \simeq 0.11$, via freeze-out. The resulting relation $g_t(m_\chi)$ is commonly referred to as the *thermal relic target*, or simply the *thermal target*—sometimes also called the *relic abundance line*.[16] This line is often displayed in parameter-space plots as a benchmark for experimental sensitivities. If the coupling is smaller than $g < g_t$, the model overproduces DM and is therefore excluded in standard cosmology, except in the extreme limit of very small couplings where DM never thermalizes with the SM. Larger couplings are allowed, but in that case the model can no longer account for the entirety of the DM abundance. In this way, the relic abundance line can also be interpreted as a lower bound on the coupling of any stable (or very long-lived) new particle. Thus, freeze-out provides a predictive and testable framework, setting the stage for the WIMP paradigm and the so-called *WIMP miracle*.

2.3.4 WIMPs: the standard Dark Matter particle

A leading hypothesis for the nature of this new non-baryonic component of the universe is the Weakly Interacting Massive Particle (WIMP). The relic abundance of WIMPs is set as they fall out of equilibrium with the high-temperature plasma of the early Universe. When the temperature T drops below the WIMP mass m_χ, the equilibrium distribution becomes Boltzmann-suppressed, $n_\chi \sim \exp(-m_\chi/T)$. Soon after, the expansion rate H exceeds the DM annihilation rate $\Gamma = \langle\sigma v\rangle n_\chi$, preventing further annihilation into SM particles and thereby *freezing out* the DM density, which subsequently evolves only through dilution, $n_\chi \propto a^{-3}$. See fig. 2.9 for a detailed example of the freeze-out process.

In general, the annihilation cross section σ can be expanded in terms of the relative velocity v between the annihilating DM particles. One finds

$$\sigma v = a + bv^2 + \mathcal{O}(v^4)\,, \tag{2.62}$$

where a is the s-wave coefficient and b the p-wave coefficient. Such expansion makes sense since freeze-out occurs for non-relativistic particles ($m_\chi \gg T \sim m_\chi v^2$, hence $v \ll 1$).[17] Thermal averaging then yields [228]

$$\langle\sigma v\rangle = a + b\frac{6T}{m_\chi} + \mathcal{O}(T^2) = a + \frac{6b}{x} + \mathcal{O}(x^{-2})\,, \tag{2.63}$$

where in the last step we introduced the dimensionless variable $x \equiv m_\chi/T$.

[16] More generally, the thermal target denotes the region of parameter space where the thermal freeze-out mechanism yields the observed relic abundance.

[17] This expansion may fail if $2m_\chi$ lies near a kinematic threshold for heavier final states, where the kinetic energy permits annihilation, or near a resonance (pole) in the cross section [44].

Using this expansion, one can obtain approximate analytical results for the relic abundance [135], or solve the full Boltzmann equation numerically, keeping only the leading coefficient. The latter approach has been carried out in Ref. [228], yielding

$$a \approx 2.2 \times 10^{-26}\,\mathrm{cm}^3/\mathrm{s}\,, \tag{2.64}$$

$$b \approx 17 \times 10^{-26}\,\mathrm{cm}^3/\mathrm{s}\,. \tag{2.65}$$

For $m_\chi \lesssim 10$ GeV, changes in the relativistic degrees of freedom across the QCD phase transition can enhance these values by up to a factor of ~ 3. These results are robust and essentially independent of the annihilation channel.

Remarkably, for DM interacting with the SM through weak gauge bosons, one generically finds [8, 135]

$$\sigma v \sim \frac{\pi}{16} G_F^2 m_\chi^2\,(1 \text{ or } v^2) \;\approx\; 2.2 \times 10^{-26}\,\mathrm{cm}^3/\mathrm{s} \times \frac{m_\chi^2}{m_Z^2}(1 \text{ or } v^2)\,, \tag{2.66}$$

via s-channel exchange, or alternatively [67]

$$\sigma v \sim \frac{g_{\mathrm{weak}}^4}{16\pi^2 m_\chi^2}(1 \text{ or } v^2) \;\approx\; 2.2 \times 10^{-26}\,\mathrm{cm}^3/\mathrm{s} \times \frac{m_W^2}{m_\chi^2}(1 \text{ or } v^2)\,, \tag{2.67}$$

through t- and u-channel processes, with $g_{\mathrm{weak}} \simeq 0.65$.

In either case, if DM has masses of order the weak scale (m_W, m_Z) and interacts via the weak force, it naturally yields the correct relic abundance. More broadly, any DM with couplings $g_\chi \sim \mathcal{O}(1)$ to the SM and masses around the electroweak scale $v_{\mathrm{EW}} = 246$ GeV generically accounts for the observed DM abundance—unless the particle is unstable and decays away, or if the cosmological history deviates from the standard picture. This coincidence of scales, often dubbed the *WIMP miracle*, together with the robustness of thermal freeze-out and the appearance of weak-scale particles in theories addressing the hierarchy problem [190], elevated WIMPs to the status of the "standard" DM candidate.

However, null results from a wide range of WIMP searches, together with the absence of new physics at the LHC associated with the Higgs boson and the hierarchy problem, have significantly diminished the appeal of WIMPs [68]. Today, WIMPs compete with a diverse set of alternative candidates. Furthermore, many variations of the WIMP scenario have by now developed into distinct and well-motivated frameworks in their own right, as we will discuss in chapter 3. For further review on WIMPs, see Ref. [67].

2.4 Searches for the Dark Matter particle

With so many observations supporting the existence of DM, determining its nature has become a central challenge in physics. A wide range of strategies aim

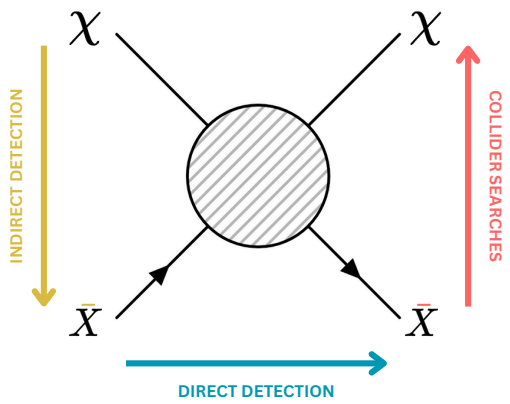

Figure 2.10: Illustration of the complementarity between the three main DM search strategies. WIMPs (or more generally freeze-out DM) require efficient annihilation of DM particles χ into SM particles X in the early universe, typically implying observable rates for indirect detection, direct detection, and collider searches.

to identify possible interactions of DM with the SM beyond gravity, but so far no conclusive evidence has been found.

The freeze-out mechanism and the WIMP miracle, however, motivate a variety of experimental signatures. The same annihilation processes that produced WIMPs in the early universe allow us to search for DM annihilation in the late universe, for instance in galaxies or compact astrophysical objects with high DM densities. Such searches are referred to as *indirect detection*. Efficient DM annihilation in the early universe generally implies that DM can also scatter off ordinary matter; searches for such scatterings are known as *direct detection*. Finally, the same annihilation processes imply the inverse reaction, where SM particles annihilate into DM pairs. These can occur in high-energy experiments, leading to *collider searches*. The interplay between these three approaches is illustrated in fig. 2.10. This web of strategies and their mutual consistency is often referred to as *DM complementarity*. In the WIMP case, the requirement of not overproducing DM in the early universe implies lower bounds on the strength of these interactions, which in turn provide promising experimental targets.

Although WIMPs have recently lost some of their central status, these searches probe generic DM models far beyond the WIMP framework,[18] and therefore continue to be of prime importance.

Besides these traditional approaches, in recent years a new experimental frontier in high-energy physics—the *intensity frontier* [230]—has emerged. This program, which includes beam-dump experiments and high-luminosity collid-

[18] They even extend to scenarios such as small primordial black holes, provided they evade evaporation [229].

ers, offers unique opportunities to probe light DM models with extremely small couplings [231].

For ultralight DM behaving as classical fields, entirely different search strategies apply. A key example is the conversion of DM fields into SM fields in environments where strong SM fields are present, as in axion haloscopes [232, 233]. For a recent review of searches for ultralight DM, see Ref. [234].

In the following, we focus on the three main search strategies for particle DM (indirect detection, direct detection, and collider searches), briefly describing their concepts and summarizing their current status. For further details on each of these approaches, see Refs. [63, 65, 235], while a broader discussion of additional search strategies can be found in Ref. [6] and references therein.

2.4.1 Indirect detection

The fact that DM plays a crucial role in structure formation implies that, although its present-day density is small on large scales, it "clumps" on smaller scales. This leads to significant density enhancements in astrophysical systems, particularly in dwarf galaxies and in the central regions of larger galaxies. In these regions, DM can still annihilate efficiently today, producing a flux of SM particles that can be detected by satellites or ground-based telescopes. In the case of decaying DM, one instead looks for the decay products emerging from these high-density regions.

Among the possible detection channels, one can distinguish two classes of indirect searches [7]: *not-so-indirect*, when the observed particles (such as photons or neutrinos) travel essentially in straight lines from the source; and *pretty indirect*, when the detected particles do not point back to the annihilation site (for example, charged particles deflected by galactic magnetic fields, or secondary low-energy photons produced during propagation). In the latter case the source cannot be identified directly, which makes background subtraction especially challenging. In both categories, astrophysical backgrounds complicate the extraction of a potential DM signal. Furthermore, the observed particles are not always direct annihilation (or decay) products of DM particles, which motivates the generic label *indirect detection*.[19]

One may also define a third, more generic category: *very indirect probes*, which constrain the effects of DM on astrophysical systems or on cosmological observables. For instance, if DM–SM scattering is efficient, DM may accumulate inside neutron stars, altering their dynamics by annihilating and injecting energy into the star [236]. These probes are considered very indirect because they rely on our modeling of complex astrophysical systems and assume that all relevant

[19] For instance, strictly speaking, in the case of annihilation into two high-energy photons, we have a pretty direct signal, but we will stick to the conventional classification.

physical processes are accounted for; in practice, the imprint of a new particle could easily be degenerate with other dynamics. A similar caveat applies to cosmological probes, which rely on our modeling of the Universe itself.

Particle flux from annihilations: For a DM particle χ annihilating through multiple channels, each with thermally averaged cross section $\langle\sigma_i v\rangle$, the annihilation rate per particle is [237]

$$\Gamma = \sum_i \frac{\rho_\chi(\vec{x})}{m_\chi}\langle\sigma_i v\rangle\,, \tag{2.68}$$

where ρ_χ is the DM energy density at the position $\vec{x}$ and m_χ the DM mass. The total annihilation rate in a volume element d^3x follows by multiplying by the number of particles in that volume:

$$\Gamma_{\rm tot} = \left(\sum_i \frac{\rho_\chi(\vec{x})}{m_\chi}\langle\sigma_i v\rangle\right) \times \left(\frac{\rho_\chi(\vec{x})}{2m_\chi}\, d^3x\right). \tag{2.69}$$

The factor of $1/2$ accounts for two particles being required in each annihilation.

To compute the flux of a given SM species $X \in \{\gamma, \nu, e^\pm, p^\pm, \dots\}$, one multiplies $\Gamma_{\rm tot}$ by dN_i/dE_X, the spectrum of X per annihilation in channel i. This quantity is in general non-trivial: heavy final states can decay through multiple channels producing long decay chains, often requiring Monte Carlo simulations to compute dN_i/dE_X. An example for the flux of photons is shown in fig. 2.11.

The position $\vec{x}$ can be parametrized in terms of the line-of-sight distance ℓ and angular coordinates Ω. The differential flux from a solid angle $\Delta\Omega$ is then

$$\frac{d\Phi}{dE_X} = \frac{1}{4\pi}\int_{\Delta\Omega} d\Omega \int d\ell\, \rho_\chi^2[\vec{x}(\ell,\Omega)] \sum_i \frac{\langle\sigma_i v\rangle}{2m_\chi^2}\,\frac{dN_i}{dE_X}\,, \tag{2.70}$$

with an extra factor of $1/2$ if DM is not its own antiparticle.

Astrophysical uncertainties are usually encapsulated in the so-called J-factor [239],

$$J = \frac{1}{\Delta\Omega}\int d\Omega \int d\ell\, \rho_\chi^2[\vec{x}(\ell,\Omega)]\,, \tag{2.71}$$

such that

$$\frac{d\Phi}{dE_X} = \sum_i \frac{\langle\sigma_i v\rangle}{2m_\chi^2}\,\frac{dN_i}{dE_X} \times \frac{J}{4\pi}\,. \tag{2.72}$$

The larger the J-factor, the more promising the target for indirect detection. Typical values are $J \sim 10^{19-20}\,\mathrm{GeV}^2/\mathrm{cm}^5$ for dwarf galaxies, $J \sim 10^{20}\,\mathrm{GeV}^2/\mathrm{cm}^5$ for Andromeda, and $J \sim 10^{22-25}\,\mathrm{GeV}^2/\mathrm{cm}^5$ for our Galactic Center.

Target selection requires balancing J-factor size with background contamination. Dwarfs are the cleanest systems since they are DM-dominated and contain

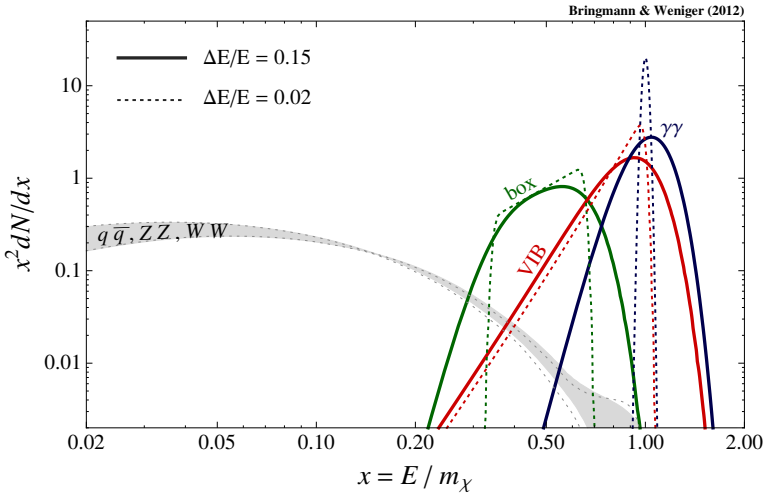

Figure 2.11: Expected photon energy spectra from DM annihilation dN_i/dE. A monochromatic line from direct annihilation into a photon pair is shown in blue, while photons from virtual internal bremsstrahlung (VIB) emission are shown in red. The box-shaped spectrum (green) arises when DM annihilates into a new state that subsequently decays into a photon pair. Secondary photons from annihilation into quarks and gauge bosons are represented by the gray band. Dotted versus solid lines compare detector energy resolutions $\Delta E/E = 0.02$ and 0.15, respectively. Reproduced from Ref. [238].

little baryonic matter. The Galactic Center provides stronger signals due to its proximity and large J-factor, but suffers from large and uncertain astrophysical backgrounds [237].

Status of indirect detection: In fig. 2.12 we summarize current bounds on DM annihilation cross sections from indirect searches. These results typically assume DM annihilates dominantly through a single channel, $\langle \sigma_i v \rangle$, for simplicity. In practice, constraints are model-dependent, since realistic scenarios involve multiple channels. Nevertheless, indirect searches strongly constrain WIMP models with $m_{\rm DM} \lesssim 100$ GeV, as it is difficult to avoid limits across all channels simultaneously.

A particularly powerful probe—often classified as very indirect—is energy injection at recombination. CMB measurements [26] are among the most precise cosmological data and probe relatively low energies, where atomic physics is extremely well understood. The CMB thus constrains both annihilation and decay without strong dependence on DM model details,[20] while being free of the large astrophysical uncertainties related to DM density profiles or particle

[20] The only relevant assumption is whether annihilation is s- or p-wave, since DM velocities at recombination are much smaller than in galaxies (or than at freeze-out).

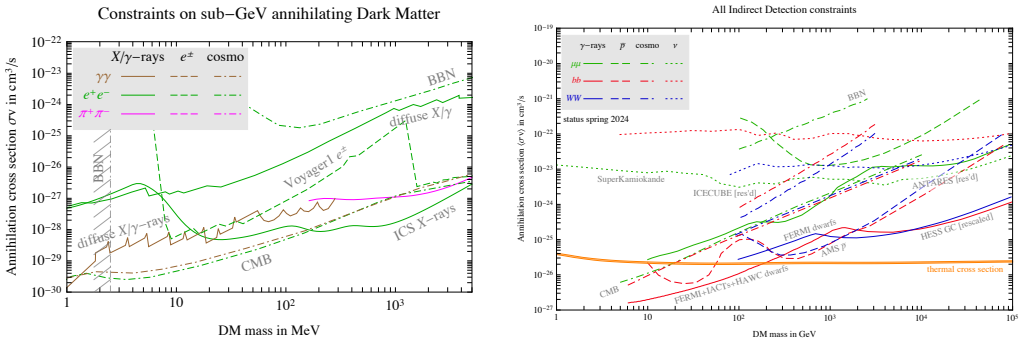

Figure 2.12: Current indirect detection bounds on DM annihilation for sub-GeV DM (left) annihilating into electrons, muons, or pions, and for heavier DM (right) annihilating into muons, b quarks, or W bosons. The orange band shows the thermal relic target for s-wave DM from (2.64). Reproduced from Ref. [6].

propagation. These measurements currently provide the strongest limits on light (s-wave) DM, $m_{\rm DM} \lesssim 100$ MeV.

2.4.2 Direct detection

The fact that DM particles surround normal matter—facilitating structure formation as inferred from galaxy rotation curves and weak lensing—and that they cannot have zero velocities (since such a distribution would be gravitationally unstable), together with the motion of the Earth and the Solar System relative to the Galactocentric rest frame, implies a non-zero DM flux passing through Earth. Assuming DM couples to the SM beyond gravity, one expects some of these particles to scatter off ordinary matter on Earth. Detectors with large numbers of target particles are therefore promising experiments to measure such interactions directly, hence the name *direct detection* (DD). The picture is similar to that of neutrino detectors—unsurprising given that neutrinos themselves contribute a small fraction of DM today.

The Dark Matter flux: A combination of astrophysical data, numerical simulations, and analytical methods yield an estimate of the local DM density $\rho_\chi^\odot$, with a commonly quoted value [6]

$$\rho_\chi^\odot \approx 0.4 \text{ GeV/cm}^3 \,. \tag{2.73}$$

This value carries systematic uncertainties of up to a factor of 2, due to the spread among different methods.

The DM velocity distribution is obtained with relatively better precision—limits vary at the $\sim 60\%$ level around the median [240]—from simulations, but

can be approximated analytically by an isothermal Maxwell–Boltzmann distribution truncated at the Milky Way escape velocity $v_{\rm esc}$ (since faster particles are unbound):[21]

$$f(v) = \begin{cases} Ce^{-v^2/v_0^2}\,, & v < v_{\rm esc}\,, \\ 0\,, & v > v_{\rm esc}\,, \end{cases} \tag{2.74}$$

where C normalizes $\int d^3v f(v) = 1$, and v_0 is the velocity dispersion. Around the solar neighborhood, one may approximate $v_{\rm esc} \approx 544$ km/s [243] and $v_0 \approx 220$ km/s [244].

In the Earth's frame, the distribution is Galilean-boosted by the Earth's velocity $\vec{v}_\oplus$ relative to the halo: $f_\oplus(\vec{v}) = f(\vec{v} + \vec{v}_\oplus)$. This results in an effective "DM wind" with average velocity $\langle v \rangle \equiv v_\chi^\oplus \approx 235$ km/s, modulated annually at the $\sim 7\%$ level due to the Earth's orbit.[22]

From the above results, ne expects a large flux of DM particles at Earth,

$$\phi = n_\chi^\oplus v_\chi^\oplus = \frac{\rho_\chi^\oplus}{m_\chi} v_\chi^\oplus \sim \frac{\rm GeV}{m_\chi}\, 10^7\ {\rm cm}^{-2}{\rm s}^{-1}\,, \tag{2.75}$$

where we approximate $\rho_\chi^\oplus \approx \rho_\chi^\odot$. The exception is ultra-heavy DM, where the flux is suppressed due to the small DM number density.

Kinematics: Such fluxes of DM particles can induce scattering in detectors, producing nuclear or electronic recoils. Nuclear recoils set the strongest constraints for $m_\chi \gtrsim$ few GeV, while electronic recoils are powerful probes for lighter DM masses. The recoil energy E_R is a key observable since it is limited by the detector's energy threshold (set by background noise and finite resolution).

A notable background is due to neutrino-induced recoils, originating from astrophysical neutrino fluxes (especially from the Sun) [246, 247]. This so-called "neutrino fog" (or "neutrino floor" in a more pessimist regard) [248, 249] will eventually slow down the progress of DD searches, potentially turning such experiments into neutrino detectors [250–253]. Hints of this background are already emerging in PandaX-4T [254] and XENONnT [255], with nearly 3σ significance.

For elastic scattering, the kinematics are straightforward: a DM particle of velocity $v \le v_{\rm esc} \ll c$ scatters off a stationary target $T \in \{N, e\}$, giving [105]

$$E_R = \frac{q^2}{2m_T} = \frac{\mu^2}{m_T} v^2 (1 + \cos\theta)\,, \tag{2.76}$$

where q is the momentum transfer, $\mu = m_\chi m_T/(m_\chi + m_T)$ the reduced mass, and θ the scattering angle.

[21] A small fraction of DM particles with $v > v_{\rm esc}$ may exist, e.g. from acceleration in cosmic ray collisions [241] or boosted from the Large Magellanic Cloud [242]. See Ref. [6] for a review.

[22] This annual modulation can help separate signal from background and is the basis for directional DD experiments [245].

The maximum recoil $E_R^{\max}$ occurs for head-on collisions ($\theta = 0$) with $m_T \simeq m_\chi$. For WIMPs of $m_\chi \sim 100$ GeV, typical nuclear recoils are $E_R^{\max} \sim 10$–100 keV: low enough for elastic scattering—smaller than typical nuclear binding energies $E_B \gtrsim 1$ MeV—but high enough to be detected in very-sensitive setups.

Given a detector threshold $E_R^{\min}$, the minimal DM speed for a detectable event is

$$v_{\min} = \sqrt{\frac{m_T E_R^{\min}}{2\mu^2}}\,. \tag{2.77}$$

For xenon detectors ($E_R^{\min} \sim$ keV), this gives $v_{\min} \sim 10^{-4}$, well below the mean DM velocity at Earth ($v_\chi^\oplus \sim 10^{-3}$).

The scattering cross section: The particle physics nature of DM is encoded in the DM–target (nucleus or electron) scattering cross section, $d\sigma_T/dE_R$. Its description is simplified by the non-relativistic nature of the collision, which allows for an expansion of the cross section in powers of the momentum transfer $q = \sqrt{2m_T E_R} \propto v$ (suppressed by the small velocities involved). This framework is known as the *Effective Field Theory of Dark Matter Direct Detection*, see Ref. [256].

After ignoring velocity-suppressed operators, two dominant possibilities remain: interactions that involve the target spin, leading to spin-dependent (SD) cross sections, or interactions that do not involve spin, leading to spin-independent (SI) cross sections. In practice, SI interactions are more common and, in the case of nuclear recoils, typically dominate over SD contributions because of a coherent enhancement proportional to the number of nucleons A (or equivalently to Z for charged nucleons). This enhancement arises since the de Broglie wavelength of DM wave packets, $\lambda \sim 1/(m_\chi v)$, is often larger than the nuclear size, so the DM particle scatters off the entire nucleus coherently.

Nuclear cross sections involve non-trivial nuclear form factors and response functions. Fortunately, these have already been worked out in great detail in the literature up to quadratic order in momentum transfer [256]. For electrons, additional complications may arise from collective excitations and other many-body effects, but these too have been studied extensively [257–259]. As a result, in most cases it is sufficient to compute the fundamental cross section for DM scattering with quarks and electrons (or the corresponding effective theory coefficients) [4, 5, 260], and then use the tabulated nuclear/electronic response functions from the literature to obtain DD constraints.

As an explicit example, consider millicharged DM, which exhibits a Rutherford-like SI cross section (approximating nuclei and electrons as free particles) [261, 262]:

$$\frac{d\sigma_T}{dE_R} = \frac{2\pi\alpha^2\epsilon^2 Z^2}{m_T E_R^2}\, F^2(E_R)\,, \tag{2.78}$$

where α is the electromagnetic fine structure constant, ϵe is the DM electric charge, and $F(E_R)$ denotes the nuclear form factor. The form factor accounts for the loss of coherence at large momentum transfer (i.e. large E_R), and is a decreasing function of the recoil energy.[23] Its standard Helm parameterization is given in Ref. [263, 264].

From eq. (2.78), one clearly sees the characteristic SI coherent enhancement with the nuclear charge Z at small momentum transfer, where the DM couples to the entire nucleus. At larger E_R, the scattering resolves individual nucleons and the enhancement is reduced.In the case of scattering with electrons, one simply sets $Z = 1$ and $F(E_R) = 1$ [261].

The event rate: Having discussed the kinematics and the scattering cross section, we are now in place to introduce the differential event rate for DD experiments, i.e. the number of scattering events per unit time and per unit recoil energy:

$$\frac{dR}{dE_R} = N_T \, n_\chi^\oplus \left\langle v \, \frac{d\sigma_T}{dE_R} \right\rangle , \tag{2.79}$$

where N_T is the number of target particles in the detector (proportional to its size), $n_\chi^\oplus$ is the local DM number density at Earth, and the average is taken over the DM velocity distribution.

Using the relation between recoil energy and scattering angle from eq. (2.76), the differential cross section can be rewritten as

$$\frac{d\sigma_T}{dE_R} = \frac{m_T}{\mu^2 v^2} \frac{d\sigma_T}{d\cos\theta} , \tag{2.80}$$

where m_T is the target particle mass, μ is the reduced mass of the DM–target system, and θ the scattering angle. Substituting this into eq. (2.79), one obtains a more explicit expression:[24]

$$\frac{dR}{dE_R} = (Z') \, M_T \, \frac{\rho_\chi^\oplus}{m_\chi} \frac{1}{\mu^2} \int_{v_{\min}}^{\infty} d^3v \, \frac{f_\oplus(v)}{v} \frac{d\sigma_T}{d\cos\theta} , \tag{2.81}$$

where M_T is the total detector mass, $Z' = 1$ for nuclear recoils and $Z' = Z$ for electronic recoils, $\rho_\chi^\oplus$ is the local DM density, and $f_\oplus(v)$ is the DM velocity distribution in the Earth's frame.

[23] For extremely small momentum transfer, the nuclear charge can itself be screened by atomic electrons, since the target is embedded in an overall neutral medium. This requires introducing an additional atomic form factor $F_A(E_R)$ satisfying $F_A(\infty) = 1$ and $F_A(0) = 0$, see Ref. [261].

[24] If one neglects the small contribution of DM particles not gravitationally bound to the Milky Way, the velocity integral upper limit can be set to $v_{\max} \simeq v_{\rm esc}$. Likewise, the recoil energy upper limit is $E_R^{\max} \simeq E_R(\theta = 0, v = v_{\rm esc})$, which is relevant for computing the total number of events, see below.

For scattering via a relatively heavy mediator ϕ ($m_\phi \gg q$), the cross section becomes approximately isotropic, since angular dependence is suppressed by $v^2/c^2 \sim 10^{-6}$ [135], i.e. $d\sigma_T/d\cos\theta \simeq$ const. In this case, the velocity average reduces effectively to $\langle v^{-1}\rangle$. It is therefore convenient to define the dimensionless function

$$\eta'(v_{\rm min}) = \frac{\rho_\chi^\oplus}{m_\chi}\int_{v_{\rm min}}^{\infty} d^3v\,\frac{f_\oplus(v)}{v}\,, \tag{2.82}$$

which encapsulates all the astrophysical uncertainties related to the local DM distributions.

For light nuclei, the DM de Broglie wavelength is typically larger than the nuclear size, so nuclear form-factor corrections are small [135], and the separation of astrophysical and particle-physics contributions through $\eta'(v_{\rm min})$ is accurate. For heavier nuclei, however, nuclear form factors must be included, which spoil this clean separation but $\eta'(v_{\rm min})$ still provides a useful estimate of astrophysical uncertainties. Additional sources of uncertainty can arise from collective nuclear effects at low momentum transfer, which are particularly relevant for low-energy scattering.

Finally, the total number of expected events in an experiment is obtained by integrating the differential event rate over the accessible recoil energies and multiplying by the observation time t_o:

$$\begin{aligned} N &= t_o\int_{E_R^{\rm min}}^{\infty} dE_R\,\frac{dR}{dE_R} \\ &= (Z')\,\epsilon\,\frac{1}{m_T}\,\frac{\rho_\chi^\oplus}{m_\chi}\int_{v_{\rm min}}^{\infty} d^3v\,v\,f_\oplus(v)\int_{\cos\theta_{\rm max}}^{1} d(\cos\theta)\,\frac{d\sigma_T}{d\cos\theta}\,, \end{aligned} \tag{2.83}$$

where $\epsilon = t_o M_T$ denotes the experimental exposure (often quoted in tonne·year), and

$$\cos\theta_{\rm max} = \frac{m_T E_R^{\rm min}}{\mu^2 v^2} - 1\,, \tag{2.84}$$

with $E_R^{\rm min}$ the detector threshold.

Status of direct detection: In figs. 2.13 and 2.14, we show the current status of bounds from DD experiments on the SI scattering cross section of DM with nucleons and electrons, respectively. It is evident that nuclear recoils provide by far the most sensitive probe of DM interactions. However, for sub-GeV DM masses, electron recoils become the dominant signature thanks to their much lower recoil energy thresholds. Remarkably, electron-recoil searches are already sensitive enough to test the spin-independent thermal target of a variety of sub-GeV DM models [265].

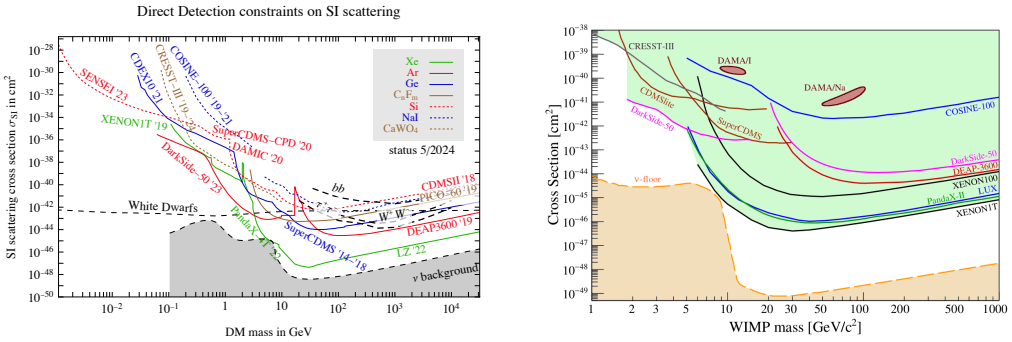

Figure 2.13: Current status of direct detection bounds on the DM–nucleon spin-independent scattering cross section for light (left) [6] and heavy (right) [269] DM masses. Results for white dwarfs denote indirect bounds applicable to efficiently annihilating DM. Note that the latest LUX-ZEPLIN results [267] improve upon XENON1T [268] by over an order of magnitude. Reproduced from Refs. [6, 269].

At higher masses, nuclear recoil experiments achieve extraordinary sensitivities. Current results are so powerful that they can even probe the thermal targets of models with velocity-suppressed cross sections, provided that the DM mass lies above the $\mathcal{O}(10\ \text{GeV})$ scale where these experiments are most effective [89, 266]. The most stringent limits come from large liquid-xenon detectors, with the LUX-ZEPLIN experiment [267] improving upon XENON1T [268] by more than an order of magnitude.

2.4.3 Collider Searches

Collider experiments provide a crucial and complementary approach to probing the nature of DM, offering a controlled, high-energy environment where DM particles and their potential mediators can be produced and studied. This strategy relies on the hypothesis that DM interacts with SM particles with strengths large enough to be detectable—a possibility that arises naturally for thermal relic candidates, allowing their production either directly or via new intermediate states in SM collisions.

Collider searches can be interpreted using different levels of theoretical description [7]:

- **Top-down approaches:** frameworks such as supersymmetry or grand unified theories, where DM candidates emerge as part of a larger structure. These scenarios may predict correlated collider signatures, e.g., cascade decays leading to displaced vertices plus missing energy [3, 271].
- **Bottom-up approaches:** including *Effective Field Theories (EFTs)*, which parametrize DM–SM interactions via higher-dimensional operators (valid

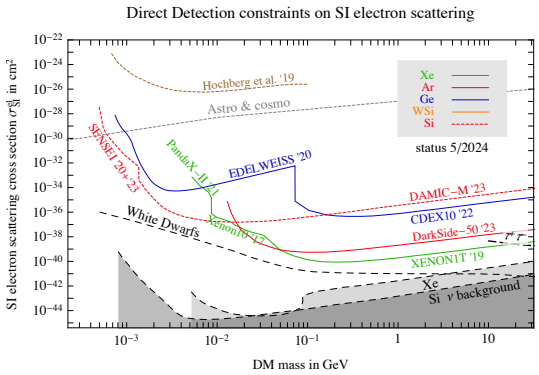

Figure 2.14: Current status of direct detection bounds on the DM–electron spin-independent scattering cross section. Results for white dwarfs denote indirect bounds applicable to efficiently annihilating DM. Note recent improvements from DAMIC-M [270]. Reproduced from Ref. [6].

if the mediator is much heavier than the collider energy), and *simplified models*, which explicitly introduce the relevant mediators when the EFT description breaks down. Both approaches, however, may miss correlations present in full UV-complete theories.

The main experimental challenge of DM searches at colliders arises from the expected properties of DM itself: feebly interacting and stable. As a consequence, DM particles typically leave no direct signature in detectors, revealing themselves only via an imbalance in (transverse) energy—and momentum—commonly referred to as missing energy signatures.

This canonical signature usually involves DM production in association with visible SM particles—often radiated from the initial states or produced in decay cascades (see fig. 2.15). Such searches are collectively referred to as *mono-X* [272], where X denotes the accompanying SM object, typically a photon or a jet [273, 274]. These objects serve both as experimental triggers and as handles to suppress backgrounds. At lepton colliders, fully invisible final states can in principle be probed thanks to the well-defined initial conditions and reduced backgrounds [275]. Hadron colliders, on the other hand, provide access to heavier candidates, in particular weak-scale DM such as WIMPs, due to their much larger center-of-mass energies.

The most basic observable in collider searches is the expected number of signal events N_{events} for a given process. This quantity can be factorized into three pieces: a collider-specific input describing the initial state (the integrated luminosity $\mathcal{L}$), a process-specific input describing the physical interaction (the total production cross section σ_{tot}), and detector-specific efficiencies ϵ_i for each SM final state particle, which account for trigger and detection requirements.

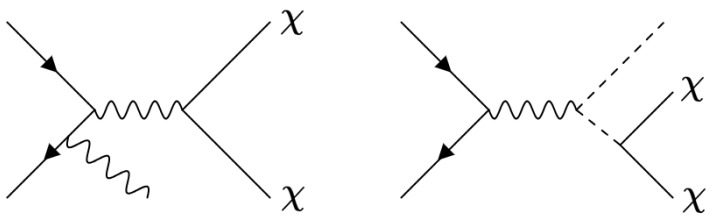

Figure 2.15: Example Feynman diagrams for DM production at colliders in association with a SM particle, leading to mono-X events.

Altogether, one obtains [8]

$$N_{\text{events}} = \sigma_{\text{tot}} \, \mathcal{L} \prod_i \epsilon_i. \tag{2.85}$$

Beyond mono-X channels, several complementary strategies are actively pursued. One notable example is the search for *invisible decays* of SM particles, in particular invisible Higgs decays, which remain relatively weakly constrained [9].[25] Another example are *precision measurements*, which may deviate from SM predictions due to contributions from virtual DM particles or, more typically, their mediators [6].

Additional signatures appear in more elaborate models of DM, such as supersymmetry, GUTs, or simplified models with extra states at collider scales. In these cases, the collider program expands from searching for DM directly to also looking for the associated new particles. Such states are usually unstable and can give striking detector signatures, for instance displaced vertices at colliders [3, 271], or long-lived mediator decays in far detectors at beam-dump facilities [276, 277]. The latter exploit extremely high luminosities and are uniquely sensitive to feebly interacting particles (FIPs) [278]. High-intensity facilities can also probe DM scattering downstream, where DM produced in collisions subsequently interacts with detector material [279, 280].

Broader overviews of collider searches can be found in Refs. [6, 65, 281], which expand on the points summarized here.

An essential consideration in interpreting collider searches is their cosmological relevance. The discovery of new invisible particles at colliders would not automatically imply that they constitute the DM dominating the Universe's matter density. Collider measurements guarantee stability only on detector timescales, $\tau \gtrsim 10^{-7}\,\text{s}$, whereas cosmological DM must survive for $\gtrsim 10^{17}\,\text{s}$ [67]. Moreover, the observed particle might represent only a subdominant DM component. Establishing a cosmological role requires complementary confirmation from DD and ID searches, ensuring consistency of the mass, couplings, and relic abundance across all probes [6]. Exceptions arise for highly predictive candidates

[25] Searches for invisible decays are sometimes grouped together with mono-X signatures.

(such as thermal relics), for which the relic abundance can be directly calculated and compared to the total DM density.[26]

Status of collider searches: The breadth of search strategies and observables, together with the strong model dependence of their predictions, makes it difficult to summarize collider searches with a single general status.

The EFT approach offers the greatest generality, and in principle one could present limits on the Wilson coefficients of DM–SM operators. However, degeneracies among coefficients typically force additional assumptions, complicating the picture—an issue already familiar from the SMEFT program [282, 283]. For comprehensive discussions of EFT interpretations and their current status, see Refs. [284–288].

For top-down models, the collider status must be evaluated in the context of each specific extension of the SM. Two of the most studied examples are supersymmetry—see Refs. [289–291] for reviews—and grand unified theories—see Refs. [292, 293].

Simplified models, though less predictive, are widely used as benchmarks and also span a wide variety of frameworks [294–298]. Nevertheless, when restricted to minimal DM models with both DM and mediators being SM singlets, only three (or four, if including operators suppressed by a single power of a heavy scale) distinct mediator possibilities remain. Since this is the framework adopted in this thesis, we will focus in the next section on these mediators—often referred to as *portals*—and review their collider status specifically in the scenarios explored later in this work.

2.5 Dark sectors and Standard Model portals

Over the past few decades, there has been a remarkable theoretical and experimental effort to explore new physics at the TeV scale, culminating in the LHC program and the design of future high-energy colliders. However, the absence of direct evidence for physics beyond the SM in these searches (as well as in direct and indirect DM searches) has motivated a shift of attention toward *light new physics* at sub-electroweak scales [299, 300]. This direction is further supported by the large variety of existing detectors already capable of probing such light scales—including electron and proton beam fixed-target experiments, e^+e^- colliders (meson factories), and even dedicated experiments at the LHC—together with a diverse set of search strategies. These strategies range from bump-hunt searches for promptly decaying resonances, to displaced-vertex and long-lived

[26] This is not a definitive proof, however, since modifications to the standard cosmological history could still alter the relic abundance.

particle searches, and to missing (transverse) energy and momentum signatures in both collisions and rare decays [301].

If such light particles exist, they must be neutral under SM gauge interactions. Otherwise, they would already have been detected in earlier experiments (recall that even neutrinos were observed decades ago).[27] The only apparent loophole would be particles carrying a tiny fractional electric charge, but such scenarios are usually disfavored since they violate the empirical law of charge quantization and clash with expectations from Grand Unification. Thus, the most natural setup for light new physics consists of states that are singlets under the SM gauge group and interact only via new mediators with feeble couplings to the SM—see fig. 2.16. These frameworks are commonly referred to as *dark sectors* or *hidden sectors*. Their suppressed interactions allow them to evade current collider limits while remaining theoretically and cosmologically well-motivated [300].

Dark sector models are compelling for several reasons. They can address some of the deepest open questions in physics, including the nature of DM, the origin of neutrino masses, the baryon asymmetry of the Universe, the hierarchy problem, and the strong CP problem [301]. They are also valuable frameworks for explaining various experimental anomalies [301]. Furthermore, hidden sectors can arise naturally from the compactification of supergravity or superstring theories, or, in the case of new (pseudo-)scalars, as pseudo–Nambu-Goldstone bosons of spontaneously broken symmetries at high scales [312, 313].[28] Within the Swampland program, weakly interacting dark sectors have even been interpreted as a natural consequence of the smallness of the observed dark energy [315]. See Refs. [301, 313, 316] for further motivation and comprehensive reviews of the dark sector framework.

This naturally raises the question: how can such hidden sectors couple consistently to the SM in a way that yields testable predictions?

One possibility is that the mediator itself directly couples to the SM, being the carrier of a new gauge force under which both SM and dark sector particles are charged. In the Abelian case, anomaly cancellation requirements (without invoking fine-tuned cancellations between SM and dark charges) restrict the options to just three flavor-dependent symmetries which can at the same time result in viable CKM matrices [317]: $U(1)_{L_\mu - L_e}$, $U(1)_{L_e - L_\tau}$, and $U(1)_{L_\mu - L_\tau}$.[29] Such scenarios are commonly studied when the mediator is heavy enough to avoid severe limits from searches for long-range forces [318, 319]; see Ref. [317] for a review. Non-Abelian mediators, by contrast, require embedding SM fermions

[27] Ultralight particles with sizable SM interactions would in addition be strongly constrained by measurements of N_{eff}.

[28] Non-Abelian hidden forces provide yet another class of examples, notably in Hidden Valley scenarios [314].

[29] If right-handed neutrinos are included, $U(1)_{B-L}$ also becomes anomaly-free and viable.

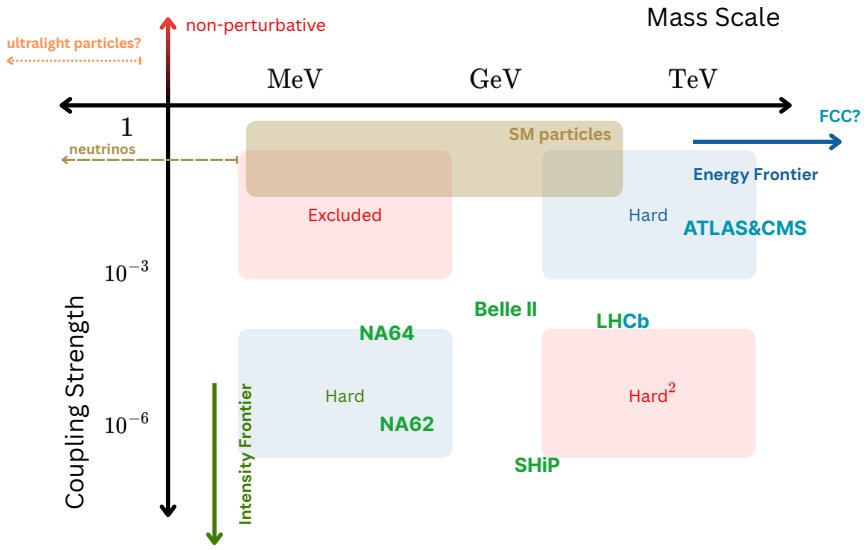

Figure 2.16: Schematic parameter space of new physics in the plane of particle mass versus coupling to the SM. The *Energy Frontier* [302] targets heavy new particles with $\mathcal{O}(1)$ couplings, requiring extremely high-energy colliders such as the LHC or the future FCC [303] (we show as examples the current detectors LHCb [304], CMS [305], and ATLAS [306]). The *Intensity Frontier* [230] focuses on lighter new particles with tiny couplings, where extremely high statistics are needed to overcome the feeble interaction strengths (examples include Belle II [91], NA62 [307], NA64 [308], and SHiP [309]). Precision measurements of SM properties probe both frontiers and can also be sensitive to ultralight states [310], forming what is sometimes called the *Precision Frontier* [311].

into new multiplets [320, 321], and must avoid confining SM states into composite objects, making such models considerably less minimal. This complexity likely explains their rarity in the light new physics literature.

A second, and more minimal, approach assumes that the SM and the dark sector do not share any new gauge force (or at least not one mediated by light particles). In this case, the mediator itself belongs to the dark sector, and interactions between the SM and hidden sector must proceed through specific interaction channels known as *portals*. This approach is by far the most common in the literature [322] and will be the focus of the following discussion.

Portals to the dark sector: A remarkable feature of the SM is that, given its gauge symmetries and field content, only three gauge- and Lorentz-invariant terms built solely from SM fields exist with mass dimension smaller than four:

$$H^\dagger H\,, \qquad B^{\mu\nu}\,, \qquad \text{and} \qquad \bar{L}_i \tilde{H} + \text{h.c.}\,, \tag{2.86}$$

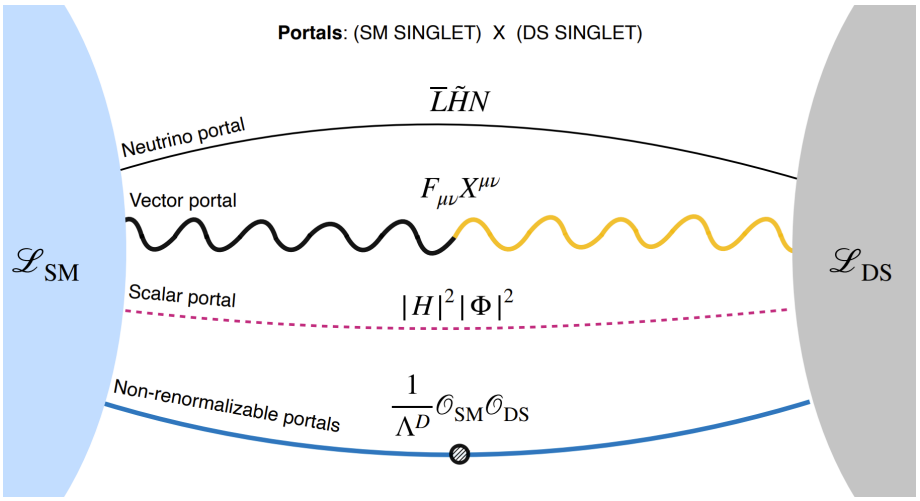

Figure 2.17: Schematic illustration of scenarios in which the Standard Model (SM) is connected to a dark sector (DS) through renormalizable or non-renormalizable portal interactions. Reproduced from Ref. [324].

where $\tilde{H}_a = \epsilon_{ab}H_b^*$ [323] with H the Higgs field and ϵ the Levi-Civita symbol, $B^{\mu\nu}$ denotes the field-strength tensor of the hypercharge gauge boson B, and L_i (with $i \in \{e, \mu, \tau\}$) the SM lepton doublets.

This implies that, in extensions of the SM featuring a dark sector where all new particles are singlets under the SM gauge group, the only renormalizable interactions connecting the SM and the dark sector can be built from one of the operators in eq. (2.86). These three possibilities are known as the *minimal portal models* (or *renormalizable portals*). They are usually classified according to the type of mediator they introduce: the **scalar portal**, associated with $H^\dagger H$; the **vector portal**, associated with $B^{\mu\nu}$; and the **fermionic (or neutrino) portal**, associated with $\bar{L}_i H$.

A schematic illustration of these possibilities is shown in fig. 2.17.

In addition to these three renormalizable portals, a fourth, relatively minimal option is widely studied: the **axion(-like) portal**. This case involves operators suppressed by a single power of a high scale $f_a \gg v$, i.e. dimension-five operators. The mediator is a gauge-singlet pseudoscalar a, usually called an *axion* or axion-like particle (ALP), which couples derivatively to the SM. These couplings reflect an approximate shift symmetry, $a(x) \to a(x) + \text{const}$, broken only softly by a bare mass term $m_{a,0}^2$ [325]. ALPs naturally arise as pseudo–Nambu-Goldstone bosons of spontaneously broken global symmetries, or as remnants of the compactification of higher-dimensional gauge fields, and can thus be much lighter than the fundamental scale f_a that generates them [301]. The specific realization of the QCD axion remains especially compelling, since it simultaneously solves the strong CP problem and provides a natural DM candidate [34].

The portal interactions in eq. (2.86), as well as the ALP portal, imply that the mediators themselves are generally unstable, making them promising targets for collider experiments. Indeed, extensive theoretical and experimental work exists on collider searches for each of these portals [322]. In what follows, we revisit the definition of each portal model, discuss their essential theoretical features, and summarize the phenomenology and current experimental status most relevant for this thesis. A more detailed discussion can be found in the comprehensive review of Ref. [301] and references therein.

The framework outlined here—DM particles residing in a hidden sector, interacting with the SM via portals, and accessible to detection across different search strategies—provides the foundation for the (not-so-)inelastic DM model that will be explored in the remainder of this thesis.

2.5.1 The scalar portal

The most minimal realization of a portal involves a new SM-singlet real scalar field h', commonly referred to as the *dark Higgs*. The most general scalar potential for the SM extended by h' can be written as [326]

$$\begin{aligned} V_{\mp}(h', H) = &- \mu_H^2 H^\dagger H + \lambda_H (H^\dagger H)^2 \mp \frac{\mu_{h'}^2}{2} h'^2 + \frac{\lambda_{h'}}{4} h'^4 + \frac{\lambda}{2} h'^2 H^\dagger H \\ &+ \frac{\mu_1^3}{\sqrt{2}} h' + \frac{\mu_3}{2\sqrt{2}} h'^3 + \frac{\mu}{\sqrt{2}} h' H^\dagger H \,, \end{aligned} \tag{2.87}$$

where H is the SM Higgs doublet, and the choice of sign in front of the h'^2 term determines whether h' develops a vacuum expectation value (vev)—at least at tree-level.

Usually, one sets $\mu_1 = \mu_3 = 0$, since these parameters often do not lead to measurable phenomenological consequences. Indeed, $\mu_1 = 0$ if the potential is expanded around a stationary configuration (otherwise $\mu_1 \neq 0$ would imply nontrivial boundary conditions), while μ_3 induces (suppressed) interactions between mediators. Moreover, if a Z_2 symmetry is imposed ($h' \to -h'$) or if a complex scalar H' with a $U(1)'$ symmetry is considered (as will be relevant later in this thesis), then $\mu_1 = \mu_3 = \mu = 0$ automatically. In what follows, we adopt $\mu_1 = \mu_3 = 0$.

The above Lagrangian induces a mass mixing between the new scalar field h' and the SM Higgs H whenever $\mu \neq 0$, or even for $\mu = 0$ if the scalar potential generates a vev for h'. The Lagrangian can be diagonalized by a simple field rotation, yielding the physical mass eigenstates

$$H_1 = \cos\theta\, h + \sin\theta\, \hat{h}' \,, \tag{2.88}$$

$$H_2 = \cos\theta\, \hat{h}' - \sin\theta\, h \,, \tag{2.89}$$

where h is the SM Higgs excitation after electroweak symmetry breaking in the unitary gauge $H = (h + v)/\sqrt{2}$, and, the shifted field is defined as $h' = \hat{h}' + w$ with the dark vev denoted by w ($w = 0$ in the case h' has no vev). For brevity, we will use h' to denote $\hat{h}'$ whenever no confusion arises.

If h' develops a vev, the scalar mixing angle θ is given by

$$\tan 2\theta = \frac{2\mu v + 2\lambda v w}{2\lambda_H v^2 - 2\lambda_{h'} w^2 + \mu v^2/(2w)}\,, \tag{2.90}$$

with minimization conditions of the scalar potential requiring, in particular,[30]

$$\mu_H^2 = \lambda_H v^2 + \frac{1}{2}\lambda w^2 + \mu w\,, \qquad \mu_{h'}^2 = \lambda_{h'} w^2 + \frac{1}{2}\lambda v^2 + \frac{1}{2}\frac{v}{w}\mu v\,. \tag{2.91}$$

If h' has no vev, the mixing angle is instead

$$\tan 2\theta = \frac{4\mu v}{(4\lambda_H - \lambda)v^2 - 2\mu_{h'}^2}\,. \tag{2.92}$$

This mixing parameter θ is commonly referred to as the *scalar mixing angle*.

For further details on the mass eigenvalues after diagonalization, see appendix A of Ref. [330]. In the limit of small mixing, the eigenmasses reduce to the usual SM Higgs mass $m_h = \sqrt{2\lambda_h}\, v$ for H_1, and a similar expression $m_{h'} = \sqrt{2\lambda_{h'}}\, w$ for the new scalar H_2.

From Eqs. (2.88–2.89), one sees that the physical Higgs H_1 inherits interactions with the dark sector suppressed by $\sin\theta$, while the dark scalar H_2 inherits interactions with SM particles suppressed by $-\sin\theta$. Conversely, both retain interactions with their original sectors weighted by $\cos\theta$.

Relevant status: In practice, the scalar portal is often parametrized more simply by the effective Lagrangian [301]

$$\mathcal{L} \supset -\frac{1}{2}\left(\sqrt{2}\,\mu\, h' + \lambda h'^2\right) H^\dagger H\,, \tag{2.93}$$

so that the phenomenology can be described by just two main parameters: the dark Higgs mass $m_{h'}$ and the scalar–Higgs mixing angle θ. In some cases, the role of the quartic coupling λ is also considered, since it enables pair production of dark Higgs bosons [95].

In fig. 2.18, we show the current experimental status of searches for visibly decaying dark Higgs bosons ($m_{h'} \leq 2m_\chi$) in the light mass regime $m_{h'} \lesssim 10$ GeV, together with the partial widths into SM states. For heavier masses, constraints are shown in fig. 2.19.

[30] More generally, minimization and vacuum stability impose additional conditions on the scalar potential parameters. Assuming both initial mass terms are negative ($V_i(H_i) \supset -\mu_i^2|H_i|^2$ with $\mu_i^2 > 0$), one obtains (at tree level): ${\lambda_{h'h}}^2 < 4\lambda_{h'}\lambda_h$, $\lambda_{h'h} + \lambda_{h'} + \lambda_h > 0$, and $\lambda_{h'}, \lambda_h > 0$. For a full discussion see Refs. [327–329].

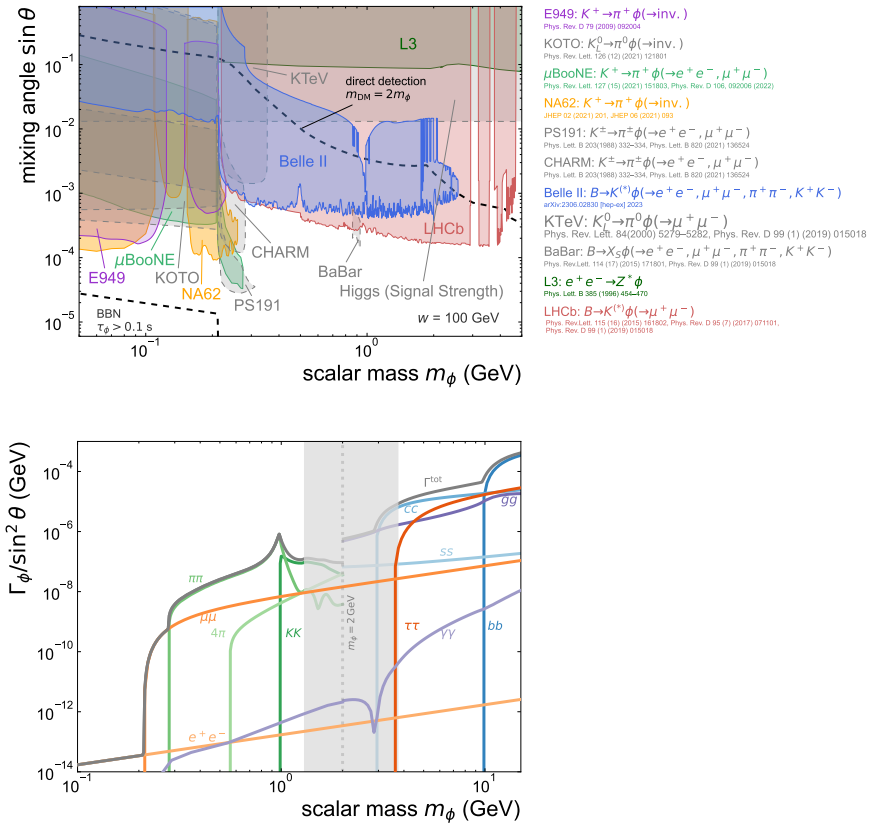

Figure 2.18: Top: Current constraints on the scalar portal for a visibly decaying mediator, shown as upper limits on the scalar mixing angle $\sin\theta$ as a function of the scalar mass $m_{h'}$. **Bottom:** Partial and total decay widths of a dark Higgs boson into SM states, illustrating the strong dependence on $m_{h'}$ as heavier final states with larger Yukawa couplings become accessible. Both plots focus on light dark Higgs bosons. Reproduced from Ref. [331].

Since we will also be interested in invisibly decaying dark Higgs bosons ($m_{h'} > 2m_\chi$), we show the current status for sub-GeV masses in fig. 2.20. For heavier $m_{h'}$, the most stringent bound is simply the SM-like Higgs signal strength, already illustrated in fig. 2.19. For a comprehensive review of the dark Higgs boson, see Ref. [331].

2.5.2 The vector portal

The inclusion of a vector mediator is, in some respects, more straightforward than that of the scalar portal thanks to the gauge symmetry intrinsically associated with any fundamental vector field. Since the only gauge-invariant field strength is that of a $U(1)$ symmetry, the renormalizable spin-1 mediator A'—dubbed the "dark photon" in the sub-GeV regime or "Z'" at higher masses—must be

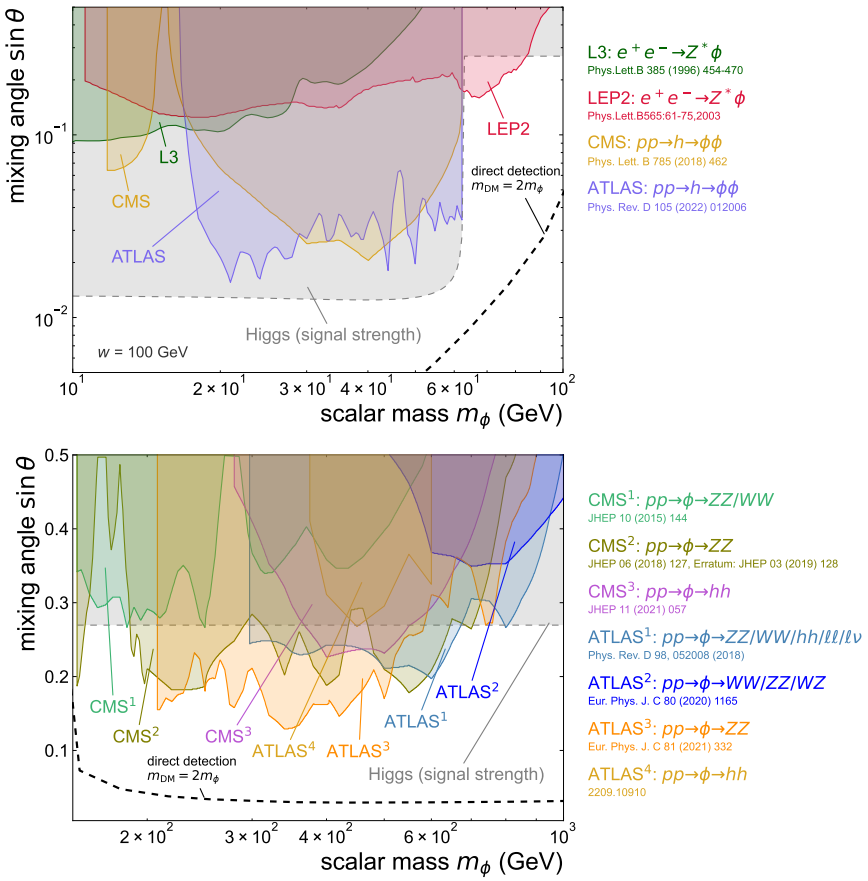

Figure 2.19: Constraints on the scalar portal for a heavy visibly decaying mediator, shown as upper limits on $\sin\theta$ as a function of the scalar mass $m_{h'}$. Reproduced from Ref. [331].

associated with a new $U(1)'$ dark force [332] (multiple $U(1)$ factors can also be introduced). The minimal extension of the SM Lagrangian simply adds the standard kinetic term for A' together with a kinetic mixing between A' and the SM hypercharge gauge boson B [301]:

$$\mathcal{L} \supset -\frac{1}{4}A'^{\mu\nu}A'_{\mu\nu} - \frac{\epsilon}{2\cos\theta_w}A'^{\mu\nu}B_{\mu\nu} - \frac{m_{A'}^2}{2}A'^{\mu}A'_{\mu}\,, \tag{2.94}$$

where θ_w is the weak mixing angle, $A^{\mu\nu}$ is the field-strength tensor of the new vector boson, and the parameter ϵ is referred to as the *kinetic mixing*.

In eq. (2.94), we have also included a possible mass term for A', which can arise from the Stueckelberg mechanism [333] in the most minimal case, or from spontaneous breaking of $U(1)'$ in more elaborate dark sectors. If the dark photon is massless, one can always redefine the vecotr fields such that a vector field is completely decoupled and another behaves exactly like the SM photon—such

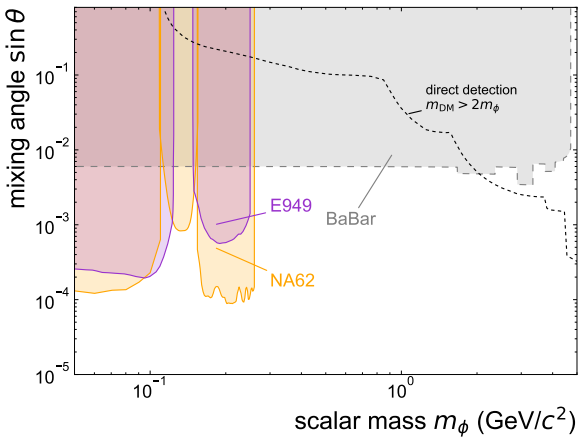

Figure 2.20: Constraints on the scalar portal for an invisibly decaying mediator, shown as upper limits on $\sin\theta$ as a function of the scalar mass $m_{h'}$. Reproduced from Ref. [331].

that A' has no physical implications—provided no particles charged under the new $U(1)'$ exist [334, 335]. Even if such particles exist, a massless dark photon is strongly constrained: it would mediate long-range forces [318, 336, 337], possibly allow for DM bound state formation [338, 339], and contribute new relativistic degrees of freedom in the early universe [340], all of which are tightly bounded by data. For this reason, in the remainder of this thesis we will restrict to the case $m_{A'} \neq 0$.[31]

The Lagrangian in eq. (2.94) induces kinetic mixing of A' with both the photon and the Z boson, requiring a diagonalization to obtain the physical propagating fields. Neglecting $\mathcal{O}(\epsilon^2)$ terms, this can be achieved by the following field redefinitions:

$$A^\mu \to A^\mu = \hat{A}^\mu - \epsilon \hat{A}'^\mu \,, \tag{2.95}$$

$$Z^\mu \to Z^\mu = \hat{Z}^\mu + \frac{m_{A'}^2}{m_{A'}^2 - m_Z^2} \epsilon \tan\theta_w \, \hat{A}'^\mu \equiv \hat{Z}^\mu + \epsilon_{A'} \hat{A}'^\mu \,, \tag{2.96}$$

$$A'^\mu \to A'^\mu = \hat{A}'^\mu + \frac{m_Z^2}{m_Z^2 - m_{A'}^2} \epsilon \tan\theta_w \, \hat{Z}^\mu \equiv \hat{A}'^\mu - \epsilon_Z \hat{Z}^\mu \,, \tag{2.97}$$

where the hats denote physical fields. Here we have assumed no near-degeneracy between the new vector boson and the SM Z boson, i.e. $|m_Z/(m_Z - m_{A'})| < 1$. A full diagonalization keeping all powers of ϵ can be found in Refs. [341, 342].

From these transformations we see that the physical mediator $\hat{A}'$ couples to SM particles with photon-like couplings suppressed by ϵ, and with Z-like couplings suppressed by $\epsilon_{A'}$. Conversely, the Z boson inherits suppressed couplings

[31] In addition, DM freeze-out would proceed dominantly into dark photons, thereby greatly reducing the predictive power of the scenario.

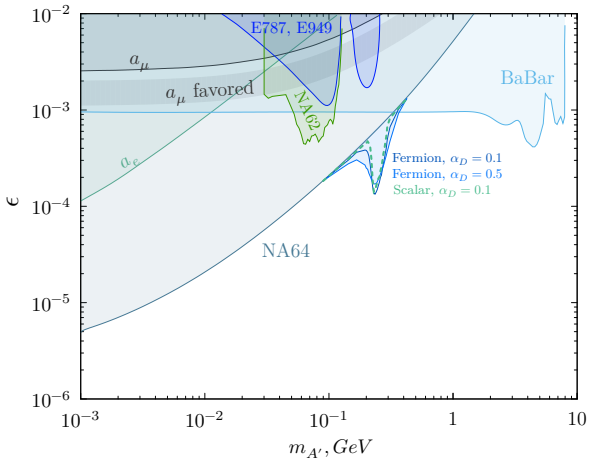

Figure 2.21: Current constraints on the vector portal for an invisibly decaying mediator, presented as upper limits on the kinetic mixing ϵ as a function of the mediator mass $m_{A'}$. The figure focuses on the dark photon case $m_{A'} \lesssim 10$ GeV. Reproduced from Ref. [344].

to dark-sector states proportional to ϵ_Z. Importantly, dark-sector particles remain neutral under electromagnetism and do not couple to the physical photon $\hat{A}$.

In the limit $m_{A'} \ll m_Z$, the Z–A' mixing is negligible ($\epsilon_{A'}, \epsilon_Z \ll \epsilon$), and only the photon mixing remains relevant. In this case, all SM particles appear to be charged under the new $U(1)'$ with effective millicharges $Q' = -\epsilon Q$, where Q is the electromagnetic charge. This is precisely the scenario typically referred to as the "dark photon."

Relevant status: The phenomenology of the vector portal is essentially governed by two parameters: the dark photon (Z') mass $m_{A'}$ and the kinetic mixing ϵ. This is in contrast to the scalar portal, which typically involves additional couplings. If new particles are charged under $U(1)'$, the dark gauge coupling e' and the corresponding charges and masses may also be considered as relevant parameters.[32]

In fig. 2.21, we show the current status of searches for invisibly decaying dark photons ($m_{A'} > 2m_\chi$) in the light-mass regime, $m_{A'} \lesssim 10$ GeV. For a comprehensive review of dark photon phenomenology and searches, see Ref. [343].

[32] If only a single new $U(1)'$-charged particle exists, its charge can be absorbed into the definition of e'.

2.5.3 The fermionic portal

For completeness, we briefly describe the fermionic portal, also known as the neutrino portal. This portal introduces a gauge-singlet spin-1/2 fermion, commonly referred to as a *heavy neutral lepton (HNL)* or *sterile neutrino* (ν_s). We denote it here as a right-handed fermion N, which couples to the SM lepton doublets L_i and the Higgs doublet H via Yukawa interactions [301, 345]:

$$\mathcal{L} \supset -y_i \, \bar{L}_i \tilde{H} N + \text{h.c.}\,. \tag{2.98}$$

Since N is a SM singlet, a Majorana mass term for N is also allowed in the Lagrangian.

After electroweak symmetry breaking, a mixing arises between the HNL and the SM neutrinos, so that HNLs inherit the weak interactions of neutrinos, albeit suppressed by the corresponding mixing angles. A common convention in the literature assumes that the HNL mixes predominantly with one particular neutrino flavor. The phenomenology of the fermionic portal is therefore characterized by the HNL mass m_N and the mixing angle U_i, with $i \in \{e, \mu, \tau\}$ depending on which flavor dominates the mixing.

With the introduction of at least two HNLs, one can generate nonzero neutrino masses through the seesaw mechanism [346, 347].[33] Moreover, light HNLs with $m_N \sim$ keV (commonly referred to as sterile neutrinos) are excellent DM candidates, since such light masses (along with tiny mixings) render ν_s cosmologically stable [349]—although in this case they can no longer explain neutrino masses in a minimal or natural way. However, strong bounds on the mixing angle, together with constraints from BBN on N_{eff}, prevent ν_s from being a thermal relic in standard cosmology. Instead, a freeze-in(-like) mechanism is typically invoked for these DM candidates [6].

Finally, we note that if HNLs were to carry charges under a new gauge symmetry, such charges would need to be carefully aligned with those of the Higgs and/or lepton doublets in order to preserve the fermionic portal coupling. In particular, HNLs cannot be charged under a purely dark sector gauge force. This is precisely the reason why the fermionic portal will not be further explored in this thesis.

[33] For two HNLs, one active neutrino remains massless. At least three HNLs are required for all neutrinos to be massive; in such scenarios, these models can also account for the baryon asymmetry of the Universe via leptogenesis [348].

Chapter 3

The case for (not-so-)inelastic Dark Matter

As discussed in the previous chapter, the dark matter (DM) particle has been extensively studied over the past decades and faces a broad range of experimental constraints; yet, no conclusive evidence of its nature has been found. Looking again at fig. 2.13, we observe that direct detection (DD) experiments place strong bounds on heavy DM candidates with masses above a few GeV, $m_{\rm DM} \gtrsim 10$ GeV [267]. On the other hand, indirect detection (ID) experiments constrain light DM models with masses below a few GeV, $m_{\rm DM} \lesssim 10$ GeV [26, 235, 350] (see fig. 2.12), essentially excluding most DM models based on thermal decoupling (i.e., the freeze-out mechanism), including the traditional WIMP paradigm [351].

Henceforth, we adopt the terms "WIMP" or "WIMP-like" to refer broadly to any DM model whose relic abundance is set via thermal freeze-out. These models typically involve only modest deviations from the original assumptions underlying the WIMP miracle and thus occupy a nearby region within the broader theoretical landscape of DM particle models.

Despite increasing pressure from experimental bounds, the thermal freeze-out mechanism continues to stand out as one of the most compelling scenarios for DM production, due to its independence from initial cosmological conditions and strong predictive power. Consequently, alternative strategies for generating DM via thermal decoupling have been proposed in the literature, and several remain viable to this day [44, 352–355].[1]

Persisting with weak-scale or heavier DM masses: In this case, ID bounds are easily evaded since they are strongest for DM masses below the weak scale [64]. Evading DD bounds requires, however, highly suppressed DM-SM scattering rates, as DD searches depend on DM interactions with nuclei or electrons. Achieving such suppression often leads to fine-tuned or less natural

[1] We focus on scenarios consistent with the standard ΛCDM cosmological model.

models. Some exceptions include fermionic DM with a scalar mediator having a pseudoscalar coupling to DM and a scalar coupling to SM particles [326, 356, 357], and inelastic DM [69, 93], discussed further below. Moreover, as DD experiments approach the so-called neutrino floor, detecting heavy DM with extremely small couplings becomes increasingly challenging [247, 249, 358].

Note also that heavy thermal DM has a natural upper bound on the DM mass of about ~ 100 TeV, imposed by unitarity constraints on the annihilation cross-section [359]—one can build models which evade this bound, but usually at the cost of increased complexity [58].

Exploring light DM masses in the sub-GeV regime: In this mass range, DD sensitivity drops off sharply. To evade ID constraints, models require velocity– or temperature-suppressed annihilation rates, since typical DM velocities at galactic scales ($v_{\rm DM} \lesssim 10^{-3}$ [360]) and relevant CMB temperatures ($T_{\rm dec}^{\rm CMB} \approx 0.3$ eV [361]) are much lower than freeze-out scales ($T_f \gtrsim$ MeV, $v_{\rm DM} \gtrsim 0.1$ [6]). This suppression can arise from p-wave annihilation cross sections ($\langle\sigma v\rangle \propto v^2$) [362], resonant annihilation via fine-tuned masses [363], or kinematically forbidden channels at low temperatures [353, 364–366].

Concrete realizations of p-wave DM include a variety of simple models, such as Majorana or complex scalar DM with vector mediators [265, 355] and scalar-mediated DM [367]—note that recent DD results from DAMIC-M now rule out complex scalar DM across much of its mass range [265].

Another path involves asymmetric DM [44, 69, 352, 353], where some asymmetry between the (co)annihilating particles suppresses late-time (co)annihilations. For example, Dirac fermion DM χ may have a depleted antiparticle $\bar{\chi}$ population by CMB time [368], analogous to the baryon asymmetry in the SM [355, 369]. While the origin of baryon asymmetry remains unknown, many mechanisms have been proposed [370, 371], and similar (or simplified) mechanisms can be constructed for the dark sector. More often, one may consider mechanisms to transfer the matter/anti-matter asymmetry from baryons into DM particles (or vice versa) [372, 373]. These, however, often lack minimality and reduce model predictability [209, 374]. In contrast, inelastic DM models realize an asymmetry in a natural way, as shown later.

Closely related are "co-scattering" or "conversion-driven freeze-out" models [52, 53], where freeze-out occurs through inelastic scattering (e.g., $\psi X \to \chi X$ with $|m_\psi - m_\chi| \ll m_\chi$). This process yields naturally suppressed couplings to the SM, evading both DD and ID constraints [375]. While sometimes absorbed into the inelastic DM framework, these models are often highly model-dependent.

Light DM scenarios have gained attention for their accessibility at collider experiments [352, 376] and potential signatures involving multiple light particles in the dark sector [313, 377–381]. They are also attractive for astrophysics [382]

and cosmology [383], since these kind of probes, so far, are often limited to temperatures well below GeV, for example $T_{\rm supernova} \lesssim 100$ MeV [384, 385] and $T_{\rm BBN} \lesssim 1$ MeV [386]. The exception being cosmic ray particles which achieve energies well above GeV and can be interesting probes for heavy DM candidates [383].

There exists a robust lower bound on the DM mass, $m_{\rm DM} \gtrsim 10$ MeV, for any DM particle thermally coupled to the SM, arising from constraints imposed by BBN and CMB observations. [387, 388].[2] Another relevant constraint is the Lee–Weinberg bound [391], $m_{\rm DM} \gtrsim 1$ GeV, which applies to thermal DM interacting via SM force mediators. However, it can be circumvented by simply introducing new particles that serve as mediators between the dark and visible sectors [355].

Hiding annihilation into "invisible" channels: A third strategy is to impose that DM annihilates only into particles that escape detection, such as new feebly interacting dark sector particles or SM neutrinos [47, 392, 393]. These invisible final states may either be directly produced in the annihilation or arise as decay products of heavier intermediates. Their feeble couplings to the rest of the SM particles naturally suppress both DD and ID signals.

The annihilation into new feebly interacting particles, generally known as *secluded freeze-out* [47], turns DM interactions with the SM irrelevant for the DM production, reducing the model's predictive power. For heavy DM, such weak couplings may prevent thermalization with the SM [394–396], necessitating an ad hoc initial abundance. On the other hand, Light DM in this regime can still maintain independence from initial conditions and remains attractive.

DM annihilation into neutrinos requires non-trivial extensions of the SM, as neutrinos are embedded within electroweak lepton doublets. Consequently, avoiding sizable contributions from associated charged lepton annihilation channels typically necessitates complex model-building [397].

To summarize, thermal freeze-out remains one of the most compelling frameworks for explaining the DM abundance, offering a predictive and testable mechanism that continues to attract significant interest from both the theoretical and experimental communities. As traditional WIMP scenarios face increasingly stringent constraints, models such as inelastic DM present a promising and timely direction for exploration, capable of evading current bounds while preserving the appealing features of thermal production.

[2] If DM only thermalizes with SM neutrinos after their decoupling, the bound can drop to keV scales [389, 390].

3.1 Inelastic Dark Matter

Inelastic dark matter (iDM) represents one of the most minimal and well-motivated frameworks for constructing WIMP-like models that remain viable in light of present-day constraints. Its appeal lies in its emergence across the three main thermal DM approaches discussed earlier, while also offering a rich landscape of phenomenological features. In particular, the inelastic structure enables efficient suppression of both direct and indirect detection signals, thereby evading many of the bounds that strongly disfavor conventional WIMP scenarios. Moreover, iDM finds theoretical support in well-studied UV completions of the SM, remaining particularly relevant in the context of supersymmetric DM models [69, 88, 398–405]. It may even represent the so-called *Last Supersymmetric Electroweak WIMP Standing* [403]. For example, Higgsino-like DM with weak-scale masses $m_{\tilde{H}} \simeq 1.1$ TeV, naturally interacting via weak bosons, remains a viable inelastic DM candidate [400, 404]. Furthermore, iDM models often imply rich dark sectors, making them ideal targets for high-intensity experiments worldwide [230, 406–412].

3.1.1 Inelastic scattering

The term *inelastic dark matter* was first introduced in 2001 by David Tucker-Smith and Neal Weiner, physicists at the University of California (Berkeley) and the University of Washington (Seattle), respectively [69]. However, key features of iDM models—such as co-annihilation and inelastic scattering—had already emerged in earlier supersymmetric frameworks. Notably, in 1997, also at the University of California (Berkeley), Lawrence J. Hall, Takeo Moroi, and Hitoshi Murayama proposed a DM model based on sneutrinos with lepton-number violation, in which they first demonstrated that inelastic scatterings could kinematically evade DD constraints [398]—they have also noted that inelastic scatterings suppress the capture of DM by astrophysical bodies.

Tucker-Smith and Weiner's iDM model was originally motivated by the DAMA anomaly, first reported in 1998 [413]. The anomaly arose from an apparent tension between results from two DD experiments: while the DAMA/NaI experiment [414] observed an annual modulation in its event rate consistent with WIMP DM, the CDMS experiment [415] appeared to exclude the region favored by DAMA/NaI. At the time, alternative explanations such as DM with purely spin-dependent interactions were considered, but these typically ran into conflicts with either ID data or other DD constraints [69, 416].

The iDM proposal posits that DM consists of two states, χ_1 and χ_2, where one is slightly heavier: $m_2 = m_1 + \delta$ with $\delta > 0$, referred to as the *mass splitting*. These states are also denoted χ (or χ_-) for the ground state and χ^* (or χ_+) for the excited state, with $m_{\chi^*} = m_\chi + \delta = (1 + \Delta_m) m_\chi$, where Δ_m is the

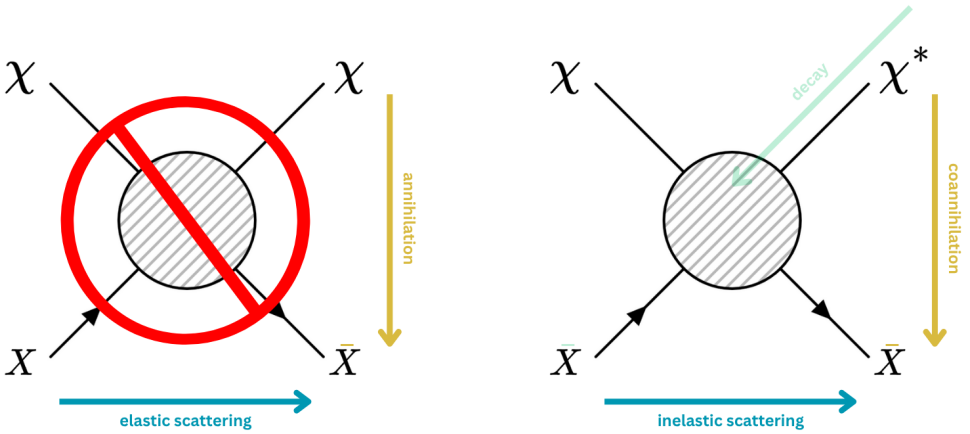

Figure 3.1: Schematic representation of the three main features of inelastic dark matter models and their interplay. Here, X represents a SM particle—typically a quark or electron—as these are the components of target materials in direct detection experiments.

normalized mass splitting commonly used in the literature. The key idea is to forbid, at least at tree level, elastic scattering of ground-state DM off SM particles, $\chi X \not\to \chi X$, while allowing inelastic scattering into the excited state: $\chi X \to \chi^* X$, as illustrated in fig. 3.1. In this setup, a DM particle cannot scatter off a nucleus N unless it has sufficient kinetic energy to excite itself:

$$v_\chi^2 \frac{\mu_{N\chi}}{2} > \delta \,, \tag{3.1}$$

where v_χ is the DM velocity and $\mu_{N\chi} = m_N m_\chi/(m_N + m_\chi)$ is the reduced mass of the nucleus–DM system. For typical galactic velocities $v_\chi \sim 10^{-3}$, this leads to $\Delta_m \gtrsim 10^{-6}$. Alternatively, this condition can be recast in terms of the minimal velocity $v_{\min}$ required to induce a nuclear recoil with energy E_R:

$$v_{\min} = \frac{1}{\sqrt{2 m_N E_R}} \left(\frac{m_N E_R}{\mu_{N\chi}} + \delta \right) , \tag{3.2}$$

which reduces to the standard elastic case (see eq. (2.77)) in the limit $\delta \to 0$. In summary, the inelastic nature of the interaction provides a simple kinematic mechanism to suppress signals in DD experiments.

One way to implement this scenario for a DM particle interacting with the SM via a mediator a is by forbidding diagonal couplings of the form[3]

$$\mathcal{L} \not\supset g_\chi \, a \chi \chi \,, \tag{3.3}$$

while introducing off-diagonal couplings of the type

$$\mathcal{L} \supset g_\chi \, a \chi^* \chi \,. \tag{3.4}$$

[3]The Lagrangian notation is schematic, as the precise form depends on the DM spin, mediator type, and Lorentz structure of the interaction.

Off-diagonal couplings to mediators are among the most common mechanisms used to realize iDM scenarios in the literature (see [3, 70, 71, 73, 417–421] and references therein).

Tucker-Smith and Weiner observed that DAMA/NaI employed iodine ($A = 127$) as a target, while CDMS used the lighter element germanium ($A = 73$). For a DM mass of $m_\chi = 100$ GeV and velocity $v_\chi \approx 220$ km/s (a typical DM velocity for DD), CDMS could probe mass splittings up to ∼11 keV, while DAMA/NaI would be sensitive to splittings as large as ∼15 keV. Thus, a splitting of $\delta \approx 13$ keV would allow both results to be reconciled. Taking into account the velocity distribution in DM halos, the viable window for reconciliation actually widens to $\delta \sim 50$–100 keV [69].

However, the parameter space for iDM as an explanation for the DAMA anomaly has become increasingly constrained by updated results from new DD experiments [422–425]. Furthermore, the COSINE-100 [426] and ANAIS–112 [427] experiments, which use the same target material as DAMA/LIBRA [428] in an effort to reproduce its annual modulation signal,[4] have so far found no evidence for such a modulation. Each experiment independently disfavors the DAMA signal at approximately 3σ, and their combined six-year datasets exclude DAMA at 3.53–4.68σ confidence level [431].

Magnetic iDM [432], which further leveraged the large magnetic moment of iodine to enhance scattering rates, was proposed as an alternative explanation of the DAMA anomaly. However, the absence of expected (albeit weaker) signals in the XENON [433] and CRESST [434] experiments, together with null results from COSINE-100 and ANAIS–112, turn this scenario strongly disfavored as well.

As a result, recent interest in iDM has shifted away from the DAMA anomaly and toward its broader phenomenological implications at colliders, as well as its relevance in astrophysical and cosmological contexts.

It is worth noting that iDM models have also been considered in the context of explaining other anomalies, such as the INTEGRAL 511 keV line [435–437], as well as the excesses reported by ATIC [438] and PAMELA [439], particularly in scenarios involving exciting or decaying DM [401, 402, 440, 441].

3.1.2 Asymmetric dark matter from inelasticity

The same inelastic interaction introduced for the process $\chi X \to \chi^* X$ in DD experiments implies the presence of decay-type processes such as $\chi^* \to \chi X \bar{X}$ in the theory, as illustrated in fig. 3.1. If these decays are not kinematically

[4] The DAMA/LIBRA experiment, a successor to DAMA/NaI at the same facility, confirmed the annual modulation with a significance improved from 6.3σ [429] to 11.8σ, reaching a combined significance of 13.7σ [430].

forbidden ($2m_X < \delta$), the excited state χ^* can decay into the ground state χ and the SM particles X and $\bar{X}$. Loop induced decays into lighter or even massless SM particles are, in general, always possible. However, such processes are typically highly suppressed, often resulting in excited-state lifetimes longer than the age of the universe. Therefore, in most cases where tree-level decays are kinematically forbidden, one considers a two-component DM scenario composed of both χ and χ^*. For models with the off-diagonal coupling introduced in eq. (3.4), if the mediator mass satisfies $m_a < \delta$, the decay $\chi^* \to \chi a$ becomes allowed and typically dominates the χ^* decay width.

With a decaying excited state, it becomes straightforward to generate an asymmetry in the cosmological abundance of the two states. It suffices to ensure that χ^* decays on cosmological timescales, so that its population can be safely neglected in the late universe. For lifetimes shorter than a few hundredths of a second, $\tau_* \lesssim 0.02$ s, the excited state has negligible effects during both BBN and CMB epochs [442].

Another crucial feature of iDM models is *coannihilation* [44].[5] In thermal iDM scenarios, freeze-out is typically dominated by coannihilation processes of the form $\chi\chi^* \to X\bar{X}$, as the inelastic interaction structure naturally suppresses the standard annihilation channel $\chi\chi \to X\bar{X}$. This suppression arises from the off-diagonal nature of the DM–SM coupling, as illustrated in fig. 3.1. However, standard annihilation can dominate DM production if the final states are not SM particles, for instance $\chi\chi \to aa$. Such scenarios fall under the secluded freeze-out paradigm, which, as discussed, lacks a clear thermal target and thus is significantly less predictive. For this reason, most iDM models kinematically forbid annihilation into non-SM final states—for example, by imposing $m_\chi \ll m_a$ in the case of mediator final states—thereby ensuring that DM is produced via coannihilation into SM particles, $\chi\chi^* \to X\bar{X}$.[6]

A notable feature of coannihilation in iDM models is that large mass splittings require exponentially larger DM–SM couplings compared to standard annihilations. This is because, at freeze-out, the number density of the excited state is Boltzmann suppressed relative to the ground state:

$$\Gamma_{\text{coa}} = n_* \langle \sigma v \rangle_{\text{coa}} = (1 + \Delta_m)^{3/2} e^{-\Delta_m x} n_- \langle \sigma v \rangle_{\text{coa}} \,, \tag{3.5}$$

where $x = m_\chi / T$ is the usual dimensionless inverse temperature parameter, and n_-, n_* denote the number densities of the ground and excited states, respectively. In contrast, the standard annihilation rate is given by:

$$\Gamma_{\text{ann}} = n_- \langle \sigma v \rangle_{\text{ann}} \,. \tag{3.6}$$

[5] Here we focus exclusively on thermal production. An alternative is non-thermal production via freeze-in [443–445], where the excited state may remain cosmologically populated, leading to non-trivial dynamics in the late universe.

[6] Other interesting, though less conventional, possibilities involve resonance-enhanced coannihilation through an s-channel mediator, where $m_\chi + m_{\chi^*} \simeq m_a$ [78] or forbidden annihilation channels when $1 \lesssim m_{A'}/m_\chi \lesssim 2$ [446].

Assuming the (co)annihilation cross sections are proportional to the square of the DM–SM coupling, $\langle\sigma v\rangle_i \propto \epsilon_i^2$, and that all other mass parameters are fixed, the ratio becomes:

$$\frac{\langle\sigma v\rangle_{\rm coa}}{\langle\sigma v\rangle_{\rm ann}} = \frac{\epsilon_{\rm coa}^2}{\epsilon_{\rm ann}^2}\,. \tag{3.7}$$

To obtain a similar rate for both processes at freeze-out ($x_f \simeq 20$) $\Gamma_{\rm coa} \approx \Gamma_{\rm ann}$, ensuring a similar DM relic abundance, one must satisfy:[7]

$$\epsilon_{\rm coa} \simeq \frac{e^{10\Delta_m}}{(1+\Delta_m)^{3/4}}\epsilon_{\rm ann}\,. \tag{3.8}$$

For $\Delta_m \sim 1$, this implies $\epsilon_{\rm coa} \sim 10^4\epsilon_{\rm ann}$. Thus, iDM models with $\Delta_m \gtrsim 1$ (i.e., $\delta \gtrsim m_\chi$) generally cannot achieve the observed relic density via freeze-out unless they invoke exponentially large couplings to the SM—values that are either excluded by experimental bounds or violate perturbative unitarity. For an alternative explanation of why iDM scenarios typically require larger couplings, see Section IV of Ref. [70].

One could alternatively consider DM masses exponentially lighter than the weak scale [354]. However, such models are often excluded by combined BBN and CMB observations if thermal equilibrium with the SM is achieved [387, 388].

Combining the fact that DM is produced via coannihilation between χ and χ^* with the instability of χ^* leads to an elegant suppression of ID signals. Since the excited state decays after freeze-out, it is absent at late times, thereby eliminating coannihilations $\chi\chi^* \to X\bar{X}$ during the CMB epoch or in astrophysical environments. In this way, iDM models naturally evade ID constraints by dynamically removing the coannihilation partner from the thermal bath shortly after freeze-out.

3.1.3 Further implications from inelasticity

Although the concept of iDM was originally proposed to explain the DAMA anomaly, it was soon recognized that iDM models have much broader implications. These include modifications to cosmology, such as altered structure formation due to inelastic and dissipative self-interactions [447–451], and to astrophysics, notably the potential to impact the evolution of compact stellar objects [72, 403, 452–455].

Another class of signatures arises from excitation and de-excitation processes—commonly referred to as up- and down-scattering—where transitions between DM states can produce distinctive signals [73, 440, 456–461]. One notable example is *luminous dark matter*, in which a ground state DM particle up-scatters

[7] This relation holds in the absence of s-channel resonances. In resonant cases, one must also account for differing center-of-mass energies between annihilation and coannihilation.

into the excited state within Earth and subsequently decays back to the ground state via photon emission, potentially inside a neutrino or DD detector [456].

In this thesis, however, we focus on the phenomenological implications of iDM at collider experiments. For a detailed account of its cosmological and astrophysical aspects, the reader is referred to the references above. Moreover, these effects are generally irrelevant in the regions of parameter space considered here, and we therefore refrain from discussing them further.

The most striking consequence of iDM for high-energy experiments lies in the unique experimental signatures enabled by the same decays that suppress ID signals. These decays can give rise to multiple displaced vertices and semi-visible signatures at particle colliders, as well as long-lived particle (LLP) candidates suitable for exploration at beam-dump facilities, all within a broad array of experimental strategies [3, 70, 462–465].

Another particularly interesting experimental signature is the so-called *double-bang* (or "double-cascade") topology—analogous to that of ultra-high-energy tau neutrinos [466–468]. In this scenario, the first "bang" results from the up-scattering process $\chi X \to \chi^* X$ via interaction with a SM target, followed by the delayed decay of χ^* back to χ, producing a second SM shower within the detector.

Furthermore, iDM models frequently emerge from extensions of the SM that involve rich dark sectors, often containing multiple new particles and interactions. Owing to the inelastic structure of these models, the associated new states can remain light and thus accessible to a broad array of experimental probes [71, 80, 90, 300, 469, 470]. Altogether, the combination of distinctive experimental signals, theoretical consistency, and compatibility with thermal freeze-out for light DM makes iDM an especially promising framework for discovery at current and future collider experiments.

3.1.4 The case for small mass splittings

A particularly interesting scenario arises when the mass splitting δ is very small, such that tree-level decays of the excited state χ^* are kinematically forbidden. In this regime, DM generally consists of two nearly degenerate components, with χ^* being a metastable state with a lifetime well exceeding the age of the universe, $\tau_* \gg 10^{17}$ s.

It is convenient to define the fraction of DM in the excited state as

$$f_* \equiv \frac{n_*}{n_- + n_*} = \frac{n_*}{n_{\rm DM}}\,, \tag{3.9}$$

where n_* and n_- denote the number densities of the excited and ground states, respectively, and $n_{\rm DM}$ is the total DM number density assuming the DM is entirely composed of χ and χ^*. Although both states are effectively stable, an

asymmetry between their abundances can still arise through processes such as $\chi^* X \to \chi X$ (from inelastic scattering) and $\chi^*\chi^* \to \chi\chi$ (present in models with mediators). Importantly, these processes do not change the total DM abundance.

If these interactions are efficient, they maintain chemical equilibrium between the two states. In this case, the population ratio is given by

$$\xi \equiv \frac{n_*}{n_-} = (1+\Delta_m)^{3/2}\, e^{-\delta/T_\chi}\,, \tag{3.10}$$

where T_χ is the temperature of the dark sector. If the dark sector remains in kinetic equilibrium with the SM or with itself, T_χ reflects the bath temperature. Otherwise, it can often be interpreted as an effective temperature associated with the momentum distribution of the excited state.

From this, the excited state fraction in equilibrium is given by

$$f_*^{\rm eq} = \frac{\xi}{1+\xi} \approx \frac{e^{-\delta/T_\chi}}{1+e^{-\delta/T_\chi}}\,. \tag{3.11}$$

The temperature T_χ can be computed from entropy conservation or, in the absence of kinetic equilibrium, by redshifting particle momenta due to cosmic expansion. Eventually, fraction changing interactions decouple at a temperature $T_\chi^{\rm dec}$ and the excited state fraction freezes out to a constant value:

$$f_*^{\infty} \approx \frac{e^{-\delta/T_\chi^{\rm dec}}}{1+e^{-\delta/T_\chi^{\rm dec}}}\,. \tag{3.12}$$

If $f_*^\infty \ll 1$, a significant asymmetry between χ and χ^* develops, suppressing ID signals. In this case, the DM coannihilation rate is approximately

$$\Gamma_{\rm coann} \approx 2 f_*^\infty n_{\rm DM} \langle\sigma v\rangle_{\rm coann}\,, \tag{3.13}$$

which is suppressed because of the small residual excited state fraction.

Conversely, if a substantial population of excited states remains today, DD constraints become severe. Down-scattering processes in which χ^* transitions to χ can deposit sizable recoil energies $\sim \delta \gg m_\chi v_\chi^2$, producing distinctive "exothermic DM" signals [471]. These signals are strongly constrained by existing DD data, excluding splittings $\delta \gtrsim 200$ eV for $\delta \ll m_\chi$ [73, 75, 419].

Further complications arise if the mass splitting satisfies $\delta \lesssim m_\chi v_\chi^2$. In this regime, up-scattering of ground state particles into the excited state becomes kinematically accessible at DD experiments. In some cases, up-scattering may even restore chemical equilibrium between states in localized astrophysical environments (e.g., galactic centers), reactivating coannihilation channels at late times. This reopens the possibility of DM annihilation into SM particles and brings back the relevance of ID constraints for splittings $\delta \lesssim 10$ eV, as discussed in [419]—see also fig. 3.2.

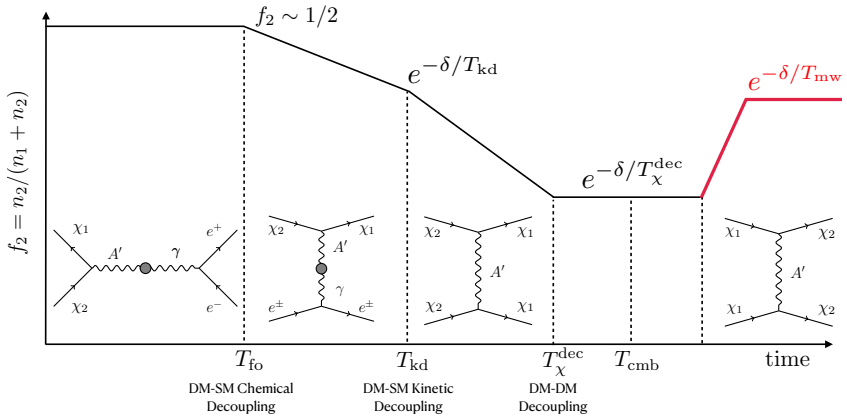

Figure 3.2: Schematic timeline of key events in the cosmological evolution of iDM with tiny mass splittings, $\delta \ll m_\chi$, such that χ^* is metastable ($\chi_1 = \chi, \chi_2 = \chi^*$). For concreteness, we adopt a dark photon mediator A'. Coannihilations $\chi\chi^* \to X\bar{X}$ freeze out at $T_{\rm fo} \sim m_\chi/20 \gg \delta$, initially leaving a symmetric DM population with $f_* \approx 1/2$. Subsequently, χ^* is depleted through DM–SM ($\chi^* X \to \chi X$) and DM–DM ($\chi^*\chi^* \to \chi\chi$) transitions. The dark sector remains in kinetic equilibrium with the SM until decoupling at $T_{\rm kd}$. The final chemical freeze-out occurs at $T_\chi^{\rm dec}$, yielding a suppressed excited state fraction $f_*^\infty \ll 1$. However, for splittings $\delta \lesssim 10$ eV, up-scattering in galaxies, e.g., the Milky Way, may regenerate χ^* with $f_* \sim e^{-\delta/T_{\rm mw}}$, where $T_{\rm mw}$ is an effective DM temperature at the Milky Way. Reproduced from Ref. [419].

In summary, the small mass splitting regime of iDM can still generate a cosmological asymmetry that suppresses ID signals while potentially evading DD constraints. However, the dynamics are significantly more intricate and model-dependent, requiring detailed treatment of freeze-out, kinetic decoupling, and local astrophysical conditions. We further discuss some elements of this scenario in section 3.1.6 in the context of a specific realization: pseudo-Dirac inelastic Dark Matter.

3.1.5 Pseudo-Dirac Dark Matter

Although iDM can consistently arise within well-motivated BSM frameworks—such as supersymmetric theories [398–400, 404, 472] or minimal extensions that gauge global SM symmetries like $U(1)_B$ [420, 473]—its appeal as a WIMP-like DM candidate has motivated the construction of a wide range of simplified models in the literature, many of which are of significant phenomenological interest.

Among these, models in which DM is a *pseudo-Dirac* fermion—i.e., a Dirac fermion split into two nearly degenerate Majorana mass eigenstates—represent one of the simplest and most elegant realizations of the iDM concept [70, 87, 88]. These models are not only minimal but can also be embedded within UV-

complete frameworks in a straightforward manner [418]. In particular, the inelastic nature of the interaction emerges naturally when a dark electromagnetic force, $U'(1)$, is introduced in the hidden sector [88, 470, 474]. The mass splitting between the Majorana states can then arise via a dark Higgs mechanism, which simultaneously breaks the $U'(1)$ symmetry and generates a mass for the associated dark photon [418].

Other iDM realizations often require larger gauge sectors [475], non-renormalizable portal interactions with the SM [417, 432, 465, 476, 477], or the introduction of multiple new fields [477–479], typically leading to an increase in model complexity and parameter space, as well as challenges in achieving full UV completeness.

A scalar analogue of the pseudo-Dirac setup can be constructed by introducing a real scalar mass term that breaks the $U'(1)$ gauge symmetry [70, 470]. However, generating this term through a minimal dark Higgs mechanism, as in the fermionic case, significantly complicates the scalar model. Unlike the fermionic scenario, which involves a single Yukawa interaction, the scalar case allows for multiple interaction terms—quadratic, trilinear, and quartic couplings with the dark Higgs. Furthermore, when the dark Higgs mass is not much heavier than the rest of the dark sector—which is often the case in models with sizable gauge couplings—all these interactions can become relevant for DM production and self-interactions, rendering the scalar iDM framework less minimal and more computationally involved.

Additional motivations for the fermionic scenario include the fact that fermion masses are radiatively stable, thus avoiding the hierarchy problem typically associated with scalar masses. Achieving radiative stability for bosonic masses would generally require either spin-1 particles (or scalars embedded within more complex models). However, to date, no viable vector iDM models have been proposed in the literature—to the best of the author's knowledge. Moreover, by analogy with the SM, where fermions constitute the matter content and bosons act as force carriers or symmetry-breaking agents, fermionic DM may appear to be a more natural candidate for accounting for the bulk of matter in the universe.

3.1.6 The status of pseudo-Dirac and Majorana Dark Matter

In this section, we briefly review the current status of dark photon portal models involving pseudo-Dirac inelastic DM (piDM) and Majorana DM (mDM). Both serve as viable sub-GeV, WIMP-like fermionic DM candidates.[8] These models

[8] Dirac DM scenarios typically require fine-tuning of the dark sector masses to enable resonance-enhanced annihilation cross sections, or the introduction of an asymmetry between DM and anti-DM to evade stringent CMB bounds [355]. For this reason, we do not discuss Dirac DM further.

for DM are among the most studied in collider and beam-dump experiments due to their predictive thermal relic targets, which remain within reach of current and upcoming facilities [90, 265, 279, 322, 408, 480–485].

In what follows, we introduce simplified interaction Lagrangians for both DM models:

- **Pseudo-Dirac inelastic Dark Matter:**

  For piDM, the interaction Lagrangian between the ground state $\chi = \chi^c$ and the excited state $\chi^* = \chi^{*c}$ mediated by a dark photon A' is given by

$$\mathcal{L}_I^{\text{iDM}} \supset \frac{i}{2} e' A'_\mu \bar{\chi} \gamma^\mu \chi^* - \frac{i}{2} e' A'_\mu \bar{\chi}^* \gamma^\mu \chi \,, \tag{3.14}$$

  where e' is the dark electromagnetic coupling ($\alpha' \equiv e'^2/4\pi$).

- **Majorana Dark Matter:**

  For mDM, the DM $\chi = \chi^c$ interaction with the dark photon A' is axial, and the simplified Lagrangian is

$$\mathcal{L}_I^{\text{mDM}} \supset \frac{1}{2} e' A'_\mu \bar{\chi} \gamma^5 \gamma^\mu \chi \,. \tag{3.15}$$

In both cases, the dark photon A' interacts with the SM via kinetic mixing:

$$\mathcal{L} \supset -\frac{1}{2} \frac{\epsilon}{\cos\theta_w} B^{\mu\nu} A'_{\mu\nu} \,, \tag{3.16}$$

where ϵ is the kinetic mixing parameter, θ_w is the weak mixing angle, and $B_{\mu\nu}$ ($A'_{\mu\nu}$) denotes the hypercharge (dark photon) field strength.

A useful dimensionless parameter widely used in the literature is

$$y \equiv \epsilon^2 \alpha' \left(\frac{m_\chi}{m_{A'}} \right)^4 . \tag{3.17}$$

In the limit $m_{A'} \gg m_\chi, m_{\chi^*}$ and for $\delta \ll m_\chi$, the relic density depends solely on this variable [3].

In the pseudo-Dirac limit,

$$\delta \equiv m_{\chi^*} - m_\chi = \Delta_m m_\chi \ll m_\chi \,, \tag{3.18}$$

the excited state χ^* is typically stable at collider scales, but may still decay rapidly enough to avoid cosmological constraints. Thus, the searches for decays of LLPs are often not considered in the analysis [90, 344, 485], as illustrated in fig. 3.3. This limit is technically natural, as $\delta \to 0$ restores a $U(1)$ symmetry in

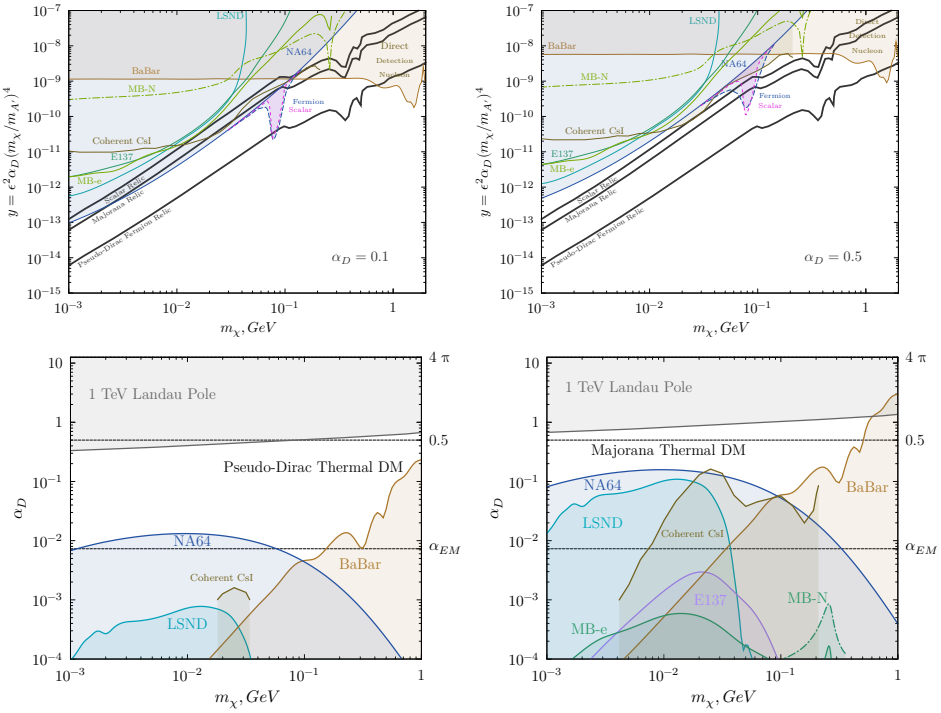

Figure 3.3: Top: exclusion limits in the (m_χ, y) plane for $\alpha' = 0.1$ (left) and $\alpha' = 0.5$ (right), assuming $m_{A'} = 3m_\chi$. **Bottom:** same limits in the (m_χ, α') plane for pseudo-Dirac (left) and Majorana (right) DM. Shaded regions show excluded parameter space from NA64 [92],LSND [279, 486], E137 [483], MiniBooNE [487], BaBar [488], COHERENT [489], and XENON10 [490], obtained in Refs.[316, 344, 376, 491–493]. Thermal relic targets for different DM models are also shown. Reproduced from Ref. [344].

the dark sector. We first focus on this regime, where piDM is often simply referred as pseudo-Dirac DM, in comparison with the mDM case, before discussing scenarios with larger mass splittings, which yield a richer phenomenology.

As shown in fig. 3.3, the thermal targets for both models survive current constraints for $m_{A'} = 3m_\chi$. However, Majorana DM is excluded for $\alpha' \lesssim 0.1$, whereas pseudo-Dirac DM remains viable down to $\alpha' \sim \alpha \approx 1/137$ (the SM electromagnetic fine-structure constant). The heavy mediator regime, $m_{A'} \gg m_\chi$, is essentially excluded for both models, as the ϵ thermal target scales roughly as $m_{A'}^2$ [90]. This motivates the frequent use of $m_{A'} = 3m_\chi$ as a benchmark.

With mediator masses and couplings pushed toward resonant and/or non-perturbative regimes, these models are expected to be comprehensively tested in the sub-GeV mass range by current and upcoming experiments such as NA64 [344], LDMX [90], and Belle II [3]; see Refs. [3, 89, 90, 344, 493] and references therein.

A similar picture holds for DM masses above the GeV scale; however, ex-

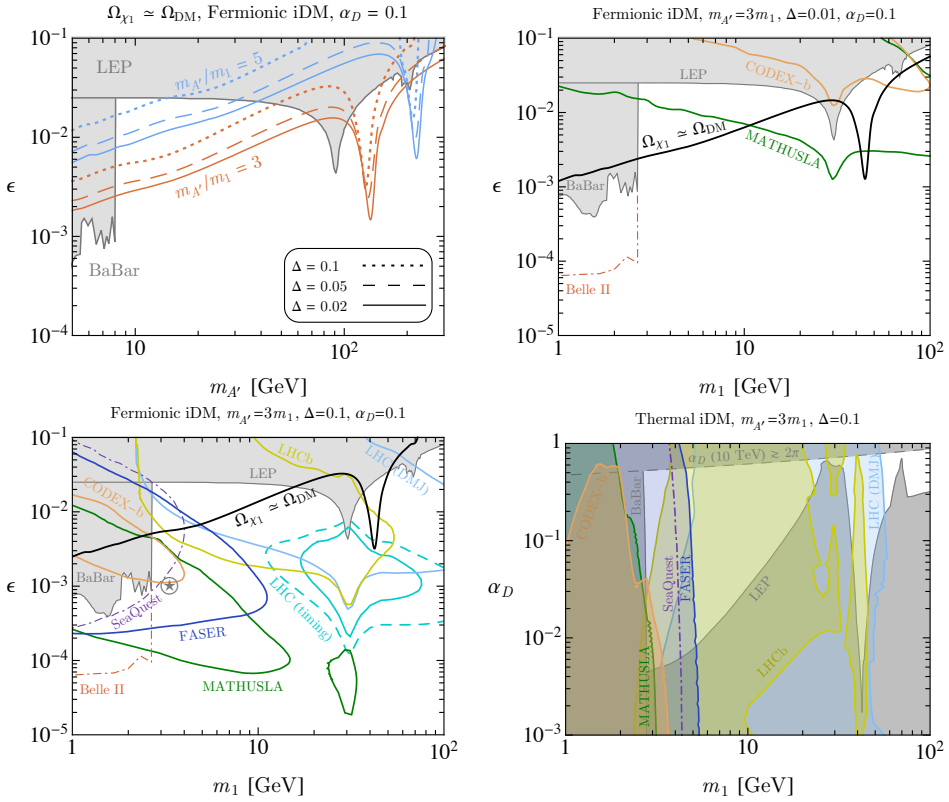

Figure 3.4: Collider and beam-dump sensitivities to piDM in various planes of (m_χ, ϵ) and (m_χ, α') for different mass splittings. The current most stringent limits are from BaBar [488, 496] and LEP [494, 495]. Projected sensitivities are shown for ATLAS [70, 306], CMS [70, 305, 497], LHCb [498–500], CODEX-b [501], FASER [502], MATHUSLA [503], Belle II [91] and SeaQuest [280]. Thermal relic targets are also shown. Recent CMS results [81] strengthen the exclusion limits on long-lived excited states for $m_\chi \gtrsim 3$ GeV. Reproduced from Ref. [71].

ploring the remaining viable parameter space in this regime will require future high-energy colliders capable of surpassing current limits from electroweak precision measurements at LEP [494, 495], as illustrated in the top-left panel of fig. 3.4.

Out of the pseudo-Dirac limit, the excited state χ^* may decay at collider scales, thereby enabling constraints from LLP searches. A wide range of current and proposed experimental facilities are sensitive to this regime, as shown in figs. 3.4 and 3.5.[9] The large number of detectors sensitive to piDM has significantly strengthened the interest in this type of models. As seen in the plots,

[9] Other experiments with relevant sensitivity include NA62 [504], SeaQuest [280], BDX [505], MiniBooNE [506], ANUBIS [507], and FACET [508]. See also [89, 90, 470] for additional coverage.

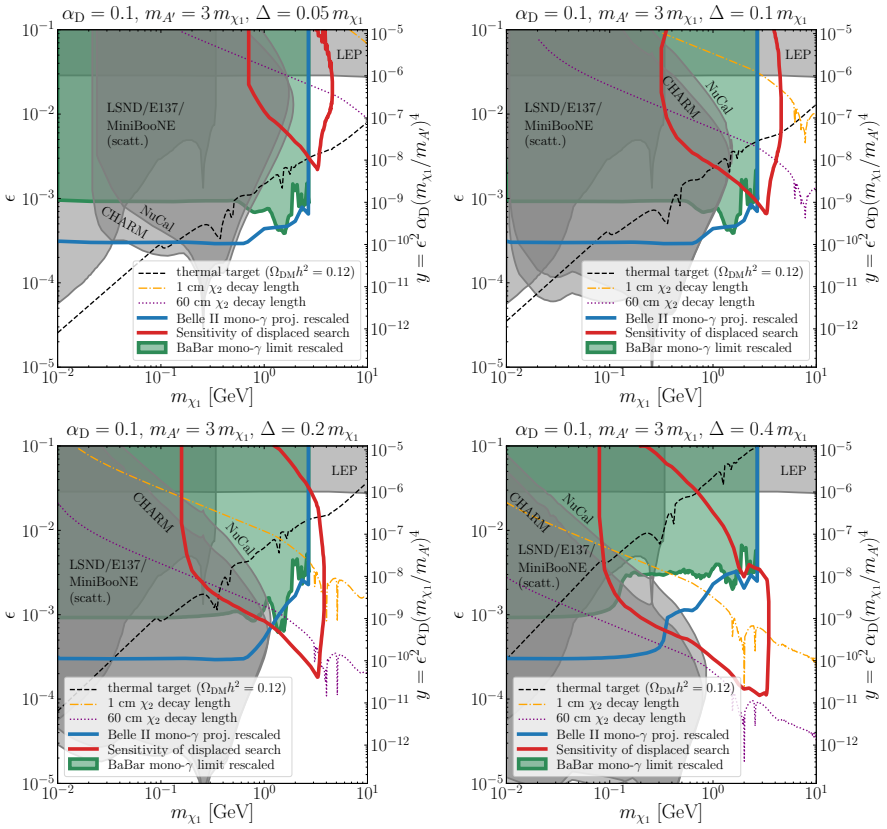

Figure 3.5: Constraints on pseudo-Dirac DM in the (m_χ, ϵ) plane for $\alpha' = 0.1$ and $m_{A'} = 3m_\chi$ with mass splittings $\Delta_m = \{0.05, 0.1, 0.2, 0.4\}$. Current bounds from NuCal [463], CHARM [463], LSND [279], E137 [280], MiniBooNE [506], LEP [494], and BaBar [488] are shown, along with projected sensitivities from Belle II [3]. Thermal targets are indicated with dashed black lines. Contours of constant χ^* decay length are also included. Reproduced from Ref. [3].

the combination of searches for decays of LLPs and missing energy signatures—together with the large kinetic mixing ϵ values required by freeze-out—places stringent constraints on large mass splittings. In general, only splittings $\Delta_m \lesssim 0.1$ remain viable, as larger values lead to a Boltzmann-suppressed excited state population during freeze-out, thereby requiring excessively large DM–SM couplings.

For mass splittings below the electron threshold, $\delta \leq 2m_e$, the decay $\chi^* \to \chi e^+ e^-$ becomes kinematically forbidden, rendering χ^* cosmologically stable [75]. This naturally arises in the pseudo-Dirac limit and requires consideration of constraints from ID and DD due to a residual excited state fraction $f_* \nsim 0$ [73].

Figure 3.6 summarizes the constraints in this regime. As shown in the figure,

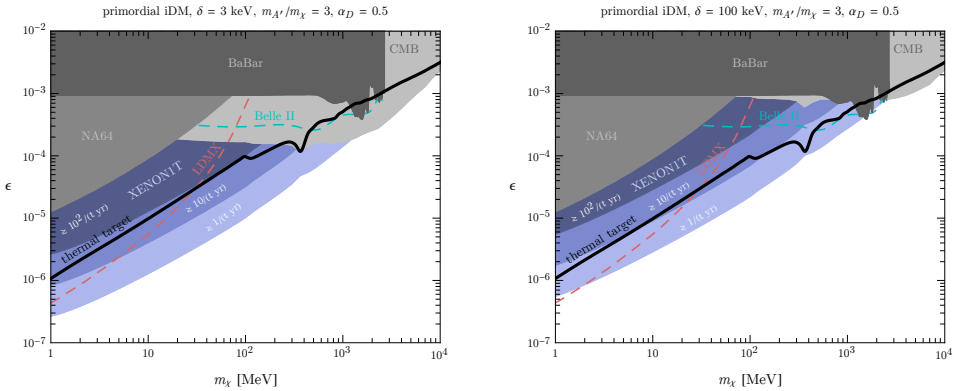

Figure 3.6: Constraints on cosmologically stable piDM in the (m_χ, ϵ) plane for $\alpha' = 0.5$ and $m_{A'} = 3m_\chi$, assuming $\delta = 3$ keV (left) and $\delta = 100$ keV (right). Direct detection bounds from XENON1T [73, 512] are shown in blue. Light and dark gray regions represent constraints from CMB [26] and missing energy searches at NA64 [513] and BaBar [488], respectively. Projected sensitivities from LDMX [90, 376, 491, 514] and Belle II [91] are shown with dashed lines. Thermal targets appear as solid black curves. Reproduced from Ref. [73].

previous DD experiments like XENON1T could already probe thermal piDM for $\delta \gtrsim$ keV via exothermic down-scattering $\chi^* e^- \to \chi e^-$, which produces a unique mono-energetic recoil signal. Current experiments such as CRESST-II [434], XENONnT [433], PandaX-4T [509], and LZ [267] have sensitivity down to splittings of a few hundred eV, $\delta \gtrsim 200$ eV [73, 75, 419, 510].[10] CMB constraints are also relevant in this scenario, excluding DM candidates down to several hundred MeV in mass.

For even smaller mass splittings, $\delta \lesssim 100$ eV, direct detection loses sensitivity, and indirect detection becomes the dominant probe. As shown in fig. 3.7, mass splittings below $\delta \lesssim 10$ eV are essentially excluded by a combination of CMB data [26] and gamma-ray observations of the Milky Way halo [419, 515–518].[11] Future ID experiments and next-generation CMB measurements [519] are expected to further probe this regime. These include proposed gamma-ray satellites such as e-ASTROGAM [520], AMEGO-X [521], and MAST [522], as well as CMB observatories like the Observatory [523] and Simons Array [524].

It should be noted that for extremely small mass splittings, $\Delta_m \lesssim 10^{-6}$, DM particles possess sufficient kinetic energy to scatter in DD experiments via $\chi e^- \to \chi^* e^-$, producing signals nearly indistinguishable from those of mDM. As

[10] Additional enhancements to low-energy detection may come from Migdal effect signals [77] or cosmic-ray accelerated DM [74] as well as non-galactic diffuse DM components [511].

[11] See [419] for the definition of the effective cross section $\langle \sigma v \rangle_{\rm eff}$, which accounts for non-standard halo profiles for excited state DM generated by up-scattering processes in galaxies. Experimental ID limits must be appropriately recast using this effective cross section.

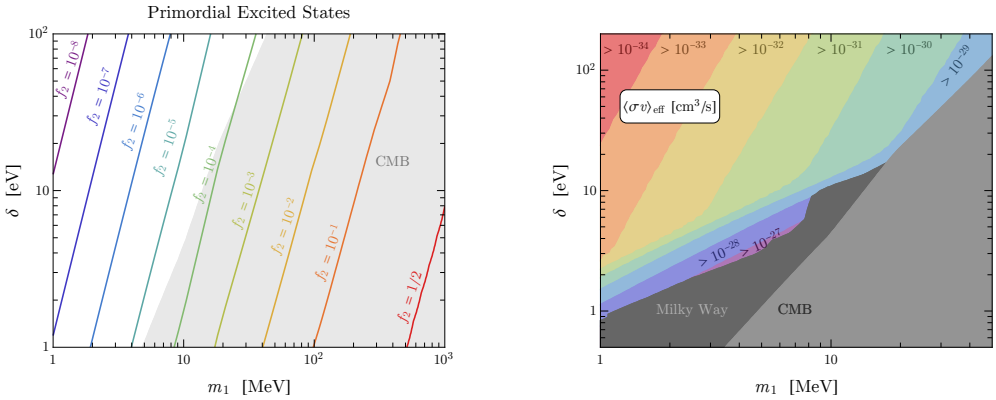

Figure 3.7: Left: Contours of the excited state fraction $f_* = n_*/(n_- + n_*)$ in the early Universe after chemical decoupling in the (m_χ, δ) plane, assuming $\alpha' = 0.5$, $m_{A'} = 3m_\chi$, and ϵ chosen to yield the correct relic abundance via freeze-out. CMB constraints from Planck [26] exclude the gray region. **Right:** Effective coannihilation cross section $\langle\sigma v\rangle_{\rm eff}$ in the same plane. Constraints from ID in the Milky Way halo are shown in dark gray [515–518]. Reproduced from Ref. [419].

a result, conventional DD WIMP searches may effectively probe this regime.

In summary, piDM exhibits a remarkably rich phenomenology across a wide range of mass splittings and energy scales. For large splittings ($\delta > 2m_e$), the excited state χ^* is short-lived, decaying rapidly into χ and visible SM particles, giving rise to distinctive collider and beam-dump signatures, including missing energy and prompt or displaced vertex signals. At lower mass splittings ($\delta \lesssim 2m_e$), χ^* becomes metastable, leading to strong constraints from DD via down-scattering. For even smaller splittings ($\delta \lesssim 100$ eV), ID observables—particularly gamma rays from the Galactic halo and CMB observations—place strong limits on piDM thermal production. These different regimes are summarized in table 3.1. Taken together, these features make piDM one of the most robust and versatile WIMP-like scenarios still open to exploration.

3.2 Not-so-inelastic Dark Matter

As discussed above, fermionic DM with a dark photon mediator ranks among the most widely studied simplified DM models and remains one of the main targets of current and future intensity frontier experiments (including beam-dump and collider searches), as it can naturally predict WIMP-like DM in the sub-GeV regime [90, 322, 408]. Among the two models compared previously, iDM and mDM,[12] one might argue that mDM constitutes the minimal model, as it involves

[12] Henceforth, we will refer to pseudo-Dirac inelastic DM (piDM) simply as iDM, since it is the most commonly studied realization and the focus of this work. Thus, iDM ≡ piDM.

Table 3.1: Summary of key phenomenological regimes in pseudo-Dirac iDM as a function of the mass splitting δ.

Mass splitting	χ^* **lifetime**	**Phenomenology**	**Experiments**
$\delta \gtrsim m_\chi$	prompt	missing energy searches	BaBar, NA64, Belle II, LDMX
$\delta \gtrsim 2m_e$	long-lived	displaced and missing energy searches	NA64, NA62, Belle II, CMS, SHiP, LDMX
$\delta \sim 100\,\text{keV}$	metastable	down-scattering in DD and ID (CMB)	XENON1T, SuperCDMS, CRESST, LZ
$\delta \lesssim 100\,\text{eV}$	metastable	ID (CMB and re-excitation at galaxies)	Planck, Fermi-LAT, e-ASTROGAM, MAST

only a single Majorana particle, whereas iDM introduces a second Majorana fermion with one additional free parameter, the mass splitting δ between the two DM states.

However, constructing a minimal UV-complete theory for mDM with a $U'(1)$ mediator requires introducing at least one additional fermionic field to ensure anomaly cancellation [525]. As a result, both iDM and mDM in their minimal UV-complete forms involve the same number of fields and parameters. This observation motivates a unified framework in which both models are embedded as specific parameter limits. In fact, the most common UV-completion of iDM already includes as special cases the effective Lagrangians of iDM and mDM, as shown in eqs. (3.14) and (3.15).

This UV-completion is commonly implemented via the inclusion of two chiral fermions, χ_L and χ_R, charged under a new $U'(1)$ gauge symmetry, accompanied by Dirac and Majorana mass terms m_d, m_L, and m_R [3, 88]. Since Majorana mass terms explicitly break the $U'(1)$ symmetry, their inclusion requires spontaneous symmetry breaking—typically via a dark Higgs mechanism [418]. In the limit $m_d \gg m_L, m_R$, one obtains a pseudo-Dirac fermion, i.e., two nearly degenerate Majorana eigenstates.[13]

The "inelasticity" of interactions in this framework—i.e., the suppression of elastic scatterings involving only the ground state—results from imposing $m_L \approx m_R$, which corresponds to a nearly parity-conserving dark sector [79]. However, this symmetry is difficult to justify, especially when DM couples to SM particles, where parity is maximally violated in the weak interactions [479].

[13] The mDM case can be recovered in a seesaw-like configuration with $m_d \sim m_R \gg m_L$ (or the $L \leftrightarrow R$ counterpart), or more simply in the limit $m_R \gg m_L, m_d$ (or $L \leftrightarrow R$), yielding $m_{\chi^*} \gg m_\chi$ and allowing one to integrate out the heavy Majorana field [376].

In this thesis, we emphasize that the condition $m_L \approx m_R$ is not necessary—in fact, no assumptions regarding parity, charge-conjugation, or time-reversal symmetries are required within the dark sector (except from the general $\mathcal{CPT}$ invariance [227]). The presence of diagonal (elastic) interactions does not undermine the attractive features of iDM. Since the two mass eigenstates are Majorana particles, their elastic scattering and annihilation cross sections are suppressed in the non-relativistic limit, rendering such interactions negligible in ID and DD contexts. On the other hand, diagonal couplings can enhance the annihilation rate in the early universe—when DM was (nearly) relativistic—thereby relaxing the relic density constraint. Moreover, for very small mass splittings (metastable χ^*), diagonal interactions can help deplete the excited-state population through processes like $\chi^*\chi \to \chi\chi$, thereby enhancing the population asymmetry between states [75]. See appendix F for an example illustrating how parity violation can dramatically alter this asymmetry, even within the commonly studied pseudo-Dirac iDM scenario.

We define this general framework as *not-so-inelastic Dark matter* (niDM), with the *not-so-inelastic region* corresponding to scenarios where DM appears inelastic in DD and collider searches but freezes out as Majorana-like in the early universe. The model introduces two new parameters: a $\mathcal{CP}$ breaking phase ϕ_d, and a mass asymmetry parameter δ_y quantifying the deviation between m_L and m_R, i.e., the breaking of parity in the dark sector. The usual iDM scenario is recovered in the limit $\delta_y \to 0$ and $\phi_d = 0$. In contrast, for $\delta_y \gg 1$, the model deviates significantly from standard iDM, with relaxed relic density constraints, similar to mDM, allowing for larger viable mass splittings. In this sense, niDM smoothly interpolates between mDM and iDM, as shown in fig. 3.8. It can even encompasses the standard Dirac DM scenario when $\delta = 0$. Consequently, all simplified fermionic DM models coupled to the SM via a dark photon portal can be fully characterized within this unified framework, without loss of generality. Such a general picture also extends to DM models interacting through a dark Higgs portal [93]—see chapter 5.

More broadly, niDM can be understood as any two-state DM scenario without constraining its coupling structure. Even the most theoretically motivated iDM candidates—supersymmetric models—typically have suppressed elastic interactions due to the assumption of near-degeneracies between neutralino and chargino masses [526]. While this assumption may be justified in some regions of the parameter space (e.g., when their mass splittings arise from loop corrections or large mass hierarchies are found in the supersymmetric mass spectrum [461, 526, 527]), more general cases fall under the niDM umbrella. Thus, by extending the concept of iDM beyond rigid unnecessary assumptions, the niDM framework offers a more flexible framework for understanding DM interactions.

In what follows, we focus on a specific fermionic niDM model often employed

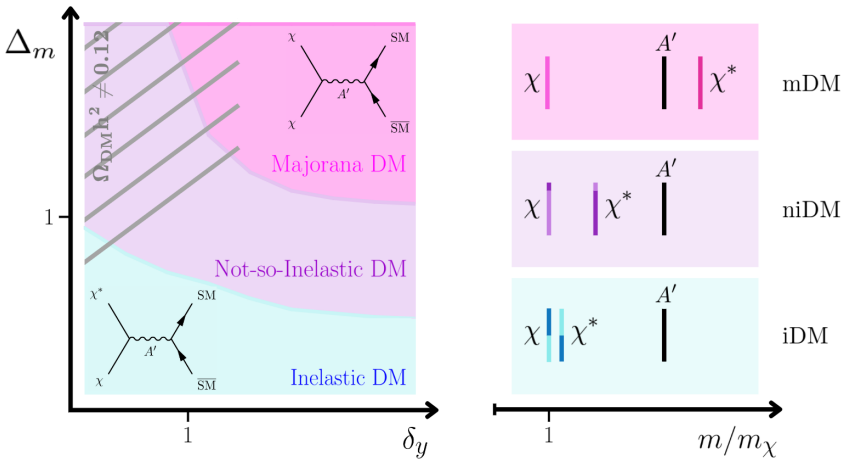

Figure 3.8: Schematic illustration of the particle spectrum and the continuous transition from inelastic DM (iDM) over not-so-inelastic DM (niDM) to Majorana DM (mDM). The left panel shows the effect of the normalized mass splitting Δ_m and Yukawa asymmetry δ_y, see eqs. (3.29) and (3.40), where we indicate also the relevance of the elastic (diagonal) and inelastic (off-diagonal) interactions. The right panel shows the typical relative mass spectrum of χ, χ^* and A' for different regimes of the normalized mass splitting Δ_m. Reproduced from Ref. [89].

in studies of pseudo-Dirac iDM.[14] This specific version without the ϕ_d phase has appeared in previous studies [70, 88, 418, 528, 529]. While Ref. [528] identifies both the iDM and mDM regimes, it overlooks the intermediate not-so-inelastic region. Ref. [529] partially explores this regime, but still restricts attention to $\delta_y \ll 1$, $\Delta_m \leq 0.4$, and relies on strong s-channel resonances with $m_{A'} \approx m_{\chi^*} + m_\chi$. Crucially, the phase ϕ_d is not a trivial extension—it is a physical free parameter of the model and can play a significant role, as we will demonstrate in chapter 5. To conclude, we advocate for this more general formulation of iDM and mDM models—captured within the niDM framework—which enables a complete characterization of fermionic DM and reveals novel phenomenological features that remained hidden in more restrictive approaches.

3.2.1 The general Lagrangian

In this section, we present a minimal anomaly-free UV-complete realization of fermionic niDM featuring a spontaneously broken $U'(1)$ symmetry, though its essential features can be adapted to other niDM constructions. This model is often used as a UV-complete starting point for the standard pseudo-Dirac iDM.

We consider a dark sector containing a new $U'(1)$ gauge symmetry, character-

[14] Unless otherwise stated, niDM refers to this specific realization.

ized by a gauge coupling e' (with its corresponding dark fine-structure constant $\alpha' \equiv e'^2/4\pi$). The matter content includes two 2-component Weyl fermions of opposite chirality, χ_L and χ_R, both singlets under the SM gauge groups but carrying the same $U'(1)$ charge q_χ. This charge assignment ensures the cancellation of gauge anomalies in our extension of the SM [525].

To generate Majorana masses and spontaneously break the $U'(1)$ symmetry, we introduce a complex scalar field H' with charge $q_{H'} = -2q_\chi$ under $U'(1)$, which acquires a vacuum expectation value (vev) $\langle H' \rangle = w/\sqrt{2}$. The vev induces a mass for the $U'(1)$ gauge boson A', as well as Majorana mass terms for both χ_L and χ_R.

The full Lagrangian involving the new fields and their interactions with the SM is given by

$$\mathcal{L}_{\rm NP} = \mathcal{L}_\chi + \mathcal{L}_V + \mathcal{L}_S \,, \tag{3.19}$$

where

$$\mathcal{L}_\chi = i\bar{\chi}_L \not{D} \chi_L + i\bar{\chi}_R \not{D} \chi_R - m_D^* \bar{\chi}_L \chi_R - y_L H' \bar{\chi}_L^c \chi_L - y_R H' \bar{\chi}_R^c \chi_R + \text{h.c.}, \tag{3.20}$$

$$\mathcal{L}_V = -\frac{1}{4} A'^{\mu\nu} A'_{\mu\nu} - \frac{1}{2} \frac{\epsilon}{\cos\theta_w} B^{\mu\nu} A'_{\mu\nu} \,, \tag{3.21}$$

$$\mathcal{L}_S = (D^\mu H')^* (D_\mu H') + \mu_{h'}^2 |H'|^2 - \lambda_{h'} |H'|^4 - \lambda_{h'h} |H'|^2 |H|^2 \,, \tag{3.22}$$

with the SM Higgs field denoted by H, the hypercharge gauge boson by B, the weak mixing angle by θ_w, and the covariant derivative defined as $iD_\mu \phi = i\partial_\mu \phi - q_\phi e' A'_\mu \phi$. The charge-conjugated field is given by $\psi^c = C\gamma_0^T \psi^*$, with C the charge conjugation matrix. The field strength tensor for each gauge boson is denoted by the gauge field variable A with two indices $A^{\mu\nu}$.

The parameters in $\mathcal{L}_\chi$ can be made real and positive by suitable field redefinitions, up to a single physical complex phase, which we assign to the Dirac mass: $m_D = m_d e^{i\phi_d}$ with $m_d \geq 0$. The gauge sector parameters ϵ and e' are taken real and positive by analogous redefinitions. We assume that H' acquires a nonzero vev, spontaneously breaking the $U'(1)$ symmetry, and that the scalar potential is (meta)stable. This imposes constraints on the parameters of the scalar potential; see section 2.5 and references therein. A phase in w can be absorbed via a redefinition of H', and we set $q_\chi = 1$ without loss of generality, as any other charge value can be absorbed into e'.

In the above Lagrangian, parity can be broken by either $y_R \neq y_L$ or $\phi_d \neq 0$, since we take $\mathcal{P}$ to act in the fermion fields as $\chi_L \to \chi_R$ [530]. In contrast, according to our definition, charge conjugation is always conserved. More generally, there is always an accidental Z_2 if one were to define charge conjugation in a different way [531].[15]

[15] For example, Ref. [479] defines a different $\mathcal{C}$ differently and always have $\mathcal{CP}$ conserved.

After symmetry breaking, the dark photon acquires a mass,

$$m_{A'} = 2e'w\,, \tag{3.23}$$

and the fermion mass term in the Lagrangian becomes

$$\mathcal{L}_\chi \supset -m_D^*\bar{\chi}_L\chi_R - \frac{1}{2}m_L\bar{\chi}_L^c\chi_L - \frac{1}{2}m_R\bar{\chi}_R^c\chi_R + \text{h.c.}\,, \tag{3.24}$$

with Majorana masses given by $m_{L/R} = \sqrt{2}y_{L/R}w$.

We diagonalize the fermion mass matrix with the usual Takagi [532] diagonalization via a unitary transformation of the Weyl fields $(\chi_L, \chi_R^c)^T$ using the mixing matrix

$$U = \begin{pmatrix} \cos\theta & e^{i\phi}\sin\theta \\ -e^{-i\phi}\sin\theta & \cos\theta \end{pmatrix}\,, \tag{3.25}$$

leading to two Majorana mass eigenstates χ and χ^*, with $m_{\chi^*} > m_\chi$ by convention (the diagonalization procedure is discussed in detail in appendix A). The corresponding masses are

$$m^2_{\chi^{(*)}} = m_d^2 + w^2(y_L^2 + y_R^2) \mp wD \tag{3.26}$$

where

$$D^2 = w^2(y_R^2 - y_L^2)^2 + 2m_d^2|\kappa|^2\,, \quad \text{with} \quad \kappa = y_L e^{i\phi_d} + y_R e^{-i\phi_d}\,. \tag{3.27}$$

Note that the Majorana masses do not depend on ϕ_d at linear order.

The fermion interactions with the dark photon A' and the dark Higgs H', in the unitary gauge h', are given by ($\chi_i \in \{\chi, \chi^*\}$):

$$\mathcal{L}_\chi^I = \frac{1}{2}e'A'^\mu\,\bar{\chi}_i(i\alpha_{ij} + \beta_{ij}\gamma^5)\gamma_\mu\chi_j - \frac{1}{2}y_L h'\,\bar{\chi}_i(\hat{\alpha}_{ij} + i\hat{\beta}_{ij}\gamma^5)\chi_j\,, \tag{3.28}$$

where the coupling coefficients $\alpha_{ij}, \beta_{ij}, \hat{\alpha}_{ij}, \hat{\beta}_{ij}$ are listed in tables 3.2 and 3.3 with the lower-script "$*$" denoting the excited state index and "_" the ground state one.[16] These coefficients and "flavor" changing interactions share conceptual similarities with the quark sector of the SM and the CKM matrix V_{ij}.

The normalized left–right Yukawa asymmetry δ_y appearing in tables 3.2 and 3.3 is defined as

$$\delta_y \equiv \frac{y_R - y_L}{y_L} = \frac{m_R - m_L}{m_L}\,, \tag{3.29}$$

and is taken to be positive without loss of generality—this can always be achieved by an appropriate re-labeling of $\chi_L \leftrightarrow \chi_R^c$. Note that even for large values of

[16] Note that in our model the diagonal couplings $\chi\chi A'$ and $\chi^*\chi^* A'$ are equal in norm and given by $|e'\cos 2\theta|$. This is a consequence of our assumption of equal $U'(1)$ charges of χ_L and χ_R as required for anomaly cancellation when introducing only two chiral fermionic fields.

Table 3.2: Coefficients for interactions between dark fermions and dark photons.

$\alpha_{**} = 0$	$\beta_{**} = -\cos 2\theta$
$\alpha_{*-} = \sin\left((2\phi + \gamma_* - \gamma_-)/2\right) \sin 2\theta$	$\beta_{*-} = \cos\left((2\phi + \gamma_* - \gamma_-)/2\right) \sin 2\theta$
$\alpha_{-*} = -\alpha_{*-}$	$\beta_{-*} = \beta_{*-}$
$\alpha_{--} = 0$	$\beta_{--} = \cos 2\theta$

Table 3.3: Coefficients for interactions between dark fermions and dark Higgs.

$$\hat{\alpha}_{**} = \sqrt{2}(\delta_y + 1)\cos\left(2\phi + \gamma_*\right)\sin^2\theta + \sqrt{2}\cos\gamma_*\cos^2\theta$$
$$\hat{\beta}_{**} = \sqrt{2}(\delta_y + 1)\ \sin\left(2\phi + \gamma_*\right)\sin^2\theta + \sqrt{2}\ \sin\gamma_*\cos^2\theta$$
$$\hat{\alpha}_{*-} = \sin 2\theta\big[(\delta_y + 1)\cos\left((2\phi + \gamma_* + \gamma_-)/2\right) - \cos\left((2\phi - \gamma_* - \gamma_-)/2\right)\big]/\sqrt{2}$$
$$\hat{\beta}_{*-} = \sin 2\theta\big[(\delta_y + 1)\ \sin\left((2\phi + \gamma_* + \gamma_-)/2\right) + \ \sin\left((2\phi - \gamma_* - \gamma_-)/2\right)\big]/\sqrt{2}$$
$$\hat{\alpha}_{-*} = \hat{\alpha}_{*-} \qquad \hat{\beta}_{-*} = \hat{\beta}_{*-}$$
$$\hat{\alpha}_{--} = \sqrt{2}(\delta_y + 1)\cos\gamma_-\cos^2\theta + \sqrt{2}\cos\left(2\phi - \gamma_-\right)\sin^2\theta$$
$$\hat{\beta}_{--} = \sqrt{2}(\delta_y + 1)\ \sin\gamma_-\cos^2\theta - \sqrt{2}\ \sin\left(2\phi - \gamma_-\right)\sin^2\theta$$

$\delta_y \gg 1$ (e.g., $y_L \ll y_R$), perturbativity remains intact. Actually, $\delta_y \to \infty$ just corresponds to $y_L = 0$ and the model still remains well defined. The complex phase ϕ is defined as

$$e^{i\phi} = \frac{\kappa}{|\kappa|}\,. \tag{3.30}$$

The phases γ_i are given by

$$e^{i\gamma_*} = \frac{\sigma_*}{|\sigma_*|} \qquad \text{and} \qquad e^{i\gamma_-} = \frac{\sigma_-}{|\sigma_-|}\,, \tag{3.31}$$

where

$$\sigma_* = \frac{w(y_L^2 + 2y_L y_R e^{-2i\phi_d} + y_R^2) + D}{\kappa\, e^{-i\phi_d}} \tag{3.32}$$

and

$$\sigma_- = \frac{w(y_L^2 + 2y_L y_R e^{-2i\phi_d} + y_R^2) - D}{\kappa^*\, e^{-i\phi_d}}\,. \tag{3.33}$$

Finally, the $\chi_{L/R}$ fermion fields mixing angle θ is given by

$$\tan\theta = \frac{w(y_R^2 - y_L^2) + D}{\sqrt{2}m_d|\kappa|}\,. \tag{3.34}$$

In summary, the model has nine independent parameters, which we take to be

$$\epsilon, \quad \theta_{h'h}, \quad \alpha', \quad y_L, \quad \delta_y, \quad \phi_d, \quad m_d, \quad m_{A'}, \quad m_{h'}\,, \tag{3.35}$$

where $\theta_{h'h}$ is scalar mixing angle between the SM h and dark h' Higgs (see details about the DM-SM portals in section 2.5). The dark vev w is fixed by $m_{A'}$, and the scalar potential parameters are mapped to the scalar masses and mixing angle. While it is technically possible to trade (m_d, ϕ_d) for (m_χ, m_{χ^*}), the inversion is nontrivial and generally yields multiple solutions for ϕ_d in the complex plane (one for each quadrant) and non-trivial constraints on the choices of masses.[17] In practical applications, we often fix ϕ_d to special values (e.g., 0 or $\pi/2$) where this inversion becomes simple. In such cases, the parameter set reduces to

$$\epsilon, \quad \theta_{h'h}, \quad \alpha', \quad \delta_y, \quad m_\chi, \quad \Delta_m, \quad m_{A'}, \quad m_{h'}\,. \tag{3.36}$$

We emphasize the role of δ_y as a key parameter controlling the interaction structure. When $\delta_y = 0$, the mixing angle becomes $\theta = \pi/4$, leading to purely off-diagonal interactions with the dark photon. In this regime, the ϕ_d phase affects only relative signs of interaction coefficients and not the interaction structure itself. The mass splitting in this case is

$$m_{\chi^*}^2 - m_\chi^2 = 4 m_d m_M |\cos\phi_d|\,, \tag{3.37}$$

with $m_M = m_L = m_R$, consistent with the standard iDM result for $\phi_d = 0$. Thus, we see that the sole effect of the phase ϕ_d, for $\delta_y = 0$, is to reduce the mass splitting between the Majorana fermions. For $\phi_d = \pi/2$, the mass splitting even vanishes.

Our analysis in the subsequent chapters focuses primarily on the phenomenology arising from $\delta_y > 0$, which has the most significant impact on dark sector dynamics. Eventually exploring the effects of a non-zero ϕ_d only in chapter 5, while in the next section, we will demonstrate how setting $\phi_d = 0$ leads to considerable simplifications.

Feynman rules for niDM

From the spontaneously broken Lagrangian in eq. (3.28), one can extract the Feynman rules governing the interactions of the physical fermionic fields in the niDM model. These interaction vertices are summarized in fig. 3.9, where, for simplicity, the mediators are shown in their mixed (non-physical) basis. The effects of scalar mixing $\theta_{h'h}$ and vector kinetic mixing ϵ can be incorporated straightforwardly when computing physical amplitudes, as detailed in section 2.5.

Because the vertices involve only Majorana fermions, we adopt the standard convention of treating them as Dirac fermions with arbitrary arrow orientations—so long as no two arrows point into the same vertex. This greatly simplifies diagrammatic calculations. A comprehensive discussion of this prescription can be found in Ref. [533].

[17] In the small-ϕ_d limit, results simplify, allowing straightforward inversion at linear order.

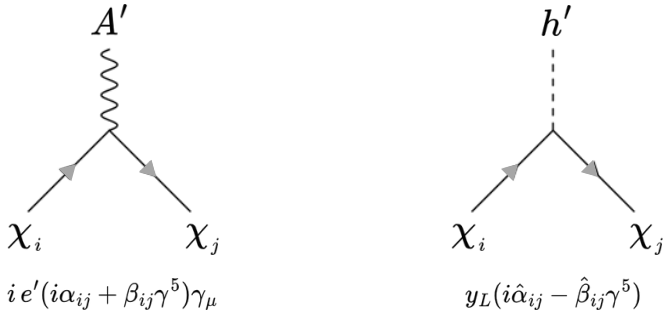

Figure 3.9: Feynman rules for the interactions of the fermionic DM states—the ground state χ and the excited state χ^*—with the DM-SM mediators: the dark photon A' and the dark Higgs h'. The interaction coefficients are listed in tables 3.2 and 3.3. Gray-colored arrows on the fermion lines indicate the Majorana nature of the states, for which particle flow is convention-dependent. See Ref. [533] for further discussion on Feynman rules for Majorana fermions.

To facilitate future studies of the niDM model introduced in this work, we provide a publicly available `FeynRules` [534] implementation.[18] This implementation can be used to generate input files for a variety of DM and high-energy physics tools. In this thesis, we employ it with the `MicrOmegas` [375] and `CalcHEP` [535] toolkits. Additional details regarding the specific features of our `FeynRules` implementation are provided in appendix B.

3.2.2 Reproducing the standard pseudo-Dirac case

To recover the standard pseudo-Dirac iDM model with a dark photon mediator—the most widely studied iDM scenario in the literature—we assume $\phi_d = 0$, corresponding to assuming that the only source of parity breaking in the dark sector is δ_y.[19] We further have to assume $m_d \geq \sqrt{m_R m_L}$, which holds in the pseudo-Dirac limit $m_d \gg m_L, m_R$. Violating this inequality alters the nature of dark photon-mediated coannihilations from s-wave to p-wave, as detailed in section 3.2.3.

Under these assumptions, the Majorana masses simplify considerably:

$$m_{\chi^{(*)}} = \sqrt{m_d^2 + \frac{1}{4}(m_R - m_L)^2} \mp \frac{1}{2}(m_R + m_L)\,. \tag{3.38}$$

The interaction coefficients simplify to those in table 3.4, and the fermionic

[18] The model files are available at `gdvgarcia/niDM_feynrules`. Please cite this thesis and Ref. [89] when using the implementation.

[19] As discussed above, allowing for a complex phase with $\delta_y \neq 0$ would introduce a p-wave contribution to coannihilations via the dark photon, which has no impact on high-energy phenomenology.

Table 3.4: Coefficients for interactions between dark fermions and dark photons, and between dark fermions and dark Higgs bosons, in the regime $m_d \geq \sqrt{m_R m_L}$.

$\alpha_{--} = 0$	$\beta_{--} = \cos 2\theta$	$\hat{\alpha}_{--} = -\sqrt{2}(1 + \delta_y \cos^2\theta)$	$\hat{\beta}_{--} = 0$
$\alpha_{-*} = \sin 2\theta$	$\beta_{-*} = 0$	$\hat{\alpha}_{-*} = 0$	$\hat{\beta}_{-*} = \delta_y \sin 2\theta/\sqrt{2}$
$\alpha_{*-} = -\alpha_{-*}$	$\beta_{*-} = 0$	$\hat{\alpha}_{*-} = 0$	$\hat{\beta}_{*-} = \hat{\beta}_{-*}$
$\alpha_{**} = 0$	$\beta_{**} = -\beta_{--}$	$\hat{\alpha}_{**} = \sqrt{2}(1 + \delta_y \sin^2\theta)$	$\hat{\beta}_{**} = 0$

mixing angle reduces to[20]

$$\cos 2\theta = -\frac{m_R - m_L}{\sqrt{4m_d^2 + (m_R - m_L)^2}} = -\frac{\delta_y \Delta_m}{(2 + \delta_y)(2 + \Delta_m)}\,, \tag{3.39}$$

where we used the normalized Yukawa (Majorana mass) asymmetry δ_y [eq. (3.29)] and the normalized mass splitting between Majorana eigenstates,

$$\Delta_m \equiv \frac{m_{\chi^*} - m_\chi}{m_\chi}\,, \tag{3.40}$$

to further simplify the expression.

Looking at table 3.4, we note that the dark photon's interactions with DM can be simply characterized by two effective couplings: the elastic (diagonal) fine-structure constant $\alpha'_{\rm el}$ and the inelastic (off-diagonal) one $\alpha'_{\rm inel}$:[21]

$$\alpha'_{\rm el} = \alpha' \cos^2 2\theta\,, \qquad \alpha'_{\rm inel} = \alpha' \sin^2 2\theta\,. \tag{3.41}$$

It follows from eq. (3.39) that $\delta_y = 0$ implies $\theta = \pi/4$, thus, $\alpha'_{\rm el} = 0$ and $\alpha'_{\rm inel} = \alpha'$, reproducing the *pure iDM scenario*. In this case, the Majorana masses reduce even further to

$$m_{\chi^{(*)}} = m_d \mp m_M\,, \tag{3.42}$$

where $m_M = m_L = m_R$. In the literature, this parity-conserving limit is often implicitly assumed from the start, with a Lagrangian written as

$$\mathcal{L}_\chi = \bar{\psi}(i\not{D} - m_d)\psi - m_M \bar{\psi}^c \psi + \text{h.c.}\,, \tag{3.43}$$

where $\psi = \chi_L + \chi_R$ is a Dirac field. The Majorana mass generation mechanism is typically neglected, and the Dirac mass is taken to be real ($\phi_d = 0$) by default. With the full model now in hand, it is clear just how specific the traditional iDM scenario really is.

Let us examine how the interplay between the two parameters δ_y and Δ_m defines three important regimes, illustrated in fig. 3.8:

[20] These coefficients follow from tables 3.2 and 3.3 with $\phi = \gamma_* = 0$ and $\gamma_- = \pi$.

[21] The terms "elastic" and "inelastic" make connection with the fact that niDM can be seen as a generalization of iDM models.

- **iDM:** For $\Delta_m \ll 1$, the two Majorana states are nearly degenerate, effectively forming a pseudo-Dirac fermion. In this limit, diagonal couplings to the dark photon are suppressed, independently of δ_y, and the off-diagonal interaction dominates. This corresponds to the canonical inelastic DM scenario and emerges naturally from a separation of scales where $m_d \gg m_{L,R}$. Although suppressed, the diagonal coupling can still contribute to enhancing the DM asymmetry in scenarios with a metastable χ^* [75]; see, for example, appendix F.

- **mDM:** For $\Delta_m \gg 1$ and $\delta_y \gg 1$, one finds $m_L \ll m_R$ and $m_d \ll m_R$, leading to a seesaw-type spectrum: $m_\chi \simeq m_d^2/m_R - m_L \ll m_{\chi^*} \simeq m_R$. The mixing angle θ can differ significantly from $\pi/4$, and diagonal interactions become sizable. The heavier state decouples, and the model effectively reduces to a standard Majorana DM framework.

- **niDM:** A third intermediate regime appears for $\Delta_m \sim 1$ and $\delta_y \gtrsim 1$, where diagonal and off-diagonal interactions coexist. While DM phenomenology at colliders and DD often resembles iDM, the relic density computation is closer to mDM. This not-so-inelastic DM regime is the main focus of chapter 4. When ambiguity may arise between the more general $\phi_d \neq 0$ case and this specific subset, we will explicitly refer to the "niDM framework in full generality."

We also note a fourth regime, $\Delta_m \gtrsim 1$ and $\delta_y \sim 1$, where the mass splitting is large but diagonal interactions remain suppressed. In this region, it is generally not possible to simultaneously satisfy relic density and experimental constraints, so we will not discuss it further.

To conclude, we emphasize that BBN imposes a robust lower bound of $m_\chi \gtrsim 10$ MeV on DM particles in thermal equilibrium with the SM [388]. In the not-so-inelastic regime ($\Delta_m \gtrsim 1$), this ensures that the decay $\chi^* \to \chi e^+ e^-$ is always kinematically allowed. As we will show in the next chapter, this implies that excited states are generically short-lived on cosmological timescales in the niDM scenario.

3.2.3 Optional: **The p-wave coannihilation case**

The condition $m_d \geq \sqrt{m_R m_L} = w\sqrt{2 y_R y_L}$ is often motivated by naturalness, since the limit $w = 0$ restores a global $U(1)_{\rm DM}$ symmetry, analogous to baryon number in the SM [87, 536]. However, this assumption is not required for a consistent UV-complete theory. Furthermore, traditional naturalness arguments have recently been challenged in light of the absence of evidence for new physics at the LHC. Alternative ideas, such as anthropic selection in a multiverse, have

Table 3.5: Coefficients for interactions between dark fermions and dark photons, and between dark fermions and dark Higgs bosons, in the regime $m_d < 2w\sqrt{y_R y_L}$.

$\alpha_{--} = 0$	$\beta_{--} = \cos 2\theta$	$\hat{\alpha}_{--} = \sqrt{2}(1 + \delta_y \cos^2\theta)$	$\hat{\beta}_{--} = 0$
$\alpha_{-*} = 0$	$\beta_{-*} = \sin 2\theta$	$\hat{\alpha}_{-*} = \delta_y \sin 2\theta/\sqrt{2}$	$\hat{\beta}_{-*} = 0$
$\alpha_{*-} = 0$	$\beta_{*-} = \beta_{-*}$	$\hat{\alpha}_{*-} = \hat{\alpha}_{-*}$	$\hat{\beta}_{*-} = 0$
$\alpha_{**} = 0$	$\beta_{**} = -\beta_{--}$	$\hat{\alpha}_{**} = \sqrt{2}(1 + \delta_y \sin^2\theta)$	$\hat{\beta}_{**} = 0$

gained attraction [537, 538], motivating us to explore the complementary regime $m_d < 2w\sqrt{y_R y_L}$, still assuming $\phi_d = 0$ for simplicity.

In this regime, the interaction coefficients take the form shown in table 3.5, where the fermion mixing angle is given by[22]

$$\cos 2\theta = -\frac{\delta_y(2 + \Delta_m)}{\Delta_m(2 + \delta_y)}\,. \tag{3.44}$$

To be consistent with the assumption of real mass parameters ($\phi_d = 0$), one must impose $\Delta_m \geq \delta_y$. Remarkably, in this scenario, even a small breaking of parity symmetry can lead to significant changes in the ratio of elastic to inelastic interaction strengths. Additionally, looking at table 3.5, we see that the off-diagonal interaction of DM with the dark photon is of axial-vector type, implying that freeze-out into SM particles via the vector portal proceeds through a p-wave process—hence the name *the p-wave coannihilation case*.

By solving for the normalized mass splitting,

$$\Delta_m = 2\frac{w}{m_\chi}(y_L + y_R) - 2 = y_L \frac{R_{A'}}{e'}(2 + \delta_y) - 2\,, \tag{3.45}$$

with $R_{A'} = m_{A'}/m_\chi$, and applying the constraint $\Delta_m \geq \delta_y$, we find the consistency condition

$$y_L \geq \frac{e'}{R_{A'}}\,. \tag{3.46}$$

This inequality has interesting implications in secluded freeze-out scenarios $\chi\chi \to h'h'$, where for sub-GeV DM one typically expects $y_L \lesssim 0.1$. For relatively small mass splittings $\Delta_m \lesssim 1$ and heavy vector mediators ($R_{A'} \gtrsim 1$), this leads to a naturally small dark gauge coupling, $\alpha' \lesssim 10^{-3} \ll \alpha$.

Although this p-wave co-annihilation scenario presents an intriguing alternative with distinct phenomenological features—such as the complete avoidance of ID constraints on DM annihilations, facilitating the possibility of metastable excited states, and naturally suppressed dark gauge couplings in secluded scenarios—it will not be explored in detail in this thesis. A more thorough investigation of its implications is left for future work.

[22] These coefficients follow from tables 3.2 and 3.3 with $\phi = \gamma_* = \gamma_- = 0$.

Chapter 4

Not-so-inelastic Dark Matter: the vector portal

In this chapter,[1] following the results established in the literature on (pseudo-Dirac) inelastic Dark Matter (iDM) models, we focus exclusively on the vector portal, neglecting the scalar sector for phenomenological purposes. Our primary interest lies in the sub-GeV DM mass range, where the not-so-inelastic DM (niDM) framework can be tested across the wide variety of experiments at the intensity frontier. In this light DM regime, the vector portal is more effective than the scalar mediator, as it couples universally to all fermion families and avoids the strong Yukawa suppressions that suppress scalar interactions with light SM particles $(e, \mu, \pi, p, ...)$ typically relevant at the intensity frontier.

Constraints on the scalar portal for light DM are already severe: the Higgs couplings are strongly Yukawa-suppressed, and direct limits on scalar portal couplings (see section 2.5) ensure that it plays a negligible role in DM–SM scattering processes at both colliders and direct detection experiments. To guarantee that scalar annihilation channels, $\chi\chi \to \phi\phi$, are irrelevant for relic density calculations, we require

$$m_s \gtrsim 1.5\, m_\chi \,,$$

a condition that is easily satisfied in the parameter space we explore. However, because we will study large values of the dark gauge coupling, perturbativity prevents $m_s \gg m_{A'}$, and dark Higgs production could therefore be relevant at accelerator searches such as those in Ref. [79][2]. A systematic study of such scalar signatures is beyond the scope of this chapter, but, in section 4.5, we will discuss their possible impact on the results presented here, while scenarios with a light dark Higgs ($m_{h'} \lesssim m_\chi$) will be explored in chapters 6 and 7.

In short, for the main results of this chapter we introduce the scalar sector only to ensure consistent $U(1)'$ symmetry breaking. The scalar Lagrangian $\mathcal{L}_S$

[1] With the exception of section 4.5, the material in this chapter is fully based on Ref. [89].

[2] This remains true even for tiny scalar mixing angles compared to the dark photon kinetic mixing, $\theta_{h'h} \ll \epsilon$.

given in eq. (5.4) therefore serves primarily as a concrete example, and our discussion will not depend sensitively on its specific form.

Dark photon models are subject to stringent bounds from missing energy searches at electron–positron colliders. In our framework such signatures arise when the dark photon decays invisibly into a pair of lighter DM states via diagonal couplings, or when an excited state produced through off-diagonal couplings decays outside the detector acceptance. We will calculate the resulting bounds from BaBar [488], estimate the sensitivity of Belle II [91], and analyze complementary constraints from ongoing beam dump experiments such as NA62 [539] and NA64 [540]. We also study the impact of (in)direct detection experiments, which now receive contributions from elastic (diagonal) interactions characteristic of niDM models.

The remainder of this chapter is structured as follows. We close this introduction with a discussion of the parameter space that will guide our analysis. In section 4.1, we then study the decay modes of the excited state fermion. Section 4.2 is devoted to relic density calculations, while section 4.3 addresses direct and indirect detection prospects. Collider and accelerator sensitivities are considered in section 4.4, while the impact of a dark Higgs on these results is analyzed in section 4.5. Our main results are presented in section 4.6, and we conclude in section 4.7. Additional details on beam dump and electron–positron collider analyses are provided in appendices C and D.

Parameter space. To reduce the dimensionality of the parameter space, we follow a common approach in the literature and fix benchmark values for certain parameters:

$$\alpha' = 0.5\,, \qquad m_{A'} = 3m_\chi\,. \tag{4.1}$$

These values are optimistic, as they both enhance experimental sensitivity and relax the relic density constraint.

It is also useful to recall the most important definitions from chapter 3, which will guide the analysis in this chapter. The diagonal and off-diagonal fine-structure constants are defined as

$$\alpha'_{\rm el} = \alpha' \cos^2 2\theta \qquad \text{and} \qquad \alpha'_{\rm inel} = \alpha' \sin^2 2\theta\,, \tag{4.2}$$

where θ is the fermionic mixing angle, given by

$$\cos 2\theta = -\frac{\delta_y\,\Delta_m}{(2+\delta_y)(2+\Delta_m)}\,, \tag{4.3}$$

in terms of two dimensionless variables: the normalized dark left–right Yukawa asymmetry and the relative mass splitting between the two DM states,

$$\delta_y = \frac{y_R - y_L}{y_L} \qquad \text{and} \qquad \Delta_m = \frac{m_{\chi^*} - m_\chi}{m_\chi}\,. \tag{4.4}$$

Without loss of generality, we take $\delta_y > 0$.

In summary, the independent parameters relevant for the DM phenomenology of this chapter are

$$\epsilon,\ \alpha',\ \delta_y,\ \Delta_m,\ m_\chi,\ m_{A'}\,. \tag{4.5}$$

Our focus will be on the novel regime specific to niDM, the *not-so-inelastic* regime, characterized by $\Delta_m \sim 1$, which interpolates between the iDM and mDM cases (see chapter 3). Restricting ourselves to predictive thermal scenarios, BBN imposes $m_\chi \gtrsim 10\,\mathrm{MeV}$, ensuring that the decay $\chi^* \to \chi e^+ e^-$ is always kinematically allowed in our analysis. As we will show in the next section, this guarantees that the excited state is always short-lived on cosmological timescales.

4.1 Excited Dark Matter decays

The presence of excited DM particles in niDM models, which may decay into SM states, is a key feature of their phenomenology. From a cosmological perspective, the excited state must be short-lived compared to cosmological timescales in order to evade stringent bounds on decaying DM.[3] For collider phenomenology, by contrast, the relevant quantities are the branching ratios into different final states, which determine the observable signatures.

If the interactions between the dark and visible sectors are dominantly mediated by the dark photon, then above the kinematic threshold $\Delta_m m_\chi > 2m_f$ the spin-averaged squared amplitude for the decay $\chi^* \to \chi f \bar{f}$ is approximately

$$\overline{|\mathcal{M}|^2}(\chi^* \to \chi f \bar{f}) \approx \alpha_{\rm dec} Q_f^2 \left[4\Delta_m(x_\chi - 1) - 2x_f x_\chi - x_f^2 - 2(x_\chi - 1)^2\right], \tag{4.6}$$

with

$$\alpha_{\rm dec} = 64\pi^2 \epsilon^2 \alpha\, \alpha'_{\rm inel} \frac{m_\chi^4}{m_{A'}^4}\,. \tag{4.7}$$

Here we adopt the notation $x_\chi = m_{\chi P}^2/m_\chi^2$ and $x_P = m_{P\bar{P}}^2/m_\chi^2$ for final states $\chi P \bar{P}$, where $m_{P_1 P_2}$ denotes the invariant mass of the particle pair $P_1 P_2$. From the amplitude in eq. (4.6), the corresponding partial width is

$$\Gamma(\chi^* \to \chi f \bar{f}) \approx N_c Q_f^2 \frac{\alpha_{\rm dec}}{240\pi^3} \Delta_m^5 m_\chi\,, \tag{4.8}$$

with $N_c = 3$ for quarks and $N_c = 1$ for leptons. Throughout this section we assume, for compactness, that SM fermions are light compared to the splitting and that the splitting is small compared to both the DM and dark photon masses:

$$m_f \ll \Delta_m m_\chi \ll m_\chi, \qquad m_{f\bar{f}}^2 \leq \Delta_m^2 \ll m_{A'}^2\,.$$

[3] The excited state could in principle be metastable, leading to a two-component DM framework. However, given the large mass splittings we consider, we will see that this scenario is not viable in our setup.

Full mass dependence is nevertheless retained in all our numerical results.

From these perturbative decays into fermions, we can estimate the lifetime of the excited state as

$$\tau_{\chi^*} \sim 10^{-15}\,\mathrm{s} \left(\frac{0.5}{\Delta_m}\right)^5 \frac{0.5}{\alpha'_{\mathrm{inel}}} \left(\frac{0.01}{\epsilon}\right)^2 \frac{500\,\mathrm{MeV}}{m_\chi} \left(\frac{m_{A'}}{m_\chi}\right)^4 . \tag{4.9}$$

This estimate shows that excited DM states are expected to be extremely short-lived in the niDM regime. Consequently, their cosmological abundance after thermal decoupling is negligible, and their phenomenology is instead restricted to signatures at high-energy experiments.

To correctly describe non-perturbative QCD effects in χ^* decays into hadrons, we adopt the data-driven approach of appendix A in Ref. [79]. This method employs the measured ratio

$$R(s) \equiv \frac{\sigma(e^-e^+ \to \textit{hadrons})}{\sigma(e^-e^+ \to \mu^-\mu^+)}$$

from e^+e^- collisions at center-of-mass energy $\sqrt{s}$ [541] to rescale the analytically calculated decay width $\Gamma(\chi^* \to \chi\mu^+\mu^-)$ into $\Gamma(\chi^* \to \chi + \textit{hadrons})$. While this prescription provides the total hadronic width, it does not yield partial widths or correct kinematic distributions for exclusive channels. Since such information is necessary for simulating χ^* decays, we also employ vector meson dominance (VMD) [542, 543] to obtain matrix elements for exclusive three-body decay modes:

$$\overline{|\mathcal{M}|^2}(\chi^* \to \chi\pi^+\pi^-) = \frac{\alpha_{\mathrm{dec}}}{4}\, G(x_\chi, x_\pi)\, \left|F_\pi(m^2_{\pi\pi})\right|^2, \tag{4.10}$$

$$\overline{|\mathcal{M}|^2}(\chi^* \to \chi KK) = \frac{\alpha_{\mathrm{dec}}}{36} m_\rho^4 \frac{G'(x_\chi, x_K)}{(m^2_\phi - x_K m^2_\chi)^2 + \Gamma^2_\phi m^2_\phi}, \tag{4.11}$$

where

$$G(x_\chi, x_\pi) = 4\big[(x_\chi{-}1)(x_\pi{+}x_\chi{-}1){-}\Delta_m(x_\pi{+}2x_\chi{-}2)\big]{-}\Delta_m^2(x_\pi{+}4x_\chi{-}8)\,, \tag{4.12}$$

$$G'(x_\chi, x_K) = x_K(4x_\chi - (\Delta_m + 2)^2) + \big[(\Delta_m + 2)\Delta_m - 2x_\chi + 2\big]^2\,, \tag{4.13}$$

and $F_\pi(q^2)$ is the pion electromagnetic form factor extracted from VMD fits to experimental data [543, 544]. Here, KK denotes both K^+K^- and $K^0\bar{K}^0$, neglecting their small mass differences. The analytical results in eqs. (4.10) and (4.11) are valid above the respective decay thresholds and in the limit $m^2_{A'}, m^2_\chi \gg \Delta^2_m m^2_\chi$.

Figure 4.1 shows the resulting branching fractions for leptonic and hadronic final states. Unlike for dark photon decays [545], no sharp resonances appear in the hadronic modes of χ^*, since the widths involve an integration over the

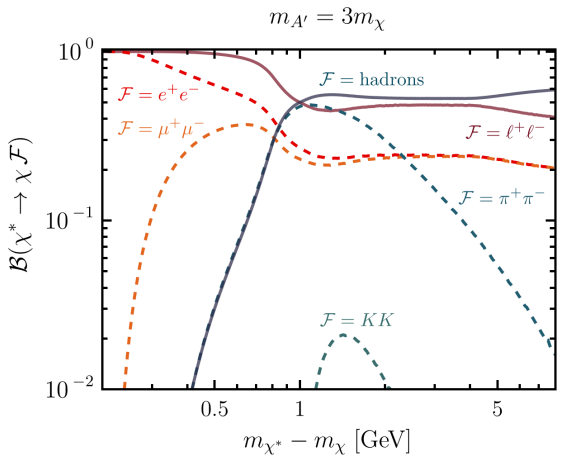

Figure 4.1: Decay branching fractions of the excited DM state χ^* in the niDM model as a function of the mass splitting between dark fermionic states. Reproduced from Ref. [89].

invariant mass of the hadronic system. By comparing the pion and kaon channels to the total hadronic width, we find that additional hadronic modes remain subdominant (contributing below ∼35%) up to $\Delta_m m_\chi \approx 2$ GeV. For higher masses, one could in principle use eq. (4.6) to compute widths into free quarks and perform hadronisation numerically. However, missing energy searches at current and past e^+e^- colliders (see section 4.4.3) only probe $m_{A'} \lesssim 8$ GeV, so such large splittings are irrelevant in the context of our benchmark $m_{A'} = 3m_\chi$.

Finally, we note that while fig. 4.1 assumes $m_{A'} = 3m_\chi$, the branching fractions are nearly independent of this choice for sufficiently heavy dark photons. Since $m_{A'}$ appears only through the propagator, $1/(m^2_{f\bar{f}} - m^2_{A'})$, and $m^2_{f\bar{f}} \leq \Delta^2_m m^2_\chi$, the propagator can be approximated as $-1/m^2_{A'}$ for $m^2_{A'} \gg \Delta^2_m m^2_\chi$, which cancels in the ratios. Moreover, provided the decays $\chi^* \to 3\chi$ and $\chi^* \to \chi A'$ remain kinematically forbidden, the branching fractions depend only on the absolute mass splitting $\Delta_m m_\chi = m_{\chi^*} - m_\chi$. Thus, the results of fig. 4.1 apply both to iDM models where $\Delta_m \ll 1$ and to niDM models allowing larger normalizaed mass splittings $\Delta_m \gtrsim 1$.

4.2 Relic abundance

In this section we present the calculation of the DM relic abundance in the niDM model, focusing on the interplay between the parity breaking parameter δ_y and the dark-fermion mass splitting Δ_m—see eq. (4.4).

We compute relic abundances using the `MicrOmegas (v5.3.41)` code [375], with a `CalcHEP` model file [535] as input, generated using the Mathematica® pack-

age `FeynRules v2.3.49` [534]. To account for non-perturbative QCD effects, we follow the standard approach of Refs. [90, 492], implementing modifications to the annihilation cross sections within `MicrOmegas`. Specifically: for $\chi^{(*)}\chi^{(*)}$ annihilations with center-of-mass energy $\sqrt{s} \approx m_{\chi^{(*)}} + m_{\chi^{(*)}}$ below the pion mass, we set the annihilation cross section into light quarks (u, d, s, c) to zero; while for energies above the pion mass, we replace the annihilation cross section into light quarks by the analytically calculated annihilation cross section into muons, rescaled by the measured cross-section ratio $R(s)$ [541],

$$\sigma(\chi^{(*)}\chi^{(*)} \to \textit{hadrons}) = R(s)\,\sigma(\chi^{(*)}\chi^{(*)} \to \mu^+\mu^-)\,, \tag{4.14}$$

see appendix A of Ref. [79].

In the present work we restrict ourselves to $m_{A'} \gtrsim 1.5 m_\chi$, which forbids pure dark sector annihilations $\chi\chi \to A'A'$. Such channels would instead lead to a secluded dark sector with only tiny couplings to the SM. Co-annihilations of the form $\chi\chi^* \to A'A'$ are also negligible: with our benchmark choice $m_{A'} = 3m_\chi$, they require $\Delta_m > 4$ to be kinematically open, which implies a severe Boltzmann suppression of the χ^* population.

Figure 4.2 shows the required kinetic mixing parameter ϵ that reproduces the observed DM abundance as a function of m_χ, for various values of δ_y ranging from 0 (the iDM limit) up to 1000 (essentially corresponding to maximal parity breaking). The plots also show model-independent bounds on ϵ from the muon anomalous magnetic moment [546] and from electroweak precision measurements at LEP [494]. These bounds arise because a kinetically mixed dark photon can contribute virtually to SM processes.

The impact of δ_y strongly depends on the mass splitting Δ_m. For small splittings, $\Delta_m \lesssim 0.2$ (upper left panel), freeze-out is essentially independent of δ_y, since annihilation is dominated by off-diagonal couplings as in conventional iDM. This results from two effects: (i) when χ^* is only slightly heavier than χ, Boltzmann suppression is mild, so both states efficiently participate in annihilations; (ii) for small Δ_m, the mixing angle θ (and thus the ratio $\alpha'_{\rm el}/\alpha'_{\rm inel}$) becomes nearly independent of the value of δ_y, see eq. (4.3).

For larger mass splittings, $\Delta_m \gtrsim 0.6$ (bottom row), the Boltzmann suppression of χ^* becomes extremlly relevant. In this case, large values of δ_y enhance the annihilation rate because diagonal interactions gain relative importance (cf. eqs. (4.2) and (4.3)). As a consequence, the required values of ϵ can be reduced by more than an order of magnitude compared to the $\delta_y = 0$ case. For $\delta_y \gg 1$, the effect saturates, since $\cos 2\theta \propto \delta_y/(2+\delta_y) \to 1 - 2/\delta_y$.

These features are further illustrated in fig. 4.3, which shows ϵ in the (δ_y, Δ_m) plane for $m_\chi = 200$ and 500 MeV. In the pseudo-Dirac limit ($\Delta_m \lesssim 0.2$), the relic abundance is independent of δ_y. For $\Delta_m \gtrsim 0.4$, however, increasing δ_y allows smaller ϵ to yield the correct relic abundance.

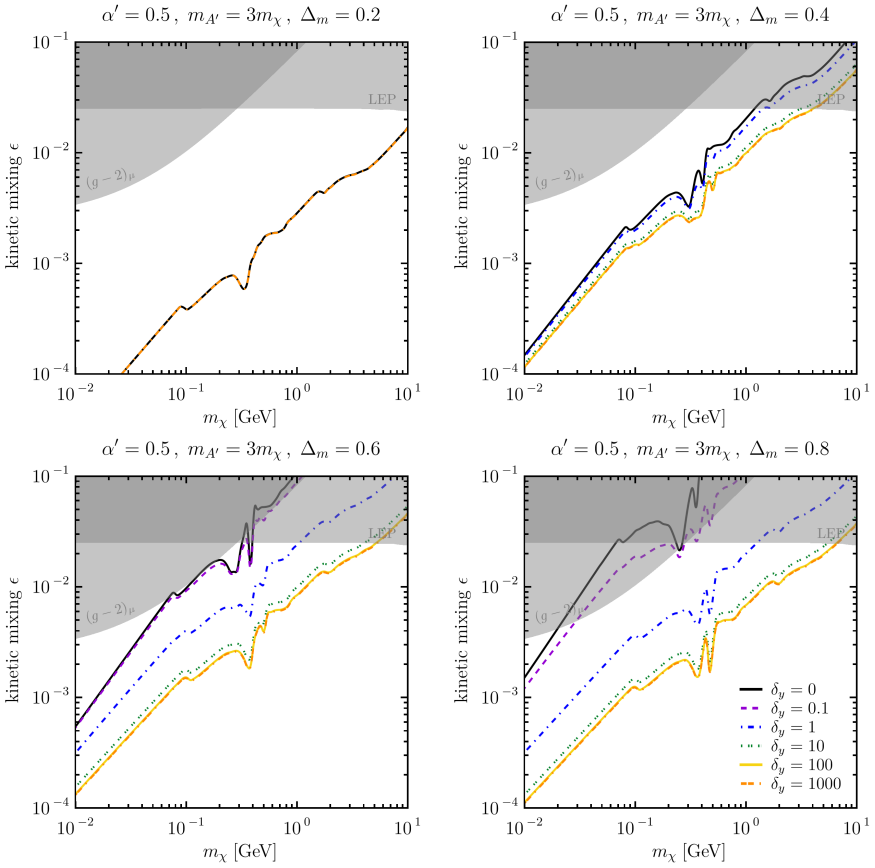

Figure 4.2: Values of the kinetic mixing ϵ that reproduce the observed DM relic abundance $\Omega_{\rm DM}h^2 = 0.12$, shown as a function of the DM mass. Panels correspond to different normalized mass splittings $\Delta_m = (0.2, 0.4, 0.6, 0.8)$. The various curves show different values of parity breaking δ_y, with the iDM limit ($\delta_y = 0$) in black. Gray shaded regions indicate model-independent bounds on ϵ (see text for details). Reproduced from Ref. [89].

The black-dashed curves in fig. 4.3 indicate the relative contribution of off-diagonal interactions to the DM relic abundance, which we denote by $f_{\rm iDM}$ and define following Ref. [547]. In the standard freeze-out approximation, the inverse of the relic density is proportional to the thermal average of the total annihilation cross section. Since annihilation processes in niDM models can proceed through both elastic (diagonal) and inelastic (off-diagonal) interactions, this framework allows us to write

$$\frac{1}{\Omega_{\rm DM}} = \frac{1}{\Omega^{\rm el}_{\rm DM}} + \frac{1}{\Omega^{\rm inel}_{\rm DM}}\,. \tag{4.15}$$

Here $\Omega^{\rm el}_{\rm DM}$ and $\Omega^{\rm inel}_{\rm DM}$ are the relic densities that would be obtained if only the respective contributions were present. Based on this decomposition, we define

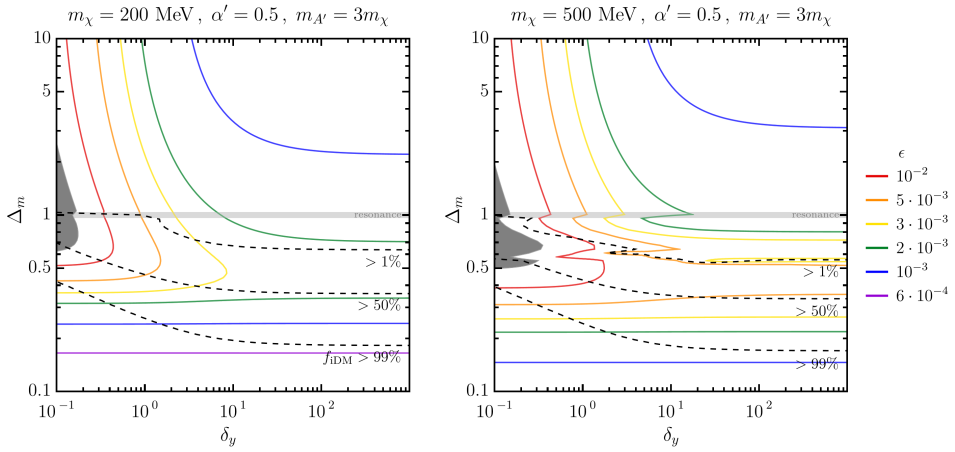

Figure 4.3: Contours of kinetic mixing ϵ reproducing the observed relic abundance $\Omega_{\rm DM}h^2 = 0.12$ as a function of δ_y and Δ_m. The two panels correspond to $m_\chi = 200$ and 500 MeV. Dashed black lines indicate the relative contribution of co-annihilation channels (see text). The horizontal light-gray band indicates resonance in the co-annihilation channel when $m_\chi + m_\chi^* \simeq m_{A'} \pm 1\%$. Dark gray regions are excluded by model-independent bounds on ϵ. Reproduced from Ref. [89].

the relative importance of off-diagonal processes as

$$f_{\rm iDM} \equiv \frac{\Omega_{\rm DM}}{\Omega_{\rm DM}^{\rm inel}} \,. \tag{4.16}$$

From fig. 4.3, we see that the not-so-inelastic regime typically corresponds to $f_{\rm iDM} \lesssim 50\%$, demonstrating that diagonal couplings provide at least half of the total annihilation rate and therefore play a crucial role in determining the relic abundance. We also note that contours of constant $f_{\rm iDM}$ do not coincide with contours of constant $\alpha'_{\rm inel}/\alpha' = \sin^2 2\theta$. The reason is that for sizeable mass splittings Δ_m the heavier state χ^* is Boltzmann suppressed relative to χ, which reduces the efficiency of co-annihilation channels even when $\alpha'_{\rm inel}$ is large.

4.3 (In)Direct detection

For the mass splittings considered here, inelastic DM scattering in direct detection (DD) experiments is strongly kinematically suppressed and therefore irrelevant.[4] In the not-so-inelastic regime, however, sizeable elastic (diagonal)

[4] The loop-induced elastic scattering process studied in Ref. [548] is kinematically allowed, but the cross section is too small to be observable even in future DD experiments.

couplings are present, leading to the effective low-energy interactions

$$\mathcal{L}_{\text{eff}} = \sum_f \frac{Q_f}{\Lambda^2}(\bar{\chi}\gamma_\mu\gamma_5\chi)(\bar{f}\gamma^\mu f) \,, \tag{4.17}$$

with

$$\Lambda = \frac{m_{A'}}{\sqrt{g_\chi \cos 2\theta\, \epsilon e}} \,. \tag{4.18}$$

The γ^5 in the DM current arises from the Majorana nature of the ground state, and, because the SM fermion current lacks a γ^5, it implies that the scattering cross section vanishes in the non-relativistic limit. Nevertheless, the same γ^5 lack in the SM current coherent enhancems the DM–nucleus scattering cross section, which can partially compensate for the velocity suppression.

To calculate the sensitivity of DD experiments, we must map the effective interaction in eq. (4.17) onto the non-relativistic effective theory of DM–nucleon interactions [256]. Using the public tool `DirectDM` [260], we find that the niDM model, defined at scale $\mu_c = 2$ GeV, induces the operators $\mathcal{O}_8^N \propto \vec{v}_\perp$ and $\mathcal{O}_9^N \propto \vec{q}$ with coefficients

$$c_8^p = \frac{2}{\Lambda^2} \,, \quad c_8^n = 0 \,, \quad c_9^p = \frac{5.586}{\Lambda^2} \,, \quad c_9^n = -\frac{3.826}{\Lambda^2} \,, \tag{4.19}$$

following the conventions of Ref. [260].

As described in Ref. [5], these coefficients can be passed to `DDCalc` [4], which provides likelihood functions for a wide range of DD experiments. For the local DM distribution, we use results from Ref. [549], which account for the effect of the Large Magellanic Cloud (LMC) on the velocity distribution (see appendix B of Ref. [89] for details). We find that, depending on the values of δ_y and Δ_m, current experiments such as LZ [267] already probe viable regions of parameter space at the upper end of the considered mass range ($m_\chi \sim 10\,\text{GeV}$). We also estimate the projected sensitivities for SuperCDMS [550] and DARWIN [551], which can reach values of $\epsilon \cos 2\theta$ as small as 10^{-3} across a wide mass range. These experiments will therefore provide complementary tests of niDM models.

For indirect detection (ID), off-diagonal interactions are irrelevant: excited states χ^* are too heavy to be produced via cosmic-ray upscattering [76, 454] and too short-lived to be efficiently generated in astrophysical systems [73, 445, 459]. Moreover, there is no cosmological abundance of χ^*, since the exponential suppression of the excited state together with its annihilation into ground states ($\chi^*\chi^* \to \chi\chi$) depletes its density—its decays further increase this depletion. Diagonal annihilations, on the other hand, are p-wave suppressed in the non-relativistic limit [330], such that no relevant ID constraints apply.

Finally, elastic scattering via diagonal couplings may induce sizeable DM self-interactions. The corresponding cross section can be approximated as

$$\sigma_{\text{SIDM}} \sim \frac{\alpha_{\text{el}}^2 m_\chi^2}{m_{A'}^4} \,, \tag{4.20}$$

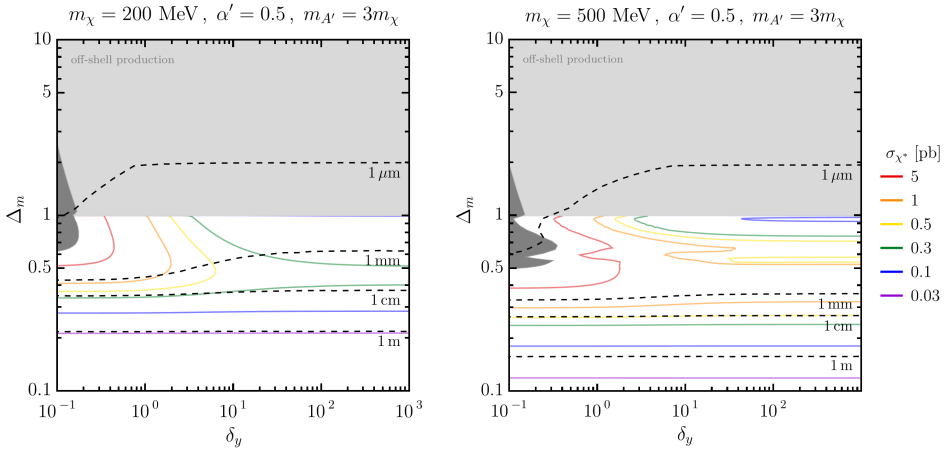

Figure 4.4: Cross section for χ^* production, as defined in eq. (4.21), at an electron–positron collider with center-of-mass energy $E_{\rm CM} = m_{\Upsilon(4S)} = 10.58$ GeV for the thermal target $\epsilon_{\rm DM}$. Each panel corresponds to a different DM mass $m_\chi = (200, 500)$ MeV. Dashed black lines show the proper decay length of χ^*. In the light gray region, χ^* production from e^+e^- annihilation requires an off-shell dark photon and is therefore suppressed. Dark gray shaded regions are excluded by model-independent bounds on ϵ. Reproduced from Ref. [89].

which remains below current astrophysical bounds [193] for $m_\chi = m_{A'}/3 > 10\,\text{MeV}$ and $\alpha_{\rm el} < 0.5$.[5]

4.4 Collider searches

The values of the kinetic mixing parameter $\epsilon_{\rm DM}$ obtained from the freeze-out calculation in section 4.2 are sufficiently large that DM particles can potentially be produced at current high-energy facilities, such as colliders and beam dump experiments. As an illustration, fig. 4.4 shows the cross section for producing excited states χ^*, defined as

$$\sigma_{\chi^*} = \sigma(e^+e^- \to A'\gamma) \times \left[\text{Br}(A' \to \chi\chi^*) + 2\,\text{Br}(A' \to \chi^*\chi^*)\right] , \tag{4.21}$$

evaluated at the typical center-of-mass energy of e^+e^- colliders which are used as B-factories, $E_{\rm CM} = m_{\Upsilon(4S)} = 10.58$ GeV. Production of χ^* is particularly relevant since, for $\Delta_m \leq 2$, the excited state can decay into a ground state χ and visible SM particles.

The proper decay length of χ^* is also displayed in fig. 4.4 and can be compared to the size of central detectors at experiments such as Belle II, which typically range from 10 cm to 1 m. For $m_\chi = 200\,\text{MeV}$ (left panel), signatures range

[5] Loop-induced self-interactions are negligible [73].

from invisible decays outside the detector for $\Delta_m \lesssim 0.2$, to prompt decays for $\Delta_m \gtrsim 0.6$. In the intermediate region $\Delta_m \approx 0.3$–0.5, decays occur at displaced vertices, which are usually vetoed by standard analyses but could be targeted in dedicated searches. For $m_\chi = 500\,\mathrm{MeV}$ (right panel), the decay width increases, shifting the lines of constant decay length to smaller Δ_m.

Even if χ^* decays outside the main detectors, its signatures may still be observable at beam dump experiments. In addition, missing energy searches at active beam dumps and DM scattering in downstream detectors provide complementary probes. In the remainder of this section, we discuss these experiments and how we implement them in our analysis. Readers primarily interested in results may proceed directly to section 4.6.

4.4.1 Proton beam dump experiments

Proton beam dumps employ high-intensity proton beams colliding on thick targets, potentially producing long-lived particles that can decay within displaced decay volumes. Null results from past searches translate into constraints on the niDM parameter space.

In our model, the key signal arises from χ^* decays. The most relevant regions for niDM ($m_{\chi^*} \lesssim 1\,\mathrm{GeV}$, $\Delta_m \gtrsim 0.3$) correspond to lifetimes $c\tau_{\chi^*} \lesssim 1$ m, as indicated in fig. 4.4. The expected number of decays is exponentially suppressed by the decay probability,

$$P_{\mathrm{decay}} \approx \exp\left(-\frac{l\, m_{\chi^*}}{\tau_{\chi^*} |\mathbf{p}_{\chi^*}|}\right) , \tag{4.22}$$

where l is the radial decay length. Hence, the largest couplings that can be probed depend on the ratio $p_{\mathrm{max}}/l_{\mathrm{min}}$, with p_{max} the maximum momentum of χ^* decaying inside the volume, and l_{min} the distance between the production point and the start of the decay volume.

To compute event yields, several steps are needed: (i) dark photon flux calculation, (ii) their decay into χ^*, (iii) subsequent χ^* decays within the detector volume, (iv) propagation of decay products, and (v) application of experiment-specific cuts. For this purpose, we extended `SensCalc` [1], a Mathematica®-based sensitivity evaluator.[6]

The default version of `SensCalc` evaluates event rates as a function of LLP mass and coupling, averaging over precomputed acceptances. This approach is insufficient for niDM, where many parameters influence the rate. We therefore implemented a module that takes experimental geometry, tabulated dark photon angle-energy distributions, and decay acceptance routines, and then generates χ^* events on-the-fly, in analogy with Monte Carlo simulations. Dark photon

[6] This extended module is not yet public, but can be provided on request.

4-momenta are sampled followed by corresponding A' decays into χ^* via $A' \to \chi\chi^*$ or $A' \to \chi^*\chi^*$. Only χ^* within the polar acceptance are selected, with azimuthal angles chosen such that their trajectories intersect the decay volume. Decay vertices are then sampled distributed according to $c\tau_{\chi^*}$, and the decays $\chi^* \to \chi e^+e^-, \chi\mu^+\mu^-, \chi\pi^+\pi^-$[7] are generated. SM decay products are propagated through the detector, including possible dipole magnets, and finally the decay products' acceptance is calculated.

The proton beam dump experiments considered in this work (NuCal, CHARM, BEBC, NA62) are review in appendix C of Ref. [89] along with comparisons with results from Ref. [463]. BEBC is studied here for the first time in the context of (n)iDM and yields constraints similar to NuCal at small masses and lifetimes. NA62, a currently running experiment, collected 1.4×10^{17} protons-on-target (PoT) in 2021 [504] (with no new physics observed) and aims for 10^{18} PoT before LS3 (2025) [552]. Thanks to its high beam energy and on-axis geometry, NA62 provides the strongest proton beam dump constraints, although a dedicated analysis by the collaboration would be required to validate our projections; further discussion of NA62 can also be found appendix C of Ref. [89].

4.4.2 NA64

The fixed-target experiment NA64 at CERN uses a 100 GeV electron beam impinging on an active beam dump. The detector consists of a ∼1 m electromagnetic calorimeter (ECAL), corresponding to about 40 radiation lengths ($40X_0$), followed by a ∼6.5 m hadronic calorimeter (HCAL), corresponding to ∼ 30 nuclear interaction lengths, with a high-efficiency veto counter (VETO) placed between them [553]. The NA64 collaboration searches for missing-energy events with $E_{\text{missing}} > 50$ GeV, selecting events with $E_{\text{ECAL}} < 50$ GeV and $E_{\text{HCAL}} < 1$ GeV, no activity in the VETO, and additional requirements on the incoming electrons (see refs. [344, 513]). Such events may arise from the production of energetic dark photons via electron–nucleus bremsstrahlung or via resonant annihilation of secondary positrons with atomic electrons, followed by the dark photon decaying into DM particles that escape the detector.

In the niDM scenario, dark photons can also decay into excited states which may themselves decay within the ECAL or HCAL. Decays inside the ECAL reduce the measured missing energy (and may also produce VETO activity from the daughters' showers), while decays in the HCAL typically veto the event completely. Both cases weaken the sensitivity of NA64 missing-energy searches, which are therefore most sensitive when χ^* has a very long decay length. The analogous effect in iDM models has been studied in detail [80, 479]. Since the production rate and kinematics of dark photons are identical for iDM and niDM (and also mDM), we can directly use these results to extract the relevant detector

[7] As noted in section 4.1, heavier meson modes are sub-dominant in the relevant mass range.

properties and analytically recast the NA64 bounds to the niDM case. Details are provided in appendix C.

NA64 has also performed dedicated searches for semi-visible dark photon decays. Results for iDM [479, 554] indicate that these analyses probe only regions already excluded by proton beam dump experiments or NA64 missing-energy searches. Looking ahead, missing-energy measurements with high-energy muon beams at NA64 are expected to extend sensitivity to dark photon masses up to about 3 GeV, potentially covering the full unexplored parameter space for sub-GeV masses [555]. Further dedicated studies will be needed to confirm this reach.

4.4.3 Electron–positron colliders

Electron–positron colliders such as PEP-II and SuperKEKB operate at fixed center-of-mass energies $\sqrt{s}$, providing well-defined event kinematics and a much cleaner background environment compared to hadronic machines. A particularly sensitive channel for dark photon production with invisible decays is the single-photon process $e^+e^- \to \gamma A'(\to \chi\chi)$, which searches for a single energetic photon signal (and missing energy), vetoing events with extra visible particles. This search was carried out by BaBar [488] and currently provides the most stringent bounds on invisibly decaying dark photons in the mass range 400 MeV–8 GeV [343, 344]. Belle II is expected to push these limits substantially further [91].

In the context of niDM, these constraints are expected to weaken: dark photons may decay to excited states that subsequently decay to SM particles inside the detector, leading to vetoed events. To analyse this effect, we developed a Mathematica®-based event simulation.[8] Events are generated in the centre-of-mass frame and boosted to the lab frame. We sample the dark photon production cross section $\sigma(e^+e^- \to \gamma A')$ and simulate its decays into χ and χ^* with the appropriate branching ratios.[9] If a χ^* is produced, we sample its decay length and channel. Tree-level cross sections and branching ratios are calculated analytically, with VMD used for $\chi^* \to \chi\pi^+\pi^-$. We neglect three-body kaon channels and higher-multiplicity decays since they are subdominant in the mass range of interest—see section 4.1. Following Ref. [3], charged pions are treated as muons for the detector response.

To derive constraints, we rescale the existing limits on invisibly decaying dark photons from BaBar and Belle II, $\epsilon_{\text{mono-}\gamma}$, to obtain the effective niDM sensitivity

[8] Available at https://github.com/gdvgarcia/MissingEnergyEEcolliders.

[9] Strictly speaking, $e^+e^- \to \gamma\chi\chi^*$ should not be factorised into production and decay, since the A' width is non-negligible. However, this mainly smears the photon and χ^* energies and is negligible within our accuracy goals [3].

ϵ_{niDM}. We compute the fraction of vetoed events,

$$R_{\text{veto}} = \frac{N_{\text{vetoed}}}{N_{\text{photon-only}}}, \tag{4.23}$$

and use it to rescale the sensitivity as

$$\epsilon_{\text{niDM}} = \frac{\epsilon_{\text{mono-}\gamma}}{\sqrt{1 - R_{\text{veto}}}}\,. \tag{4.24}$$

Since R_{veto} itself depends on ϵ_{niDM}, the above equation is an implicit definition and numerical results have to be computed iteratively.

Details of the selection criteria at BaBar and Belle II are given in appendix D. There we also validate our simulation by reproducing published iDM results from Ref. [3], finding good agreement.

4.4.4 Dark Matter scattering searches

If dark photons are produced in collisions and followed by invisible decays, they give rise to a flux of relativistic DM particles (both χ and χ^*) traversing downstream detectors. Such particles can scatter on the detector material, producing visible signals. Measurements from LSND [279, 556], E137 [483, 557], and MiniBooNE [506] have placed strong constraints on light DM with masses below a few hundred MeV. We adopt the bounds of Ref. [280], obtained by rescaling published results to the appropriate α'. These apply to our model independently of (δ_y, Δ_m) in the parameter ranges considered, since $\chi^{(*)}$ are produced with highly relativistic energies, much larger than the mass splitting between states.

4.5 The influence of a light dark Higgs

Before proceeding, we comment on the possible impact of a non-decoupled dark Higgs h' in the mass spectrum of our theory. For $m_{h'} \gtrsim 1.5\, m_\chi$ (a requirement for a predictive freeze-out scenario), we find that corrections to our bounds from colliders and fixed-target experiments are typically at the 25% level (and up to 40% for scattering searches, which is comparatively less relevant for our conclusions).[10] Neglecting h' in our main analysis is therefore a good approximation, and these corrections do not affect our main conclusions. Nevertheless, h' may open up additional search channels—for instance, through visible decays when $m_{h'} > 2m_\mu$ (see chapter 7)—which merit further dedicated study.

We now briefly summarize how the dark Higgs may affect the different classes of experiments considered in our analysis.

[10] A dedicated study assuming both the dark photon and the dark Higgs to decay fully invisibly was performed in Ref. [558], finding corrections below the 5% level.

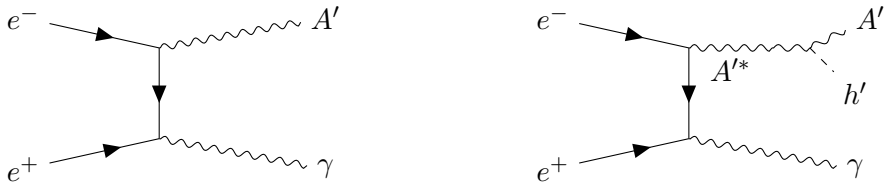

Figure 4.5: Representative tree-level contributions to mono-photon production in e^+e^- collisions. Left: standard dark-photon channel, $e^+e^- \to \gamma\, A'$. Right: same, with final-state radiation of a dark Higgs boson from the dark-photon line. Loop corrections do not modify such production decomposition based on the final-state particles.

Mono-photon searches at electron–positron colliders

Since the scalar portal coupling to the light SM particles relevant for our analysis is far too small to yield observable rates (additionally, one can always assume $\theta_{h'h} \ll \epsilon$), we only need to consider events mediated through the dark photon.

The total number of mono-photon events can be written decomposed as

$$N_\gamma = N_a + N_b + \dots \,, \tag{4.25}$$

corresponding to the representative tree-level diagrams shown in fig. 4.5—loop corrections would not modify this production decomposition. Since the dark photon is the only relevant portal, the number of events is proportional to the number of dark photons produced,

$$N_\gamma \propto N_{A'} \equiv \epsilon^2 n \,, \tag{4.26}$$

where $N_{A'}$ denotes the total dark photon yield.

We introduce a suppression factor $f_a \leq 1$ for N_a events, which accounts for possible χ^* decays inside the detector that would veto the corresponding mono-photon signal. For N_b, additional suppression arises from the three-body phase space (f_3) and the off-shell propagator at the dark photon vertex (f_*). Furthermore, the emission of an extra h' reduces the boost of the $\chi^{(*)}$, thereby increasing the probability that the excited state decays inside the detector, suppressing the mono-photon signal even further ($f_b \leq f_a$).[11]

Collecting these effects, we define

$$N_a = f_a\, \epsilon^2 n_a \,, \qquad N_b = f_a f'\, \epsilon^2 n_b \,, \qquad f' \equiv \frac{f_3 f_* f_b}{f_a} < 1 \,. \tag{4.27}$$

[11] Dark Higgs bosons can also decay visibly inside the detector (or into χ^* which then decays visibly), further reducing the mono-photon yield. These effects are absorbed into f_b, which further justifies the inequality $f_b \leq f_a$.

From the diagrams in fig. 4.5, one expects $n_b \approx \alpha' n_a$, provided that channels with additional dark Higgs final states are not strongly kinematically suppressed (i.e. $m_{A'} + m_{h'} \ll \sqrt{s}$). The experimental bound $N_\gamma < N_{\rm exp}$ can thus be written as

$$f_a \epsilon^2 n_a (1 + f' \alpha') + \cdots < N_{\rm exp} \,, \tag{4.28}$$

where the ellipsis denotes higher-multiplicity production modes. Neglecting these subdominant contributions, we obtain

$$\epsilon < \frac{\epsilon_{\rm exp}^{{\rm no}\, h'}}{\sqrt{1 + f' \alpha'}} \,, \tag{4.29}$$

with $(\epsilon_{\rm exp}^{{\rm no}\, h'})^2 \equiv N_{\rm exp}/(f_a n_a)$. We see that the actual bounds are expected to become relatively stronger than those without the inclusion of the dark Higgs in the analysis. In particular, for $\alpha' = 0.5$, this implies that our estimates carry an uncertainty of less than 25% (assuming the conservative case $f' = 1$).

In principle, the kinematics of the two production channels could alter the above reasoning and lead to $f' > 1$. However, Ref. [558] has shown that such final-state radiation effects have only minor impact, which further supports the robustness of our approximation.

NA64 missing energy

At NA64, dark Higgs bosons can also be produced via final-state radiation from Bremsstrahlung-generated dark photons, and subsequently escape detection, thereby increasing the number of missing energy events. If, however, the h' or its decay products deposit energy in the detector or veto system, these additional events are suppressed. Taking into account analogous suppression factors (f_3, f_*, f_b), the overall modification to our bounds is again expected to remain below 25%. Moreover, these estimates are even more robust than in the e^+e^- collider case, since at beam-dump experiments the final-state particles are highly boosted in the forward direction, making the details of production kinematics less relevant. In addition, NA64 is an active beam dump experiment, thus fully covering the interaction point, which further reduces possible losses of decay products.

Scattering

For scattering signatures, additional events may arise from channels producing $\chi^{(*)}$ together with a dark Higgs h'. In this case, one expects $f_a \simeq f_b$, since we now focus on scattering in the far-forward direction, where the dominant suppression originates from the interaction cross section, while both channels yield similarly energetic DM particles. Following eq. (4.28), the presence of h'

leads to a relative increase of approximately $2f_* f_3 \alpha'$ in the number of events if h' decays visibly, and $\approx 4f_* f_3 \alpha'$ if h' decays into $\chi^{(*)}$ pairs. Scatterings involving h' itself are strongly Yukawa-suppressed and are therefore neglected. We thus expect our estimates to be reliable at the 40% level if h' decays visibly, and up to 70% if it decays predominantly invisibly into DM states before reaching the detector. Although these uncertainties are relatively large, scattering bounds only probe DM masses up to $m_\chi \lesssim 300$ MeV and therefore do not affect the main conclusions of this work. Moreover, in our benchmark scenario we expect h' to decay visibly due to perturbative unitarity—see chapter 6.

Beam dump experiments

In proton beam dump setups, the situation is analogous to scattering, but with an additional factor of 1/2 for extra events due to h', since only excited states contribute to these searches.[12] Thus, including the dark Higgs in the mass spectrum typically modifies our estimates by less than 25%. A special case arises if $m_{h'} > 2m_\mu$, where visible h' decays may occur inside the detector, opening up additional search channels. This primarily affects the region $m_\chi \gtrsim 100$ MeV, where beam dump experiments are in any case less constraining for the niDM thermal target—furthermore, extremely small $\theta_{h'h}$ values can be used to avoid such signatures. A dedicated study of h' decays would be required to obtain a complete picture in this mass range.

Summary

In summary, although the dark Higgs can affect individual experimental signatures, its overall impact on our constraints remains below the 25% level. The main conclusions on the viability of the niDM parameter space—presented in the next section—are therefore robust.

4.6 Results

Having discussed the different experiments capable of probing the niDM model, we are now in a position to determine the allowed regions of parameter space. To illustrate the main features, we consider two benchmark DM masses, 200 and 500 MeV, and explore the (δ_y, Δ_m) plane, where δ_y denotes the dark left–right Yukawa asymmetry and Δ_m the relative mass splitting between dark fermions (see eq. (4.4)). These two masses were chosen to highlight the complementarity of different collider searches.

[12] The dark Higgs could in principle decay into excited states, but for our benchmark choices this would imply a breakdown of perturbativity (see chapter 6).

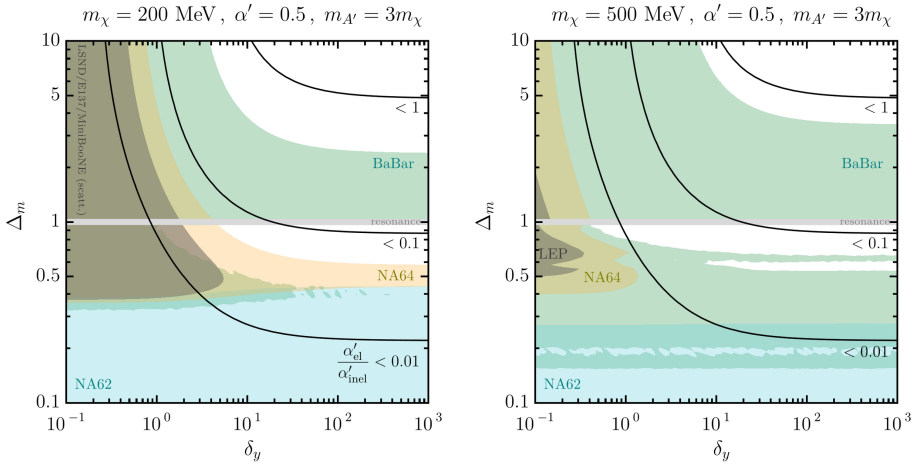

Figure 4.6: Excluded regions in the (δ_y, Δ_m) parameter plane where the kinetic mixing required to reproduce the observed DM relic abundance is inconsistent with experimental results. Black lines show the ratio of elastic (diagonal) to inelastic (off-diagonal) couplings. Reproduced from Ref. [89].

Figure 4.6 summarizes the constraints on the niDM parameter space. At each point in the (δ_y, Δ_m) plane we determine the value of the kinetic mixing parameter ϵ required to reproduce the observed DM relic abundance and then check whether this value is excluded by existing data. Shown in blue are the strongest constraints from proton beam dump experiments (NA62 [559]), in yellow those from active electron beam dumps via missing energy searches at NA64 [344], and in green those from mono-photon searches at BaBar [488]. In gray we indicate model-independent bounds on ϵ from electroweak precision measurements at LEP [494], as well as limits from DM scattering in far detectors (LSND, E137, and MiniBooNE) following Ref. [280]. The light gray bands mark the resonance condition $m_\chi + m_{\chi^*} = m_{A'} \pm 1\%$. Black lines indicate contours of constant ratio of diagonal to off-diagonal couplings.

From fig. 4.6 we draw several conclusions. First, the traditional iDM regime with negligible diagonal interactions ($\delta_y \ll 1$ or $\Delta_m \ll 1$) is fully excluded for both DM masses and parameter ranges considered. At the other extreme, in the mDM regime ($\Delta_m \gg 1$ and $\delta_y \gg 1$), where the heavier state decouples and diagonal interactions dominate, all current constraints can be satisfied. For intermediate values, the BaBar bound strengthens as Δ_m approaches 1 from above, since the production of the correct DM abundance requires larger values of ϵ.

For $\Delta_m < 1$, however, BaBar constraints are significantly weakened. This is because the decay $A' \to \chi\chi^*$ opens up, and the subsequent χ^* decays often lead to event vetoes in the missing-energy analysis. Sizable allowed parameter regions therefore emerge for $\Delta_m \sim 0.6$–0.9 and $\delta_y \gtrsim 1$. This corresponds precisely to

the not-so-inelastic regime, where diagonal interactions shape the relic density, while off-diagonal interactions control laboratory signatures.

The prospects for testing this parameter space in the near future are promising. NA62, running in proton beam dump mode, aims to collect $\sim 10^{18}$ protons-on-target by 2025 [552]. Because the sensitivity scales only logarithmically with intensity, we expect modest improvements compared to current results [504]. Much more significant progress is anticipated from Belle II [91], which has already accumulated more than 424 fb^{-1} of data [560] and, even with only ~ 20 fb^{-1}, could surpass BaBar and cover essentially all unexplored regions in the (δ_y, Δ_m) plane. Additional advances are expected from NA64, which continues to increase its electron-on-target dataset toward a target of 10^{13} EoT within the next decade [561].

The impact of these improvements is more transparent in the (m_χ, ϵ) plane shown in fig. 4.7. Different rows correspond to different values of Δ_m, while columns correspond to different choices of δ_y, selected to lie within the most interesting regions of parameter space. The solid black curve indicates the ϵ value required for the observed relic abundance; the dashed black curve shows the corresponding iDM prediction ($\delta_y = 0$ with the same Δ_m). Projected sensitivities of the various ongoing experiments are shown as dashed colored lines. We find that collecting 10^{18} PoT at NA62 would only marginally strengthen the lower bound on ϵ, whereas NA64 could reduce the upper bound by more than a factor of three. The most decisive improvements are expected from Belle II, which will probe the relic density line up to $m_\chi \sim 3$ GeV for all parameter choices considered. Further gains may come from upcoming NA64 searches with high-energy muon beams, which are projected to cover dark photon masses up to 3 GeV with a reach comparable to the Belle II mono-photon analysis [555].

Finally, in addition to collider bounds, we show in fig. 4.7 the exclusions from the LZ DD experiment [267], which probes $m_\chi \gtrsim 7$ GeV and is therefore highly complementary to collider searches. We also include projections for future DD facilities: the next-generation DARWIN [551], targeting the same heavy-mass region as LZ, and the near-future SuperCDMS [550], which extends sensitivity down to sub-GeV masses. For $\delta_y = 50$ we find an intriguing gap in coverage around $m_\chi \sim 5$ GeV, where DD experiments are challenged by the solar ^{8}B neutrino background [247]. Exploring strategies to fill this gap represents an exciting direction for future experimental efforts.

4.7 Concluding remarks

In this chapter we have investigated the consequences of relaxing parity conservation in the dark sector of fermionic inelastic Dark Matter (iDM) models with a vector mediator. Most of the existing literature assumes parity to be

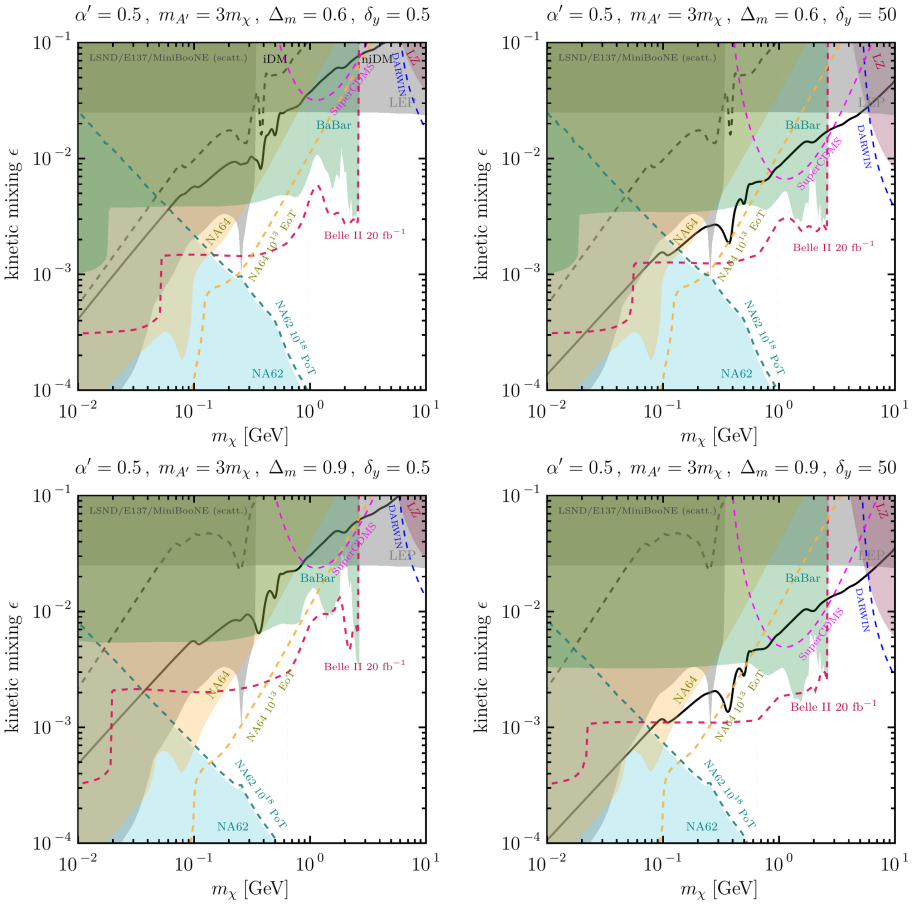

Figure 4.7: Current bounds and projected sensitivities to the kinetic mixing parameter ϵ as a function of the DM mass in the niDM model. Solid black curves show the relic density requirement for the chosen (Δ_m, δ_y) in each panel; dashed black curves indicate the iDM ($\delta_y = 0$) relic density with the same mass splitting. Reproduced from Ref. [89].

conserved (or only weakly broken), but as we have shown, this assumption is not necessary. Allowing for sizeable parity breaking not only preserves the attractive features of iDM but also opens up new, viable parameter space. We refer to this generic extension as "not-so-inelastic Dark Matter" (niDM), in which elastic (diagonal) interactions $\chi X \to \chi X$ occur alongside the inelastic (off-diagonal) processes $\chi X \to \chi^* X$. As in conventional iDM, the excited state χ^* can yield distinctive decay signatures at laboratory experiments.

We have explored a UV-complete realization of niDM with fermionic DM charged under a broken abelian gauge symmetry, which was introduced in chapter 3. The connection to the SM is provided by the traditional kinetic mixing of the dark photon A' with the SM photon (see section 2.5). This framework naturally interpolates between the iDM limit ($\delta_y \to 0$) and the Majorana DM

(mDM) limit where the heavier state decouples. The phenomenology is governed primarily by the fermion mass splitting Δ_m and the left–right asymmetry parameter δ_y. The not-so-inelastic regime of interest is characterized by $\Delta_m \sim 1$ and $\delta_y \gtrsim 1$. While the pure iDM limit is tightly constrained and largely excluded, we showed that allowing for parity breaking (that is, a non-zero δ_y) opens up new thermal freeze-out solutions consistent with all existing bounds. For our benchmark setup, two DM mass windows remain viable: $m_\chi \simeq 400$ MeV and $m_\chi \simeq 5$ GeV.

We then explored the phenomenology of these regions in detail. At higher masses ($m_\chi \sim 5$ GeV), direct detection experiments such as LZ, and in the future SuperCDMS and DARWIN, offer potential sensitivity. However, we find that the relic density curve lies in the region obscured by the solar ^{8}B neutrino background, leaving a challenging gap in experimental coverage. Identifying new strategies to probe this region remains an important direction for future work.

In the sub-GeV regime, collider and beam-dump experiments provide the most powerful probes. Production and subsequent decay of the excited state leads to distinctive signatures, which we simulated and recast across a wide range of facilities: proton beam dumps (NuCal, CHARM, BEBC, NA62), active electron beam dumps (NA64), and e^+e^- colliders (BaBar, Belle II). We found that existing data exclude large parts of parameter space, but leave open a window around $m_\chi \simeq 400$ MeV for suitable (Δ_m, δ_y). Importantly, this window will be fully tested in the near future: Belle II mono-photon searches and upcoming NA64 analyses are expected to cover the entire viable parameter space for sub-GeV niDM. In addition, missing energy searches with high-energy muon beams at NA64 promise sensitivity up to $m_{A'} \sim 3$ GeV, potentially reaching beyond the coverage of electron beam dump setups.

To summarize, this chapter has shown that the vector-portal realization of niDM retains the advantages of both iDM and mDM, while avoiding some of their strongest constraints, thereby reopening parameter space for thermal DM in the sub-GeV and few-GeV mass ranges. While our analysis here focused on the vector portal—the most extensively studied mediator in the sub-GeV DM literature—we will see in the following chapters that similar conclusions can be drawn for scalar mediators and for scenarios where both portals are present. Together, these cases broaden the phenomenology of not-so-inelastic dark matter and establish it as a robust framework for thermal dark matter.

Chapter 5

Not-so-inelastic Dark Matter: the scalar portal

Having analyzed the case where the dark sector communicates with the SM through the vector portal—the most commonly studied setup in the inelastic Dark Matter (iDM) literature—we now turn to scenarios where the scalar portal provides the dominant connection.[1] In contrast to the purely vector-mediated case, removing the vector portal altogether does not render the theory inconsistent. The essential ingredient for generating two fermionic DM states with a mass splitting, and hence a non-trivial flavor structure as required in not-so-inelastic Dark Matter (niDM) models, is the presence of Majorana mass terms, which can naturally arise from couplings to a dark scalar.

In this chapter, rather than building directly on the general niDM framework introduced in chapter 3 and fixing a maximal $\mathcal{CP}$-violating phase $\phi_d = \pi/2$, we adopt a different but equivalent perspective. We construct a minimal setup with a Dirac fermion χ_D coupled to a real pseudoscalar field a. In the limit where the parity-violating parameter vanishes, this setup preserves all discrete symmetries ($\mathcal{C}$, $\mathcal{P}$, and $\mathcal{T}$). Throughout this chapter, we will work close to this nearly $\mathcal{CP}$-conserving limit. Importantly, this formulation avoids the need for introducing an additional dark $U(1)'$ gauge force.

Scalar portal models are notoriously constrained in the sub-GeV mass range. In this regime, reproducing the observed DM abundance through thermal freeze-out would require unreasonably large scalar mixing with the SM Higgs, while stringent experimental bounds further reduce the available parameter space (see section 2.5). Consequently, the scalar portal can provide a viable thermal DM candidate only at masses above roughly 10 GeV. At these higher masses, however, direct detection limits become extremely stringent, making predictive scalar-mediated thermal DM scenarios particularly difficult to realize.

In the framework developed here, we construct a scalar portal model in which

[1] The material in this chapter is fully based on Ref. [93].

interactions are dominantly inelastic (off-diagonal). Such behavior requires parity violation in the dark sector, since in a parity-conserving scenario the interactions would instead be purely elastic (diagonal). This mechanism suppresses the otherwise dominant elastic scattering channels and thereby relaxes the stringent constraints from direct detection. As we will argue, this setup constitutes one of the most minimal realizations of fermionic iDM found in the literature. In what follows, we compute the direct detection limits from LZ [267], estimate the future reach of DARWIN [94], and analyze complementary constraints from collider experiments, perturbative unitarity, and cosmology, ultimately showing that our scalar portal niDM scenario provides an ideal target for upcoming direct detection searches.

The remainder of this chapter is structured as follows. In section 5.1, we introduce the scalar portal framework for niDM and discuss its relation to the SM. We then study the decay modes of the excited state and the theoretical constraints from perturbative unitarity. In section 5.2, we analyze the DM relic abundance via thermal freeze-out. Indirect and direct detection bounds, arising from both elastic and inelastic interactions, are presented in section 5.3. Collider constraints, primarily from precision Higgs measurements, are discussed in section 5.4. We then combine these results with relic abundance requirements and cosmological considerations in section 5.5, before concluding in section 5.6. Appendix E provides a brief discussion of the methods used to compute the DM relic abundance in this chapter.

5.1 A new minimalistic model

The simple WIMP model of a fermionic DM coupled to a dark Higgs mediator in a $\mathcal{CP}$-conserving setup [562] is essentially ruled out by direct detection constraints in the visible freeze-out regime, where the relic abundance is thermally generated through DM annihilation into SM particles ($\mathrm{DM\,DM} \leftrightarrow \mathrm{SM\,SM}$) [330]. One proposed remedy is to replace the scalar mediator with a pseudoscalar (the so-called Coy Dark Matter scenario), or alternatively, to introduce sizable CP violation in the dark sector [326, 356, 357]. However, these solutions come at the cost of suppressing the prospects for probing DM in direct detection experiments [563, 564], and they additionally face stringent indirect detection bounds for DM masses below 10–100 GeV [565].

In this analysis, we pursue a different route: we substitute the usual Dirac-type Yukawa couplings ($\bar{\chi}\chi$) in the dark sector with Majorana-type Yukawas ($\bar{\chi^c}\chi$), which are often neglected in simple singlet extensions of the SM. Allowing for a small breaking of parity then transforms the setup into one of the most minimal realizations of iDM [69], where indirect detection limits can be naturally avoided due to the efficient depletion of the heavier state, e.g. through its decays.

Indeed, iDM models commonly found in the literature are realized in a variety of more complex ways: via the vector portal, which introduces a new $U(1)$ gauge boson together with a symmetry-breaking mechanism (typically a dark Higgs mechanism); through non-renormalizable portal operators; or by extending the SM with a larger number of new particles—see Refs. [70, 417, 418, 420, 432, 465, 476, 477]. By contrast, we show that introducing only a single real pseudoscalar acquiring a vacuum expectation value (vev) suffices to build a UV-complete fermionic iDM model, provided that the dark sector exhibits a small but non-zero amount of parity violation. Owing to its minimality, we will refer to this setup as *minimal-inelastic Dark Matter* (miDM).[2]

The miDM framework developed here features a predictive visible freeze-out regime, testable by upcoming direct detection experiments such as DARWIN, and subject to complementary cosmological probes from Big Bang Nucleosynthesis (BBN) and the Cosmic Microwave Background (CMB), as well as collider searches at the LHC. In the remainder of this section, we introduce the model in detail and clarify its relation to the niDM setup discussed in chapter 3.

5.1.1 The framework

We consider a real pseudoscalar field A with a nonzero vacuum expectation value (vev) $\langle A\rangle = w$, and a Dirac fermion $\chi_D = \chi_L + \chi_R$, where both fields are singlets under all SM gauge groups. To reduce the number of allowed terms in the Lagrangian, we impose a Z_4 symmetry,

$$\chi \to i\chi\,, \qquad A \to -A\,, \tag{5.1}$$

under which the most general Lagrangian consistent with the SM gauge group and the Z_4 symmetry can be written as

$$\mathcal{L}_{\rm NP} = \mathcal{L}_\chi + \mathcal{L}_A\,, \tag{5.2}$$

with

$$\mathcal{L}_\chi = \bar\chi(i\partial\!\!\!/ - m_d)\chi - \frac{1}{\sqrt{2}}\, y\, A\, \bar{\chi^c}\,(\delta_P + \gamma_5)\chi + \text{h.c.}\,, \tag{5.3}$$

$$\mathcal{L}_A = \frac{1}{2}(\partial^\mu A)(\partial_\mu A) + \frac{\mu_a^2}{2}A^2 - \frac{\lambda_a}{4}A^4 - \frac{\lambda_{ah}}{2}A^2|H|^2\,, \tag{5.4}$$

where H denotes the SM Higgs doublet, and charge conjugation is defined by $\psi^c = C\gamma_0^T\psi^*$ with C the charge conjugation matrix.

[2] A related model was discussed in Ref. [440] in the context of the INTEGRAL/SPI 511 keV line, though their focus was on the $\mathcal{CP}$-conserving regime and a secluded freeze-out scenario rather than the predictive visible freeze-out considered here. Other minimal (n)iDM constructions exist for scalar DM [441, 566], though their iDM limits are typically less natural.

If $\delta_P = 0$ and y is real, both $\mathcal{P}$ and $\mathcal{CP}$ are exact symmetries of the Lagrangian, in which case the setup reduces to a Coy Dark Matter model [356]. In what follows, we instead allow for a small real parity-breaking parameter $\delta_P = \delta_P^* \ll 1$ together with a real Yukawa coupling y.[3] The origin of a small non-zero δ_P could lie in a fully $\mathcal{CP}$-conserving extension of the dark sector where parity violation is radiatively induced by interactions with the SM weak sector. Here, however, we remain agnostic about its origin and focus instead on its phenomenological consequences.

Adopting the unitary gauge, we expand

$$A = a + w\,, \qquad H = \frac{1}{\sqrt{2}}(0,\, h + v)^T\,, \tag{5.5}$$

where $v = 246$ GeV is the SM Higgs vev. The fermion mass terms then take the form

$$\mathcal{L}_\chi \supset -m_d \bar{\chi}_L \chi_R + \frac{1}{2} m_L \bar{\chi}_L^c \chi_L - \frac{1}{2} m_R \bar{\chi}_R^c \chi_R + \text{h.c.}\,, \tag{5.6}$$

with Majorana masses related to the Yukawa couplings by $m_{L/R} = 2 y_{L/R} w$ and $y_{L/R} = y(1 \mp \delta_P)/\sqrt{2}$. It is technically natural to have $w \ll m_d$, in which case we define

$$\delta_d \equiv \frac{m_L}{m_d} \propto \frac{w}{m_d} \ll 1\,. \tag{5.7}$$

To obtain nearly off-diagonal couplings of the DM states to the dark pseudoscalar, following table 3.3, one requires $\delta_i \ll 1$. Thus, eq. (5.7) together with $\delta_P \ll 1$ allows us to systematically expand in both δ_d and δ_P. Unless otherwise specified, all results below are given at leading order in these parameters, while numerical results include the full dependence on δ_i.

After diagonalizing the fermion mass terms, the Lagrangian becomes

$$\mathcal{L}_\chi = \frac{1}{2}\bar{\chi}_i (i\partial\!\!\!/ - m_i)\chi_i - \frac{1}{2} y_L\, a\, \bar{\chi}_i \big(\alpha_{ij} + i\beta_{ij}\gamma^5\big)\chi_j\,, \tag{5.8}$$

with Majorana masses

$$m_{\chi^{(*)}} = m_d \left(1 + \frac{1}{2}\delta_d\big(\delta_d \mp 2\delta_P\big)\right)\,, \tag{5.9}$$

and normalized mass splitting

$$\Delta_m \equiv \frac{m_{\chi^*} - m_\chi}{m_\chi} = 2\delta_d \delta_P\,. \tag{5.10}$$

The interaction coefficients are collected in table 5.1, where "$*$" denotes the excited state and "$-$" the ground state. From eq. (5.10), it is evident that parity

Table 5.1: Coupling coefficients of dark fermions to the dark pseudoscalar in the limit $\delta_i \ll 1$.

$\alpha_{**} = 2(\delta_d + \delta_P + \Delta_m + \delta_P^2)$	$\beta_{**} = 0$
$\alpha_{*\text{-}} = 0$	$\beta_{*\text{-}} = 2 + 2\delta_P + 2\delta_P^2 - \delta_d^2$
$\alpha_{\text{-}*} = 0$	$\beta_{\text{-}*} = \beta_{*\text{-}}$
$\alpha_{\text{--}} = 2(\delta_d - \delta_P + \Delta_m - \delta_P^2)$	$\beta_{\text{--}} = 0$

conservation ($\delta_P = 0$) implies $\Delta_m = 0$, i.e. the two states are degenerate and only elastic interactions remain.

Defining the dark Yukawa fine-structure constant $\alpha_y = y^2/4\pi$, the effective elastic and inelastic constants read

$$\alpha_{\text{el-}} = \alpha_y \alpha_{\text{--}}^2 \,, \qquad \alpha_{\text{el}*} = \alpha_y \alpha_{**}^2 \,, \qquad \alpha_{\text{inel}} = \alpha_y \beta_{*\text{-}}^2 \,. \tag{5.11}$$

A notable feature from the coupling structure in table 5.1 is that the diagonal couplings differ between ground and excited states, as in the i2DM scenario [478]. This allows mediator decays into two excited states, potentially leading to striking signatures such as double displaced vertices—see chapter 7.

Finally, interactions with the SM arise from a mass mixing between A and H, induced by the λ_{ah} term in $\mathcal{L}_A$. The mixing angle θ is given by[4]

$$\tan 2\theta = \frac{\lambda_{ah} v w}{\lambda_h v^2 - \lambda_a w^2} \,, \tag{5.12}$$

such that the physical pseudoscalar $\hat{a}$ couples to SM states and the SM Higgs $\hat{h}$ couples to dark fermions, both with couplings suppressed by $\sin\theta$. The corresponding scalar mass eigenvalues can be found in section 2.5, where a more detailed discussion of the scalar portal is also provided. For simplicity, we will continue to denote the SM-like scalar by h and the dark pseudoscalar by a.

As a final remark, promoting the pseudoscalar A to a complex field would instead allow for a global $U(1)$ continuous symmetry in place of the discrete Z_4. If this symmetry were gauged, one would effectively recover the niDM model of chapter 3 upon shifting the pseudoscalar into a scalar and introducing a maximal phase $\phi_d = \pi/2$ for the Dirac mass. Such a $U(1)$ symmetry would simplify the Lagrangian in a manner similar to the considered Z_4, but analyzing the consequences of the associated Nambu–Goldstone boson or of a new gauge boson goes beyond the scope of this chapter. To make the correspondence with chapter 3 explicit, we identify

$$\delta_y \equiv \frac{2\delta_P}{1-\delta_P} \,, \qquad y_L^{(\text{chap. 3})} \equiv \frac{1}{\sqrt{2}} y_L^{(\text{chap. 5})} \,. \tag{5.13}$$

[3] We assume δ_P real for simplicity. A complex value would lead to similar phenomenological consequences, except that $\mathcal{CP}$ is restored for an imaginary δ_P for a real y.

[4] In this chapter we denote the scalar mixing simply by θ, since there is no risk of confusion with the dark-fermion mixing angle introduced in previous chapters.

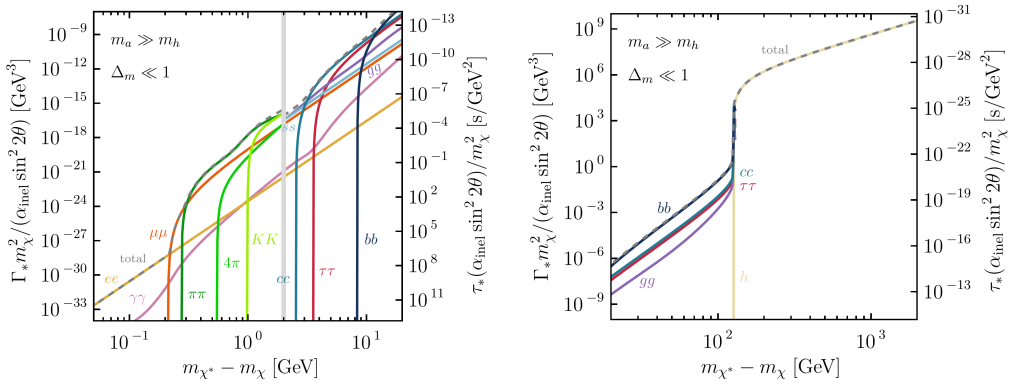

(a) Light mass splittings. **(b)** Heavy mass splittings.

Figure 5.1: Total decay width of the excited state, Γ_* (dashed gray), and partial widths $\Gamma(\chi^* \to \chi\mathcal{F})$ into selected SM final states $\mathcal{F}$ (solid colors), shown for (a) small and (b) large mass splittings. Only the dominant modes are presented. The right-side vertical scale indicates the corresponding lifetime τ_*. The light gray band at $\Delta_m m_\chi = 2$ GeV marks the region where neither dispersive analyses nor perturbative spectator models are reliable [331, 568, 571], resulting in the discontinuity of the total width. For Higgs final states, we approximate $\cos\theta \approx 1$. Reproduced from Ref. [89].

5.1.2 Excited Dark Matter decays

If kinematically accessible, decays into the mediator would dominate the width of the excited state Γ_*. However, in the miDM framework the mass splitting is naturally small, $\Delta_m \ll 1$, such that $\chi^* \to 3\chi$ is always forbidden, while $\chi^* \to \chi a$ is inaccessible in the visible freeze-out regime (DM DM $\leftrightarrow$ SM SM). Consequently, decays into SM final states are of central importance, and we compute the corresponding partial widths shown in fig. 5.1.[5]

Loop-induced decays into photons [567] and gluons [568, 569] (with $\alpha_s(s)$ from [138]) as well as non-perturbative decays into mesons [568] are obtained from the standard results for dark Higgs decays, through the amplitude relation [6]

$$\overline{|\mathcal{M}|^2}(\chi^* \to \chi\, 2\mathcal{F}) = \frac{\beta_e}{\beta_\mathcal{F}} \frac{\Gamma_{a^* \to 2\mathcal{F}}}{\Gamma_{a^* \to 2e}} \overline{|\mathcal{M}|^2}(\chi^* \to \chi\, 2e)\,, \tag{5.14}$$

where $2\mathcal{F}$ denotes a SM fermion–antifermion or boson–antiboson pair, and $\beta_\mathcal{F}^2 = m_{2\mathcal{F}}^2 - 4m_\mathcal{F}^2$, with $m_{P_1P_2}$ the invariant mass of the pair. The decay width Γ_{a^*} corresponds to that of an off-shell pseudoscalar with effective mass $m_{2\mathcal{F}}$.

[5] We neglect the reduced phase space due to confinement effects: for instance, charm (bottom) production requires $\Delta m\, m_\chi > 2m_D$ ($2m_B$), rather than simply $2m_c$ ($2m_b$).

[6] As emphasized in [570], hadronic decay rates suffer from sizable uncertainties that must be considered for precise cosmological studies of miDM.

In the perturbative regime, the decay width into light fermions, $2m_f < \Delta_m m_\chi \ll m_\chi$, takes the form

$$\Gamma_*(\chi^* \to \chi \bar{f} f) \approx N_c \frac{\alpha_{\rm inel} \sin^2 2\theta}{560\pi^2} \frac{m_f^2}{v^2} \frac{(\Delta_m^2 - \tau_f^2)^4}{\Delta_m + \tau_f} \left(\frac{1}{m_h^2} - \frac{1}{m_a^2}\right)^2 m_\chi^5 , \quad (5.15)$$

with $N_c = 3$ (1) for quarks (leptons) and $\tau_f = 2m_f/m_\chi$.

For very light dark scalars, $m_a < \Delta_m m_\chi \ll m_\chi$, the two-body decay $\chi^* \to \chi\, a$ opens up. In this case, for $\theta \ll y$,

$$\Gamma_* \approx \frac{1}{2} \alpha_{\rm inel} \cos^2\theta \left(\Delta_m^2 - \frac{m_a^2}{m_\chi^2}\right)^{3/2} m_\chi \, . \quad (5.16)$$

Considering $m_\chi \in [10, 10^4]$ GeV, for $m_a \ll m_h$ and couplings typical of freeze-out ($\theta, y \gtrsim 10^{-1}$), the excited state lifetime falls well below one second once the splitting exceeds the kaon threshold,

$$\Delta_m m_\chi > 2m_K \, .$$

For heavier dark scalars, $m_a \gg m_h$, this happens above the B-meson threshold,

$$\Delta_m m_\chi > m_B \, .$$

In these regimes, cosmological abundances of χ^* are negligible. By contrast, for $m_a \simeq m_h$, destructive interference between the two scalar portals may render χ^* long-lived, in which case a dedicated relic abundance analysis would be necessary.

5.1.3 Perturbative Unitarity

Visible freeze-out requires

$$m_a \simeq \sqrt{2\lambda_a}\, w > m_\chi \simeq m_d \, . \quad (5.17)$$

At the same time, suppressing diagonal couplings demands $\delta_d \ll 1$, i.e. $\sqrt{2}\, y_L w \ll m_d$. Taken together, these conditions tend to push λ_a to large values, potentially violating perturbativity. Following [330], we impose

$$3(\lambda_h + \lambda_a) \pm \sqrt{9(\lambda_h - \lambda_a)^2 + \lambda_{ha}^2} < 16\pi \, , \quad (5.18)$$

ensuring perturbative unitarity in $aa \to aa$ and $hh \to hh$ scattering.[7] We also exclude regions where the dark Yukawa becomes non-perturbative, $\alpha_y \geq 1$. These requirements already constrain much of the visible freeze-out parameter space.

[7] Stronger bounds could in principle be obtained by including additional processes [572].

For intuition on the allowed range of δ_d, consider first $\lambda_{ha} \simeq 0$ (hence $\theta \simeq 0$), for which eq. (5.18) simplifies to $\lambda_a < 8\pi/3$. Demanding $m_a > m_\chi$ then implies

$$\delta_d \gtrsim \sqrt{\frac{3}{8\pi}}\, y\,. \tag{5.19}$$

Note that we also take $\delta_P \ll 1$ throughout our analysis in order to suppress direct detection constraints.

Second, within the freeze-out approximation, the thermally averaged annihilation cross section is

$$\langle \sigma v \rangle \approx \frac{y_{\rm SM}^2 y^2 \theta^2}{16\pi m_\chi^2}\, e^{-x_f \Delta_m} \approx 10^{-10}\ \text{GeV}^{-2}\,, \tag{5.20}$$

where $y_{\rm SM}$ denotes the SM Higgs coupling to the heaviest SM state available for annihilation (simply taken $\mathcal{O}(1)$ for $m_\chi \gg$ GeV), and $x_f = m_\chi/T_f \simeq 20$ with T_f the freeze-out temperature. From this condition we estimate

$$\delta_d \gtrsim 0.25 \left(\frac{0.1}{\theta}\right) \left(\frac{m_\chi}{1\ \text{TeV}}\right) e^{10\Delta_m}\,. \tag{5.21}$$

This rough estimate indicates that $\alpha_{\text{el-}}$ cannot be arbitrarily suppressed in the visible freeze-out regime, since $\alpha_{\text{--}} \sim 2\delta_d$ (unless one fine-tunes $\delta_d \simeq \delta_P$). We therefore expect relatively large mixing angles, $\theta \gtrsim 0.1$, and small normalized mass splittings, $\Delta_m \lesssim 0.1$, to remain compatible with perturbativity.

In summary, theoretical consistency requires modest mass splittings, non-negligible diagonal couplings, and sizable Higgs–dark scalar mixing angles. This renders the model a highly predictive framework and a well-motivated target for experimental searches. These expectations will serve as guiding benchmarks for the numerical analysis of the relic abundance and the experimental constraints presented in the following sections.

5.2 Relic abundance

In order to predict the DM relic abundance, we have developed a dedicated Mathematica® package to solve the Boltzmann equations for the case of up to two DM particles in kinetic equilibrium with the SM during freeze-out (see appendix E for details).[8] The package also implements a refined freeze-out approximation, adapted to scenarios with two DM states, which allows us to efficiently generate the figures presented in this chapter. In practice, we compute the full numerical solution for a limited number of benchmark points in each figure,

[8] Since we consider large scalar mixing angles, kinetic equilibrium between DM and the SM should be preserved during freeze-out [394].

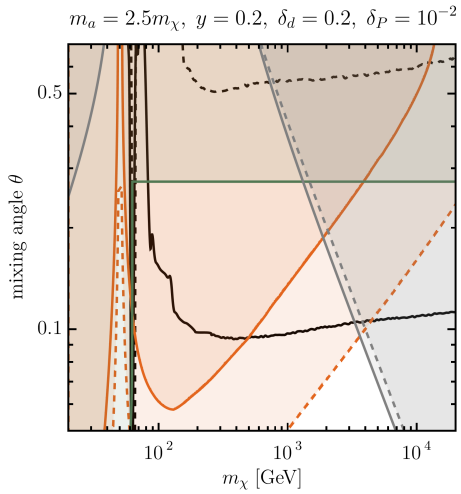

Figure 5.2: Values of the scalar mixing angle θ that reproduce the observed DM relic abundance $\Omega_{\rm DM}h^2 = 0.12$ as a function of the DM mass (black lines). The gray shaded regions correspond to perturbativity bounds. Higgs signal strength constraints from CMS and ATLAS [573, 574] are shown in green, while orange regions indicate the bounds from LZ [267]—see text for details. Solid lines correspond to the miDM scenario, while dashed ones correspond to the elastic scalar portal DM case. Reproduced from Ref. [89].

thereby controlling the accuracy of the freeze-out approximation and reducing its error.

To remain in a theoretically controlled regime, we restrict our study to DM masses $m_\chi \geq 10$ GeV, thereby avoiding non-perturbative QCD effects in the relic density calculation. Lighter masses are in any case expected to be excluded by a combination of existing experimental constraints and the strong Yukawa suppression of annihilations into light SM final states.

A key difference between miDM and the standard *elastic* scalar portal—the $\mathcal{CP}$-conserving Higgs-portal with Majorana DM which will be denoted simply by mDM in this chapter—is that the off-diagonal interactions in miDM allow for *s-wave coannihilations* into SM final states, $\chi\chi^* \to \text{SM}\,\text{SM}$. This is a feature it shares with pseudoscalar (Coy) DM, though in that case the s-wave applies directly to $\chi\chi$ annihilations. By contrast, mDM leads to p-wave–suppressed annihilations, $\chi\chi \to \text{SM}\,\text{SM}$. As a result, miDM can reproduce the observed relic density with smaller couplings than the standard scalar portal, thereby alleviating (though not removing) direct detection constraints while remaining predictive. To illustrate this point, fig. 5.2 compares the thermal targets of the elastic mDM scenario (dashed) and the (not-so-)inelastic miDM scenario (solid). As shown, miDM can evade current bounds while still lying within the reach of upcoming searches.

5.3 (In)direct detection

Indirect detection bounds from off-diagonal (inelastic) co-annihilation or from χ^* decays are negligible in the parameter region where the excited state lifetime is much shorter than a second. In this case, the abundance of χ^* during BBN or CMB is vanishingly small.[9] For $\tau_* \gtrsim 0.02$ s [442], the abundance of χ^* becomes non-negligible and its cosmological implications deserve a dedicated study. Bounds from energy injection during BBN are expected to be particularly stringent in such cases. One possible way to evade these limits would be to consider extremely long-lived states ($\delta_P \approx 0$), corresponding to late-universe decaying DM scenarios. We do not pursue this possibility further in the present work.

On the other hand, diagonal (elastic) annihilations are p-wave suppressed, leaving no relevant constraints from indirect detection on the annihilation cross section. Potential constraints could also arise from the visible decays of the pseudoscalar mediator. However, in the mass range of interest, $m_a \gtrsim 10$ GeV, and for the mixing angles considered, $\theta \gtrsim 10^{-2}$, we find $\tau_a \ll 0.02$ s, so the abundance of a is negligible already at the BBN epoch.

Turning to direct detection, inelastic scatterings are suppressed in two ways: kinematically, when the mass splitting exceeds the kinetic energy of DM in the halo ($\Delta_m \gtrsim v^2 \sim 10^{-6}$), and dynamically, since the pseudoscalar nature of the interaction generates only momentum-suppressed operators in the non-relativistic effective theory, in particular $\mathcal{O}_{10,11} \propto \vec{q}$ [256].[10]

By contrast, elastic couplings induce unsuppressed spin-independent cross sections for DM–nucleus scatterings, which are tightly constrained. The LUX-ZEPLIN (LZ) experiment [267] currently provides the strongest limits on such interactions, and the future DARWIN project [94] is expected to extend the reach further. Following ref. [330], the corresponding cross section reads

$$\sigma^{\mathrm{SI}} = \frac{\mu_{\chi N}^2 m_N^2 f_N^2 \alpha_{\text{el-}} \sin^2 2\theta}{v^2} \left(\frac{1}{m_h^2} - \frac{1}{m_a^2} \right)^2 , \tag{5.22}$$

where $\mu_{\chi N}$ is the reduced DM–nucleon mass, m_N the nucleon mass, and $f_N \simeq 0.3$ the effective Higgs–nucleon coupling [575]. The only way to relax these constraints is by suppressing $\alpha_{\text{el-}}$ sufficiently, which however conflicts with perturbativity. Consequently, much of the visible freeze-out regime consistent with perturbativity remains within the projected sensitivity of these detectors.

[9] See e.g. Ref. [454] for scenarios with large mass splittings, where indirect detection signals from iDM can arise.

[10] Off-diagonal couplings also induce loop-level spin-independent interactions. Results from Ref. [564], applicable in the $\Delta_m \ll 1$ limit, show that such loop contributions remain about an order of magnitude above the thermal target.

5.4 Colliders

Collider constraints on an invisibly decaying scalar portal ($m_a > 2m_\chi$), relevant for most of the visible freeze-out regime, arise primarily from precision Higgs measurements. Possible deviations of the Higgs properties in our model from those of the SM Higgs can be captured by a signal strength modifier μ, which rescales all production and decay modes of the SM-like Higgs uniformly while leaving branching ratios unchanged [331]. This behavior is precisely what is expected in the framework of our miDM model.

The combination of ATLAS and CMS measurements requires $\mu > 0.93$ at 95% CL [573, 574]. In our scalar mass-mixing scenario, μ takes the form [576]

$$\mu = \cos^2\theta \, \frac{\cos^2\theta \, \Gamma_h^{\mathrm{SM}}}{\cos^2\theta \, \Gamma_h^{\mathrm{SM}} + \Gamma_h^{\mathrm{dark}}} \,, \tag{5.23}$$

where $\Gamma_h^{\mathrm{SM}} = 4.1$ MeV [577] denotes the SM prediction for the total decay width of the Higgs, and Γ_h^{dark} is the partial width into dark-sector states. Equation (5.23) thus provides a generic constraint on our model that applies to either a visibly or an invisibly decaying pseudoscalar mediator, independent of specific search channels.

In this work, we will focus on constraints from Higgs signal strength measurements, since they dominate in the mass range $m_a \gtrsim 10$ GeV when a decays invisibly, which is particularly relevant for visible freeze-out [331]. Nonetheless, parts of the parameter space where a decays visibly ($m_a < 2m_\chi$) remain testable through direct searches for the mediator at ATLAS [574, 578], CMS [579], and LEP [580], illustrating the complementarity of different search strategies and the promising prospects offered by upcoming HL-LHC data—see the summary of constraints in section 2.5. Even in the invisibly decaying regime, additional signals may arise from the decays of the excited DM state, in close analogy to the vector portal scenario.

5.5 Results

In fig. 5.3, we present the combined constraints on the freeze-out parameter space. Each panel corresponds to a different choice of the mixing angle θ, the vev-Dirac mass ratio δ_d, and the parity-breaking parameter δ_P. For every pair of dark-sector masses (m_χ, m_a), the dark Yukawa coupling y is fixed by requiring the observed DM relic abundance to be produced via freeze-out. Opaque regions are currently excluded by experimental data or perturbativity, while shaded/hatched regions indicate projected sensitivities of future searches. The gray bands mark the resonant region $m_a \in (2 \pm 10\%)m_\chi$, where early kinetic decoupling is expected to affect the relic abundance calculation [78]. Overall,

we find that perturbativity imposes some of the strongest constraints across the parameter space.

In the *visible freeze-out regime*, perturbativity effectively rules out the limit of very small $\delta_d \ll 0.1$, forcing the Dirac mass scale m_d to be comparable to the dark vev w. As a consequence, elastic interactions remain relevant and subject to direct detection constraints. This was expected, since the dark scalar mass scales as $m_a \sim w \sim \delta_d m_d$ and must exceed the DM mass $m_\chi \sim m_d$ for freeze-out to occur through the visible channel. While the inelastic nature of miDM opens new viable regions, they are strongly bounded by perturbativity and will be almost fully covered by next-generation direct detection experiments. Only finely tuned configurations with $\delta_P \approx \delta_d$ can completely evade these bounds, and even then only for small values $\delta_i \lesssim 0.2$, as large normalized mass splittings are exponentially suppressed. Furthermore, small scalar mixing angles $\theta \lesssim 0.1$ are also excluded by a combination of perturbativity and the relic abundance requirement, making collider probes potentially relevant in this regime.

In the *secluded regime*, much larger portions of parameter space survive. Here, the dark scalar is naturally lighter than DM, so direct detection constraints can be relaxed by taking smaller δ_i. Nevertheless, Higgs signal strength measurements remain constraining and require $\theta \lesssim 10^{-2}$ to be avoided entirely. Importantly, wide regions of parameter space unconstrained by Earth-based experiments contain long-lived excited states with $\tau_* \gtrsim 0.02$ s [442], due to suppressed mass splittings. Such lifetimes can be in tension with BBN and CMB bounds, suggesting that cosmological probes may be decisive in testing this parameter space. Notably, reducing δ_i and θ to weaken terrestrial constraints tends to enlarge this cosmologically sensitive region, underscoring the complementarity between laboratory searches and cosmology.

In summary, visible freeze-out in miDM is highly predictive and testable in the near future, while the secluded regime remains more open but strongly linked to cosmological signatures. Together, these results highlight the balance between perturbativity, collider limits, direct detection, and cosmological probes in shaping the viable parameter space of the model.

5.6 Concluding remarks

We have introduced a renormalizable pseudo-Dirac dark matter (DM) model adopting a dark Higgs mechanism with a real pseudoscalar field, which simultaneously mediates DM–SM interactions via the scalar portal. The pseudo-Dirac nature is generated via a Majorana–Yukawa term ($\bar{\chi^c}\chi$) by allowing for parity breaking in the dark sector. In the case of small parity breaking, the diagonal couplings between dark fermions are suppressed, and the model realizes an inelastic DM (iDM) behavior. The absence of an extra massive gauge boson,

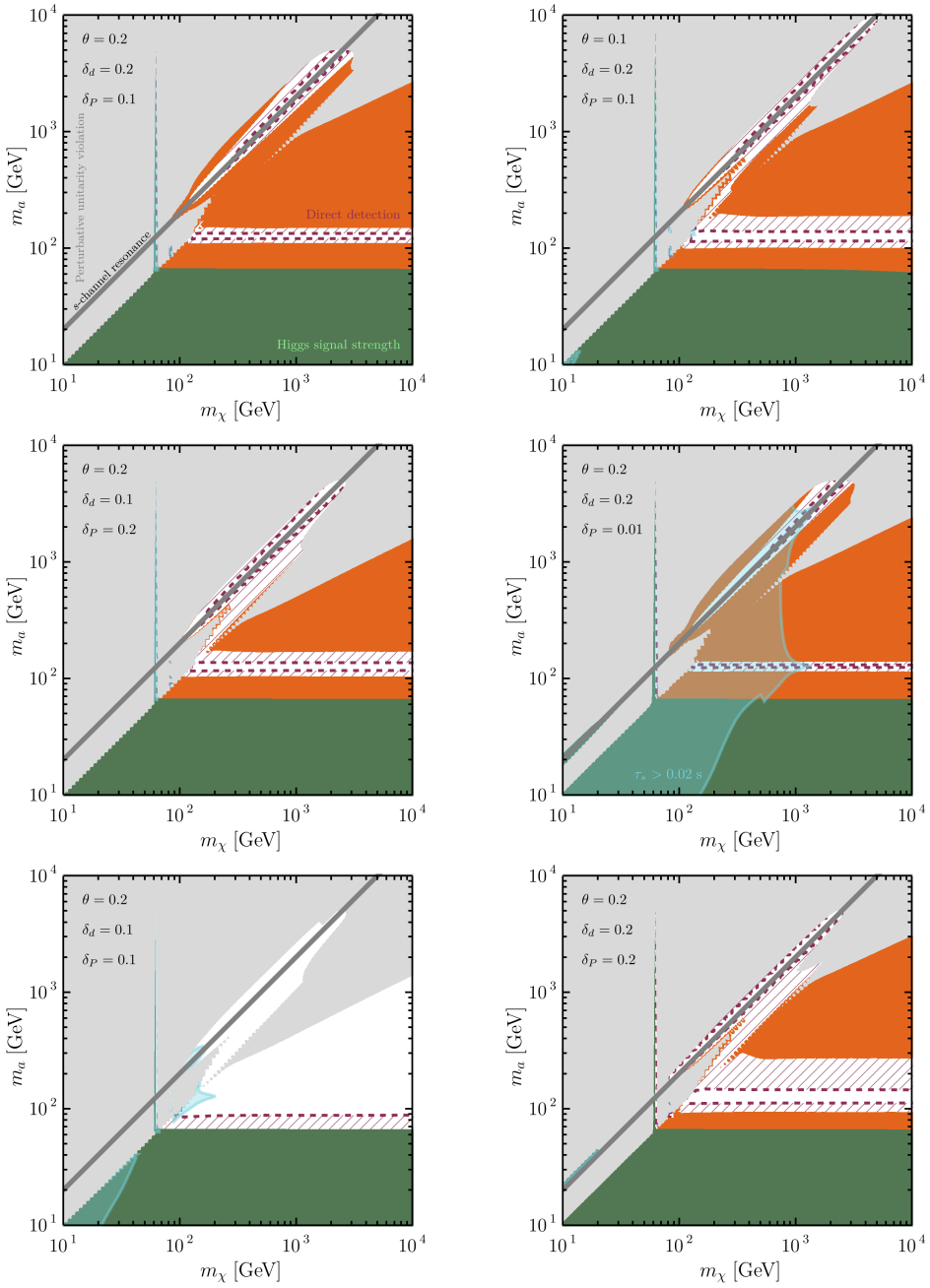

Figure 5.3: Regions in the (m_χ, m_a) plane excluded by current and projected searches. Light gray: perturbativity. Green: Higgs signal strength [573, 574]. Orange: direct detection (LZ [267]). Red-hatched: DARWIN [94] sensitivity. Blue: regions where $\tau_* \geq 0.02$ s, potentially in conflict with BBN [442]. Gray bands: resonant region $m_a \in (2 \pm 10\%) m_\chi$. See text for details. Reproduced from Ref. [93].

usually present in pseudo-Dirac iDM models, establishes this framework as one of the most minimal realizations of iDM in the literature. For this reason, we refer to it as *minimal-inelastic Dark Matter* (miDM).

From another perspective, miDM can be viewed as a minimal deformation of the standard dark Higgs portal with Majorana DM, yet this modest modification leads to a qualitatively new cosmological history and novel experimental signatures. In this chapter, we introduced this new possibility and studied its properties in the regime of weak scale DM masses. We focused on the initial-conditions–independent scenario of DM production via freeze-out, considering a dark sector in equilibrium with the SM bath. In the visible freeze-out regime, we found the model to be tightly constrained by perturbative unitarity, requiring mediator masses below $m_a \lesssim 3m_\chi$, i.e. near an s-channel resonance. In comparison, the standard $\mathcal{CP}$-even portal with Majorana DM is essentially ruled out in this regime, while the $\mathcal{CP}$-odd portal remains largely untested for masses above a few hundred GeV—and out of reach of direct detection searches.

In contrast, the secluded regime offers a larger viable parameter space, even for sizeable scalar mixing angles $\theta \gtrsim 10^{-2}$, where the standard scalar portal would already be excluded by direct detection searches (except in the fine-tuned region $m_a \approx m_h$). Moreover, miDM can accommodate lighter DM candidates while avoiding indirect detection constraints, in contrast to the $\mathcal{CP}$-odd case, and allows for regions where the excited DM state can be long-lived, opening up interesting signatures at both cosmological and collider scales.

Finally, we emphasize that the most predictive part of parameter space, where DM is produced via visible freeze-out, will be nearly completely tested by the next generation of direct detection experiments, such as DARWIN, with the exception of narrowly fine-tuned corners ($\delta_P \approx \delta_d \ll 1$ or $m_a \approx 2m_\chi$). This makes the miDM model a particularly timely and well-motivated target for upcoming direct DM searches.

Taken together with the vector-portal construction analyzed in the previous chapter, this study highlights parity violation as a unifying mechanism for realizing inelastic dark matter across different portals. By systematically exploring both vector and scalar mediators, this thesis demonstrates how modest deformations of otherwise standard dark matter models can qualitatively change their phenomenology and experimental prospects. In this sense, the scalar portal miDM scenario developed here not only enlarges the landscape of viable iDM models, but also reinforces the central theme of this work: that the role of parity in the dark sector is both non-trivial and experimentally testable, offering one of the cleanest pathways toward connecting particle physics models of dark matter with the next generation of experimental data.

Chapter 6

Not-so-inelastic Dark Matter with two mediators

In the previous chapters, we have explored each portal separately. While the scalar portal can in principle serve as a standalone mediator [93] (particularly since the scalar is essential to generating the mass splitting that enables inelastic interactions), this simplification does not extend to the vector portal. Indeed, the vector model (e.g., the Lagrangian in eq. (3.43)), in which the $U'(1)$ gauge symmetry is explicitly broken by Majorana mass terms, necessarily requires a scalar field to spontaneously break the symmetry in order to render the theory a consistent UV-complete realization [339].[1]

The scalar portal alone may give rise to the minimal-inelastic DM (miDM) model [93]. However, as seen in chapter 5, it cannot serve as a predictive thermal model for sub-GeV DM due to Yukawa suppression in annihilations to light SM particles. One may consider a secluded freeze-out for miDM, but such a setup implies that DM states are only produced via suppressed off-shell diagrams at colliders. Consequently, the only relevant collider signals would arise from dark Higgs decays, resulting in minimal novelty for DM phenomenology beyond existing dark Higgs searches.

Despite its non-minimality, the vector portal remains particularly compelling. It permits predictive WIMP-like sub-GeV DM scenarios, and—under parity conservation in the dark sector—can realize exact iDM models with purely off-diagonal interactions, unlike the scalar portal which always retains some residual elastic couplings. Furthermore, the dark photon couples to all SM fermion families without any suppression other than the kinetic mixing ϵ, making it easier to be produced in a wider range of high-energy experiments, and thus richer in experimental signatures.

In chapter 4, we studied the vector portal neglecting the effects of the dark Higgs. However, given the large gauge couplings typically required for successful freeze-out, the dark Higgs cannot be much heavier than the other dark sector

[1] Or a more elaborate mechanism for the $U'(1)$ breaking.

particles if perturbative unitarity is to be preserved [329, 581]. As such, the dark Higgs should be considered an active component of the particle spectrum. Although, as shown in section 4.5, the presence of a dark Higgs does not drastically alter the constraints or sensitivities presented earlier (typically within a 20% error margin), it does open the door to a number of important phenomenological consequences, which we now explore in detail.

To clarify under what conditions the dark Higgs can be decoupled, we recall the perturbative unitarity condition. From eq. (5.18), and assuming $\lambda_{h'h} \approx 0$ (which is generally justified since $\theta_{h'h} \ll 1$ by experimental bounds [331]), the unitarity constraint simplifies to [330]:

$$\lambda_{h'} \lesssim \frac{8}{3}\pi \,. \tag{6.1}$$

Furthermore, with $\lambda_{h'h} \approx 0$, the dark Higgs mass is approximately

$$m_{h'} \approx \sqrt{\lambda_{h'}} w = \frac{\sqrt{\lambda_{h'}}}{2g_\chi} m_{A'} \lesssim 1.3 \sqrt{\frac{0.1}{\alpha'}} m_{A'} \,, \tag{6.2}$$

where in the last inequality we have saturated the bound on $\lambda_{h'}$ using Eq. (6.1). Therefore, assuming $m_{h'} \gg m_{A'}, m_{\chi^*}$ in order to fully decouple the dark Higgs from the low-energy theory is only possible for very small $\alpha' \ll 0.1$. Such small gauge couplings make thermal freeze-out viable only via narrow s-channel resonances [78], fine-tuned forbidden channels [446], or a cold secluded sector with reduced predictivity. Hence, within a minimal perturbative framework, it is neither possible nor phenomenologically compelling to fully decouple the dark Higgs when $\alpha' \gtrsim 0.1$.

The phenomenology of the dark Higgs in the mass spectrum depends on whether it is light or heavy. In the former case, it decays visibly and offers long-lived particle (LLP) signatures, while in the latter, it typically decays invisibly, increasing the multiplicity of dark sector states. For the visible-decay regime, one generally requires kinematic suppression of dark sector final states ($m_{h'} \leq 2m_\chi, 2m_{A'}$), as these would otherwise dominate due to the small scalar mixing angle $\theta_{h'h} \ll 1$ and the Yukawa suppression of SM light particles [83]. The invisible-decay regime usually occurs when this kinematic suppression is lifted.

The implications of the dark Higgs in the context of iDM and niDM were already studied in relative detail in Refs. [329, 418, 528] nearly a decade ago. However, only recently has the richness of new signatures at colliders of these models gained attention [79, 83, 529], culminating in a dedicated search for dark Higgs decays in iDM scenarios by the Belle II collaboration itself [82].

To understand these implications concretely, we categorize the scenarios as follows:

Heavy Dark Higgs: For an invisible dark Higgs (e.g., $h' \to \chi\chi$), one expects more standard signatures, such as a SM pair plus missing energy ($e^+e^- \to A'h'$ with $A' \to \bar{f}f$ and $h' \to$ inv) [582–584], or a small influence in other searches (as in our niDM case discussed in chapter 4). For instance, Ref. [558] showed that final-state radiation of dark Higgs particles in such scenarios can increase bounds on A' by up to 5%, specifically in mono-photon searches at BaBar [488].

If the decay $h' \to A'A'$ are kinematically allowed, multi-lepton final states can arise, such as $e^+e^- \to A'h' \to 3A' \to 6\ell$ [582], motivating searches via both Higgs-strahlung [585–587] and rare meson decays [588].

Including iDM or niDM into the picture allows for a visibly decaying LLP (the excited DM state χ^*) even if both the dark Higgs and dark photon remain invisible, thereby opening up additional discovery channels. Consequently, studies of (n)iDM with a heavy dark Higgs typically focus on the regime in which h' can decay into at least one excited state [83, 529].

Ref. [529] investigated the specific scenario where excited states are produced solely via dark Higgs decays, while the dark photon A' decays invisibly into χ particles. Their results highlight the critical role of the dark Higgs in probing the parameter space, since in its absence constraints would arise only from DM scattering and traditional searches for invisible dark photons. Notably, they demonstrate that searches targeting excited-state decays at FASER [589] can significantly enhance sensitivity to (n)iDM models—reaching all the way to the thermal relic target—even in nearly resonant regimes such as $m_{A'} \approx 2m_\chi$. However, their analysis is confined to a compressed dark sector with small mass splittings $\Delta_m \leq 0.4$, which enhances the s-channel (co)annihilation due to resonance (since $m_{A'} \leq m_\chi + m_{\chi^*} \leq 2.4m_\chi$ is required). It remains an open and interesting question how these results would change under more generic mass hierarchies, which become accessible by introducing significant parity breaking in the dark sector (i.e., allowing $\delta_y \neq 0$).

An additional and more generic signature was explored in Ref. [83], namely the production of two visibly decaying particles within a single event—a feature we will refer to as *"di-decay"* events. These arise due to the presence of the dark Higgs boson and, as we will discuss in the next chapter, can also be generated in niDM models even without the dark Higgs, or from the dark Higgs portal alone [95]. Ref. [83] considered the case of a heavy dark Higgs with $m_{h'} > 2m_{\chi^*}$, such that the decay $h' \to \chi^*\chi^*$ is kinematically allowed. They focused on the Belle II and GAZELLE experiments within the standard iDM framework ($\delta_y = 0$). For large values of the gauge coupling α', they analyzed the Higgs-strahlung process producing up to three excited states per collision, while for smaller α' they considered B-meson decays $B \to K^{(*)}h'$ with two excited states emerging from the dark Higgs decay. These novel signatures are illustrated in fig. 6.1. In both setups, they found that for moderate mass splittings $\Delta_m \gtrsim 0.1$, previously unconstrained regions of parameter space could be explored. However, aside from

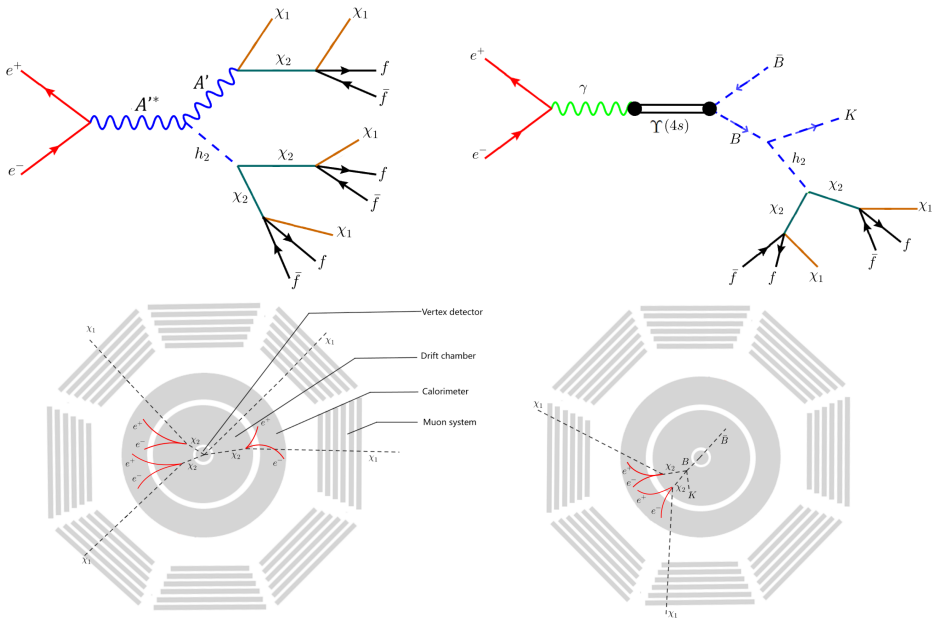

Figure 6.1: Feynman diagrams and schematic event topologies illustrating signatures due to a heavy dark Higgs boson in iDM models at Belle II. The left panels show production via the dark Higgs-strahlung process, $e^+e^- \to A'h'$, while the right panels depict production through rare B-meson decays, $e^+e^- \to \Upsilon(4S) \to B\bar{B}$ followed by $B \to Kh'$. The bottom diagrams present corresponding displaced vertices signatures in the transverse plane of the Belle II detector. Reproduced from Ref. [83].

a finely tuned resonant configuration ($m_{A'} = 2.01 m_\chi + \delta$), the majority of these regions would overproduce DM. This reinforces the importance of investigating larger mass splittings enabled by the more generic niDM framework with $\delta_y \neq 0$.

Light Dark Higgs: This scenario is motivated by large gauge couplings $\alpha' \gtrsim 0.1$, as required for thermal relics from $\chi^{(*)}\chi^{(*)} \to A' \to \bar{f}f$, and leads naturally to visible dark Higgs decays. Light h' can participate in secluded freeze-out via the p-wave annihilation $\chi\chi \to h'h'$ [79], though s-wave enhancement may occur through bound state formation [339, 590]. In contrast, light vectors mediate s-wave freeze-out which is excluded by CMB constraints for $m_\chi \lesssim 10$ GeV [26].

Since a light dark Higgs decays visibly, it is subject to numerous standard experimental searches, which in turn impose stringent constraints on the mixing angle, typically requiring $\theta_{h'h} \lesssim 10^{-4}$ [331] (see section 2.5.1).

Ref. [79] investigated in detail the case of a light dark Higgs within the standard iDM framework, focusing on scenarios where the scalar is produced via Higgs-strahlung processes at Belle II. They analyzed a novel di-decay topology in which both the dark Higgs and the excited DM state χ^* can decay visibly,

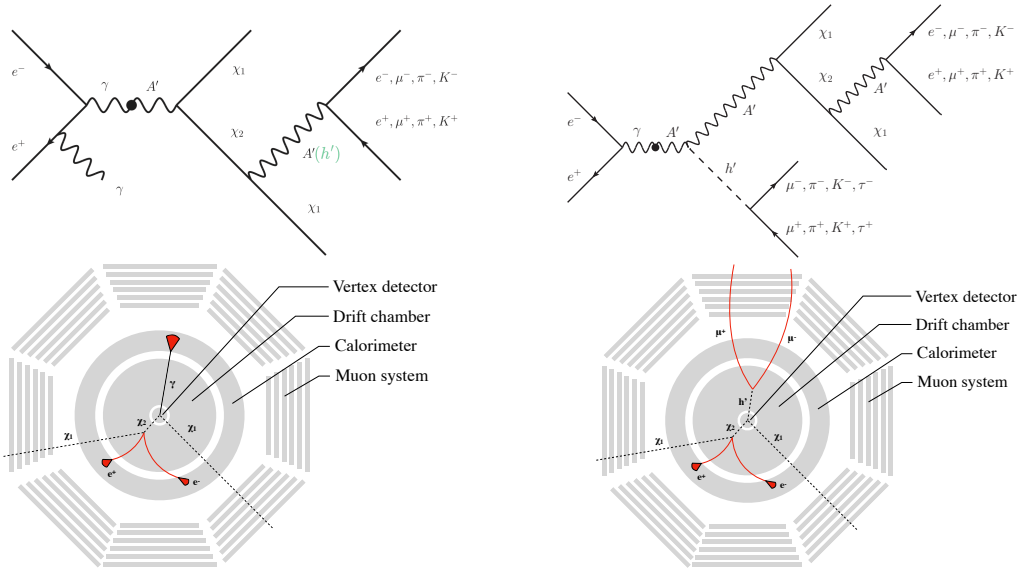

Figure 6.2: Feynman diagrams and schematic event topologies illustrating distinct iDM signatures at Belle II. The left panels depict the canonical vector portal iDM process, featuring a high-energy photon and a displaced vertex: $e^+e^- \to \gamma A' \to \gamma\chi\chi^*$, followed by the visible decay $\chi^* \to \chi\bar{f}f$. The right panels show a di-decay signature enabled by a light dark Higgs boson, produced via Higgs-strahlung $e^+e^- \to A'h' \to \chi\chi^* h'$, with both h' and χ^* decaying visibly. The lower diagrams illustrate the corresponding displaced vertices signatures in the transverse plane of the Belle II detector. Reproduced from Refs. [3, 79].

leading to a di-decay event with two different invariant masses. This distinctive signature is schematically shown in fig. 6.2, alongside the more conventional iDM signal: a single displaced vertex from χ^* decay in association with a high energy photon. Their analysis demonstrates that Belle II has excellent sensitivity to this di-decay signature, particularly for large gauge couplings $\alpha' \gtrsim 0.1$, as illustrated in fig. 6.3.

Although the light Higgs scenario generally lacks the full predictive power of a visible freeze-out model, it still constitutes a consistent and phenomenologically rich DM framework. It naturally arises in dark sectors with large gauge couplings, offering multiple distinct and complementary discovery channels. Notably, the promising collider signatures associated with this scenario—particularly the di-decay events arising from Higgs-strahlung—have already motivated a dedicated search by the Belle II collaboration itself [82].

Finally, the niDM framework is not expected to drastically change the above-mentioned searches (at least in the regions of parameter space they explored), except in one key regime: when the mass splitting $\delta > m_{h'}$ and parity is broken $\delta_y \neq 0$, since now the decay $\chi^* \to \chi h'$ becomes possible. Due to the typically

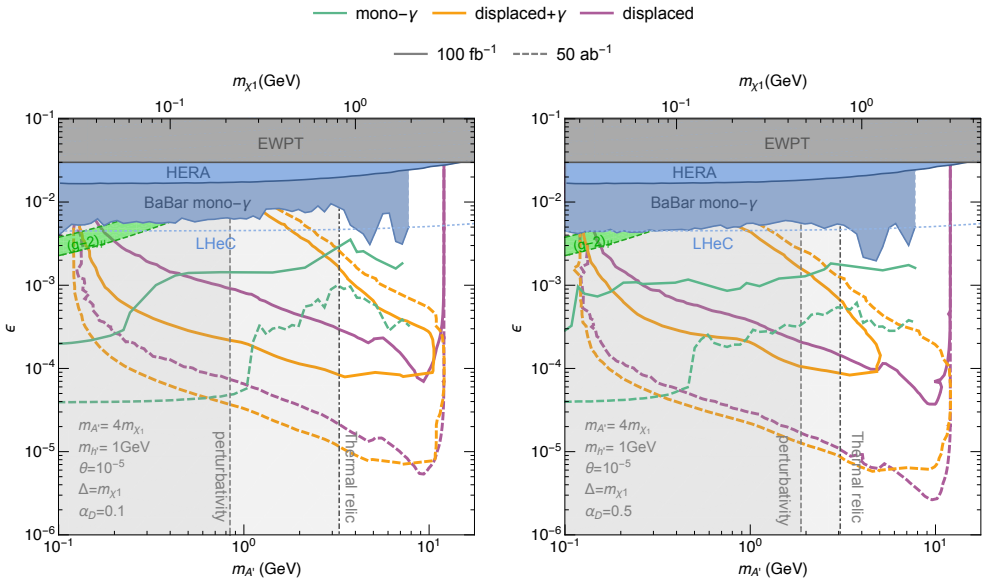

Figure 6.3: Projected sensitivities of various search channels at Belle II for integrated luminosities of $100\,\mathrm{fb}^{-1}$ (solid lines) and $50\,\mathrm{ab}^{-1}$ (dashed lines). The panels correspond to different values of the dark gauge coupling: $\alpha' = 0.1$ (left) and $\alpha' = 0.5$ (right). The signal labeled "displaced" refers to di-decay events originating from the Higgs-strahlung process $e^+e^- \to A'h'$, where both the dark Higgs and the excited dark matter state decay visibly. Reproduced from Ref. [79].

small kinetic mixing $\epsilon \ll 1$ [343], this new decay is expected to dominate over decays into SM particles $\chi^* \to \chi \bar{f} f$. The rest of this chapter is dedicated to studying the implications of this newly opened decay channel.

6.1 Dark Higgs via dark photons

The presence of parity-breaking excited state decays enables the production of dark Higgs bosons through on-shell processes arising from dark photon decay chains, $A' \to \chi^{(*)}\chi^* \to \chi(h')\chi h'$. The dark photon itself can be efficiently produced at electron-positron colliders via standard e^+e^- annihilation processes, $e^+e^- \to \gamma A'$, and at beam dumps via standard nucleus-induced bremsstrahlung, $pZ \to pZ + A'$ or $e^-Z \to e^-Z + A'$. Unlike Higgs-strahlung or B-meson decay channels, these decay chains allow for dark Higgs production even at small gauge couplings $\alpha' \ll 0.1$ and scalar mixing angles $\theta_{h'h} \ll 1$, since they rely on the kinetic mixing ϵ between vector bosons, which can be as large as $\epsilon \lesssim 10^{-2}$ in iDM scenarios [79].

Typical dark Higgs-strahlung searches assume large values of $\alpha' = 0.1$ or even $\alpha' = 0.5$, close to where perturbativity breaks down and loop corrections

become significant. These large couplings also result in Landau poles near the TeV scale [344]. In contrast, smaller α' values are more natural, aligning with the choice made by nature in QED. Moreover, adopting $\alpha' \sim \alpha$ points to an appealing unification of forces at scales similar to those predicted by grand unified theories (GUTs) of the SM [188, 591]. Hence, relaxing the ad hoc assumption of parity conservation in the dark sector opens the door to probing dark Higgs bosons in regions of parameter space previously inaccessible to standard visible dark Higgs searches.

Ref. [528] was among the first to highlight the potential for light dark Higgs production via parity-breaking decays like $\chi^* \to \chi h'$. However, they ultimately disregarded this possibility by neglecting the mixing angle between scalars $\theta_{h'h}$, which typically leads to dark Higgs bosons with lifetimes too long to be probed in collider or beam dump experiments. An exception arises if the dark Higgs can decay into a dark photon and fermion pair (its dominant mode when $2m_\chi > m_{h'} > m_{A'} + 2m_e$ for $\theta_{h'h} = 0$). However, in that case, mediators cannot decay into DM particles, and the χ states are only produced via suppressed off-shell channels, making $\chi^* \to \chi h'$ largely irrelevant. In addition, this setup tends to result in either a secluded freeze-out scenario—requiring suppression of s-wave annihilation channels such as $\chi\chi \to A'A'$ [330] and bound state formation $\chi\chi \to h'(\chi\chi)$ or $\chi\chi \to A'(\chi\chi)$ [79, 339]—or a compressed mass spectrum with $2m_\chi > m_{h',A'} > m_\chi$, pushing the model into resonant or forbidden freeze-out regimes [528].

Their motivation for neglecting scalar mixing lies in avoiding fine-tuning between the dark Higgs potential's quadratic term $\mu_{h'}^2$ and the quartic mixing $\lambda_{h'h}$, especially for sub-GeV dark Higgs where $\theta_{h'h} \lesssim 10^{-6}$ would be required [418], as seen from the minimization condition in eq. (2.92). However, taking a phenomenological approach and treating $\theta_{h'h}$ as a free parameter, ignoring this way any fine-tuning discussion, allows for the emergence of novel and testable collider signatures [79, 83, 529]. Notably, experimental efforts are increasing their interest on probing light dark Higgs scenarios, with current bounds reaching $\theta_{h'h} \sim 10^{-4}$ [331] and future projections offering further sensitivity [592] (see section 2.5, section 2.5.1).

In the next sections, we explore the novel opportunity to search for light dark Higgs bosons through the standard iDM collider signature: a high-energy photon accompanied by a displaced vertex (plus missing energy) [3], hereafter referred to as "displaced+γ" for compactness; see the left panels of fig. 6.2.[2] This signature is a general prediction of niDM models with $m_{h'} < \delta$ and parity violation ($\delta_y \neq 0$), and can occur even with small dark sector couplings, as will be detailed in section 6.2.

In particular, section 6.2 outlines the conditions under which the displaced+γ

[2] A similar signature arises in minimal visibly decaying dark photon models, $e^+e^- \to \gamma A' \to \gamma l^+ l^-$, but without missing energy [593].

analysis becomes parametrically independent of the specific values of the dark sector couplings. This section also defines the benchmark scenario adopted throughout the study and justifies the choice of the Belle II experiment as the primary experimental focus. Subsequently, section 6.3 demonstrates that freeze-out via the process $\chi\chi \to h'h'$ naturally leads to niDM models satisfying the aforementioned independence conditions. It also shows that bound state formation—potentially induced by light mediators—can be safely neglected in our context. In section 6.4.1, we assess the relevance of direct and indirect detection constraints for the parameter space probed by Belle II under our benchmark assumptions. We find that these constraints are negligible for the mass range accessible to Belle II; however, BBN constraints and direct detection bounds become significant for lower and higher mass regimes, respectively. Then, in section 6.4.2, we detail the methodology used to estimate Belle II's sensitivity to displaced+γ signatures and review current limits from other collider searches. Finally, we present our main results in section 6.5, and conclude in section 6.6.

6.1.1 Optional: **Dark photons via dark Higgs**

Before delving deeper into dark Higgs production via the vector portal, we briefly comment on the inverse situation: dark photon production through the scalar portal. Analogous to the light dark Higgs scenario, excited state decays $\chi^* \to \chi A'$ can also arise naturally for light dark photons—even in the parity-conserving case $\delta_y = 0$.[3] In this case, dark photons emerge from the decay chain of the scalar mediator: $h' \to \chi^{(*)}\chi^* \to \chi(A')\chi A'$. Alternatively, dark photons can be produced directly from the decay $h' \to A'A'$ [588]. However, DM annihilation into gauge bosons requires careful control of the gauge coupling to satisfy ID constraints. This consideration may naturally lead to dominant $h' \to \chi^{(*)}\chi^{(*)}$ decays, governed by an independent Yukawa coupling.

The process $\chi\chi \to A'A'$ is s-wave due to t- and u-channel diagrams, while the s-channel Higgs-mediated contribution is p-wave. To ensure p-wave freeze-out and evade CMB bounds [26], one requires $e' \ll y$, where $y \propto y_R$ is the effective Yukawa coupling. This requirement generally leads to dominant $h' \to \chi^{(*)}\chi^{(*)}$ decays since the decay width $\Gamma_{h'\to A'A'} \propto e'^2$, whereas $\Gamma_{h'\to\chi^{(*)}\chi^{(*)}} \propto y^2$. However, since $\Gamma_{h'\to A'A'}$ grows faster with $m_{h'}$, the assumption $h' \to \chi\chi \gg A'A'$ must be reassessed at higher masses [83].

For instance, in the mDM regime, Ref. [330] provides the cross section:

$$\sigma v_\chi(\chi\chi \to Z'Z') \simeq \frac{e'^4}{16\pi m_\chi^2} + \frac{y_R^4}{48\pi\, m_\chi^2}\, v_\chi^2, \tag{6.3}$$

where $m_s \gg m_\chi \gg m_{A'}$ and SM contributions are neglected. For p-wave dom-

[3] Due to dark Higgs pair production, discussed in section 7.1.1, this scenario may result in up to four decaying dark photons being produced from dark Higgs decay chains.

inance at freeze-out ($v_\chi^2 = 3/x_f \approx 0.1$), the s-wave contribution must satisfy $\langle\sigma v\rangle_s \lesssim 10^{-4}\langle\sigma v\rangle_p$, which implies $e' \lesssim 0.05 y_R$.

However, even for this hierarchy, $h' \to \chi\chi$ dominates over $h' \to A'A'$ only for $m_{h'} \lesssim 10 m_\chi$ when $m_{A'} \sim m_\chi$. For $m_{A'} = 0.1 m_\chi$, a stronger suppression $e' \lesssim 0.005 y_R$ is needed for the same dominance within the same mass range. This highlights the model-dependent nature of light dark photon scenarios.

An alternative is to engineer a forbidden freeze-out by fine-tuning $m_{A'} = m_\chi + \Delta$ with $0 < \Delta \ll 1$, such that $\chi\chi \to A'A'$ is kinematically blocked at late times. But compared to annihilation into scalars ($\chi\chi \to h'h'$), which is naturally p-wave, both alternatives for the vector channel are more restrictive and constrained. However, interestingly, the light dark photon case can result in significantly lighter LLPs due to the absence of Yukawa suppression in their decays to electrons.

In summary, dark photon production via the scalar portal is a more intricate and model-dependent scenario with highly intertwined parameters. For this reason, we do not pursue it further here, leaving its phenomenology to future studies of secluded iDM models.

6.2 Dark Higgs production and decays

We focus here on light niDM scenarios to avoid DD constraints. Heavier DM masses could, in principle, be explored at LHC experiments, but would require proximity to the standard iDM regime or extremely small mixing angles $\epsilon, \theta_{h'h}$ to evade DD bounds. For the light DM case, Belle II offers one of the most suitable currently operating collider setups to search for niDM signatures. Although LHCb has promising potential, Belle II benefits from cleaner backgrounds and better-defined initial collision conditions provided by lepton colliders. Therefore, our analysis will focus exclusively on Belle II. Moreover, we restrict our attention to the standard niDM setup where $\phi_d = 0$ for simplicity.

A light dark Higgs, $m_{h'} \lesssim m_b$, can already be directly constrained via B-meson decays due to its mixing angle $\theta_{h'h}$. However, we highlight the novelty of producing dark Higgs particles via dark photon decays, which can enhance Belle II's sensitivity for extremely small angles $\theta_{h'h} \lesssim 10^{-4}$.

Importantly, this production mechanism enables a largely coupling-independent analysis, since after A' production the subsequent decay chains are prompt over a wide range of dark sector parameters. Let us, discuss this point in detail:

1. We consider on-shell production of dark photons at Belle II through annihilation processes $e^+e^- \to \gamma A'$, such that the number of produced A's depends solely on the kinetic mixing parameter: $N_{A'} \propto \epsilon^2$.

2. The dark photon A' can decay either to DM or SM particles. Assuming one dominant decay mode and light final states ($m_f, m_{\chi^{(*)}} \ll m_{A'}$), its lifetime is approximately:

$$\tau_{A'} \approx 10^{-20}\ \text{s} \left(\frac{\alpha}{\alpha'}\right) \left(\frac{\text{GeV}}{m_{A'}}\right) \tag{6.4}$$

if decaying to DM, or

$$\tau_{A'} \approx 10^{-18}\ \text{s} \left(\frac{0.01}{\epsilon}\right)^2 \left(\frac{\text{GeV}}{m_{A'}}\right) \tag{6.5}$$

if decaying to SM fermions. Thus, for $\epsilon^2 \ll 10^{-2}\alpha'/\alpha$, decays into DM dominate. Since model-independent bounds constrain $\epsilon \lesssim 10^{-2}$ [494, 546, 594], dark photon decays into DM dominate for $\alpha' \gtrsim 10^{-4}$ [83]. Moreover, for $m_{A'} \gtrsim 100$ MeV and these coupling values, such decays are prompt at Belle II.

3. Excited states produced from A' decays are also expected to decay promptly to h'. For $m_{h'} \ll \delta \sim m_\chi$, the lifetime of $\chi^* \to \chi h'$ is:[4]

$$\tau_* \approx \frac{10^{-16}\ \text{s}}{\delta_y^2 \sin^2 2\theta} \left(\frac{10^{-3}}{y}\right)^2 \left(\frac{\text{GeV}}{m_\chi}\right) \tag{6.6}$$

while if decaying via $\chi^* \to \chi f \bar{f}$ (for $2m_f \ll \delta$):

$$\tau_* \approx \frac{10^{-12}\ \text{s}}{\sin^2 2\theta} \frac{\alpha}{\alpha'} \left(\frac{0.01}{\epsilon}\right)^2 \left(\frac{\text{GeV}}{m_\chi}\right) \left(\frac{R_{A'}}{5}\right)^4 \tag{6.7}$$

with

$$R_{A'} \equiv \frac{m_{A'}}{m_\chi}\,. \tag{6.8}$$

Thus, decays into h' dominate when:

$$\delta_y y_L \gtrsim 10^{-1} \epsilon \sqrt{\alpha'}/R_{A'}^2\,. \tag{6.9}$$

For $R_{A'} > 2$ (to allow $A' \to \chi\chi$) and $\epsilon \lesssim 10^{-2}$ (from generic constraints [494, 546, 594]), it is sufficient to require $\delta_y y_L \gg 10^{-4}\sqrt{\alpha'}$, or simply $\delta_y y_L \gg 10^{-4}$ (as $\alpha' < 1$), for the excited DM states to decay dominantly to dark Higgs bosons. These decays are also prompt for $m_{\chi^*} \gtrsim 100$ MeV given $\delta_y y_L \gg 10^{-4}$.

[4] Here we assume that the decay is dominated by the off-diagonal Yukawa coupling. Loop-induced decays via gauge interactions can become relevant in scenarios with large values for α' and δ_y, but with negligible Yukawa couplings. However, we do not consider this possibility in the present work.

In summary, for kinematically allowed processes of the form:

$$e^+e^- \to \gamma A' \to \gamma\chi^{(*)}\chi^* \to \gamma\chi(h')\chi h' \,,$$

a sizable number of h' boson can be produced at Belle II, depending only on the specific values of $m_{A'}$ and ϵ for dark sector masses above $\gtrsim 100$ MeV, provided that the following "independence" conditions are satisfied:

$$\alpha' \gtrsim 10^{-4} \qquad \text{and} \qquad \delta_y y_L \gg 10^{-4} \,. \tag{6.10}$$

These processes occur promptly at the collision point and yield signatures similar to standard iDM, but with visible final-state fermions from $h' \to f\bar{f}$ carrying a fixed invariant mass $m_{ff} \simeq m_{h'}$, thereby offering improved background discrimination when compared to the standard iDM 3-body decays $\chi^* \to \chi\bar{f}f$.

As we will discuss in section 6.3, for large mass splittings $\delta \gtrsim m_\chi$, the dark sector couplings naturally fall in the above-mentioned intervals (6.10) if one requires the correct DM relic abundance to be produced via thermal freeze-out. Therefore, the process $e^+e^- \to \gamma h'(\to ff)+$missing energy is naturally expected to arise in niDM with light dark Higgs particles.

To conclude, decays of h' to SM particles are well studied [331, 528, 568, 595] and usually dominated by the scalar mixing $\theta_{h'h}$ (rather than loop-induced vector portal processes). Therefore, standard results for the scalar portal decay widths can be used [595] and depend only on $m_{h'}$ and $\theta_{h'h}$, see section 2.5.1. Given the strong constraints on $\theta_{h'h} \lesssim 10^{-4}$ [331], visible decays occur within Belle II only for $m_{h'} > 2m_\mu$, as $h' \to e^+e^-$ is highly Yukawa-suppressed.

6.2.1 Parameter Space

We focus on sub-GeV DM to target intensity frontier experiments. Due to Belle II's center-of-mass (c.m.) energy $\sqrt{s} \approx 10$ GeV, we limit $m_{A'} \lesssim 10$ GeV. To ensure decays within the detector, we set $m_{h'} \gtrsim 100$ MeV. We require $\delta > m_{h'}$ for $\chi^* \to \chi h'$ to be kinematically allowed. We study the niDM regime, i.e., $\delta \sim m_\chi$ and $\delta_y \gtrsim 1$. Larger splittings may suppress A' production since we also require $m_{A'} > 2m_\chi + \delta$ to allow for $A' \to \chi\chi^*$ decays, while smaller δ_y favors χ^* decays to SM fermions, taking us back to the standard iDM signature.

Following these considerations, as our *benchmark* scenario, we fix the mass hierarchy and parity-breaking parameter as follows:

- $\Delta_m = 1$,
- $m_{A'} = 2.5\, m_{\chi^*} = 5\, m_\chi \equiv R_{A'} m_\chi$,
- $m_{h'} = 0.9\, \delta = 0.9\, m_\chi$,
- $\delta_y = 1$.

While the dark sector couplings e' and y_L will be fixed via the DM thermal freeze-out, as discussed in the next section. We take $2m_\mu \approx 200$ MeV $< m_\chi <$

$\sqrt{s}/R_{A'} \approx 2$ GeV, with the largest viable values for $\epsilon \lesssim 10^{-2}$ [79] and $\theta_{h'h} \lesssim 10^{-4}$ [331] to ensure Belle II accessibility and thermal equilibrium [394].

Finally, although our couplings are set by freeze-out, our results will remain fairly general since the assumed dark prompt decays ($c\tau \ll 1$ mm) occur for wide coupling ranges as long as parity is broken in the dark sector. In the next section, we show how freeze-out naturally leads to such values.

6.3 Dark Matter freeze-out

As previously discussed, the prompt decays of both the dark photon and the excited DM state allow our signal to be remarkably robust against variations in the dark sector couplings, provided the conditions in eq. (6.10). This inherent independence from precise coupling values highlights the naturalness of our scenario. In the following, we solidify this conclusion by explicitly computing the DM relic abundance and demonstrating that the required Yukawa and gauge couplings lie well within the prompt decay regime, thereby justifying our earlier assumptions.

Given that we consider a light dark Higgs $m_{h'} < m_\chi$ and large mass splittings $\Delta_m \sim 1$, freeze-out production will be dominated by the secluded annihilation channel $\chi\chi \to h'h'$. While the relic density condition $\Omega_\chi h^2 = 0.11$ [26] would normally fix one parameter, our benchmark assumptions — namely $\delta_y = 1$, $\Delta_m = 1$, and $m_{A'} = 5m_\chi$ ($R_{A'} = 5$) — allow us to determine both the Yukawa and gauge couplings from relic abundance constraints.

This is done in two steps. First, the relic density condition fixes the annihilation cross section, which in turn determines the Yukawa coupling y_L. Second, using the definition of the mass splitting,

$$\Delta_m = 2y_L \frac{w}{m_\chi}(2 + \delta_y) = 2y \frac{R_{A'}}{e'}\,, \tag{6.11}$$

where $y \equiv (y_R + y_L)/2$ is the average Yukawa coupling, we can solve for the gauge coupling e'. For our benchmark, this yields $e' = 10y$.

This relation $e' = 10y$ in turn implies that a secluded freeze-out dominates over a visible one. Secluded annihilation scales as y^4, while the visible annihilation via the vector portal proceeds with a cross section proportional to $\cos^2(2\theta)\epsilon^2 e^2 e'^2/R_{A'}^4$. The scalar portal contribution is subleading for light DM due to Yukawa suppression of the final states and the hierarchies $\epsilon \gg \theta_{h'h}$ and $e' = 10y \gg y$. We also neglect all contributions involving excited states in the Feynman diagrams for annihilation processes since $\Delta_m \gtrsim 1$. In this way, only the ground state coupling to the dark Higgs, $y_L\hat{\alpha}_{--}$, contributes and is given by

$$|y_L\hat{\alpha}_{--}| = \frac{1}{\sqrt{2}}\,|y_R + y_L + (y_R - y_L)\cos 2\theta|\,. \tag{6.12}$$

For angles close to $\theta \approx \pi/4$ (standard iDM), this coupling approximates $\sqrt{2}y$. For the mDM limit $\theta \to \pi/2$, it approaches $\sqrt{2}y_L$. For our benchmark ($\delta_y = 1$), we obtain $|y_L \hat{\alpha}_{--}| \approx \sqrt{2}y(1 + 1/27) \approx \sqrt{2}y$, justifying the use of iDM results. This remains accurate for $\delta_y \lesssim 2$ or $\Delta_m \lesssim 2$.

The visible/secluded annihilation cross section ratio can be estimated as:

$$\frac{\sigma v_\chi(\chi\chi \to A' \to ff)}{\sigma v_\chi(\chi\chi \to h'h')} \sim \frac{\cos^2(2\theta)}{\Delta_m^2} \frac{\epsilon^2 e^2}{y^2} \frac{4}{R_{A'}^2} \approx \left(\frac{\epsilon}{0.01}\right)^2 \left(\frac{10^{-4}}{y}\right)^2 , \tag{6.13}$$

where we used eq. (6.11) and the benchmark values. This implies that as long as we assume $y \gtrsim 10^{-4}$, we can safely neglect SM annihilation channels.

Now, to verify this assumption, we estimate the value of y required to satisfy the relic abundance constraint. We will use the freeze-out approximation for p-wave processes[5] [228],

$$b_p \approx 3 \times 10^{-25}\ \mathrm{cm}^3/\mathrm{s}\,, \tag{6.14}$$

where b_p is defined via $\sigma v = a_s + b_p v^2 + c_d v^4 + \mathcal{O}(v^6)$, and neglect contributions involving the heavy excited states. Eq. (6.14) guarantees that p-wave DM produces the correct DM relic abundance via freeze-out $\Omega_{\mathrm{DM}} h^2 = 0.12$. Here, we assume that the dark sector is in thermal equilibrium with the SM during freeze-out. This assumption is justified by mixing values probed by the Belle II experiment [394], namely $\epsilon \gtrsim 10^{-5}$ and $\theta_{h'h} \gtrsim 10^{-6}$.

According to Ref. [330], for $m_{h'} \ll m_\chi$, we have

$$\sigma v_\chi(\chi\chi \to h'h')_0 \simeq \frac{3y^4}{32\pi m_\chi^2} v_\chi^2 . \tag{6.15}$$

Taking into account a finite dark Higgs mass, the corrected cross section is

$$\sigma v_\chi(\chi\chi \to h'h') = F(y_L, \delta_y, m_{h'}, m_\chi, \lambda_{h'} w) \cdot \sigma v_\chi(\chi\chi \to h'h')_0\,, \tag{6.16}$$

where $F \approx 24$ for our benchmark. Sommerfeld enhancement is neglected due to $m_{h'} \sim m_\chi$ [590, 596, 597].

From eqs. (6.14) and (6.16), the relic abundance condition $\Omega_\chi h^2 = 0.12$ implies:

$$y \simeq 0.07 \sqrt{\frac{m_\chi}{\mathrm{GeV}}}, \tag{6.17}$$

yielding, in our benchmark scenario, $\delta_y y_L \gtrsim 0.01 \gg 10^{-4}$ for $m_\chi \gtrsim 100$ MeV. Combining this with eq. (6.11), we find:

$$\alpha' \simeq 0.04 \frac{m_\chi}{\mathrm{GeV}}, \tag{6.18}$$

[5] At $m_\chi > 3$ GeV, QCD effects lower b_p to about 1.5.

ensuring $\alpha' \gg 10^{-4}$. Thus, both conditions in eq. (6.10) are satisfied and we expect prompt decays of both A' and χ^* into dark sector particles.

We observe that for $m_\chi \gtrsim 3$ GeV, one has $\alpha' \gtrsim 0.1$, meaning Higgs-strahlung production may become dominant over χ^* decays for these masses. Values above $m_\chi \gtrsim 30$ GeV imply $\alpha' > 1$, signaling loss of perturbativity. Yet, such masses are beyond Belle II's kinematic reach due to $m_{A'} = 5m_\chi$ and we can safely only focus on the novel h' production mechanism.

Lastly, note that if α' were fixed large from the start $\alpha' \gtrsim 0.1$ (as often assumed in the literature), annihilation would proceed via s-channel Higgs exchange $\chi\chi \to h' \to h'h'$. This channel scales as $y^2\lambda_{h'}^2 \propto y^2 e'^2$, instead of y^4, generally requiring smaller y to reproduce the relic density. Therefore, a large α' value would drastically reduce Δ_m via eq. (6.11), reintroducing nearly-degeneracy between DM states and suppressing the $\chi^* \to \chi h'$ decay channel.

6.3.1 Bound State Formation

Given that the dark Higgs acts as a light mediator, it could, in principle, induce the formation of bound states of DM pairs, which is a s-wave process (i.e., this process does not depend on the DM velocities) [339, 590]. These bound states, once formed, may decay by emitting visible particles, thereby injecting energy into the SM bath. More critically, the formation of a bound state necessitates the emission of a dark Higgs h', which in our case decays into SM particles via the scalar portal. Thus, even if the bound state itself is long-lived, its formation process alone can lead to observable energy injection—facing stringent constraints from CMB measurements [26].

Ref. [590] studied the conditions under which bound state formation (BSF) becomes effective and found that if the mediator mass satisfies

$$m_{h'} > \frac{1}{4}\alpha_{\tilde{y}}^2 m_\chi \equiv m_{h'}^{\min}, \tag{6.19}$$

where $\alpha_{\tilde{y}} \equiv (y_L \hat{\alpha}_{--})^2/4\pi$ is the effective fine-structure constant for the scalar-mediated potential, BSF becomes highly suppressed and can be safely neglected (see also [79]).

This result can be physically understood through energy conservation: the DM pair must lose energy by emitting a mediator in order to transition into a bound state. The binding energy of the state is $E_B \sim \alpha_{\tilde{y}}^2 m_\chi$ [339], while the DM kinetic energy at late times or at freeze-out is negligible ($v_\chi \ll 1$). Therefore, for the emission of a real scalar to be possible, its mass must not exceed the available energy, i.e., $m_{h'} \lesssim E_B$.

In our benchmark scenario, where $\alpha_{\tilde{y}} \simeq y^2/2\pi$ and the relic abundance con-

dition fixes y as in eq. (6.17), we find

$$m_{h'}^{\min} \simeq 10^{-7} \frac{m_\chi}{\text{GeV}}. \tag{6.20}$$

This lower bound on $m_{h'}$ is far below the benchmark value $m_{h'} = 0.9\, m_\chi$, confirming that BSF is negligeble in our region of interest.

More generally, to ensure both $\chi^* \to \chi h'$ decays and the suppression of BSF, one must require $m_{h'} < \delta$ and $m_{h'} > m_{h'}^{\min}$ simultaneously. Using $\Delta_m \equiv \delta/m_\chi$ and inserting $\alpha_{\tilde{y}}$ in terms of y, we find:

$$\Delta_m > r_y \cdot \frac{1}{4}\alpha_y^2, \tag{6.21}$$

where $\alpha_y = y^2/(2\pi)$ and $r_y^4 \equiv (\hat{\alpha}_{--} y_L/\sqrt{2}y)^4$. For $\delta_y \lesssim 2$, we find $r_y \sim 1$, simplifying the condition.

On the other hand, by using eq. (6.11), we can invert this relation to define a maximum allowed mass splitting before BSF turns on:

$$\Delta_m^{\max} \equiv \left(\frac{2R_{A'}}{r_y}\right)^{4/3} \alpha'^{-2/3}. \tag{6.22}$$

For a dark photon decaying into DM particles $R_{A'} > 2$, one simply finds an upper bound $\Delta_m^{\max} \simeq 6/r_y^{4/3}$ (given that $\alpha' < 1$). In the benchmark we consider, we have $r_y \simeq 1$, thus, $\Delta_m^{\max} \simeq 6$, which is well above the mass splitting we adopt ($\Delta_m = 1$). Furthermore, in general, one already requires $\Delta_m \leq 2$ to forbid 3-body decays such as $\chi^* \to 3\chi$ which may take over $\chi^* \to \chi h'$.

We conclude that our benchmark region safely avoids the formation of DM bound states mediated by the dark Higgs and, therefore, can be made fully compatible with CMB and relic abundance constraints.

6.4 Dark Matter searches

This section reviews the experimental searches most relevant for testing our light dark Higgs scenario.

6.4.1 Direct and Indirect Detection

As discussed in previous chapters, DD constraints arise for both the vector and scalar portals due to the presence of elastic couplings in the niDM setup. These constraints are typically only significant for DM masses above a few GeV, where nucleon recoil becomes extremely constrained, as illustrated in fig. 2.13. Currently, the most stringent bounds come from the LUX-ZEPLIN experiment [267], with DARWIN [94] projected to extend sensitivity even further.

The dark photon portal leads to DM–nucleon interactions via the non-relativistic effective operators $\mathcal{O}_8^N \propto \mathbf{v}_\perp$ and $\mathcal{O}_9^N \propto \mathbf{q}$, with coefficients (in the conventions of Refs. [256, 260]):

$$c_8^p = \frac{2}{\Lambda^2}, \quad c_8^n = 0, \quad c_9^p = \frac{5.586}{\Lambda^2}, \quad c_9^n = -\frac{3.826}{\Lambda^2}, \tag{6.23}$$

where the effective scale is defined by $\Lambda = m_{A'}/\sqrt{e' \cos 2\theta \, \epsilon e}$. While, the scalar portal contributes to spin-independent DM–nucleon scattering, with the cross section given by [330]:

$$\sigma^{\mathrm{SI}} = \frac{\mu_{\chi N}^2 m_N^2 f_N^2 \alpha_{\tilde{y}} \sin^2 2\theta_{h'h}}{v^2} \left(\frac{1}{m_h^2} - \frac{1}{m_a^2} \right)^2, \tag{6.24}$$

where $\mu_{\chi N}$ is the reduced DM–nucleon mass, m_N is the nucleon mass, and $f_N = 0.3$ is the effective Higgs–nucleon coupling [575].

We neglect direct detection constraints from DM–electron scattering, since both portals exhibit strong suppression: for the vector portal, interactions are velocity- or momentum-suppressed; and for the scalar portal, electron couplings are Yukawa suppressed. Moreover, interactions using off-diagonal (inelastic) couplings are suppressed by the large mass splitting between DM states $\Delta_m \gg v_\chi^2$ [511] or by their loop-induced nature [548, 564].

For the vector portal, DD constraints can be evaluated via the DDCalc package [4], using the effective coefficients above as inputs [5]. For the scalar portal, one compares predicted cross sections from eq. (6.24) against experimental upper limits.

However, as shown in chapter 4, vector portal DD limits are only relevant for $m_\chi \gtrsim 5$ GeV. Meanwhile, the scalar portal is suppressed by small scalar mixing angles $\theta_{h'h} \lesssim 10^{-4}$ and Yukawa couplings $\alpha_{\tilde{y}} \lesssim 10^{-3}$, along with the intrinsic Yukawa suppression $y_N^2 \sim 10^{-6}$. Altogether, this gives:

$$\sigma^{\mathrm{SI}} \propto \theta_{h'h}^2 \, \alpha_{\tilde{y}} \, y_N^2 \sim 10^{-17}, \tag{6.25}$$

which is well below the thermal target for scalar DM with a dark photon portal, $\sigma^{\mathrm{SI}}_{\mathrm{scalar}} \propto \epsilon^2 \alpha' \alpha R_{A'}^{-4} \sim 10^{-11}$ for $m_\chi \gtrsim 100$ MeV and $R_{A'} \gtrsim 3$ [344]. Indeed, $\sigma^{\mathrm{SI}}_{\mathrm{scalar}}$ is at most probed down to 3 orders of magnitude for $m_\chi \lesssim 1$ GeV [265]. Therefore, as for the vector portal, DD bounds are only relevant for $m_\chi \gtrsim 5$ GeV thanks to impressive results from xenon based DD experiments, such as PandaX-4T [509], XENONnT [598] and LZ [267]. Consequently, DD constraints are irrelevant for the mass range of interest at Belle II, $m_\chi \lesssim 2$ GeV.

ID constraints are likewise negligible for two main reasons. First, the excited state is heavy and efficiently decays, making its population negligible even at

freeze-out [420], and eliminating potential co-annihilation signals. Second, DM–DM annihilation is p-wave suppressed (as discussed in section 6.3), rendering late-time annihilation signals irrelevant [330].

Constraints from exotic energy injection during BBN or the CMB are not applicable in our regime of interest. The lifetimes of unstable dark sector particles are $\tau \ll 1$ s (short enough to be probed at collider experiments), safely to avoiding these constraints [442, 599, 600]. Additionally, our dark sector particles lie above hundreds of MeV, rendering stellar cooling and supernova constraints irrelevant [331, 601–604].

Constraints on DM "re-excitation" through up-scattering (e.g., $\chi f \to \chi^* f$) are also irrelevant given our large mass splittings ($\delta \sim m_\chi \gtrsim 100$ MeV) [72, 73, 76, 419, 454, 459]. Similarly, DM self-interaction bounds do not constrain our parameter space due to both small dark sector couplings and relatively heavy dark Higgs mediators ($m_{h'} \gtrsim 0.2\, m_\chi$) [89, 597].

To summarize, we conclude that, within our chosen parameter space and benchmark scenario, DD and ID constraints are irrelevant for Belle II searches. The most relevant experimental probes are thus those at colliders, which we explore in the following section.

6.4.2 Collider searches

Our goal is to investigate the signatures arising from the new excited state decay $\chi^* \to \chi h'$ at the intensity frontier, with a particular focus on the Belle II detector. These decays are only accessible in parity-breaking dark sectors—specifically, in the niDM generalization of pseudo-Dirac DM. Hence, we concentrate on the displaced vertex plus high-energy photon signal $e^+e^- \to \gamma h' \chi\chi$ (displaced+γ), shown in the left panels of fig. 6.2.

To estimate the Belle II sensitivity to this displaced+γ process, we develop a novel *semi-analytical approach*. This method neglects the selection cuts on the final-state SM particles from LLP decays and focuses solely on the spatial distribution of decay vertices. We only use the direction of SM particles produced directly in the collision—e.g., the photon in the displaced+γ signal. The angular distribution of initial-state particles is derived from the $2 \to 2$ collision cross section in the c.m. frame,[6] while the decay distributions are isotropic in the LLP rest frame for two-body decays.

We then numerically integrate over the relevant angular ranges mapped onto the detector frame by Lorentz boosting. The decay probability within detector dimensions is computed using the particle lifetime. This semi-analytical method

[6] We restrict to $2 \to 2$ processes.

can also be applied to the standard iDM displaced+γ signal and the Higgs-strahlung signal. Its main limitation arises for three-body decays or when a mother particle in the decay chain is also a LLPs itself, neither cases present in our chosen benchmark scenario.

A detailed explanation and validation of this approach is presented in appendix D. For $m_\chi \gtrsim 100$ MeV, the estimated relative errors are typically $\lesssim 50\%$, except near the kinematic threshold $m_{A'} \sim \sqrt{s} - E_\gamma^{\min}$, where deviations can reach up to a factor of three.[7]

In our computations, we use Belle II's c.m. energy $\sqrt{s} \simeq 10.58$ GeV and a c.m. velocity $\vec{\beta} = (0.27, 0.04, 0)$, resulting from the asymmetric beam configuration of SuperKEKB (4 GeV positrons, 7 GeV electrons intersecting at 83 mrad). We conservatively assume an integrated luminosity of 100 fb^{-1}, a value already surpassed by Belle II [82].

Following Ref. [3], we adopt the following geometric cuts in the lab frame:

- Transverse decay position: $0.2\text{ cm} < R_{yz} < 60\text{ cm}$,
- Longitudinal vertex position: $-0.55\text{ m} < x < 1.4\text{ m}$,
- Polar angle between decay direction and positive x-axis: $17^\circ < \theta_{\text{lab}} < 150^\circ$,
- Photon angle in same range, and minimum energy cut $E_\gamma > 0.5$ GeV.

Although dark Higgs production via Higgs-strahlung (right panels in fig. 6.2) is also possible, such signatures are suppressed under our benchmark where $m_\chi \lesssim 2$ GeV implies $\alpha' \lesssim 0.08$ (see eq. (6.18)). Recasting bounds from Belle II's dedicated Higgs-strahlung searches for standard iDM [82] lies beyond the scope of this work.

Future facilities such as LHCb or FCC-ee may also be sensitive to these signatures, but we leave those projections to future studies.

In the following, we simply summarize the relevant current constraints from high-energy experiments:

Missing energy searches: The strongest constraints on an invisibly decaying dark photon in the range 1 GeV $\lesssim m_{A'} \lesssim 8$ GeV arise from BaBar mono-photon searches [344, 488]. While still relevant for our semi-visible scenario, a fraction of events may be vetoed due to h' decays into SM particles. Since $m_{h'} \sim m_\chi$, the energy deposited from h' decays is comparable to that from χ^* decays in iDM scenarios. However, the h' lifetime is generally much longer than that

[7] The increased errors can be mitigated by applying a smooth step-function suppression at the kinematic threshold reducing the total number of events.

of χ^*, owing to the small Higgs mixing angle $\theta_{h'h}$ and the suppressed Yukawa couplings of the Higgs to light SM fermions. These longer lifetimes render the BaBar bounds more similar to the standard mDM limits reported by the BaBar collaboration than to classic iDM results. We employ an updated version of the simulation described in chapter 4 to rescale these bounds in the present context. Further details on the simulation and the applied cuts can be found in chapter 4 and appendix D as well as in Refs. [3, 89].

The NA64 experiment, using a 100 GeV electron beam, becomes the strongest missing energy constraint for lighter dark photons masses $m_{A'} \lesssim 1$ GeV. Here, dark photons are produced via bremsstrahlung ($eZ \to eZA'$) and e^+e^- annihilation in electromagnetic showers. Missing energy events are identified by energy imbalance in the ECAL, with vetoes from downstream detectors.

Despite potential visible decays of dark photon daughters, previous studies have shown that the limits remain robust in both iDM [80, 479] and niDM scenarios [89]. Hence, we present the official NA64 limits [344], deferring detailed recasting to future work.

Proton beam dumps: Proton beam dump experiments could place strong constraints and offer promising sensitivities to a dark Higgs produced through vector portal interactions, especially as the scalar portal production is Yukawa suppressed. However, we postpone this analysis to future studies since their expected to probe only DM masses $m_\chi \lesssim 300$ MeV [89].

Dark Matter scattering: At high-energy facilities, dark photons may be produced on-shell and decay into DM particles. These boosted DM particles can scatter inside detectors like LSND [279, 556], E137 [483, 557], or MiniBooNE [506].

For $m_\chi \lesssim 500$ MeV and $\alpha' \gtrsim 0.1$, strong limits exist coming from scatterings via the vector mediator [280], but our benchmark implies $\alpha' \lesssim 0.02$ for this DM masses (from eq. (6.18)), making such constraints irrelevant for our study. Moreover, scalar portal scattering is negligible due to the strong Yukawa and mixing angle suppressions.

6.5 Results

Having examined the various theoretical and experimental constraints relevant for a light dark Higgs in niDM scenarios, we are now ready to assess the discovery potential of Belle II for this class of models. In this respect, we determine the viable regions of parameter space following the results and approximations established in the previous sections.

Figure 6.4 displays the current bounds and projected sensitivities in the (m_χ, ϵ) and (m_χ, θ) parameter planes, for our chosen benchmark values.[8] Shown in yellow are the limits from missing energy searches at NA64 using high-energy electron collisions on an active target [344], and in green from mono-photon measurements at BaBar [488]. We also show model-independent constraints from electroweak precision observables at LEP [494] and HERA [594] in gray. Standard bounds on scalar mixing angles from dark Higgs searches at PS191 [605], NA62 [606, 607], CHARM [568, 608], MicroBooNE [609, 610], Belle II [611], BaBar [568, 612] and LHCb [568, 613, 614] are also included in gray [331]. Additionally, we include in light gray constraints from BBN, requiring the dark Higgs to decay before 0.1 s [599]; stronger bounds such as $\tau_{h'} < 0.02$ s [442] apply only for $m_{h'} > 2m_\pi$, a region for which $\tau_{h'} < 0.02$ s is already automatically satisfied for all points we consider. As a visual reference, contours of constant dark Higgs proper decay length $c\tau_{h'} = 1$ km are included to highlight regions where no decays are expected to be probed at colliders.

The Belle II experiment is expected to probe much of the still-allowed parameter space. With over 424 fb^{-1} of data already collected [560], even a conservative dataset of 100 fb^{-1} offers substantial sensitivity, reaching down to $\epsilon \sim 10^{-4}$ and $\theta \sim 10^{-5}$. The projected reach for the novel displaced+γ channel—enabled by the parity-violating nature of niDM with decays $\chi^* \to \chi h'$—is shown as red dashed lines. This channel provides a distinctive probe unavailable in parity-preserving iDM models [79].

It is important to emphasize that the dark sector couplings used in our study are not arbitrary. They are chosen to reproduce the observed DM relic abundance through secluded annihilations $\chi\chi \to h'h'$, see eqs. (6.17) and (6.18). Therefore, the allowed parameter regions in fig. 6.4 represent viable models for sub-GeV DM, fully consistent with cosmological and experimental observations. Furthermore, these remaining viable parameter space can only be fully explored through the complementary interplay between missing energy searches and dedicated probes of dark Higgs decays, thereby motivating continued efforts to study these signatures at both colliders and beam dump experiments [3, 79].

Finally, we reiterate that our conclusions are robust against variations in dark sector coupling values, as long as $\alpha' \gtrsim 10^{-4}$ and $\delta_y y_L \gg 10^{-4}$ (see section 6.2). Within this regime, the displaced+γ signature remains a promising and distinctive discovery channel for parity-violating dark sectors.

6.6 Concluding Remarks

In this chapter, we have highlighted the crucial role of the dark Higgs boson in models of not-so-inelastic DM, where it arises naturally alongside the dark

[8] In this section, $\theta_{h'h}$ will be denoted by θ for simplicity.

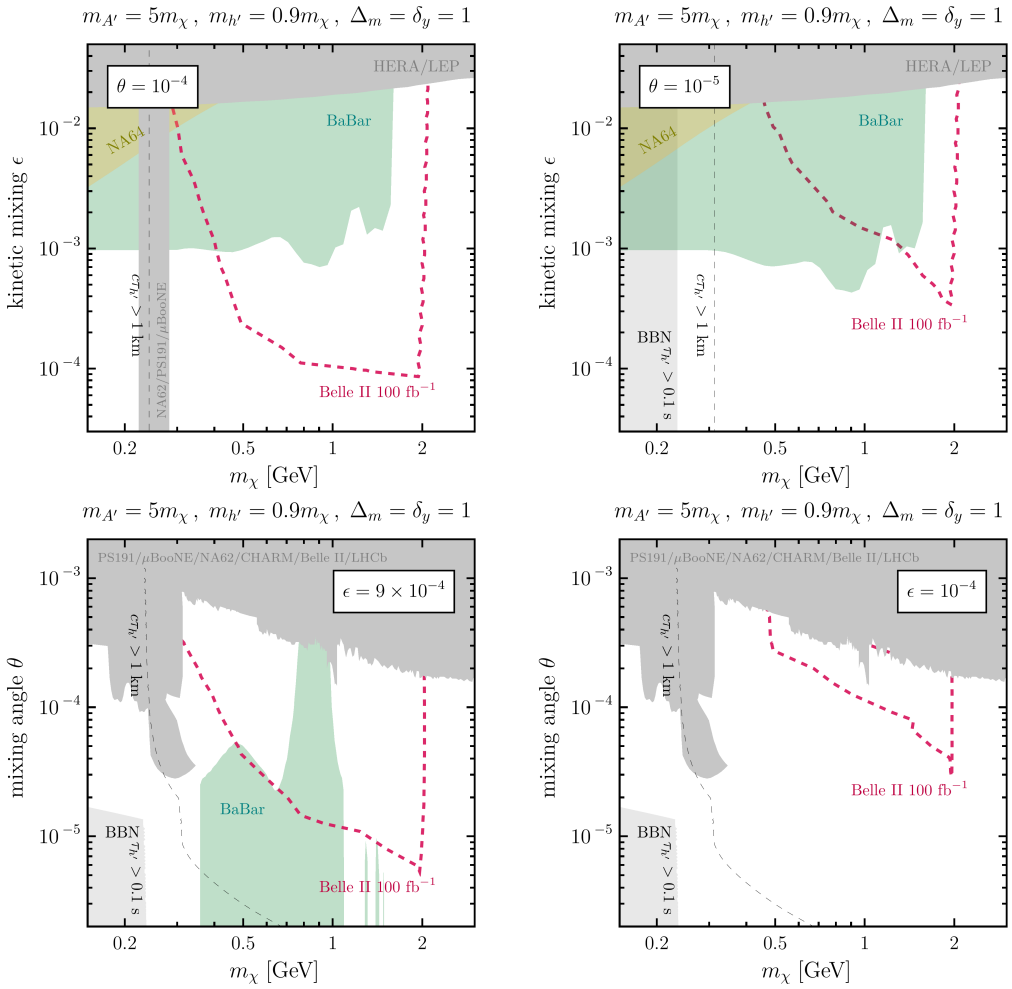

Figure 6.4: Projected sensitivity of Belle II to displaced vertex signatures from dark Higgs decays in association with a high-energy photon, shown in the (m_χ, ϵ) and $(m_\chi, \theta_{h'h})$ parameter planes. Current bounds from precision observables and direct searches for dark Higgs production via the scalar portal are shown in gray. Green and yellow shaded regions correspond to exclusions from missing energy searches at BaBar and NA64, respectively. Light gray areas are excluded by BBN constraints, requiring $\tau_{h'} < 0.1$ s. Dashed red contours indicate Belle II sensitivity for an integrated luminosity of 100 fb^{-1}, while dashed black lines represent contours of dark Higgs proper decay length $c\tau_{h'} = 1$ km. Throughout the plane, the observed DM relic abundance is satisfied via secluded freeze-out $\chi\chi \to h'h'$. See text for further discussion.

photon mediator. Specifically, we have shown that when the dark Higgs is light, $m_{h'} < \delta$, a novel decay channel for the excited DM state becomes kinematically accessible: $\chi^* \to \chi h'$. This process is only viable in parity-violating dark sectors, i.e., for $\delta_y \neq 0$, and gives rise to distinctive experimental signatures that are largely independent of the precise values of the dark sector couplings.

One of the central findings of this chapter is that light dark Higgs scenarios enable DM to freeze out through secluded annihilations, $\chi\chi \to h'h'$, thereby decoupling the relic density calculation from direct interactions with SM particles. Although this mechanism reduces the predictive link between DM cosmology and experimental signatures at colliders—in contrast to conventional visible freeze-out scenarios—it retains the appealing feature of being insensitive to the Universe's initial conditions. As a result, it permits a wider range of viable mixing parameters in both vector portal ϵ and scalar portal θ cases, expanding the space of experimentally testable WIMP-like DM models.

On the experimental front, we have shown that the Belle II detector provides a promising avenue to probe the structure of this dark sector through its distinctive signature: a displaced vertex originating from the decay of the dark Higgs h', accompanied by a high-energy photon and missing energy. This signal is further distinguished by the fixed invariant mass of the SM particle pair from the h' decay, enhancing its discriminating power against background. Remarkably, even with a relatively modest dataset of 100 fb^{-1}, Belle II can already explore significant portions of the viable parameter space, emphasizing its high sensitivity to this class of hidden sector models.

Nonetheless, important directions remain open. In particular, existing missing energy searches at BaBar [488] should be revisited in detail to account for potential energy depositions from dark Higgs decays in the detector. This is essential, as these searches provide the most stringent bounds in the mass range accessible to Belle II. Moreover, production of dark Higgs particles via dark photon decays may be explored at electron and proton beam dump experiments such as NA64 [344], NA62 [504], NuCal [615], and CHARM [616], offering complementary discovery potential. Incorporating these probes represents a crucial step toward a comprehensive exploration of the light dark Higgs scenario.

In summary, dark Higgs particles in niDM models not only enrich the theoretical structure of dark sectors but also open new experimental avenues at the intensity frontier. This strongly motivates continued efforts to develop and refine collider and beam dump strategies for long-lived particle searches in the MeV to GeV mass range.

Chapter 7

Not-so-inelastic Dark Matter: exploring new directions

While the guiding principle for constructing dark sectors or FIPs models has often been minimality, it is important to recognize that the SM itself is far from minimal—it includes a non-trivial gauge group, two mass scales, a scalar sector, and three fermion generations, each containing multiple fermionic particles. Inspired by this, a new class of *rich dark sector models* (RDSMs) has gained attention. They have even been identified as one of three "Big ideas" in RF6 Snowmass process in the US, with a special focus on rich DM models (e.g., the iDM scenario) [617]. RDSMs extend the dark sector with new gauge symmetries and a complex particle spectrum—including fermions, scalars, and multiple mediators—and are often better suited to explain various open problems in fundamental physics, such as DM, neutrino oscillations, and the baryon asymmetry of the Universe [325, 331, 408, 410, 463, 543, 545, 552, 571, 618–624]. Historical precedents for RDSMs include Hidden Valley models [314, 625, 626], mirror sectors [627–629], and Twin Higgs scenarios [630].

RDSMs exhibit a much richer phenomenology than minimal models. Whereas standard searches focus on visible (e.g., dilepton resonances) or invisible (e.g., missing energy) signals, RDSMs naturally allow for semi-visible decays, complex decay chains, and multiple displaced vertices. These features demand more inclusive experimental strategies, as traditional cuts may severely weaken sensitivity [300].

A variety of Intensity Frontier (IF) experiments, including Belle II [91], NA62 [539], FASER [631], SND@LHC [632], SHiP [633], MAPP [634], DarkQuest [635] and DUNE [636], are designed to explore the parameter space of long-lived FIPs in the MeV to a few GeV mass range. They complement prompt searches at the LHC by targeting longer lifetimes and smaller couplings [507, 637–643].

The canonical FIP signature is the mono-decay: the decay of a single long-lived particle within the detector, typically reconstructed through its visible decay products. Mono-decay events allow for the extraction of mass, decay length,

and branching ratios [644–649]. However, a fundamental limitation exists: distinct FIP models may exhibit identical decay signatures, leading to degeneracies that cannot be resolved through mono-decays alone.[1] In principle, distinguishing between FIP models could be achieved by combining information about the decay palette with knowledge of the production point. However, at IF experiments, the production vertex is usually inaccessible—occurring deep within a thick target or hidden beneath substantial backgrounds—making it extremely challenging, if not impossible, to reconstruct its position.

In this context, we propose an alternative and powerful strategy: the observation and analysis of "di-decay events," where two FIPs decay within the detector volume. Such events arise naturally in RDSMs, for which the mono-decay signature can easily mimic that of minimal "portal" benchmark models widely studied in the literature. We emphasize that di-decay events provide unique insights into the underlying production mechanisms of FIPs and enable sharper discrimination between different dark sector scenarios.[2] Moreover, when combined with more conventional search strategies, they offer the possibility of a comprehensive characterization of RDSMs, including generic realizations of niDM.

7.1 Opportunities from di-decays

The di-decay signature is a complementary strategy to the common studied mono-decay signals which can greatly improve the FIPs *differentiation* power of IF experiments. These events offer crucial kinematic handles, such as the invariant mass of the decaying pair, which encode information about the production mechanism (insights from other correlated variables can be found in appendix F of Ref. [95]). In particular, they enable one to discriminate between production via:

- Quadratic couplings to SM fields. Famous examples are quadratic operators coupled to the SM Higgs, hXX where h is the Higgs boson and X being ALPs, Higgs-like scalars, or dark photons [408, 552, 652, 654, 656, 660–667].
- Quadratic couplings to short-lived new physics resonances. Here, examples are HNLs interacting with a dark photon [668, 669] and various DM scenarios with with unstable mediators [71, 83, 622].

[1] Furthermore, theoretical uncertainties in modeling the decays of GeV-scale FIPs can span several orders of magnitude, posing additional challenges for their identification [595, 623, 650].

[2] For the ATALS and CMS detectors, the di-decay signature has been studied in Refs. [651–658]. For Belle II, the di-decay signature was previously discussed in Ref. [83, 659], however, in the context of very specific models involving multiple FIPs and without revealing the discovery power.

- Dark showers in strongly coupled dark QCD-like scenarios [670–675], where dark mesons π_D and ρ_D are typically produced with high multiplicity per event, and can mimic decays of ALPs or dark photons.

For example, suppose a IF experiment observes a dark-photon-like mono-decay signal. This signature could originate from four distinct types of FIPs: a minimal portal dark photon, a dark photon with additional quadratic coupling to the Higgs or to a scalar mediator, or even a dark ρ meson. While pair production might alter the energy spectrum of mono-decays, its impact is generally modest (unless it overwhelmingly dominates the FIP flux). Observing di-decays would immediately rule out the minimal scenario but would not suffice to distinguish among the other three cases.

Additional insight can be gained from the invariant mass distribution, $m_{\rm inv}$, of the di-decay products, as illustrated in Fig. 7.1. At SPS, a coupling of the form hXX leads to decays such as $B \to X_s + 2X$ and $B_s \to 2X$ [571, 622], where X_s is a meson containing a strange quark. In this case, the $m_{\rm inv}$ distribution is continuous for $m_{\rm inv} < m_B - m_K$ and exhibits a sharp peak at $m_{B_s}/2$. Coupling to a scalar resonance like a dark Higgs ($h'XX$) would instead produce a narrow peak at the resonance mass $m_{h'}$. In contrast, dark ρ mesons present a continuous spectrum typically enhanced at low $m_{\rm inv}$ and, depending on model details, may extend beyond $m_{B_s}/2$.

Due to these qualitatively distinct features, observing up to $\mathcal{O}(100)$ di-decay events with negligible backgrounds may allow one to distinguish between these competing FIP scenarios [95]. Di-decays thus serve as a smoking gun for RDSMs and pair-produced FIPs, offering a powerful means to resolve model ambiguities that mono-decay signatures alone cannot address. Although di-decays are generically suppressed relative to mono-decays—owing to the requirement that both FIPs decay within the detector volume, their exceptionally low backgrounds and correlated decay observables significantly enhance their discriminating power in identifying the nature of the underlying FIP scenario.

Consider a FIP X with interactions described by the following interaction Lagrangian:

$$\mathcal{L}_{\rm int} = c_1\ X \cdot \mathcal{O}_1(\Psi_{\rm SM}) + c_2\ \mathcal{O}_2(\Psi_{\rm SM}) \cdot X \cdot X \tag{7.1}$$

Here, $\mathcal{O}_{1/2}(\Psi_{\rm SM})$ are some operators only containing the SM fields $\Psi_{\rm SM}$, while $c_{1,2}$ are interaction couplings, generally independent of each other (see eq. (2.87) as an example). The interaction shown in eq. (7.1) is symbolic; the key point is that the FIP connects to the SM via linear and quadratic terms.

The $\mathcal{O}_1$ operator can produce events with a single X in SM collisions and it also controls X decays. Its contribution to the number of X produced scales as $N_X^X \propto c_1^2$, whole the lifetime of X behaves as $\tau_X \propto c_1^{-2}$. In contrast, the $\mathcal{O}_2$ operator can only contribute to the production of X in pairs, with $N_{\rm prod}^{2X} \propto c_2^2$.

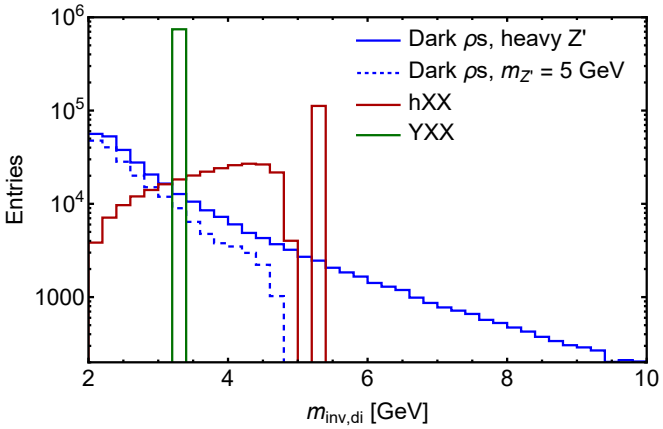

Figure 7.1: Invariant mass distribution of a pair of FIPs X with mass $m_X = 1\,\text{GeV}$ for various production scenarios at the SPS accelerator. Shown are dark ρ^0 mesons in the dark QCD model of Ref. [672], produced via a Z' mediator that is either very heavy or light with $m_{Z'} = 5\,\text{GeV}$, simulated using `PYTHIA8` [676]; 2- and 3-body decays of B mesons, corresponding to FIPs quadratically coupled to the Higgs boson (e.g., dark photons, ALPs, and Higgs-like scalars); and 2-body decays of a short-lived intermediate particle with mass $m_Y = 3\,\text{GeV}$ (e.g., HNLs or dark photons in iDM models). Reconstructing the invariant mass distribution from di-decay events allows for straightforward identification of the production mode and underlying model, even without access to the production vertex. Assuming negligible backgrounds and an invariant mass resolution of 0.1 GeV, as few as 100 di-decay events are sufficient to differentiate between the shown scenarios. Reproduced from Ref. [95].

Examples are the decays of some mother particle Y:

$$Y \to 2X, \quad Y \to Y' + 2X, \ \ldots, \tag{7.2}$$

Accordingly, at IF experiments, two types of events may occur: *mono-decays*, where a single X particle decays within the detector, and *di-decays*, where two X particles decay inside the detector volume. In the mono-decay case, both operators $\mathcal{O}1$ and $\mathcal{O}2$ contribute to production, whereas for di-decays, only $\mathcal{O}_2$ contributes.

The number of events detected for each signature can be roughly estimated as [677]:

$$N_{\text{events}}^{(\text{di})} = N_{\text{prod}}^{2X} \times \xi^2, \tag{7.3}$$

$$N_{\text{events}}^{(\text{mono})} = N_{\text{prod}}^{X+2X} \times \xi - 2N_{\text{events}}^{(\text{di})}, \tag{7.4}$$

where $N_{\text{prod}}^{X+2X} = N_{\text{prod}}^{X} + 2N_{\text{prod}}^{2X}$, $N_{\text{prod}}^{X(2X)}$ is the total number of events producing a single (pair of) particle(s) X and $\xi = \epsilon_X \cdot P_{\text{dec}}^X \cdot \epsilon_{\text{dec}} < 1$ is the suppression of the event rate due to geometric limitations, decay probability, and event selection:

– ϵ_X is the fraction of Xs whose trajectories intersect the decay volume.

– P^X_{dec} is the X's decay probability:

$$P^X_{\text{dec}} = \exp\left[-\frac{l_{\text{min}}}{\tau_X \langle\gamma v\rangle_X}\right] - \exp\left[-\frac{l_{\text{max}}}{\tau_X \langle\gamma v\rangle_X}\right], \tag{7.5}$$

with $l_{\text{min/max}}$ being the minimal and maximal distance from the collision point covered by the decay volume, and $\langle\gamma\beta\rangle_X$ the mean γ factor times velocity v of the produced X particles.

– ϵ_{dec} is the fraction of X decay events that can be successfully reconstructed. It accounts for suppressions arising from both kinematic and geometric cuts on the final-state particles, as well as their reconstruction efficiencies.

If a signature is not background-free in a particular experiment under consideration, its sensitivity in that experiment is determined by the signal strength $I = N_{\text{events}}/\sqrt{N_{\text{bg}}}$ with N_{bg} the total number of background events corresponding to the given signature; otherwise if background-free simply $I = 1$.

The signal strength ratio for di- and mono-decay events is given by

$$\eta = \frac{I_{\text{di}}}{I_{\text{mono}}} = \frac{N^{2X}_{\text{prod}}}{N^X_{\text{prod}} + 2N^{2X}_{\text{prod}}(1-\xi)} \times \xi \times \sqrt{\frac{N^{\text{mono}}_{\text{bg}}}{N^{\text{di}}_{\text{bg}}}}\,. \tag{7.6}$$

This ratio captures the non-trivial interplay between the production rates, geometric acceptance ξ and background yields, as shown in fig. 7.2.

When $N^{2X}_{\text{prod}}/N^X_{\text{prod}}$ is sizable, η becomes highly sensitive to deviations of ξ from unity. At beam dumps or colliders with strong boosts and limited angular coverage [539, 642, 678, 679], $\xi \ll 1$, making di-decays relevant only at larger couplings, though still potentially impactful.

Conversely, in setups like BelleII[91] or FCC-ee [680], where FIPs are produced with modest boosts and detectors cover large solid angles, ξ remains close to one, enhancing the visibility of di-decays.

The background suppression factor is also critical. In background-limited searches, such as in ANUBIS [507] or Belle II[611], mono-decays may suffer from irreducible noise, while di-decay signatures, involving two displaced vertices with correlated products, are much cleaner and harder to be mimicked, whether physical or combinatorial, by SM processes.

Therefore, in experiments with moderate boosts or non-negligible backgrounds, di-decays can substantially enhance or complement conventional mono-decay searches. More broadly, they offer a powerful window into the internal structure of dark sectors and can play a pivotal role in distinguishing minimal portal scenarios from richer frameworks, such as not-so-inelastic dark matter (niDM) models.

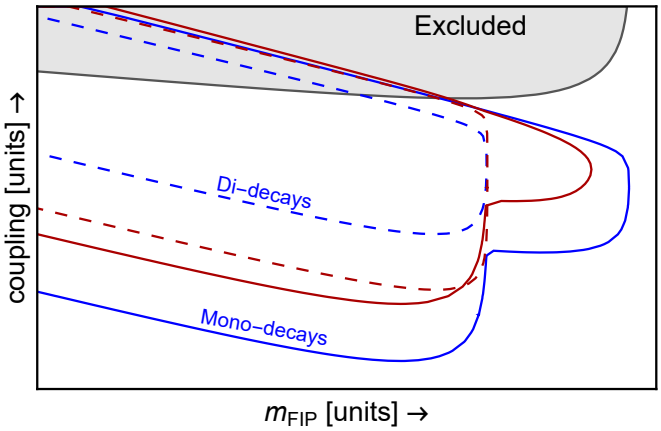

Figure 7.2: Schematic representation of the parameter space for a FIP with mass m_{FIP} coupled to SM particles, which can be produced at accelerator experiments either as a single particle or in pairs. At intensity frontier experiments, such a FIP may be probed via searches for a single decay vertex ("mono-decay") or two decay vertices within the same event ("di-decay"). The currently excluded regions of parameter space are shown in gray, while the prospective sensitivities to mono- and di-decays are indicated by solid and dashed curves, respectively. Depending on background levels, tagging requirements, experimental geometry, and FIP kinematics, di-decays may either compete with the mono-decay signature (red curves) or be sub-dominant while still providing unique insights in the event of a detection (blue curves). Reproduced from Ref. [95].

In the context of (n)iDM, previous studies have largely concentrated on the exclusion potential of di-decay signatures across various experiments [79, 83]. In contrast, our focus is on their role in model discrimination in the event of a discovery. We show how di-decays arise naturally within the niDM framework and demonstrate their power as a diagnostic tool for unraveling the underlying structure of the dark sector. In particular, we illustrate that combining multiple experimental signatures allows one to reconstruct the different dark sector's couplings and, consequently, probe the flavor dynamics characteristic of generic niDM models.

To establish a baseline, we first revisit the di-decay phenomenology in a minimal dark Higgs scenario in section 7.1.1. We then discuss, in section 7.1.2, the novel di-decay signatures enabled by parity breaking in niDM and argue that the rich phenomenology motivates a model-independent formulation of the niDM coupling structure. Building on this, section 7.2 introduces an effective Lagrangian describing generic fermionic niDM models, while section 7.2.1 explores how Belle II can probe the resulting dark sector dynamics. Finally, in section 7.2.2, we identify the regions of parameter space where Belle II can comprehensively investigate the dark flavor structure, concluding in section 7.3 with a discussion of our findings.

7.1.1 Optional: **Old di-decays signatures** (dark Higgs only)

Before analyzing di-decays in the context of niDM models, we first review their appearance in one of the most minimal FIP models, the standard dark Higgs portal also known as Higgs-like scalar introduced in section 2.5.[3] Remarkably, despite the extensive body of research on dark Higgs particles [331], the di-decay signature has remained completely unexplored at IF experiments.

We recall that this model features a light scalar S with the following effective interactions [660]:[4]

$$\mathcal{L} \supset m_h^2 \theta S h + \frac{\alpha}{2} h S^2 \,, \tag{7.7}$$

where h is the SM Higgs boson, and θ and α parameterize mixing and trilinear couplings, respectively (further details on the model can be found in section 2.5). The scalar S inherits Higgs-like decays and interactions, with rates suppressed by $\theta \ll 1$, along an addition tri-linear hSS interaction. Particularly, theoretical uncertainties on S decays can reach orders of magnitude when dominated by mixing with scalar mesons [568, 595, 681]. We follow Ref. [595] for a data-driven estimation of the scalar decay width taking into account these uncertainties. The coupling of the additional tri-linear interaction α can be directly linked to the branching ratio $\mathrm{Br}(h \to SS)$ via

$$\alpha^2 \simeq \frac{32\pi}{\sqrt{1 - \frac{4m_S^2}{m_h^2}}} \mathrm{Br}_{h\to SS} \Gamma_h m_h \,, \tag{7.8}$$

where Γ_h and m_h are the total decay width and mass of the SM Higgs. Indeed, the main constraints on α come from unobserving the decays of the type $h \to \mathrm{inv}$, setting the model-independent bound $\mathrm{Br}(h \to \mathrm{inv}) < 0.15$ at 95% CL [682].[5]

This model leads to both mono- and di-production channels via B-meson decays and Higgs boson decays:

$$B^{+/0} \to Y_{s/d} + S, \quad B_s \to \phi + S \,, \tag{7.9}$$

$$h \to SS, \quad B^{+/0} \to Y_{s/d} + SS, \quad B_s \to \phi + SS \,, \tag{7.10}$$

where $Y_{s/d}$ refers to any hadron containing a strange or down-type quark. The mono-production modes, eq. (7.9), are induced by θ, while α controls di-production, eq. (7.10). Contributions from radiative decays of vector mesons are in general negligible [95, 685].

[3] In this section, we will denote the new scalar by S in contrast with our standard notation h' to avoid any confusion between the Higgs h and the dark Higgs S. Moreover, for simplicity $\theta_{h'h}$ is denoted by θ.

[4] The quartic term $h^2 S^2$ is neglected since it is irrelevant for our analysis.

[5] With the HL-LHC runs, the sensitivity to invisible Higgs decays will be improved down to a few percent [683, 684].

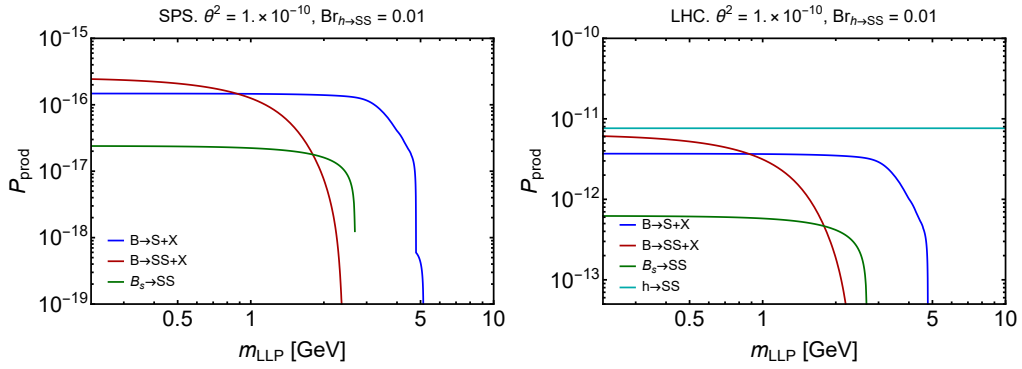

Figure 7.3: Production probabilities of Higgs-like scalars at the SPS and LHC facilities for $\theta^2 = 10^{-10}$ and $\mathrm{Br}(h \to SS) = 0.01$. Reproduced from Ref. [95].

Assuming $\mathrm{Br}(h \to SS) = 0.01$, the production probabilities of S particles at the SPS and LHC facilities, calculated using `SensCalc` [1, 2], are shown in fig. 7.3. Here, we neglect production via proton bremsstrahlung and kaon decays since they are typically subdominant in the SPS- and LHC-based experiments we will consider. At the LHC, di-production modes (7.10), specifically Higgs decays, dominate the scalar production provided that $\theta^2/\mathrm{Br}(h \to SS) \lesssim 2 \cdot 10^{-8}$. At lower energy facilities where the Higgs cannot be produced, di-production processes remain the main production mechanisms under the same condition when kinematically allowed, $m_S \lesssim m_{B_s}/2$ [660].

Sensitivity at Intensity Frontier Experiments: To assess the potential of IF experiments to explore Higgs-like scalars via di-decay signatures, we consider three complementary experiments: SHiP [686], Belle II [91], and LHCb with the recently proposed Downstream trigger scheme (hereafter Downstream@LHCb) [642, 643]. While SHiP is expected to begin operation in 2033 following its 2024 approval, both Belle II and Downstream@LHCb are already running. Details of our simulations and the experimental configurations are discussed in appendices C and D of Ref. [95].

SHiP is a proton beam dump experiment operating with a 400 GeV beam and a long, shielded decay volume. It is expected to collect the impressive amount of $6 \cdot 10^{20}$ protons on target. Its design ensures operation in a background-free regime throughout its projected 15-year runtime [633], making it especially suited for rare decay searches such as those involving FIPs.

Downstream@LHCb is an implemented trigger scheme that expands the LHCb effective decay volume beyond the inner tracker. For invariant masses above 2 GeV, the decay region is effectively background-free due to the absence of physical resonances and the suppression of combinatorial backgrounds [643, 687]. Studies are ongoing to assess the feasibility of probing lower masses. The

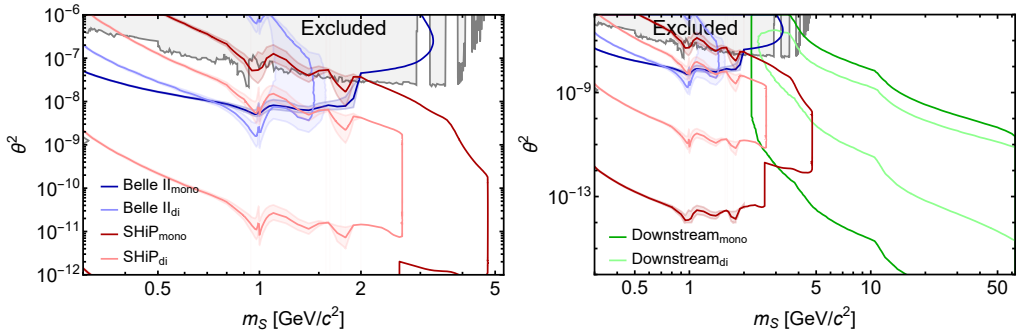

Figure 7.4: Sensitivities of SHiP, Belle II, and Downstream@LHCb for mono- and di-decay signatures from Higgs-like scalars, assuming $\mathrm{Br}(h \to SS) = 0.1$. The left panel shows the zoomed-in parameter space probed by SHiP and Belle II, while the right panel additionally includes the Downstream@LHCb experiment. Mono-decay regions constitute the exclusion potential, while, in the di-decay domain, it may be possible to distinguish between different models with similar (or even the same) decay pattern. Excluded regions (gray) are taken from Ref. [611]. Shaded colored bands represent theoretical uncertainties from scalar decay modeling [595]. Reproduced from Ref. [95].

search may continue through the LHC high-luminosity phase, targeting a total integrated luminosity of $\mathcal{L} = 300$ fb^{-1}.

At Belle II, low-boost $B\bar{B}$ meson pairs produced via e^+e^- collisions and a large angular coverage provide an excellent setup for di-decay searches. The ability to reconstruct the full decay chain is a key advantage, though it comes with significant background. For instance, the signature $B^+ \to K^+X$ [91], $X \to$ visible final states, yields 5–10 background events for $\mathcal{L} = 0.189$ fb^{-1} [611], which extrapolates to $\mathcal{O}(10^3)$ events for the full run of $\mathcal{L} = 50$ ab^{-1}. Despite this, Belle II offers unique capabilities in reconstructing displaced decays with precise kinematic control.

Fig. 7.4 presents the sensitivities of these experiments for both mono- and di-decay signatures. We see that, indeed, these three experiments complement each other: both SHiP and Belle II probe $m < m_{B_s}/2$ though in different mixing angle regimes, while Downstream@LHCb is sensitive to higher masses.

At SHiP, the sensitivity to di-decays lies entirely within the mono-decay reach, as expected due to the additional suppression from requiring two decays within the background-free detector. Nevertheless, it covers a meaningful portion of parameter space where, thanks to correlated observables, it may be possible to reconstruct the production mode and robustly discriminate the Higgs-like scalar from other models (see appendix F of Ref. [95] for further discussion).

At Belle II, mono-decay backgrounds are dominated by fake tracks and tracks with missing hits [611], rather than physical backgrounds. Similar effects could affect di-decay searches, but the probability of reconstructing two displaced ver-

tices with matching invariant masses that together with the kaon reproduce the parent B meson mass is strongly combinatorially suppressed. We thus optimistically treat the di-decay signature as background-free, though a dedicated experimental study is warranted. Given the non-negligible backgrounds for mono-decays and the mild di-decay relative suppression due to the large angular coverage of Belle II, the di-decay search is highly competitive and even dominant for scalar masses around 1 GeV.

At Downstream@LHCb, the situation mirrors SHiP: the di-decay reach is again nested within the mono-decay domain. However, the accessible mass range extends up to $m_S = m_h/2$, where scalar decays involve high-multiplicity final states. This makes such events ideal for r the new Buffer Scanner (BuSca) project of LHCb [687, 688], capable of real-time Downstream monitoring at 30 MHz for masses up to 50 GeV.

We expect similar opportunities at other IF experiments, particularly off-axis LHC detectors such as MATHUSLA, ANUBIS, and CODEX-b, where moderate FIP boosts and non-negligible backgrounds could make the clean and distinctive di-decay signature especially valuable [689].

Conclusion. In this optional section, we have elucidated how di-decay signatures can naturally emerge even in minimal dark sector scenarios, such as those involving Higgs-like scalars. While not a new prediction, since this model has already been studied at the main LHC detectors, our analysis demonstrates that these signatures can effectively probe sizable regions of parameter space at both current and future IF experiments. In particular, di-decays provide a valuable tool for identifying production mechanisms, mitigating backgrounds, and distinguishing between models with otherwise similar decay patterns. Our study highlights the complementary capabilities of Belle II, SHiP, and Downstream@LHCb in accessing this signature, thereby advancing the experimental program for FIPs searches . More broadly, the methodology developed here establishes a foundation for investigating richer dark sector scenarios, such as the case for not-so-inelastic Dark Matter, which will be discussed next.

7.1.2 New di-decay signatures

As discussed in the previous chapter, di-decay events were previously considered in the context of inelastic Dark Matter (iDM) predominantly for models involving a dark Higgs mediator in addition to the vector portal [79, 83]. In such setups, the dark Higgs can decay into two excited DM states or be produced through Higgs-strahlung processes, independently of parity-breaking assumptions.[6] Consequently, di-decay signatures naturally emerge via dark Higgs production.

[6]Throughout this work, we consistently adopt a non-zero mass splitting $\delta > 0$, which is necessary for realizing inelastic interactions.

In contrast, the not-so-inelastic Dark Matter (niDM) framework, due to its relaxed symmetry structure allowing for generic parity breaking, enables the appearance of di-decays even in scenarios involving only the dark photon mediator. Furthermore, thanks to the broader range of viable kinetic mixing values [79] (especially when compared to the scalar mixing angle [331]), dark photon-mediated di-decays probe a larger region of parameter space. While Higgs-strahlung can still allow for dark Higgs production via the vector portal, it typically requires large dark gauge couplings. In contrast, in the niDM scenario, such di-decay events can occur even for small dark couplings and remain entirely independent of scalar mixing angles $\theta_{h'h}$—thus decoupling the collider phenomenology from the properties of the dark Higgs.

Given this novel feature and its broad accessibility at current and upcoming experiments, we focus here on the dark photon portal. As partially discussed in Ref. [83], similar conclusions could be drawn for the dark Higgs portal scenario; we will return to this point later. For now, assuming the dark Higgs is lighter than the DM but heavier than the mass splittings, its role is limited to enabling secluded freeze-out via $\chi\chi \to h'h'$ and imposing DD constraints for $m_\chi \gtrsim 8$ GeV—similar to the previous chapter—while not contributing to decays of the form $\chi^* \to \chi h'$.

Turning to the dark photon interactions in niDM, the couplings introduced in table 3.2 illustrate that the dark photon generically couples to two excited DM states, enabling decays such as $A' \to \chi^*\chi^*$. These can manifest at e^+e^- colliders via processes like electron-positron annihilations $e^+e^- \to \gamma A' \to \gamma\chi^*\chi^*$, dark Higgs-strahlung $e^+e^- \to h'A' \to h'\chi^*\chi^*$ and direct production $e^+e^- \to \chi^*\chi^*$, leading to multiple distinctive signatures with two (or more) decay vertices (see fig. 7.5 for details). In the special case of parity conservation ($\delta_y = 0$), these interactions remain purely off-diagonal, and such decay channels are forbidden. Allowing for general parity violation ($\delta_y \neq 0$), however, results in non-zero diagonal couplings $\beta_{**} \neq 0$, and the possibility of significant $A' \to \chi^*\chi^*$ branching ratios arises.

To quantify this behavior, fig. 7.6 displays the branching fractions of A' into dark sector final states as a function of the normalized mass splitting $\Delta_m \equiv (m_{\chi^*} - m_\chi)/m_\chi$ across representative niDM scenarios. These include:

- The standard regime ($m_d \geq \sqrt{m_R m_L}$) with large parity breaking $\delta_y \gg 1$ but no $\mathcal{CP}$-phase ($\phi_d = 0$) as discussed in chapter 4 [89];
- The p-wave scenario ($m_d < \sqrt{m_R m_L}$) introduced in section 3.2.3 (also for $\phi_d = 0$) with small parity breaking values, $\delta_y = 0.05$ and $\delta_y = 0.5$, since necessarily $\Delta_m \geq \delta_y$;

Additionally, we include predictions for inelastic Dirac DM (i2DM) [478], where the DM consists of Dirac fermions and di-decays occur without requiring any

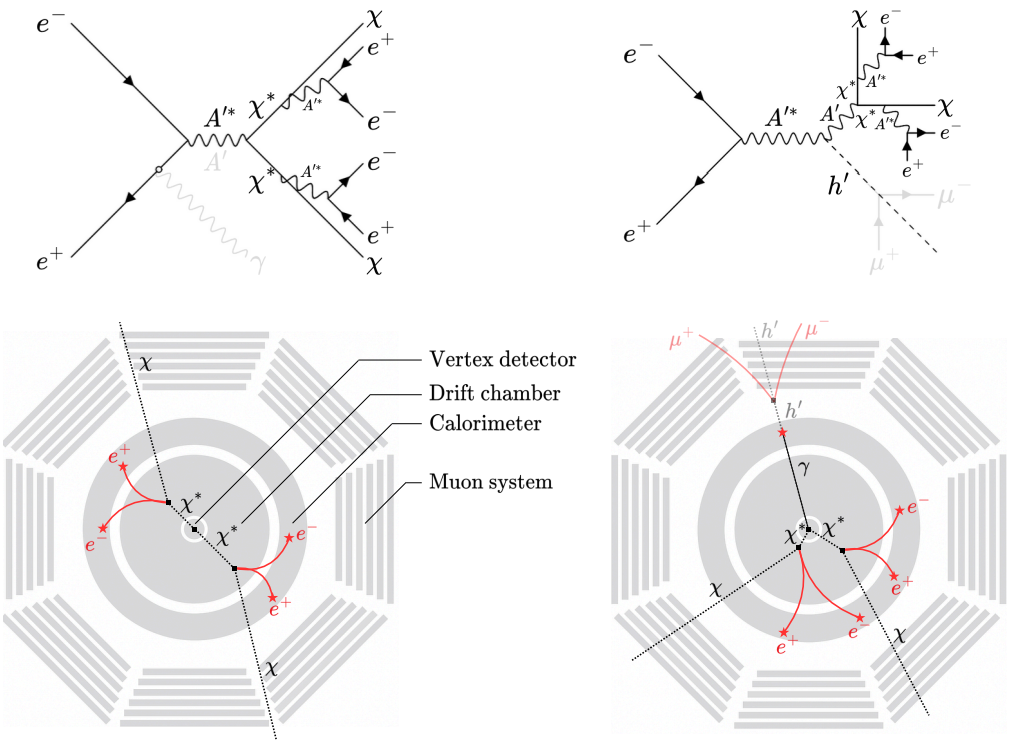

Figure 7.5: Schematic Feynman diagrams (top) illustrating the new niDM di-decay signatures—allowed only when $\delta_y \neq 0$—at Belle II, together with examples of the corresponding event topologies in the transverse plane of the detector (bottom), where we assume a promptly decaying dark photon. The top left diagram shows both direct production of an excited state pair in e^+e^- collisions via off-shell dark photons, $e^+e^- \to A'^* \to \chi^*\chi^*$, and production in association with a SM photon followed by on-shell dark photon decay, $e^+e^- \to \gamma A' \to \gamma\chi^*\chi^*$. The top right diagram depicts production via dark Higgs-strahlung, $e^+e^- \to A'h'$ (involving an off-shell A'^*), with $A' \to \chi^*\chi^*$. In this case, the dark Higgs may decay visibly within the detector or escape undetected; for $m_{h'} > 2m_\chi + \delta$, additional χ^* states can be produced, as discussed in Ref. [83]. For illustration, we show χ^* decays into electrons and h' decays into muons, though in general many SM final states are possible. The bottom panels represent the corresponding event topologies: direct production (left) and production with an additional associated particle, either a SM photon or a dark Higgs (right).

parity violation, serving as a benchmark for comparison. We set the fermionic mixing angle θ_χ driven the coupling structure of this type of models to its maximal value $\pi/4$ and also to a small value of $\pi/10$. In all cases, we assume a small kinetic mixing such that the dark photon decays dominantly into the dark sector.

These results highlight the rich variety of possible A' branching behaviors, depending on symmetry assumptions and parameter choices. Notably, mod-

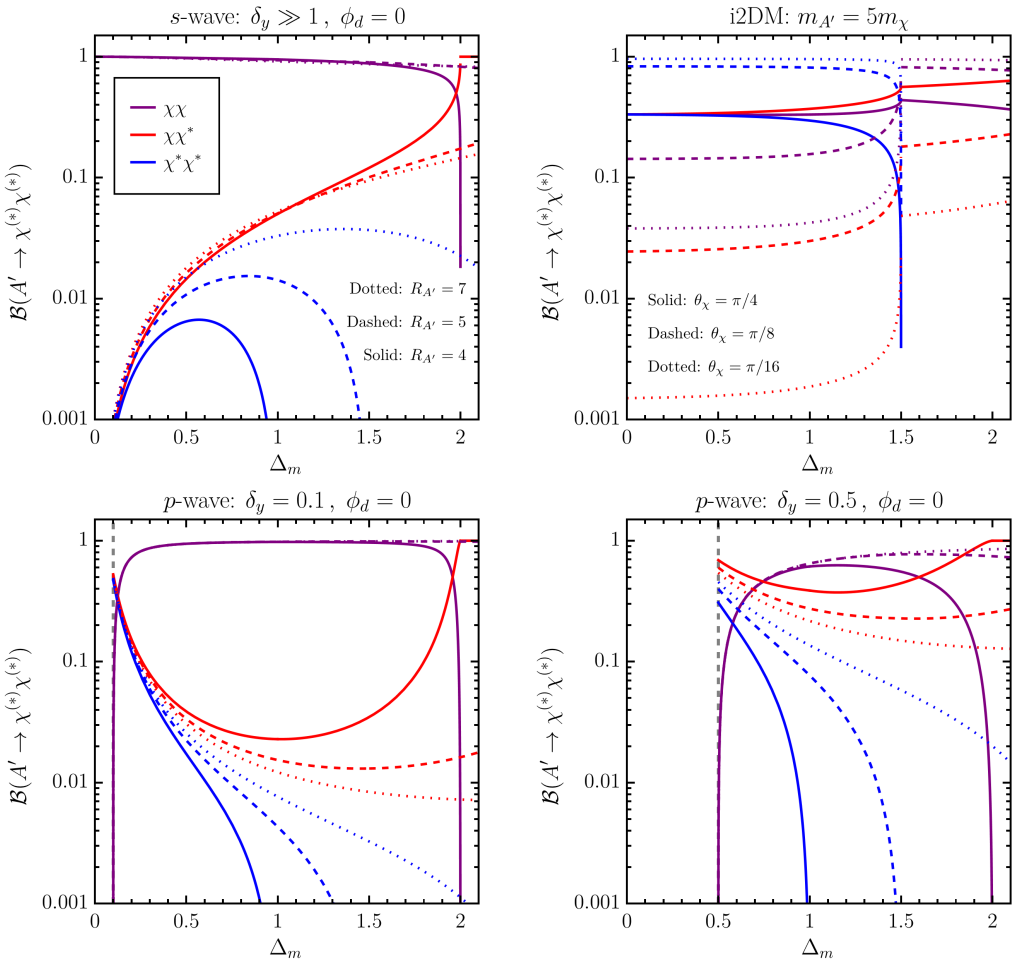

Figure 7.6: Branching fractions of an invisibly decaying dark photon A' ($\alpha' \gg \epsilon\alpha$) in various niDM scenarios as a function of the normalized mass splitting Δ_m. **Top:** standard s-wave niDM scenario ($m_d \geq \sqrt{m_R m_L}$) with $\phi_d = 0$ and strong parity breaking $\delta_y \gg 1$ (left), shown for several values of the mass ratio $R_{A'} \equiv m_{A'}/m_\chi$; and the i2DM setup [478] with fixed $R_{A'} = 5$ but varying fermionic mixing angle θ_χ (right). **Bottom:** p-wave niDM scenario ($m_d < \sqrt{m_R m_L}$) with $\delta_y = 0.1$ (left) and $\delta_y = 0.5$ (right), for the same values of $R_{A'}$ as in the s-wave case and $\phi_d = 0$. Vertical gray lines mark $\Delta_m = \delta_y$, which represents the minimal mass splitting allowed in p-wave scenarios.

els like i2DM also populate the literature and exhibit distinct phenomenological features. Motivated by this diversity, in the remainder of this chapter we advocate for a general effective description of fermionic niDM models to systematically study their experimental signatures—particularly di-decays. This model-independent approach allows experimental analyses to directly constrain the effective couplings governing dark sector interactions, without relying on ad hoc UV completion choices. In the event of a discovery, such measurements could then be mapped back to UV-complete models, enabling identification of the DM particle responsible for approximately 80% of the matter content of the Universe.

7.2 A generic picture for not-so-inelastic Dark Matter

Inspired by fermionic iDM models found in the literature [69, 70, 89, 418, 478]—particularly the niDM model introduced in chapter 3—we consider a dark sector containing two fermions: the ground DM state χ and the excited DM state χ^*, with masses

$$m_{\chi^*} = m_\chi + \delta\,, \qquad \text{where} \qquad \delta > 0\,. \tag{7.11}$$

We describe their interactions via the following effective Lagrangian:

$$\mathcal{L}^I_\chi = e' A'^\mu\, \bar{\chi}_i (i\alpha_{ij} + \beta_{ij}\gamma^5)\gamma_\mu \chi_j - y h'\, \bar{\chi}_i (\hat{\alpha}_{ij} + i\hat{\beta}_{ij}\gamma^5)\chi_j\,, \tag{7.12}$$

where two of the three renormalizable portals to the SM are included:[7] the dark photon A' and the dark Higgs h'. As in most iDM frameworks, DM is essentially only composed of the lightest state χ.

The Feynman rules presented in chapter 3 apply here as well, with the difference that the interaction coefficients are now left generic. These must satisfy:

$$\alpha_{ij} = -\alpha^*_{ji}\,, \qquad \beta_{ij} = \beta^*_{ji}\,, \qquad \hat{\alpha}_{ij} = \hat{\alpha}^*_{ji}\,, \qquad \hat{\beta}_{ij} = \hat{\beta}^*_{ji}\,, \tag{7.13}$$

which imply, for instance, that all diagonal coefficients are real except for α_{ii}, which are purely imaginary.

For Majorana fermions, the interaction terms should be rescaled by a factor of 1/2, and the following extra relations apply:

$$\alpha_{ij} = -\alpha_{ji}\,, \qquad \beta_{ij} = \beta_{ji}\,, \qquad \hat{\alpha}_{ij} = \hat{\alpha}_{ji}\,, \qquad \hat{\beta}_{ij} = \hat{\beta}_{ji}\,. \tag{7.14}$$

These imply that $\alpha_{ii} \equiv 0$ and all couplings are real. A full derivation of the relations in eqs. (7.13) and (7.14) is provided in appendix A.

[7] We neglect the heavy neutral lepton portal $F_{ij}\bar{L}_i H \chi_j$, as it is often absent in fermionic iDM scenarios due to symmetries or model specific choices [70, 89, 93, 418, 478], effectively setting $F_{ij} = 0$.

The relevant mediator parameters are their masses, $m_{A'}$ and $m_{h'}$, and their mixings with the SM: the kinetic mixing ϵ for A' and the scalar mixing angle θ for h' (see section 2.5). While additional parameters may be relevant in the scalar sector [95], such as those entering dark Higgs di-production, we neglect these in the present analysis.

In the remainder of this work, when referring generically to the off-diagonal coefficients, we will adopt the notation κ_{-*}. This parameter corresponds to either α_{-*} or β_{-*}, depending on whether the scenario under consideration is fully s-wave or fully p-wave, respectively—otherwise a complex number depending on both coefficients.

Following chapter 3, we further define the inelastic fine-structure constant as

$$\alpha'_{\text{inel}} = \kappa^2_{-*}\alpha' \,. \tag{7.15}$$

This will serve as the reference parameter in our analysis, as it directly governs the excited state lifetime τ_*. When comparing different flavor structures, we require the lifetime of the excited state to be fixed, since it can be extracted experimentally from the distribution of propagation lengths of displaced vertices, independently of assumptions about the dark flavor structure.

To facilitate phenomenological studies, we developed a Mathematica® *Handbook for Fermionic iDM*, which includes analytic expressions for decay widths and branching ratios of all states in this effective model, as well as 3-body decay amplitudes. Users can specify the coefficient values for their concrete models or simply choose the already implemented coefficients for niDM [89] and i2DM [478]. The handbook also includes differential and total cross sections for dark sector production in e^+e^- collisions. We also make available a Monte Carlo event generator (and a semi-analytical estimator) for collider signals such as mono-photon events and displaced vertex searches, see appendix D.[8] A compatible `SensCalc` interface for generic iDM can also be accessed upon request [1].

7.2.1 Probing the not-so-inelastic flavor structure

While the generality of the niDM framework may seem too broad to be predictive, its rich structure gives rise to a variety of experimental signatures that can be exploited to constrain its parameters. We focus here on the Belle II experiment, which offers clean collision environments and excellent vertex reconstruction. In particular, we concentrate on three key signatures with high discovery potential at Belle II:[9]

[8] The handbook and the generator are publicly available at /gdvgarcia/A_handbook_for_fermionic_n_iDM and /gdvgarcia/niDMatEEcolliders, respectively. Please cite the current thesis and Ref. [89] when using them.

[9] Similar signatures can also be used to probe dark sectors unrelated to DM, such as in the 3-portal model [300, 690].

- Mono-photon with missing energy (mono-γ),
- Displaced vertex plus photon (displaced+γ),
- Two decay events with at least one displaced vertex (di-decay).

We restrict our analysis to the light DM regime, $m_\chi \lesssim 5$ GeV, which is well-suited to Belle II's sensitivity to dark photons with masses up to $m_{A'} \sim 10$ GeV. This ensures that the condition $m_{A'} > 2m_{\chi^*}$ can be satisfied, allowing for on-shell decays of the form $A' \to \chi^{(*)}\chi^{(*)}$. At the lower end, we impose $m_\chi \gtrsim 10$ MeV to evade constraints from Big Bang Nucleosynthesis, which exclude thermally coupled light DM in equilibrium with the SM [388].

Additionally, we focus on scenarios with relatively large mass splittings, $\delta \gtrsim 10^{-2} m_\chi$, to ensure that the excited state χ^* decays within detector scales, i.e., proper decay lengths $c\tau_* \lesssim \mathcal{O}(\text{m})$ [89]. Within these mass ranges, collider bounds provide the dominant constraints for niDM models composed of Majorana fermions, regardless of the coupling structure. This follows from suppressed DM-SM scattering cross sections and p-wave annihilations, as discussed in chapters 4 and 6.

In contrast, Dirac niDM models face additional limits due to potentially unsuppressed diagonal couplings, which can mediate SI scattering and lead to s-wave annihilation. For this reason, and for simplicity, we focus on the Majorana case when presenting concrete results.

Let us now assess how the three signatures probe the coupling structure of the effective Lagrangian in eq. (7.12). Due to its novelty, we concentrate here on the dark photon portal. A similar analysis applies for a heavy dark Higgs ($m_{h'} > 2m_{\chi^*}$), although the corresponding signatures would arise from B-meson decays such as $B \to Kh'$. In that case, analogous signatures (mono-K, displaced+K, and di-decay) can be defined using B-tagging, albeit with additional experimental challenges.[10]

Heavy dark photon case. The expected number of events in each signature channel can be estimated as:

$$N^{(2)}_{\text{events}} = \xi_*^2 \,\text{Br}_{**}\, N_{A'}\,, \tag{7.16}$$

$$N^{(1)}_{\text{events}} = \xi_\gamma\, \xi_* \left[\text{Br}_{-*} + 2(1-\xi_*)\,\text{Br}_{**}\right] N_{A'}\,, \tag{7.17}$$

$$N^{(0)}_{\text{events}} = \xi_\gamma \left[\text{Br}_{--} + (1-\xi_*)\text{Br}_{-*} + 2(1-\xi_*)^2\text{Br}_{**}\right] N_{A'}\,, \tag{7.18}$$

where $N_{A'}$ is the total number of dark photons produced, Br_{ij} denotes the A' branching ratios, and $\xi_i < 1$ are detection probabilities (γ for photons and

[10] Complications from dark Higgs pair production (see section 7.1.1) increase final-state multiplicities. Moreover, the dark Higgs portal has more couplings with the SM than the simpler vector case.

$*$ for decay vertices of excited states), similar to ξ discussed below eqs. (7.4) and (7.16).[11]

With sufficient statistics and simulation-based estimates of ξ_i, the branching ratios—and therefore relations among effective couplings—can be inferred from ratios of the measured event rates $N^{(i)}_{\text{events}}$. While non-trivial due to ξ_*'s dependence on m_χ, this strategy, in an optimistic setup, could even provide constraints on the absolute DM mass. In specific niDM scenarios characterized by less parameters (e.g., Δ_m and δ_y as in chapter 4), the three branching ratios can be used to infer these parameters along the DM mass itself, providing a powerful discriminator among models.

The energy(angular) distributions of photons in inclusive missing energy events provide a handle on the dark photon mass. This can be inferred by analyzing events in which the photon is emitted at large angles where missing energy from detector acceptance is minimal. Importantly, the analysis must be inclusive: all events with a photon and missing energy are included, regardless of whether additional visible particles from dark sector decays are present.

The shape of the distribution reflects the A' kinematics (set by $m_{A'}$), while its normalization—the number of events per bin—can be used to extract the kinetic mixing parameter ϵ. With these two parameters, $N_{A'}$ is fixed. Focusing for simplicity on events involving a visible high-energy photon—i.e., di-decays produced in association with a photon $N^{(2)}_{\text{events}} = \xi_\gamma\, \xi_*^2\, \text{Br}_{**}\, N_{A'}$—all branching ratios can be expressed as

$$\text{Br}_{**} = \frac{n_2}{\xi_*^2}, \tag{7.19}$$

$$\text{Br}_{-*} = \frac{1}{\xi_*}\left(n_1 - 2\frac{1-\xi_*}{\xi_*}\, n_2\right), \tag{7.20}$$

$$\text{Br}_{--} = n_0 - \frac{1-\xi_*}{\xi_*}\, n_1\,, \tag{7.21}$$

where $n_i = N^{(i)}_{\text{events}}/(\xi_\gamma N_{A'})$. If visible decays are negligible—as is generally expected given the smallness of ϵ from experimental constraints—the branching ratios satisfy the unitarity relation

$$1 = \text{Br}_{--} + \text{Br}_{-*} + \text{Br}_{**}, \tag{7.22}$$

which provides a useful cross-check.

Small deviations in the $(\epsilon, m_{A'})$ extraction may occur at large $\Gamma_{A'}$ (corresponding to large α'), where off-shell effects become relevant. In this regime,

[11] In principle, the detection probabilities ξ_* depend on both the decay mode i and the experimental signature j, $\xi^{(j)}_{*i}$, but we approximate them as universal for simplicity.

additional signatures such as di-decays (or even "tri-decays") from dark Higgs-strahlung (h'-strahlung) processes—with at least one h' decaying—may also become accessible. These channels offer complementary probes of the dark sector and enable further constraints on its coupling structure.

Vertex displacement distributions encode the lifetime of χ^*, which is related to the mass splitting δ and the off-diagonal couplings as well as α' (see section 4.1). The value of the mass splitting δ can be estimated from the maximum invariant mass of the visible decay products in $\chi^* \to \chi \bar{f} f$, and, combined with lifetime measurements, can be used to determine the inelastic fine-structure constant α'_{inel} (e' times κ_{-*}).

To fully disentangle all effective couplings, certain assumptions about the dark flavor structure may be necessary—for example, setting $\beta_{-*} = 0$ as in the standard niDM scenario, or $\alpha_{-*} = 0$ as in the p-wave case. In theories with only one source of parity breaking (i.e, models with no $\mathcal{CP}$-phases), typically only one of these couplings can be nonzero, making such assumptions well motivated. Moreover, s-wave scenarios are typically considered natural in such frameworks, whereas p-wave scenarios are somewhat "unnatural" (see discussion chapter 3).

In an optimistic scenario where h'-strahlung events are also observed (i.e., $\alpha' \gtrsim 10^{-3}$ [79] and the dark Higgs has a decay length within detector reach $\theta \gtrsim 10^{-7}$ [79]), the dark gauge coupling e' can be directly extracted. This possibility remains realistic under perturbative unitarity and freeze-out abundance constraints, which disfavor both very large and very small values of $m_{h'}$.

In such favorable circumstances, one could in principle determine both the diagonal and off-diagonal couplings, as well as the absolute mass m_χ. This follows from the fact that the branching ratios take the schematic form $\text{Br}_{mn} = g(\kappa_{ij}, m_{A'}, m_\chi, \delta)$. Since the variables $(m_{A'}, \delta, \kappa_{-*})$ could already be extracted, only three unknowns remain, which can be fixed by the three independent branching ratios. In this way, the full coupling structure of the dark sector through the vector portal can in principle be reconstructed—in a very optimistic setup. The schematic flow of this analysis is shown in fig. 7.7.

The above analysis outlines an ambitious but in-principle feasible roadmap for fully reconstructing niDM models from collider data. To assess its experimental viability, we aim in future work to implement a realistic case study in collaboration with Belle II experts, including background estimates and detector effects. In the remainder of this chapter, we turn to exploring the parameter space regions where the three signatures (mono-γ, displaced+γ, and di-decay) provide overlapping sensitivity, enabling full exploitation of this reconstruction strategy. We begin by reviewing current constraints on vector portal niDM, followed by projected sensitivities at Belle II.

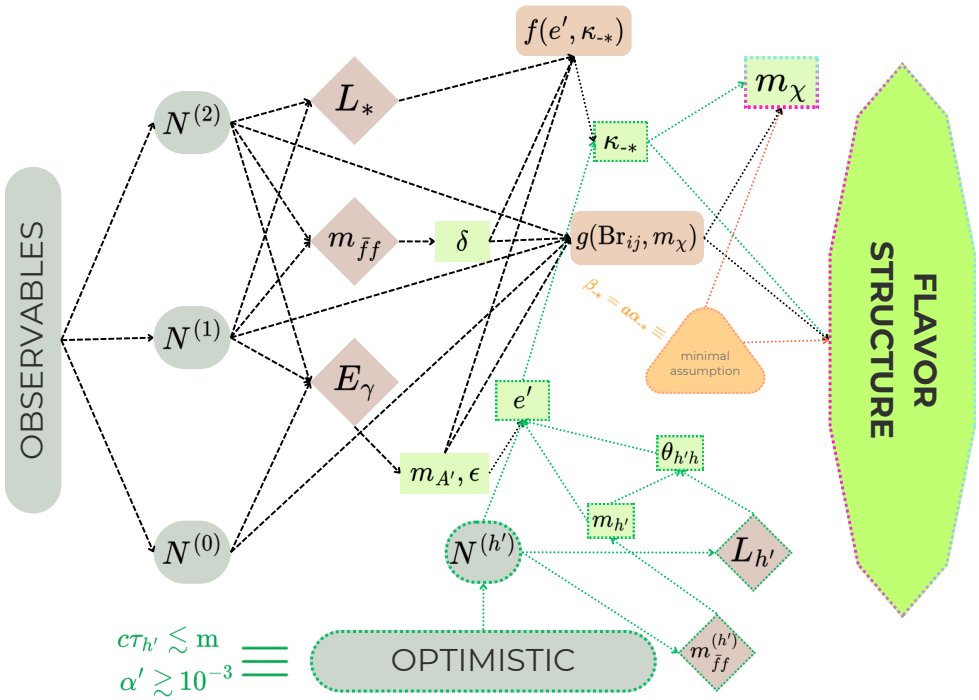

Figure 7.7: Schematic flowchart illustrating how key experimental observables can be used to probe the parameters of a generic not-so-inelastic Dark Matter effective Lagrangian. $N^{(0,1,2,h')}$ denote the number of events associated with the mono-γ, displaced+γ, di-decay, and h'-strahlung signatures, respectively. $L_{*(h')}$ and $m_{\bar{f}f}^{(h')}$ represent the vertex displacement and invariant mass distributions of χ^* (or h') decays. E_γ denotes the photon energy distribution. The effective off-diagonal coupling κ_{-*} depends on both α_{-*} and β_{-*}. The functions f and g represent relationships among the listed variables, while Br_{ij} correspond to the various A' branching ratios. The optimistic scenario refers to the case in which h'-strahlung events are observable ($\alpha' \gtrsim 10^{-3}$, $\theta_{h'h} \gtrsim 10^{-7}$, $2m_\chi \gtrsim m_{h'} \gtrsim 2m_\mu$); deductions that rely on this scenario are indicated with green arrows. A final minimal assumption (fixing the relation between κ_{-*} and the coefficients α_{-*} and β_{-*}) is required to extract all interaction coefficients from data—naturalness and no $\mathcal{CP}$-phases typically suffice. Results based on this assumption are indicated with orange arrows. *This proposed flowchart, however, must be further studied under realistic detector effects and possible parameter degeneracies.* See main text for further details.

7.2.2 Belle II sensitivity to flavor-probing signatures

Motivated by the standard s-wave and p-wave regimes of niDM introduced in chapter 3, we consider two representative choices for the off-diagonal coefficients (recalling that for Majorana fermions $\alpha_{ii} \equiv 0$ automatically). Specifically, we take $\beta_{-*} = 0$ (corresponding to the standard regime) and $\alpha_{-*} = 0$ (corresponding to the p-wave regime). In $\mathcal{CP}$-conserving scenarios, it is typically the case that at least one of these coefficients must vanish, making such assumptions well motivated. Thus, we focus on Majorana niDM models characterized by three independent flavor parameters governing the DM interactions with the dark photon.

We neglect the Higgs contribution to the χ^* decay width, as it only becomes relevant when $\alpha_y^{\text{inel}} \sim \alpha'_{\text{inel}}$ (i.e., $\hat{\kappa}_{-*} y \sim \kappa_{-*} e'$) and $\theta \sim 10\epsilon$ for large mass splittings $\delta \gtrsim$ GeV, owing to the Yukawa suppression of light SM final states. This approximation is further supported by the stringent experimental bounds on the scalar mixing angle, $\theta \lesssim 10^{-4}$ [331]. In addition, we assume the dark Higgs to be light ($m_{h'} \lesssim m_\chi$), thereby ensuring secluded freeze-out $\chi\chi \leftrightarrow h'h'$, which predicts $y \approx 0.07\sqrt{m_\chi/\text{GeV}}$ (see chapter 6)—values much smaller than the e' considered here. Taken together, these arguments further justify neglecting Higgs effects, and imply that its particular flavor structure does not play any role in the parameter space probed by Belle II.

Current constraints. As discussed in the previous section, collider constraints dominate in the mass and splitting ranges of interest. Here we briefly summarize the most relevant bounds on niDM with a vector mediator, as well as constraints that may arise from a light dark Higgs. The reader is referred to chapters 4 and 6 for further details.

Model-independent bounds on ϵ are set by measurements of deep inelastic scattering of $e^\pm$ off protons at HERA [594], which dominate around $m_{A'} \sim$ 10 GeV. For larger masses, electroweak precision tests at LEP [494] provide the strongest constraints.

At high-energy facilities, sizable DM fluxes can be produced, giving rise to scattering events in surrounding detectors. Measurements at LSND [279, 556], E137 [483, 557], and MiniBooNE [506] place strong bounds on light DM with $m_\chi \lesssim \mathcal{O}(100)$ MeV for large α'. Since the collision energies are much larger than the DM masses and splittings, these bounds are insensitive to the details of diagonal versus off-diagonal couplings. We therefore follow Ref. [280] rescaling their results by an appropriate choice of α'.

Beam-dump searches are especially powerful for $m_\chi \lesssim 2$ GeV and long-lived excited states ($c\tau_* \gtrsim 1$ m). However, such long lifetimes are outside Belle II sensitivity. Ref. [3] showed that Belle II mainly probes unexplored regions of parameter space for large mass splittings $\delta \gtrsim 0.4 m_\chi$, which correspond to shorter

lifetimes. We therefore restrict our analysis to this range and neglect beam-dump bounds, leaving the study of novel beam-dump signatures, such as niDM di-decays and h' production from dark photons, to future work.

Excited state decays at NA64 impact missing-energy searches only if they occur between the VETO and HCAL, i.e. within 1 m $\lesssim L \lesssim$ 6.5 m. Since such decay lengths are expected to be irrelevant for displaced searches at Belle II, we simply adopt the recent NA64 constraints reported in Ref. [344]. As discussed in chapter 4 (see also Refs. [80, 479]), the effects of including these decays remain confined to a narrow interval along the DM mass axis.

For electron–positron colliders, we extend the simulations presented in chapter 4 to include both dark sector decays of χ^* and visible SM decays of mediators, see appendix D. The simulation is made less model-dependent by using the generic coefficients introduced in this chapter. For mono-photon searches, we apply the cuts from Ref. [3] to recast BaBar bounds [488] and estimate Belle II sensitivity [91]. For h'-strahlung, relevant in the optimistic scenario, we use the cuts of Ref. [79] to recast the Belle II bounds for 365 fb^{-1} [82], employing the semi-analytical approach described in chapter 6.

Projected sensitivities. Belle II has already collected over 424 fb^{-1} of data [560]. To remain conservative, we estimate sensitivities for $\mathcal{L} = 100$ fb^{-1}. However, we note that the recent null results from h'-strahlung searches with 365 fb^{-1} [82] already exclude the optimistic scenario at 100 fb^{-1}. Thus, we also project results for $\mathcal{L} = 50$ ab^{-1}, the dataset expected by the end of Belle II around 2030.

Because mono-photon searches are background limited, rescaling sensitivities is non-trivial, as discussed in chapter 4. The sensitivity evolves as $S(\epsilon) \propto \mathcal{L}^{1/4}$ [79].[12] We therefore first rescale the published sensitivity from 20 fb^{-1} up to 100 fb^{-1} and 50 ab^{-1}, and then apply our updated simulation procedure to estimate mono-γ sensitivities across different niDM scenarios.

By contrast, displaced+γ, di-decays, and h'-strahlung are expected to be essentially background free under the cuts proposed in Refs. [3, 79]. We adopt these cuts directly. For di-decays, we use the same cuts as for h'-strahlung since both involve two decaying particles. In our new case, the decays originate from identical states (χ^*), producing a continuous spectrum with $m_{\bar{f}f} < \delta$, while h'-strahlung produces an invariant mass fixed at $m_{h'}$. The distinction between the two signatures can therefore be made experimentally.

Sensitivities are computed using the semi-analytical method described in appendix D, adopting the background-free assumption (90% C.L. contours correspond to 2.3 events). A more refined analysis, including background estimates and optimized cuts, would require a full Belle II detector simulation, which lies beyond the scope of this work.

[12] See Ref. [3] for the assumptions underlying this scaling.

Results. We present the combined constraints (gray shaded regions) and projected Belle II sensitivities (colored contours) for the three (four) complementary searches—mono-γ (blue), displaced+γ (yellow), di-decays (red), and h'-strahlung (green)—in figs. 7.8 and 7.9. Results are shown for $\mathcal{L} = 100$ fb^{-1} (solid) and $\mathcal{L} = 50$ ab^{-1} (dashed), considering two benchmark values of α'_{inel}: an optimistic 0.1 (fig. 7.8) and a more natural value $0.01 \sim \alpha$ (fig. 7.9). We focus on large splittings $\delta = m_\chi$, which ensure short χ^* lifetimes accessible at Belle II while avoiding beam-dump bounds. For h'-strahlung projections (only present for $\mathcal{L} = 50$ ab^{-1}) we take $\theta = 2.6 \times 10^{-4}$, consistent with the Belle II search for dark Higgs bosons associated with iDM [82]. At $\mathcal{L} = 100$ fb^{-1} we instead assume long-lived h' escaping detection—a condition easily satisfied for $\theta \ll 10^{-5}$ or for light dark Higgs masses $m_{h'} < 2m_\mu$.

We investigate three benchmarks with very distinctive flavor structures:

1. *iDM-like*: small and equal diagonal coefficients, $\beta_{ii} = 0.1$, together with a large off-diagonal one $\kappa_{-*} = 0.99$. This structure is realized in the standard niDM model from chapter 3 for $\delta_y \approx 1$ in the s-wave regime or $\delta_y \approx 0.1$ in the p-wave case.

2. *Democratic*: all non-zero coefficients equal to 0.5, corresponding to a Majorana version of the i2DM model [478] (*i2DM-like*) with maximal fermionic mixing angle $\theta_\chi = \pi/4$.

3. *Hierarchical*: $\beta_{**} = 0.9$, $\kappa_{-*} = 0.3$, and $\beta_{--} = 0.1$, also corresponding to an i2DM-like scenario but with a small mixing angle $\theta_\chi \approx \pi/10$.[13]

For iDM-like models we present both s- and p-wave cases, whereas for i2DM-like scenarios we restrict to the natural s-wave regime, since no qualitative differences arise and the only quantitative distinction originates from variations in the χ^* lifetime, $\tau^s_* \simeq 2.7\tau^p_*$ (see dotted lines in figs. 7.8 and 7.9).

As an illustrative example of p-wave i2DM-like sensitivity, fig. 7.10 considers the hierarchical benchmark, focusing exclusively on excited state di-decay events. The figure decomposes the sensitivity according to the three distinct di-decay production modes. The first two correspond to χ^* originating from dark photon decays, $A' \to \chi^*\chi^*$, with the dark photon produced either via annihilation in association with a Standard Model photon, $e^+e^- \to A'\gamma$ (solid), or through dark Higgs-strahlung, $e^+e^- \to A'h'$ (dashed). The third mode corresponds to χ^* produced directly in the high-energy collision, $e^+e^- \to \chi^*\chi^*$ (dotted). While the first channel involves only on-shell particles, the latter two proceed via an off-shell s-channel dark photon and are therefore suppressed for small α'. Moreover, the sensitivity from $e^+e^- \to A'h'$ depends on the dark Higgs lifetime: if h'

[13] We avoid very small κ_{-*} values, since with α'_{inel} fixed this would require α' larger than unity, breaking perturbativity.

decays promptly, 'tri-decay' events dominate instead. To capture these effects, we present separately the combined sensitivity of the channels independent on the dark Higgs properties in light gray, alongside the total sensitivity including h'-strahlung in red.

Figs. 7.8 and 7.9 demonstrate that even with $\mathcal{L} = 100$ fb^{-1}, Belle II can probe all three primary signatures across a broad parameter space and for diverse flavor structures. Scenarios with large diagonal couplings are particularly promising, as di-decays may surpass mono-decays sensitivity due to their multiple production channels and the photon-tagging requirement in displaced+γ searches. Democratic structures also yield interesting reach for the di-decay signature.

Although the optimistic h'-strahlung case for 100 fb^{-1} is excluded already by existing 365 fb^{-1} results [82], projections for 50 ab^{-1} reveal that Belle II could in principle probe the full dark sector coupling structure as described in section 7.2.1. Indeed, regions remain where all four signatures are accessible without being excluded by current bounds. This highlights the strong motivation for Belle II to continue accumulating data and exploring these complementary signatures, as the flavor structure of the dark sector may prove as rich and surprising as that of the SM—after all, the dark sector may be serving up a menu so exotic that Belle II could end up tasting "flavors" far spicier than the traditional quark cuisine.

7.3 Concluding remarks

In this chapter, we have investigated the potential for discovery and characterization of feebly interacting particles (FIPs) at Intensity Frontier experiments, with special attention to *di-decay signatures*—observing simultaneously the decays of two FIPs within a single event. Such signatures offer unique opportunities: they can serve as a smoking-gun signal for models predicting FIP pair production, and the reconstruction of both decays enables the identification of the production channel even when the production vertex itself is inaccessible—a common limitation at Intensity Frontier facilities. Consequently, di-decays provide a robust discriminator between different classes of FIPs that otherwise share similar decay phenomenology. Furthermore, di-decays are associated with significantly lower background rates compared to mono-decays, often requiring no tagging, and can arise from a larger variety of production channels. In certain cases, this can yield exclusion sensitivities comparable to, or even stronger than, mono-decay searches, despite the parametric suppression of the di-decay event rate.

Using a benchmark model with Higgs-like scalars, we demonstrated that di-decay searches can cover a wide parameter space at both current and upcoming Intensity Frontier experiments. More importantly, in the presence of rich dark sectors—particularly niDM models—di-decays can be combined with

other, more standard searches to probe in depth the structure of the dark sector couplings. Specifically, we have shown that for niDM scenarios, di-decay searches, in combination with mono-photon, displaced vertex plus photon, and dark Higgs-strahlung signatures, could in principle allow a *full reconstruction* of the effective dark sector flavor structure.

By estimating Belle II sensitivities to these complementary signatures, we have demonstrated that the dark flavor structure is within the reach of current and near-future datasets. In particular, di-decays not only enrich the Belle II physics program but also provide a critical handle for disentangling diagonal and off-diagonal couplings in niDM models. This makes them an invaluable addition to the FIP search strategy at Intensity Frontier facilities.

Overall, our results establish di-decays as a novel and powerful probe of new physics. Beyond niDM, the methods developed here are broadly applicable and can be extended to other classes of FIP models predicting rich phenomenology. In this way, di-decay signatures open a promising path to refining and expanding the search strategies for FIPs at the Intensity Frontier, with *tæsting* the possible flavor (structure) of the dark sector now within reach.

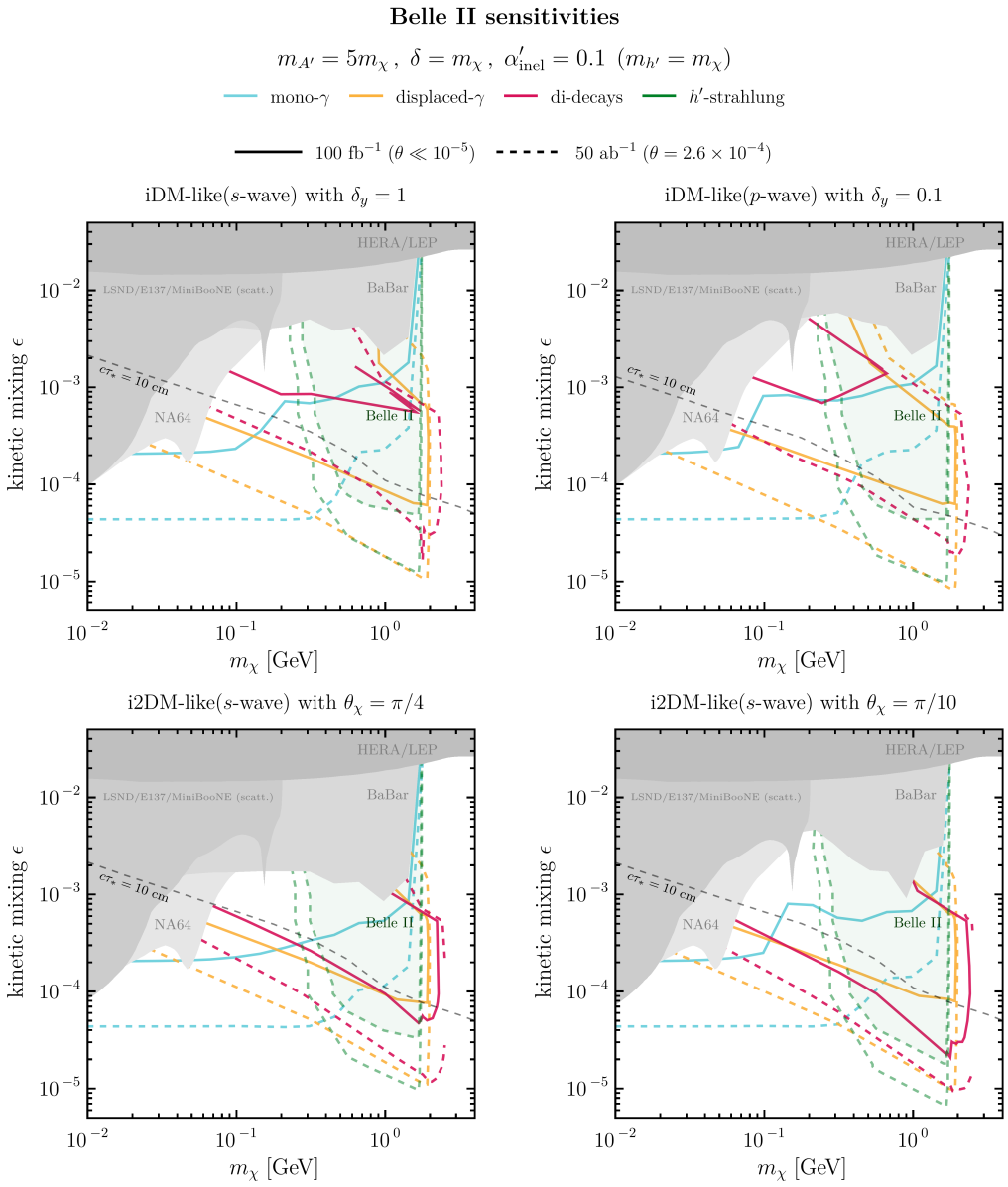

Figure 7.8: Projected sensitivities of different niDM searches at Belle II for integrated luminosities of 100 fb^{-1} (solid lines) and 50 ab^{-1} (dashed lines), assuming $\alpha'_{\rm inel} = 0.1$. Results are shown for four illustrative examples of niDM models with distinctive flavor structures. DM is taken to be Majorana (similar results are expected for Dirac DM). Current bounds are indicated in gray, except for Belle II constraints which only apply to short-lived dark Higgs bosons. Dotted black lines denote contours of excited state proper decay length $c\tau_* = 10$ cm. Across the plane, the observed DM relic abundance is satisfied via secluded freeze-out $\chi\chi \to h'h'$. A full NA64 recasting and additional beam dump constraints remain to be performed but are not expected to significantly affect the parameter space relevant for Belle II. See text for further discussion.

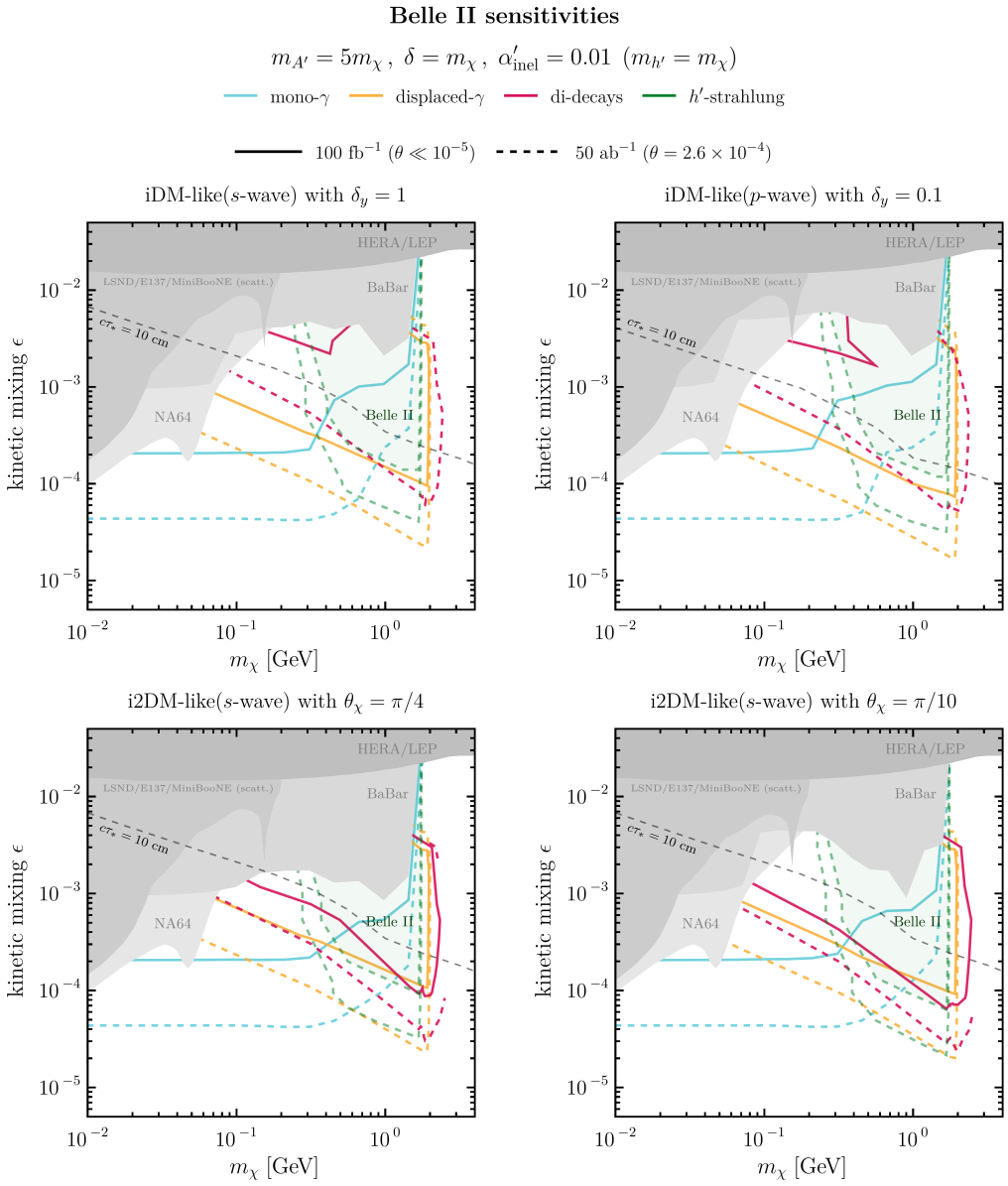

Figure 7.9: Same as fig. 7.8, but assuming $\alpha'_{\rm inel} = 0.01$.

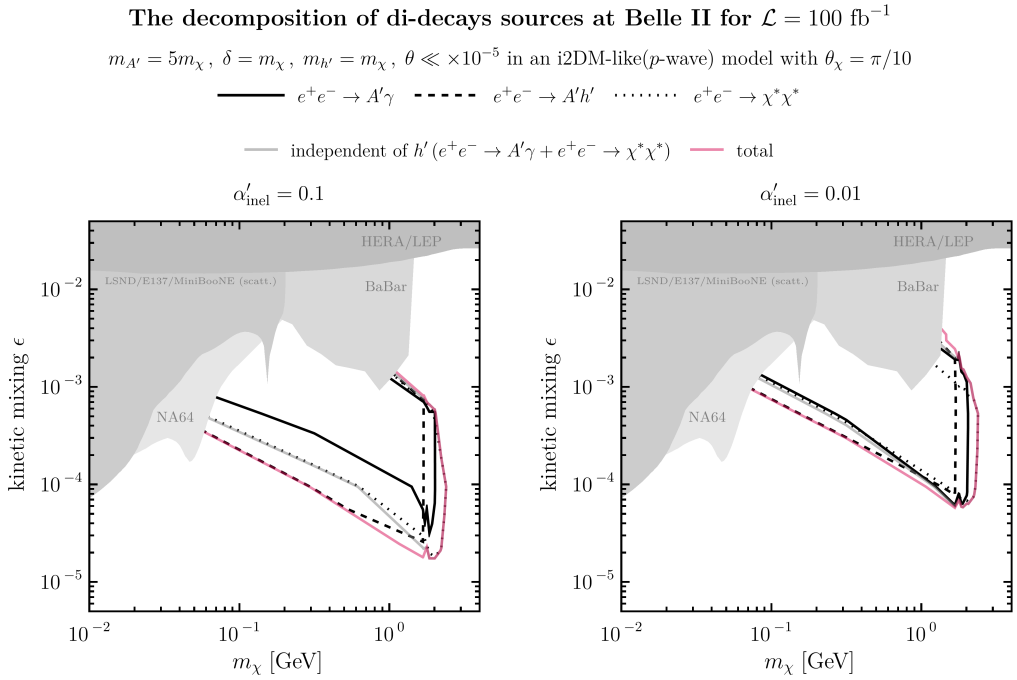

Figure 7.10: Decomposition of Belle II excited state di-decay sensitivities into different production channels for an integrated luminosity of 100 fb^{-1}. The combined sensitivity from channels independent of the dark Higgs properties is shown in light gray, while the total sensitivity including all channels is shown in red. The left panel corresponds to $\alpha'_{\rm inel} = 0.1$ and the right panel to $\alpha'_{\rm inel} = 0.01$. Current bounds are indicated in gray. Beam dump constraints will be addressed in future work but are not expected to significantly affect the Belle II reach. See the main text for further details on the production modes.

Chapter 8

Conclusion

The study of dark matter continues to pose one of the most fundamental and enduring challenges in modern physics. Although its existence is well supported by gravitational evidence, the identity of its particle nature remains unknown even after many decades of investigation. In this thesis, we have examined a class of models aimed at bridging this gap, focusing on the framework of inelastic dark matter and its generalizations. By developing theoretically motivated, minimal, and UV-complete scenarios—and evaluating their phenomenology across multiple experimental frontiers—this work provides a coherent and predictive strategy to probe hidden sectors. The results obtained contribute both conceptually and phenomenologically to our understanding of how dark matter might interact with the Standard Model, and what experimental strategies might ultimately lead to its discovery.

8.1 Summary

We began in chapter 2 by reviewing the current status of the Dark Matter (DM) problem. While its existence is firmly established through astrophysical and cosmological observations, its particle properties remain elusive to direct laboratory searches, with no conclusive evidence observed to date. To address this, a wide range of theoretical frameworks have been developed, many of which predict stable, feebly interacting particles emerging naturally in extensions of the Standard Model (SM). Among these, the thermal freeze-out scenario, particularly involving Weakly Interacting Massive Particles (WIMPs), has long been favored due to its predictive power and independence from early-universe initial conditions. The so-called "WIMP miracle" further motivates these models by intrinsically linking weak-scale masses and interactions to the observed relic abundance of DM.

However, decades of experimental searches have significantly constrained the parameter space for classic WIMP models. As discussed in chapter 3, this has led to the development of various WIMP-like frameworks that retain the appealing

features of thermal freeze-out, sometimes at the expense of strict predictivity or weak-scale masses and couplings. Among these, inelastic DM (iDM) stands out as one of the most minimal and versatile frameworks, applicable to DM masses ranging from the sub-GeV scale to masses well above the electroweak scale. It successfully evades both direct and indirect detection bounds while offering rich phenomenological consequences for collider physics, astrophysics, and cosmology.

Also in chapter 3, we reviewed the canonical pseudo-Dirac iDM model and its collider phenomenology. We examined how UV-completions of this model often rely on an ad hoc assumption of parity conservation in the dark sector. We demonstrated that this assumption is not essential: Majorana DM (mDM) models remain viable within WIMP-like scenarios, and parity violation merely interpolates smoothly between the traditional iDM and mDM regimes. Motivated by this, we introduced a general and minimal UV-complete framework—named not-so-inelastic DM (niDM)—which unifies iDM and mDM models interacting via dark photon mediators and necessarily includes a second mediator, the dark Higgs boson, associated with spontaneous symmetry breaking in the dark sector.

In the subsequent chapters, we analyzed the niDM framework across various scenarios. In chapter 4, following the typical approach adopted in the iDM literature, we considered a setup involving only the dark photon portal and sub-GeV DM masses. We showed that parity violation gives rise to a new phenomenological regime—models that resemble iDM in collider and direct detection (DD) experiments but whose thermal production mimics mDM. We labeled this parameter space as the not-so-inelastic regime. In the standard niDM model often employed in iDM studies, this regime appears for large mass splittings $\delta \sim m_\chi$, and contains two unconstrained regions: one near a few hundred MeV and another near a few GeV. This is in contrast to traditional iDM, which is excluded in the sub-GeV range for $\delta \gtrsim 0.1 m_\chi$. Current experiments such as Belle II and NA64 have the potential to fully probe the lighter mass window, while the multi-GeV region remains challenging. Heavier DM masses are constrained by DD, while lighter ones are excluded by beam-dump experiments and Big Bang Nucleosynthesis limits.

In chapter 5, we showed that a consistent iDM framework does not require a dark photon. We introduced the minimal-inelastic DM (miDM) model: a dark sector containing only a Dirac fermion and a pseudoscalar mediator a. The model behaves as iDM in the presence of small but non-zero parity violation and in the regime where the vacuum expectation value w of the pseudo-scalar is small compared to the bare Dirac mass of the fermion. This small-w regime is motivated by naturalness, as $w = 0$ restores a global Z_4 symmetry. Although miDM is not well suited for sub-GeV DM due to its Yukawa-suppressed couplings to light SM particles, it remains a highly predictive target for DD experiments at masses above the electroweak scale, as it leads to elastic DM–nucleus scattering with spin-independent cross sections. Future detectors such as DARWIN are

expected to nearly close the remaining parameter space in the visible freeze-out regime (i.e., $m_a > m_\chi$).

In chapter 6, we considered a scenario where both the dark photon and dark Higgs are active mediators. We argued that perturbativity considerations prevent integrating out the scalar mediator. We revisited the limited existing literature on niDM with both mediators and identified a new decay channel enabled by parity violation: $\chi^* \to \chi h'$. This allows dark Higgs production via dark photon decays into excited DM states, followed by their subsequent decay into ground states and scalar mediators. We found that this channel enables Belle II to probe substantial regions of parameter space that are currently unconstrained, offering simultaneous sensitivity to both the dark photon's kinetic mixing and the dark Higgs' scalar mixing—regions within which niDM yields a consistent WIMP-like DM candidate.

Finally, in chapter 7, we explored a novel class of feebly interacting particle (FIP) signatures in Intensity Frontier experiments: di-decay events, where two FIPs are produced and decay inside the detector. These events allow for identification of the FIP production modes and differentiation between FIPs with similar decay products, while also potentially suppressing backgrounds that typically plague mono-decay searches. We first considered a simple model only consisting of a Higgs-like scalar, then showed how parity-violating niDM models naturally predict di-decay signatures, even in the dark photon-only case. We introduced a general, UV-agnostic parametrization of niDM models based on effective couplings of DM states to mediators. Focusing on Belle II, we analyzed three complementary signatures (a single photon plus missing energy, a displaced vertex associated with a high-energy photon, and di-decays) and argued that, when combined,[1] they allow for the reconstruction of the DM "flavor structure", i.e., the coupling pattern between mediators and DM states.

8.2 Outlook

The results presented in this thesis open several promising avenues for further investigation.

Although briefly discussed in chapter 3, an alternative niDM scenario where naturalness is not imposed remains an intriguing possibility. We have shown that this setup leads to p-wave dominated co-annihilations, thereby evading ID bounds even in the presence of meta-stable excited states. A more detailed exploration of this scenario is planned for future work.

In chapter 4, the DM mass region near 5 GeV remains largely unexplored. Interestingly, DD experiments lose sensitivity just above this threshold, and e^+e^- collider energies typically drop off at the B-meson pair threshold, limiting their

[1] This assumes an optimistic scalar sector that allows for detectable Higgs-strahlung events.

reach from below. One possibility for extending sensitivity in this region involves direct searches for the dark Higgs boson, which cannot be much heavier than the DM due to the large gauge couplings required for successful visible freeze-out. For instance, Higgs-strahlung processes could allow e^+e^- colliders to probe masses more than 1 GeV above the current reach of mono-photon searches. Furthermore, it would be valuable to engage more closely with the Belle II and NA64 collaborations to analyze their data within the more general niDM framework, beyond the specific mDM and iDM limits. Productive conversations in this direction are already ongoing.

For chapter 5, further exploration is needed regarding cosmological bounds from long-lived excited DM states. In particular, we have not yet quantified the relic abundance of excited DM generated via freeze-out, though this could significantly constrain the parameter space. Diagonal interactions (e.g., parity-violating effects) might help suppress the excited DM fraction even for small diagonal couplings, giving the Boltzmann suppression faced by off-diagonal interactions at low dark sector temperatures. Preliminary results in this direction for the standard niDM model with a vector mediator are promising, and a dedicated study is expected to be completed soon. Additionally, scalar-mediated iDM remains largely unexplored at the LHC or in projections for the FCC. Given ongoing dark Higgs searches at the LHC, this constitutes a fruitful direction for collider studies.

The results presented in chapters 6 and 7 are largely preliminary; accordingly, the next step in both cases involves full Monte Carlo simulations to incorporate constraints from beam dump experiments. Simulations will also be essential for refining Belle II sensitivities and projecting the reach of SHiP. A key direction for further development in chapter 7 is to rigorously demonstrate how combining the complementary signatures available in niDM models can constrain the dark flavor structure. We plan to present a specific benchmark case study to illustrate this point.

Another exciting avenue involves the study of DM flavor oscillations, analogous to neutrino oscillations, which can arise in generic niDM (and even i2DM) frameworks. These oscillation signatures offer promising opportunities for probing the DM coupling structure while also suppressing SM backgrounds. A proof-of-principle is presented in appendix A, and a dedicated study is underway to assess how much of the niDM parameter space can be probed using this mechanism.

In conclusion, this thesis has explored a simple yet profound direction in iDM physics: the possibility that parity is not conserved in the dark sector. This is not an unnatural assumption, given that parity is already maximally violated in the electroweak sector of the SM. We have shown that parity violation enables a host of new phenomena: (n)iDM models with large mass splittings, a minimal iDM framework involving only a single (pseudo)scalar mediator, excited DM

states decaying into dark Higgs bosons, and distinctive di-decay signatures that, when combined with standard signals, could enable full characterization of the dark sector flavor structure.

In short, parity should not be taken for granted. It is our responsibility as physicists to investigate its role in our extensions of the SM—just as T. D. Lee [85], C. N. Yang, C. S. Wu [86], and many others did more than half a century ago to demonstrate that parity is not a symmetry of our Universe.[2]

After all, *we still do not know what dark matter looks like in the mirror.*

[2]The same logic should be applied to the charge-conjugation and time-reversal symmetries. Other foundational contributors to the study of $\mathcal{C}$, $\mathcal{P}$, and $\mathcal{T}(\mathcal{CP})$ violations include [691] E.M. Purcell [84], N.F. Ramsey [692], J.H. Smith [693], E. Ambler, R.W. Hayward, D.D. Hoppes, R.P. Hudson, J.D. Jackson [694], S.B. Treiman, H.W. Wyld, J.H. Christenson [695], J.W. Cronin, V.L. Fitch, R. Turlay, and A.D. Sakharov [696].

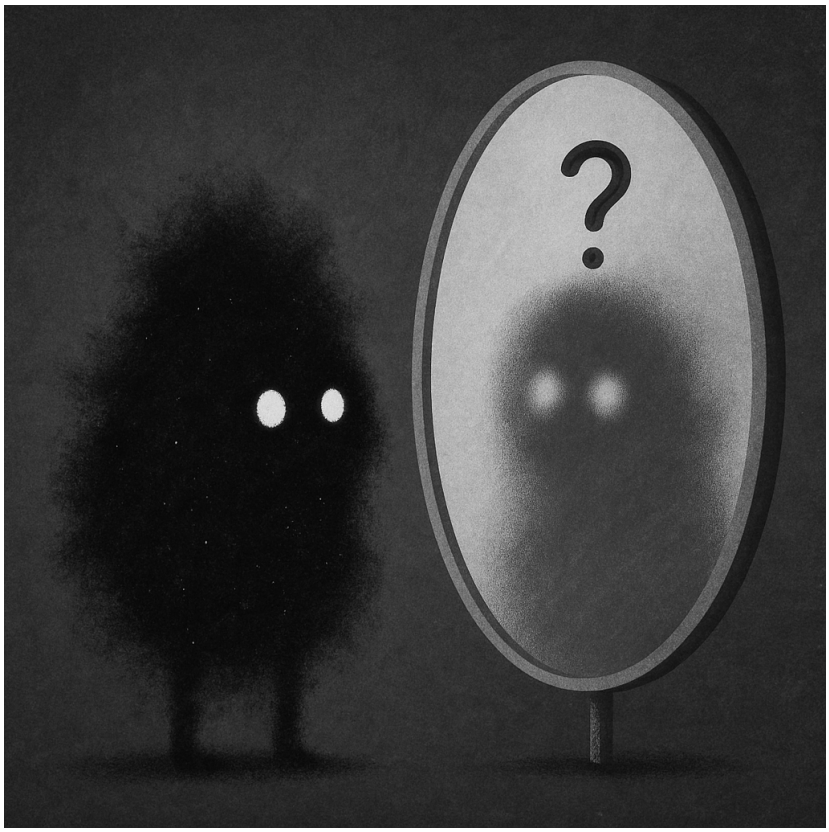

Esse estranho que mora no espelho / ... / olha-me de um jeito
de quem procura adivinhar quem sou.

– **Mario Quintana** in *O antinarciso — Caderno H*

Bibliography

[1] Maksym Ovchynnikov et al. "Sensitivities to feebly interacting particles: Public and unified calculations". In: *Phys. Rev. D* 108.7 (2023), p. 075028. DOI: 10.1103/PhysRevD.108.075028. arXiv: 2305.13383 [hep-ph].

[2] Maksym Ovchynnikov. *SensCalc*. Online at https://doi.org/10.5281/zenodo.7957784. Version 1.0.0-beta. 2023. DOI: 10.5281/zenodo.7957784. URL: https://doi.org/10.5281/zenodo.7957784.

[3] Michael Duerr et al. "Invisible and displaced dark matter signatures at Belle II". In: *JHEP* 02 (2020), p. 039. DOI: 10.1007/JHEP02(2020)039. arXiv: 1911.03176 [hep-ph].

[4] Peter Athron et al. "Global analyses of Higgs portal singlet dark matter models using GAMBIT". In: *Eur. Phys. J. C* 79.1 (2019), p. 38. DOI: 10.1140/epjc/s10052-018-6513-6. arXiv: 1808.10465 [hep-ph].

[5] Peter Athron et al. "Thermal WIMPs and the scale of new physics: global fits of Dirac dark matter effective field theories". In: *Eur. Phys. J. C* 81.11 (2021), p. 992. DOI: 10.1140/epjc/s10052-021-09712-6. arXiv: 2106.02056 [hep-ph].

[6] Marco Cirelli, Alessandro Strumia, and Jure Zupan. "Dark Matter". In: (June 2024). arXiv: 2406.01705 [hep-ph].

[7] Stefano Profumo, Leonardo Giani, and Oliver F. Piattella. "An Introduction to Particle Dark Matter". In: *Universe* 5.10 (2019), p. 213. DOI: 10.3390/universe5100213. arXiv: 1910.05610 [hep-ph].

[8] Martin Bauer and Tilman Plehn. *Yet Another Introduction to Dark Matter: The Particle Physics Approach*. Vol. 959. Lecture Notes in Physics. Springer, 2019. DOI: 10.1007/978-3-030-16234-4. arXiv: 1705.01987 [hep-ph].

[9] A. Arbey and F. Mahmoudi. "Dark matter and the early Universe: a review". In: *Prog. Part. Nucl. Phys.* 119 (2021), p. 103865. DOI: 10.1016/j.ppnp.2021.103865. arXiv: 2104.11488 [hep-ph].

[10] F. Zwicky. "Die Rotverschiebung von extragalaktischen Nebeln". In: *Helv. Phys. Acta* 6 (1933), pp. 110–127. DOI: 10.1007/s10714-008-0707-4.

[11] Gianfranco Bertone and Dan Hooper. "History of dark matter". In: *Rev. Mod. Phys.* 90.4 (2018), p. 045002. DOI: 10.1103/RevModPhys.90.045002. arXiv: 1605.04909 [astro-ph.CO].

[12] Vera C. Rubin and W. Kent Ford Jr. "Rotation of the Andromeda Nebula from a Spectroscopic Survey of Emission Regions". In: *Astrophys. J.* 159 (1970), pp. 379–403. DOI: 10.1086/150317.

[13] V. C. Rubin, N. Thonnard, and W. K. Ford Jr. "Rotational properties of 21 SC galaxies with a large range of luminosities and radii, from NGC 4605 /R = 4kpc/ to UGC 2885 /R = 122 kpc/". In: *Astrophys. J.* 238 (1980), p. 471. DOI: 10.1086/158003.

[14] A. Bosma. "21-cm line studies of spiral galaxies. 2. The distribution and kinematics of neutral hydrogen in spiral galaxies of various morphological types." In: *Astron. J.* 86 (1981), p. 1825. DOI: 10.1086/113063.

[15] T. S. van Albada et al. "The Distribution of Dark Matter in the Spiral Galaxy NGC-3198". In: *Astrophys. J.* 295 (1985), pp. 305–313. DOI: 10.1086/163375.

[16] Massimo Persic, Paolo Salucci, and Fulvio Stel. "The Universal rotation curve of spiral galaxies: 1. The Dark matter connection". In: *Mon. Not. Roy. Astron. Soc.* 281 (1996), p. 27. DOI: 10.1093/mnras/278.1.27. arXiv: astro-ph/9506004.

[17] Maxim Markevitch et al. "Direct constraints on the dark matter self-interaction cross-section from the merging galaxy cluster 1E0657-56". In: *Astrophys. J.* 606 (2004), pp. 819–824. DOI: 10.1086/383178. arXiv: astro-ph/0309303.

[18] Douglas Clowe et al. "A direct empirical proof of the existence of dark matter". In: *Astrophys. J. Lett.* 648 (2006), pp. L109–L113. DOI: 10.1086/508162. arXiv: astro-ph/0608407.

[19] Jeffrey M. Kubo et al. "The Mass Of The Coma Cluster From Weak Lensing In The Sloan Digital Sky Survey". In: *Astrophys. J.* 671 (2007), pp. 1466–1470. DOI: 10.1086/523101. arXiv: 0709.0506 [astro-ph].

[20] Raphael Gavazzi et al. "A weak lensing study of the Coma cluster". In: *Astron. Astrophys.* 498 (2009), p. L33. DOI: 10.1051/0004-6361/200911841. arXiv: 0904.0220 [astro-ph.CO].

[21] Volker Springel et al. "Simulating the joint evolution of quasars, galaxies and their large-scale distribution". In: *Nature* 435 (2005), pp. 629–636. DOI: 10.1038/nature03597. arXiv: astro-ph/0504097.

[22] Darren J. Croton et al. "The Many lives of AGN: Cooling flows, black holes and the luminosities and colours of galaxies". In: *Mon. Not. Roy. Astron. Soc.* 365 (2006). [Erratum: Mon.Not.Roy.Astron.Soc. 367, 864 (2006)], pp. 11–28. DOI: 10.1111/j.1365-2966.2006.09994.x. arXiv: astro-ph/0602065.

[23] Volker Springel, Carlos S. Frenk, and Simon D. M. White. "The large-scale structure of the Universe". In: *Nature* 440 (2006), p. 1137. DOI: 10.1038/nature04805. arXiv: astro-ph/0604561.

[24] L. F. Abbott and Mark B. Wise. "Large Scale Anisotropy of the Microwave Background and the Amplitude of Energy Density Fluctuations in the Early Universe". In: *Astrophys. J. Lett.* 282 (1984). Ed. by M. A. Srednicki, pp. L47–L50. DOI: 10.1086/184302.

[25] N. Aghanim et al. "Planck 2018 results. I. Overview and the cosmological legacy of Planck". In: *Astron. Astrophys.* 641 (2020), A1. DOI: 10.1051/0004-6361/201833880. arXiv: 1807.06205 [astro-ph.CO].

[26] N. Aghanim et al. "Planck 2018 results. VI. Cosmological parameters". In: *Astron. Astrophys.* 641 (2020). [Erratum: Astron.Astrophys. 652, C4 (2021)], A6. DOI: 10.1051/0004-6361/201833910. arXiv: 1807.06209 [astro-ph.CO].

[27] J. Silk et al. *Particle Dark Matter: Observations, Models and Searches*. Ed. by Gianfranco Bertone. Cambridge: Cambridge Univ. Press, 2010. ISBN: 978-1-107-65392-4. DOI: 10.1017/CBO9780511770739.

[28] M. Milgrom. "A Modification of the Newtonian dynamics as a possible alternative to the hidden mass hypothesis". In: *Astrophys. J.* 270 (1983), pp. 365–370. DOI: 10.1086/161130.

[29] David H. Weinberg et al. "Observational Probes of Cosmic Acceleration". In: *Phys. Rept.* 530 (2013), pp. 87–255. DOI: 10.1016/j.physrep.2013.05.001. arXiv: 1201.2434 [astro-ph.CO].

[30] Alain Blanchard et al. "ΛCDM is alive and well". In: *Open J. Astrophys.* 7 (2024), p. 117170. DOI: 10.33232/001c.117170. arXiv: 2205.05017 [astro-ph.CO].

[31] Pablo Villanueva-Domingo, Olga Mena, and Sergio Palomares-Ruiz. "A brief review on primordial black holes as dark matter". In: *Front. Astron. Space Sci.* 8 (2021), p. 87. DOI: 10.3389/fspas.2021.681084. arXiv: 2103.12087 [astro-ph.CO].

[32] Anne M. Green. "Primordial black holes as a dark matter candidate - a brief overview". In: *Nucl. Phys. B* 1003 (2024), p. 116494. DOI: 10.1016/j.nuclphysb.2024.116494. arXiv: 2402.15211 [astro-ph.CO].

[33] G. F. Giudice. "Dark Matter and Supersymmetry". In: *Beyond the Standard Model*. Jan. 1989.

[34] L. J. Rosenberg. "Axions: Dark matter and the strong CP problem". In: *30th Rencontres de Moriond: Euroconferences: Clustering in the Universe*. 1995, pp. 487–502.

[35] Sven Bjarke Gudnason, Chris Kouvaris, and Francesco Sannino. "Dark Matter from new Technicolor Theories". In: *Phys. Rev. D* 74 (2006), p. 095008. DOI: 10.1103/PhysRevD.74.095008. arXiv: hep-ph/0608055.

[36] Roshan Foadi, Mads T. Frandsen, and Francesco Sannino. "Technicolor Dark Matter". In: *Phys. Rev. D* 80 (2009), p. 037702. DOI: 10.1103/PhysRevD.80.037702. arXiv: 0812.3406 [hep-ph].

[37] Shi-Hao Chen. "SU(5) Grand Unified Model and Dark Matter". In: (Dec. 2009). arXiv: 0912.2427 [physics.gen-ph].

[38] Gary Shiu, Pablo Soler, and Fang Ye. "Milli-Charged Dark Matter in Quantum Gravity and String Theory". In: *Phys. Rev. Lett.* 110.24 (2013), p. 241304. DOI: 10.1103/PhysRevLett.110.241304. arXiv: 1302.5471 [hep-th].

[39] Melissa van Beekveld et al. "Supersymmetry with Dark Matter is still natural". In: *Phys. Rev. D* 96.3 (2017), p. 035015. DOI: 10.1103/PhysRevD.96.035015. arXiv: 1612.06333 [hep-ph].

[40] Giacomo Cacciapaglia. "Composite dark Matter and the Higgs". In: *Frascati Phys. Ser.* 65 (2017). Ed. by Gennaro Corcella et al., pp. 112–119.

[41] Rouzbeh Allahverdi et al. "Superheavy dark matter from string theory". In: *JHEP* 02 (2021), p. 026. DOI: 10.1007/JHEP02(2021)026. arXiv: 2010.03573 [hep-ph].

[42] Gi-Chol Cho, Kana Hayami, and Nobuchika Okada. "SO(10) grand unification with minimal dark matter and color octet scalars". In: *Phys. Rev. D* 105.1 (2022), p. 015027. DOI: 10.1103/PhysRevD.105.015027. arXiv: 2110.03884 [hep-ph].

[43] Sven Heinemeyer and Carlos Muñoz. "Dark Matter in Supersymmetry". In: *Universe* 8.8 (2022), p. 427. DOI: 10.3390/universe8080427.

[44] Kim Griest and David Seckel. "Three exceptions in the calculation of relic abundances". In: *Phys. Rev. D* 43 (1991), pp. 3191–3203. DOI: 10.1103/PhysRevD.43.3191.

[45] Edward W. Kolb, Daniel J. H. Chung, and Antonio Riotto. "WIMPzillas!" In: *AIP Conf. Proc.* 484.1 (1999). Ed. by H. Falomir, R. E. Gamboa Saravi, and F. A. Schaposnik, pp. 91–105. DOI: 10.1063/1.59655. arXiv: hep-ph/9810361.

[46] Jonathan L. Feng, Arvind Rajaraman, and Fumihiro Takayama. "Superweakly interacting massive particles". In: *Phys. Rev. Lett.* 91 (2003), p. 011302. DOI: 10.1103/PhysRevLett.91.011302. arXiv: hep-ph/0302215.

[47] Maxim Pospelov, Adam Ritz, and Mikhail B. Voloshin. "Secluded WIMP Dark Matter". In: *Phys. Lett. B* 662 (2008), pp. 53–61. DOI: 10.1016/j.physletb.2008.02.052. arXiv: 0711.4866 [hep-ph].

[48] Jonathan L. Feng and Jason Kumar. "The WIMPless Miracle: Dark-Matter Particles without Weak-Scale Masses or Weak Interactions". In: *Phys. Rev. Lett.* 101 (2008), p. 231301. DOI: 10.1103/PhysRevLett.101.231301. arXiv: 0803.4196 [hep-ph].

[49] Yonit Hochberg et al. "Mechanism for Thermal Relic Dark Matter of Strongly Interacting Massive Particles". In: *Phys. Rev. Lett.* 113 (2014), p. 171301. DOI: 10.1103/PhysRevLett.113.171301. arXiv: 1402.5143 [hep-ph].

[50] Duccio Pappadopulo, Joshua T. Ruderman, and Gabriele Trevisan. "Dark matter freeze-out in a nonrelativistic sector". In: *Phys. Rev. D* 94.3 (2016), p. 035005. DOI: 10.1103/PhysRevD.94.035005. arXiv: 1602.04219 [hep-ph].

[51] Eric Kuflik et al. "Phenomenology of ELDER Dark Matter". In: *JHEP* 08 (2017), p. 078. DOI: 10.1007/JHEP08(2017)078. arXiv: 1706.05381 [hep-ph].

[52] Raffaele Tito D'Agnolo, Duccio Pappadopulo, and Joshua T. Ruderman. "Fourth Exception in the Calculation of Relic Abundances". In: *Phys. Rev. Lett.* 119.6 (2017), p. 061102. DOI: 10.1103/PhysRevLett.119.061102. arXiv: 1705.08450 [hep-ph].

[53] Mathias Garny et al. "Coannihilation without chemical equilibrium". In: *Phys. Rev. D* 96.10 (2017), p. 103521. DOI: 10.1103/PhysRevD.96.103521. arXiv: 1705.09292 [hep-ph].

[54] Juri Smirnov and John F. Beacom. "New Freezeout Mechanism for Strongly Interacting Dark Matter". In: *Phys. Rev. Lett.* 125.13 (2020), p. 131301. DOI: 10.1103/PhysRevLett.125.131301. arXiv: 2002.04038 [hep-ph].

[55] Torsten Bringmann et al. "Dark Matter from Exponential Growth". In: *Phys. Rev. Lett.* 127.19 (2021), p. 191802. DOI: 10.1103/PhysRevLett.127.191802. arXiv: 2103.16572 [hep-ph].

[56] Yong Du et al. "Revisiting dark matter freeze-in and freeze-out through phase-space distribution". In: *JCAP* 04.04 (2022), p. 012. DOI: 10.1088/1475-7516/2022/04/012. arXiv: 2111.01267 [hep-ph].

[57] Nicolás Bernal, Kuldeep Deka, and Marta Losada. "Thermal dark matter with low-temperature reheating". In: *JCAP* 09 (2024), p. 024. DOI: 10.1088/1475-7516/2024/09/024. arXiv: 2406.17039 [hep-ph].

[58] Ronny Frumkin et al. "Roadmap to Thermal Dark Matter beyond the Weakly Interacting Dark Matter Unitarity Bound". In: *Phys. Rev. Lett.* 130.17 (2023), p. 171001. DOI: 10.1103/PhysRevLett.130.171001. arXiv: 2207.01635 [hep-ph].

[59] Robert J. Scherrer and Michael S. Turner. "On the Relic, Cosmic Abundance of Stable Weakly Interacting Massive Particles". In: *Phys. Rev. D* 33 (1986). [Erratum: Phys.Rev.D 34, 3263 (1986)], p. 1585. DOI: 10.1103/PhysRevD.33.1585.

[60] Paolo Gondolo and Graciela Gelmini. "Cosmic abundances of stable particles: Improved analysis". In: *Nucl. Phys. B* 360 (1991), pp. 145–179. DOI: 10.1016/0550-3213(91)90438-4.

[61] Gary Steigman, Basudeb Dasgupta, and John F. Beacom. "Precise Relic WIMP Abundance and its Impact on Searches for Dark Matter Annihilation". In: *Phys. Rev. D* 86 (2012), p. 023506. DOI: 10.1103/PhysRevD.86.023506. arXiv: 1204.3622 [hep-ph].

[62] Andrzej Hryczuk. "Dark Matter Freeze-out and Freeze-in beyond Kinetic Equilibrium". In: *LHEP* 2023 (2023), p. 344. DOI: 10.31526/lhep.2023.344.

[63] Marcin Misiaszek and Nicola Rossi. "Direct Detection of Dark Matter: A Critical Review". In: *Symmetry* 16.2 (2024), p. 201. DOI: 10.3390/sym16020201. arXiv: 2310.20472 [hep-ph].

[64] Carlos Pérez de los Heros. "Status, Challenges and Directions in Indirect Dark Matter Searches". In: *Symmetry* 12.10 (2020), p. 1648. DOI: 10.3390/sym12101648. arXiv: 2008.11561 [astro-ph.HE].

[65] Antonio Boveia and Caterina Doglioni. "Dark Matter Searches at Colliders". In: *Ann. Rev. Nucl. Part. Sci.* 68 (2018), pp. 429–459. DOI: 10.1146/annurev-nucl-101917-021008. arXiv: 1810.12238 [hep-ex].

[66] Gary Steigman and Michael S. Turner. "Cosmological Constraints on the Properties of Weakly Interacting Massive Particles". In: *Nucl. Phys. B* 253 (1985), pp. 375–386. DOI: 10.1016/0550-3213(85)90537-1.

[67] Jonathan L. Feng. "The WIMP paradigm: Theme and variations". In: *SciPost Phys. Lect. Notes* 71 (2023), p. 1. DOI: 10.21468/SciPostPhysLectNotes.71. arXiv: 2212.02479 [hep-ph].

[68] Giorgio Arcadi et al. "The Waning of the WIMP: Endgame?" In: *Eur. Phys. J. C* 85.2 (2025), p. 152. DOI: 10.1140/epjc/s10052-024-13672-y. arXiv: 2403.15860 [hep-ph].

[69] David Tucker-Smith and Neal Weiner. "Inelastic dark matter". In: *Phys. Rev. D* 64 (2001), p. 043502. DOI: 10.1103/PhysRevD.64.043502. arXiv: hep-ph/0101138.

[70] Eder Izaguirre, Gordan Krnjaic, and Brian Shuve. "Discovering Inelastic Thermal-Relic Dark Matter at Colliders". In: *Phys. Rev. D* 93.6 (2016), p. 063523. DOI: 10.1103/PhysRevD.93.063523. arXiv: 1508.03050 [hep-ph].

[71] Asher Berlin and Felix Kling. "Inelastic Dark Matter at the LHC Lifetime Frontier: ATLAS, CMS, LHCb, CODEX-b, FASER, and MATHUSLA". In: *Phys. Rev. D* 99.1 (2019), p. 015021. DOI: 10.1103/PhysRevD.99.015021. arXiv: 1810.01879 [hep-ph].

[72] Nicole F. Bell, Giorgio Busoni, and Sandra Robles. "Heating up Neutron Stars with Inelastic Dark Matter". In: *JCAP* 09 (2018), p. 018. DOI: 10.1088/1475-7516/2018/09/018. arXiv: 1807.02840 [hep-ph].

[73] Masha Baryakhtar et al. "Electromagnetic signals of inelastic dark matter scattering". In: *JHEP* 06 (2022), p. 047. DOI: 10.1007/JHEP06(2022)047. arXiv: 2006.13918 [hep-ph].

[74] Jie-Cheng Feng et al. "Revising inelastic dark matter direct detection by including the cosmic ray acceleration". In: *JHEP* 04 (2022), p. 080. DOI: 10.1007/JHEP04(2022)080. arXiv: 2110.08863 [hep-ph].

[75] Mariana Carrillo González and Natalia Toro. "Cosmology and signals of light pseudo-Dirac dark matter". In: *JHEP* 04 (2022), p. 060. DOI: 10.1007/JHEP04(2022)060. arXiv: 2108.13422 [hep-ph].

[76] Nicole F. Bell et al. "Cosmic-ray upscattered inelastic dark matter". In: *Phys. Rev. D* 104 (2021), p. 076020. DOI: 10.1103/PhysRevD.104.076020. arXiv: 2108.00583 [hep-ph].

[77] Nicole F. Bell et al. "Low-mass inelastic dark matter direct detection via the Migdal effect". In: *Phys. Rev. D* 104.7 (2021), p. 076013. DOI: 10.1103/PhysRevD.104.076013. arXiv: 2103.05890 [hep-ph].

[78] Nirmalya Brahma, Saniya Heeba, and Katelin Schutz. "Resonant pseudo-Dirac dark matter as a sub-GeV thermal target". In: *Phys. Rev. D* 109.3 (2024), p. 035006. DOI: 10.1103/PhysRevD.109.035006. arXiv: 2308.01960 [hep-ph].

[79] Michael Duerr et al. "Long-lived Dark Higgs and Inelastic Dark Matter at Belle II". In: *JHEP* 04 (2021), p. 146. DOI: 10.1007/JHEP04(2021)146. arXiv: 2012.08595 [hep-ph].

[80] Martina Mongillo et al. "Constraining light thermal inelastic dark matter with NA64". In: *Eur. Phys. J. C* 83.5 (2023), p. 391. DOI: 10.1140/epjc/s10052-023-11536-5. arXiv: 2302.05414 [hep-ph].

[81] Aram Hayrapetyan et al. "Search for Inelastic Dark Matter in Events with Two Displaced Muons and Missing Transverse Momentum in Proton-Proton Collisions at s=13 TeV". In: *Phys. Rev. Lett.* 132.4 (2024), p. 041802. DOI: 10.1103/PhysRevLett.132.041802. arXiv: 2305.11649 [hep-ex].

[82] I. Adachi et al. "Search for a dark Higgs boson produced in association with inelastic dark matter at the Belle II experiment". In: (May 2025). arXiv: 2505.09705 [hep-ex].

[83] P. Ko et al. "Searching for elusive dark Higgs boson in spin-1/2 inelastic dark matter models at Belle II". In: (Apr. 2025). arXiv: 2504.19067 [hep-ph].

[84] E. M. Purcell and N. F. Ramsey. "On the Possibility of Electric Dipole Moments for Elementary Particles and Nuclei". In: *Phys. Rev.* 78 (1950), pp. 807–807. DOI: 10.1103/PhysRev.78.807.

[85] T. D. Lee and Chen-Ning Yang. "Question of Parity Conservation in Weak Interactions". In: *Phys. Rev.* 104 (1956), pp. 254–258. DOI: 10.1103/PhysRev.104.254.

[86] C. S. Wu et al. "Experimental Test of Parity Conservation in β Decay". In: *Phys. Rev.* 105 (1957), pp. 1413–1414. DOI: 10.1103/PhysRev.105.1413.

[87] Yanou Cui et al. "Candidates for Inelastic Dark Matter". In: *JHEP* 05 (2009), p. 076. DOI: 10.1088/1126-6708/2009/05/076. arXiv: 0901.0557 [hep-ph].

[88] Andrea De Simone, Veronica Sanz, and Hiromitsu Phil Sato. "Pseudo-Dirac Dark Matter Leaves a Trace". In: *Phys. Rev. Lett.* 105 (2010), p. 121802. DOI: 10.1103/PhysRevLett.105.121802. arXiv: 1004.1567 [hep-ph].

[89] Giovani Dalla Valle Garcia et al. "Not-so-inelastic Dark Matter". In: *JHEP* 02 (2025), p. 127. DOI: 10.1007/JHEP02(2025)127. arXiv: 2405.08081 [hep-ph].

[90] Asher Berlin et al. "Dark Matter, Millicharges, Axion and Scalar Particles, Gauge Bosons, and Other New Physics with LDMX". In: *Phys. Rev. D* 99.7 (2019), p. 075001. DOI: 10.1103/PhysRevD.99.075001. arXiv: 1807.01730 [hep-ph].

[91] W. Altmannshofer et al. "The Belle II Physics Book". In: *PTEP* 2019.12 (2019). Ed. by E. Kou and P. Urquijo. [Erratum: PTEP 2020, 029201 (2020)], p. 123C01. DOI: 10.1093/ptep/ptz106. arXiv: 1808.10567 [hep-ex].

[92] P. Crivelli. "Status and prospects of the NA64 experiment at the CERN SPS". In: *Workshop on Feebly-Interacting Particles*. Jan. 2023. arXiv: 2301.09905 [hep-ex].

[93] Giovani Dalla Valle Garcia. "A minimalistic model for inelastic dark matter". In: *Phys. Lett. B* 862 (2025), p. 139320. DOI: 10.1016/j.physletb.2025.139320. arXiv: 2411.02147 [hep-ph].

[94] J. Aalbers et al. "DARWIN: towards the ultimate dark matter detector". In: *JCAP* 11 (2016), p. 017. DOI: 10.1088/1475-7516/2016/11/017. arXiv: 1606.07001 [astro-ph.IM].

[95] Giovani Dalla Valle Garcia and Maksym Ovchynnikov. "Di-decay signature of new physics particles at intensity frontier experiments". In: (Mar. 2025). arXiv: 2503.01760 [hep-ph].

[96] P. A. R. Ade et al. "Planck 2013 results. XVI. Cosmological parameters". In: *Astron. Astrophys.* 571 (2014), A16. DOI: 10.1051/0004-6361/201321591. arXiv: 1303.5076 [astro-ph.CO].

[97] Ofer Lahav. "Observational tests for the cosmological principle and world models". In: *NATO Sci. Ser. C* 565 (2001). Ed. by Robert G. Crittenden and Neil G. Turok, pp. 131–142. DOI: 10.1007/978-94-010-0540-1_7. arXiv: astro-ph/0001061.

[98] Albert Einstein. "The Field Equations of Gravitation". In: *Sitzungsber. Preuss. Akad. Wiss. Berlin (Math. Phys.)* 1915 (1915), pp. 844–847.

[99] Albert Einstein. "The foundation of the general theory of relativity." In: *Annalen Phys.* 49.7 (1916). Ed. by Jong-Ping Hsu and D. Fine, pp. 769–822. DOI: 10.1002/andp.19163540702.

[100] Albert Einstein. "Cosmological Considerations in the General Theory of Relativity". In: *Sitzungsber. Preuss. Akad. Wiss. Berlin (Math. Phys.)* 1917 (1917), pp. 142–152.

[101] Dominik J. Schwarz. "Thoughts on the Cosmological Principle". In: *Fundamental Interactions*. WORLD SCIENTIFIC, Sept. 2009, pp. 267–276. ISBN: 9789814277839. DOI: 10.1142/9789814277839_0015. URL: http://dx.doi.org/10.1142/9789814277839_0015.

[102] Edward Arthur Milne. "Kinematics, dynamics, and the scale of time". In: *Proceedings of the Royal Society of London. Series A, Mathematical and Physical Sciences* 158.894 (1937), pp. 324–348. DOI: 10.1098/rspa.1937.0023.

[103] C. L. Bennett et al. "Structure in the COBE Differential Microwave Radiometer First-Year Maps". In: *The Astrophysical Journal Letters* 396 (1992), pp. L7–L12. DOI: 10.1086/186504.

[104] Konstantinos Migkas. "Galaxy clusters as probes of cosmic isotropy". In: *Phil. Trans. Roy. Soc. Lond. A* 383.2290 (2025), p. 20240030. DOI: 10.1098/rsta.2024.0030. arXiv: 2406.01752 [astro-ph.CO].

[105] Diego Blas. "Introduction to dark matter". Online accessed: 2024-04-01. 2019. URL: https://conference.ippp.dur.ac.uk/event/1291/attachments/6076/8176/DM_Blas1.pdf.

[106] Sean M. Carroll. "Lecture notes on general relativity". In: (Dec. 1997). arXiv: gr-qc/9712019.

[107] R. L. Workman et al. "Review of Particle Physics". In: *PTEP* 2022 (2022), p. 083C01. DOI: 10.1093/ptep/ptac097.

[108] Edwin Hubble. "A Relation between Distance and Radial Velocity among Extra-Galactic Nebulae". In: *Proceedings of the National Academy of Sciences* 15.3 (1929), pp. 168–173. DOI: 10.1073/pnas.15.3.168.

[109] A. G. Adame et al. "DESI 2024 VI: cosmological constraints from the measurements of baryon acoustic oscillations". In: *JCAP* 02 (2025), p. 021. DOI: 10.1088/1475-7516/2025/02/021. arXiv: 2404.03002 [astro-ph.CO].

[110] Nandan Roy. "Dynamical dark energy in the light of DESI 2024 data". In: *Phys. Dark Univ.* 48 (2025), p. 101912. DOI: 10.1016/j.dark.2025.101912. arXiv: 2406.00634 [astro-ph.CO].

[111] Marina Cortês and Andrew R. Liddle. "Interpreting DESI's evidence for evolving dark energy". In: *JCAP* 12 (2024), p. 007. DOI: 10.1088/1475-7516/2024/12/007. arXiv: 2404.08056 [astro-ph.CO].

[112] Jerome Martin. "The Theory of Inflation". In: *Proc. Int. Sch. Phys. Fermi* 200 (2020). Ed. by E. Coccia, J. Silk, and N. Vittorio, pp. 155–178. DOI: 10.3254/ENFI200008. arXiv: 1807.11075 [astro-ph.CO].

[113] Ana Achúcarro et al. "Inflation: Theory and Observations". In: (Mar. 2022). arXiv: 2203.08128 [astro-ph.CO].

[114] John Ellis and David Wands. "Inflation (2023)". In: (Dec. 2023). arXiv: 2312.13238 [astro-ph.CO].

[115] H. E. S. Velten, R. F. vom Marttens, and W. Zimdahl. "Aspects of the cosmological "coincidence problem"". In: *Eur. Phys. J. C* 74.11 (2014), p. 3160. DOI: 10.1140/epjc/s10052-014-3160-4. arXiv: 1410.2509 [astro-ph.CO].

[116] Michael S. Turner. "The Hot big bang and beyond". In: *AIP Conf. Proc.* 342 (1995), pp. 43–62. DOI: 10.1063/1.48810. arXiv: astro-ph/9503017.

[117] Andreas Ekstedt and Johan Löfgren. "A Critical Look at the Electroweak Phase Transition". In: *JHEP* 12 (2020), p. 136. DOI: 10.1007/JHEP12(2020)136. arXiv: 2006.12614 [hep-ph].

[118] Tillmann Boeckel, Simon Schettler, and Jurgen Schaffner-Bielich. "The Cosmological QCD Phase Transition Revisited". In: *Prog. Part. Nucl. Phys.* 66 (2011). Ed. by Amand Faessler and Vadim Rodin, pp. 266–270. DOI: 10.1016/j.ppnp.2011.01.017. arXiv: 1012.3342 [astro-ph.CO].

[119] David S. Pereira et al. "Baryogenesis: A Symmetry Breaking in the Primordial Universe Revisited". In: *Symmetry* 16.1 (2024), p. 13. DOI: 10.3390/sym16010013. arXiv: 2312.14080 [gr-qc].

[120] Xi-He Hu and Ye-Ling Zhou. "Gravitational waves of GUT phase transition during inflation". In: *Phys. Rev. D* 111.11 (2025), p. 115003. DOI: 10.1103/kbzd-kgdr. arXiv: 2501.01491 [hep-ph].

[121] B. P. Abbott et al. "Observation of Gravitational Waves from a Binary Black Hole Merger". In: *Phys. Rev. Lett.* 116.6 (2016), p. 061102. DOI: 10.1103/PhysRevLett.116.061102. arXiv: 1602.03837 [gr-qc].

[122] Gabriella Agazie et al. "The NANOGrav 15 yr Data Set: Evidence for a Gravitational-wave Background". In: *Astrophys. J. Lett.* 951.1 (2023), p. L8. DOI: 10.3847/2041-8213/acdac6. arXiv: 2306.16213 [astro-ph.HE].

[123] Eric Madge et al. "Primordial gravitational waves in the nano-Hertz regime and PTA data — towards solving the GW inverse problem". In: *JHEP* 10 (2023), p. 171. DOI: 10.1007/JHEP10(2023)171. arXiv: 2306.14856 [hep-ph].

[124] Douglas Scott. "The Cosmic Neutrino Background". In: *International School of Physics "Enrico Fermi" in collaboration with the summer schools ISAPP: Neutrino Physics, Astrophysics and Cosmology*. Feb. 2024. arXiv: 2402.16243 [astro-ph.CO].

[125] Ryan Cooke. "Big Bang Nucleosynthesis". In: (Sept. 2024). arXiv: 2409.06015 [astro-ph.CO].

[126] Max Pettini. "Introduction to Cosmology". Online accessed: 2024-04-17. 2018. URL: https://people.ast.cam.ac.uk/~pettini/Intro%20Cosmology/Lecture07.pdf.

[127] Michael Dine and Alexander Kusenko. "The Origin of the matter - antimatter asymmetry". In: *Rev. Mod. Phys.* 76 (2003), p. 1. DOI: 10.1103/RevModPhys.76.1. arXiv: hep-ph/0303065.

[128] Brian D. Fields. "The primordial lithium problem". In: *Ann. Rev. Nucl. Part. Sci.* 61 (2011), pp. 47–68. DOI: 10.1146/annurev-nucl-102010-130445. arXiv: 1203.3551 [astro-ph.CO].

[129] Ruth Durrer. "The cosmic microwave background: the history of its experimental investigation and its significance for cosmology". In: *Class. Quant. Grav.* 32.12 (2015), p. 124007. DOI: 10.1088/0264-9381/32/12/124007. arXiv: 1506.01907 [astro-ph.CO].

[130] Saleem Zaroubi. "The Epoch of Reionization". In: (June 2012). DOI: 10.1007/978-3-642-32362-1_2. arXiv: 1206.0267 [astro-ph.CO].

[131] Christian L. Reichardt. "Observing the Epoch of Reionization with the Cosmic Microwave Background". In: (Nov. 2015). DOI: 10.1007/978-3-319-21957-8_8. arXiv: 1511.01117 [astro-ph.CO].

[132] Jeanette Kazmierczak (NASA). "Cosmic History". Online accessed: 2024-04-17. 2024. URL: https://assets.science.nasa.gov/dynamicimage/assets/science/astro/universe/internal_resources/497/Universe_History_2.png?w=6667&h=3750&fit=clip&crop=faces%2Cfocalpoint.

[133] Mark Trodden and Sean M. Carroll. "TASI lectures: Introduction to cosmology". In: *Theoretical Advanced Study Institute in Elementary Particle Physics (TASI 2002): Particle Physics and Cosmology: The Quest for Physics Beyond the Standard Model(s)*. Jan. 2004, pp. 703–793. arXiv: astro-ph/0401547.

[134] David Wands, Oliver F. Piattella, and Luciano Casarini. "Physics of the Cosmic Microwave Background Radiation". In: *Astrophys. Space Sci. Proc.* 45 (2016). Ed. by Júlio C. Fabris et al., pp. 3–39. DOI: 10.1007/978-3-319-44769-8_1. arXiv: 1504.06335 [astro-ph.CO].

[135] David G. Cerdeño. "DARK MATTER 101 - From production to detection". Online accessed: 2024-04-03. URL: https://www.ippp.dur.ac.uk/~dcerdeno/Dark_Matter_Lab_files/DM.pdf.

[136] Roman N. Lee. "Electron-positron annihilation to photons at $O(\alpha^3)$ revisited". In: *Nucl. Phys. B* 960 (2020), p. 115200. DOI: 10.1016/j.nuclphysb.2020.115200. arXiv: 2006.11082 [hep-ph].

[137] David Silva Pereira et al. "Thermodynamics of the Primordial Universe". In: *Entropy* 26.11 (2024), p. 947. DOI: 10.3390/e26110947. arXiv: 2411.03018 [gr-qc].

[138] S. Navas et al. "Review of particle physics". In: *Phys. Rev. D* 110.3 (2024), p. 030001. DOI: 10.1103/PhysRevD.110.030001.

[139] Michal Malinský. "Theoretical cosmology II (NTMF333)". Online accessed: 2025-09-07. URL: https://ipnp.cz/~malinsky/courses/NTMF333/Lectures.pdf.

[140] A. D. Dolgov. "Baryogenesis, 30 years after". In: *25th ITEP Winter School of Physics*. July 1997. DOI: 10.1080/01422419808240874. arXiv: hep-ph/9707419.

[141] Cristina Benso, Thomas Schwetz, and Drona Vatsyayan. "Large neutrino mass in cosmology and keV sterile neutrino dark matter from a dark sector". In: *JCAP* 04 (2025), p. 054. DOI: 10.1088/1475-7516/2025/04/054. arXiv: 2410.23926 [hep-ph].

[142] Max Aker et al. "Direct neutrino-mass measurement based on 259 days of KATRIN data". In: *Science* 388.6743 (2025), adq9592. DOI: 10.1126/science.adq9592. arXiv: 2406.13516 [nucl-ex].

[143] Julien Lesgourgues and Sergio Pastor. "Neutrino cosmology and Planck". In: *New J. Phys.* 16 (2014), p. 065002. DOI: 10.1088/1367-2630/16/6/065002. arXiv: 1404.1740 [hep-ph].

[144] Ivan Esteban et al. "NuFit-6.0: updated global analysis of three-flavor neutrino oscillations". In: *JHEP* 12 (2024), p. 216. DOI: 10.1007/JHEP12(2024)216. arXiv: 2410.05380 [hep-ph].

[145] D. M. Webber et al. "Measurement of the Positive Muon Lifetime and Determination of the Fermi Constant to Part-per-Million Precision". In: *Phys. Rev. Lett.* 106 (2011), p. 041803. DOI: 10.1103/PhysRevLett.106.079901. arXiv: 1010.0991 [hep-ex].

[146] Glennys R. Farrar. "6-quark Dark Matter". In: *PoS* ICRC2017 (2018), p. 929. DOI: 10.22323/1.301.0929. arXiv: 1711.10971 [hep-ph].

[147] Glennys R. Farrar and Zihui Wang. "Constraints on long-lived di-baryons and di-baryonic dark matter". In: (June 2023). arXiv: 2306.03123 [hep-ph].

[148] F. Zwicky. "On the Masses of Nebulae and of Clusters of Nebulae". In: *Astrophys. J.* 86 (1937), pp. 217–246. DOI: 10.1086/143864.

[149] Edwin Hubble and Milton L. Humason. "The Velocity-Distance Relation among Extra-Galactic Nebulae". In: *Astrophys. J.* 74 (1931), pp. 43–80. DOI: 10.1086/143323.

[150] F. W. Bessel. "On the variations of the proper motions of Procyon and Sirius". In: 6 (Dec. 1844), pp. 136–141. DOI: 10.1093/mnras/6.11.136.

[151] B. L. Welther. "The discovery of Sirius B: a case of strategy or serendipity?" In: 16 (Jan. 1987), p. 34.

[152] J. M. Schaeberle. "DISCOVERY OF THE COMPANION TO PROCYON". In: *Publications of the Astronomical Society of the Pacific* 8.53 (Dec. 1896), 314a. DOI: 10.1086/121125. URL: https://dx.doi.org/10.1086/121125.

[153] Gabriel Rodríguez-Moris and José A. Docobo. *The Discovery of Neptune Revisited*. 2024. arXiv: 2405.06310 [astro-ph.EP]. URL: https://arxiv.org/abs/2405.06310.

[154] Albert Einstein. "Explanation of the Perihelion Motion of Mercury from the General Theory of Relativity". In: *Sitzungsber. Preuss. Akad. Wiss. Berlin (Math. Phys.)* 1915 (1915), pp. 831–839.

[155] *Gravitational lensing in action*. https://esahubble.org/images/heic1106c/. Accessed: 2025-08-11.

[156] Raul E. Angulo and Oliver Hahn. "Large-scale dark matter simulations". In: *Liv. Rev. Comput. Astrophys.* 8.1 (2022), p. 1. DOI: 10.1007/s41115-021-00013-z. arXiv: 2112.05165 [astro-ph.CO].

[157] Joerg P. Dietrich et al. "Weak lensing evidence for a filament between the clusters A 222 and A 223 and its quantification". In: *Astron. Astrophys.* 440 (2005), pp. 453–471. DOI: 10.1051/0004-6361:20041523. arXiv: astro-ph/0406541.

[158] Nicolas Martinet et al. "Weak lensing study of 16 DAFT/FADA clusters: substructures and filaments". In: *Astron. Astrophys.* 590 (2016), A69. DOI: 10.1051/0004-6361/201526444. arXiv: 1603.04696 [astro-ph.CO].

[159] Tianyi Yang, Michael J. Hudson, and Niayesh Afshordi. "How dark are filaments in the cosmic web?" In: *Mon. Not. Roy. Astron. Soc.* 498.3 (2020), pp. 3158–3170. DOI: 10.1093/mnras/staa2547. arXiv: 2001.10943 [astro-ph.CO].

[160] Tien-Tien Yu. "2024 TASI Lectures: A Dark Matter Primer". In: (June 2025). arXiv: 2506.05234 [hep-ph].

[161] Brian D. Fields et al. "Big-Bang Nucleosynthesis after Planck". In: *JCAP* 03 (2020). [Erratum: JCAP 11, E02 (2020)], p. 010. DOI: 10.1088/1475-7516/2020/03/010. arXiv: 1912.01132 [astro-ph.CO].

[162] Celine Boehm. "Particle dark matter versus modified gravity". In: *Nucl. Phys. B* 1003 (2024), p. 116503. DOI: 10.1016/j.nuclphysb.2024.116503.

[163] Shin'ichi Nojiri and Sergei D. Odintsov. "Dark energy, inflation and dark matter from modified F(R) gravity". In: *TSPU Bulletin* N8(110) (2011), pp. 7–19. arXiv: 0807.0685 [hep-th].

[164] Jose A. R. Cembranos. "Modified gravity and dark matter". In: *J. Phys. Conf. Ser.* 718.3 (2016), p. 032004. DOI: 10.1088/1742-6596/718/3/032004. arXiv: 1512.08752 [hep-ph].

[165] Taishi Katsuragawa and Shinya Matsuzaki. "Dark matter in modified gravity?" In: *Phys. Rev. D* 95.4 (2017), p. 044040. DOI: 10.1103/PhysRevD.95.044040. arXiv: 1610.01016 [gr-qc].

[166] Stacy S. McGaugh et al. "The Baryonic Tully-Fisher relation". In: *Astrophys. J. Lett.* 533 (2000), pp. L99–L102. DOI: 10.1086/312628. arXiv: astro-ph/0003001.

[167] Kris Pardo and David N. Spergel. "What is the price of abandoning dark matter? Cosmological constraints on alternative gravity theories". In: *Phys. Rev. Lett.* 125.21 (2020), p. 211101. DOI: 10.1103/PhysRevLett.125.211101. arXiv: 2007.00555 [astro-ph.CO].

[168] Stacy S. McGaugh. "A tale of two paradigms: the mutual incommensurability of ΛCDM and MOND". In: *Can. J. Phys.* 93.2 (2015), pp. 250–259. DOI: 10.1139/cjp-2014-0203. arXiv: 1404.7525 [astro-ph.CO].

[169] Xin Li et al. "Finslerian MOND vs. observations of Bullet Cluster 1E0657-558". In: *Mon. Not. Roy. Astron. Soc.* 428.4 (2013), pp. 2939–2948. DOI: 10.1093/mnras/sts237. arXiv: 1209.3086 [astro-ph.GA].

[170] Jacob D. Bekenstein. "Relativistic gravitation theory for the MOND paradigm". In: *Phys. Rev. D* 70 (2004). [Erratum: Phys.Rev.D 71, 069901 (2005)], p. 083509. DOI: 10.1103/PhysRevD.70.083509. arXiv: astro-ph/0403694.

[171] Jacob D. Bekenstein. "Tensor-vector-scalar-modified gravity: from small scale to cosmology". In: *Phil. Trans. Roy. Soc. Lond. A* 369 (2011), pp. 5003–5017. DOI: 10.1098/rsta.2011.0282. arXiv: 1201.2759 [astro-ph.CO].

[172] B. P. Abbott et al. "GW170817: Observation of Gravitational Waves from a Binary Neutron Star Inspiral". In: *Phys. Rev. Lett.* 119.16 (2017), p. 161101. DOI: 10.1103/PhysRevLett.119.161101. arXiv: 1710.05832 [gr-qc].

[173] R. H. Sanders. "Does GW170817 falsify MOND?" In: *Int. J. Mod. Phys. D* 27.14 (2018), p. 14. DOI: 10.1142/S0218271818470272. arXiv: 1805.06804 [gr-qc].

[174] Riccardo Scarpa. "Modified newtonian dynamics, an introductory review". In: *AIP Conf. Proc.* 822.1 (2006). Ed. by Eric J. Lerner and Jose B. Almeida, pp. 253–265. DOI: 10.1063/1.2189141. arXiv: astro-ph/0601478.

[175] B. Paczynski. "Gravitational Microlensing by the Galactic Halo". In: 304 (May 1986), p. 1. DOI: 10.1086/164140.

[176] Kim Griest. "Galactic Microlensing as a Method of Detecting Massive Compact Halo Objects". In: 366 (Jan. 1991), p. 412. DOI: 10.1086/169575.

[177] Karsten Jedamzik. "Could MACHOS be primordial black holes formed during the QCD epoch?" In: *Phys. Rept.* 307 (1998). Ed. by D. B. Cline, pp. 155–162. DOI: 10.1016/S0370-1573(98)00067-2. arXiv: astro-ph/9805147.

[178] Bernard Carr and Florian Kuhnel. "Primordial black holes as dark matter candidates". In: *SciPost Phys. Lect. Notes* 48 (2022), p. 1. DOI: 10.21468/SciPostPhysLectNotes.48. arXiv: 2110.02821 [astro-ph.CO].

[179] P. Ivanov, P. Naselsky, and I. Novikov. "Inflation and primordial black holes as dark matter". In: *Phys. Rev. D* 50 (1994), pp. 7173–7178. DOI: 10.1103/PhysRevD.50.7173.

[180] Manuel Drees and Encieh Erfani. "Dark Matter Primordial Black Holes and Inflation Models". In: (May 2012). arXiv: 1205.4012 [astro-ph.CO].

[181] Nilanjandev Bhaumik and Rajeev Kumar Jain. "Primordial black holes dark matter from inflection point models of inflation and the effects of reheating". In: *JCAP* 01 (2020), p. 037. DOI: 10.1088/1475-7516/2020/01/037. arXiv: 1907.04125 [astro-ph.CO].

[182] Guillermo Ballesteros et al. "Primordial black holes as dark matter and gravitational waves from single-field polynomial inflation". In: *JCAP* 07 (2020), p. 025. DOI: 10.1088/1475-7516/2020/07/025. arXiv: 2001.08220 [astro-ph.CO].

[183] Virgile Dandoy, Valerie Domcke, and Fabrizio Rompineve. "Search for scalar induced gravitational waves in the international pulsar timing array data release 2 and NANOgrav 12.5 years datasets". In: *SciPost Phys. Core* 6 (2023), p. 060. DOI: 10.21468/SciPostPhysCore.6.3.060. arXiv: 2302.07901 [astro-ph.CO].

[184] Will Barker, Benjamin Gladwyn, and Sebastian Zell. "Inflationary and gravitational wave signatures of small primordial black holes as dark matter". In: *Phys. Rev. D* 111.12 (2025), p. 123033. DOI: 10.1103/4hrv-zfch. arXiv: 2410.11948 [astro-ph.CO].

[185] S. Clesse, V. Dandoy, and S. Verma. "Probing Primordial Black Hole Mergers in Clusters with Pulsar Timing Data". In: (Dec. 2024). arXiv: 2412.15989 [astro-ph.CO].

[186] J. Casas et al. "Origins of neutrino masses and mixings and the impact of radiative corrections". In: *Nucl. Instrum. Meth. A* 451 (2000). Ed. by B. Autin, pp. 69–75. DOI: 10.1016/S0168-9002(00)00374-0.

[187] Robert Foot, H. Lew, and R. R. Volkas. "Electric charge quantization". In: *J. Phys. G* 19 (1993). [Erratum: J.Phys.G 19, 1067 (1993)], pp. 361–372. DOI: 10.1088/0954-3899/19/3/005. arXiv: hep-ph/9209259.

[188] Stuart Raby. "Grand Unified Theories". In: *2nd World Summit: Physics Beyond the Standard Model*. Aug. 2006. arXiv: hep-ph/0608183.

[189] Alessandro Strumia. "Solving the strong CP problem". In: *16th Conference on Quark Confinement and the Hadron Spectrum*. Jan. 2025. arXiv: 2501.16427 [hep-ph].

[190] Michael E. Peskin. "What is the Hierarchy Problem?" In: *Nucl. Phys. B* 1018 (2025), p. 116971. DOI: 10.1016/j.nuclphysb.2025.116971. arXiv: 2505.00694 [hep-ph].

[191] Erik Zackrisson and Teresa Riehm. "Gravitational Lensing as a Probe of Cold Dark Matter Subhalos". In: *Advances in Astronomy* 2010.1 (Nov. 2009). Ed. by Regina Schulte-Ladbeck. ISSN: 1687-7977. DOI: 10.1155/2010/478910. URL: http://dx.doi.org/10.1155/2010/478910.

[192] Aurel Schneider. "Structure formation with suppressed small-scale perturbations". In: *Mon. Not. Roy. Astron. Soc.* 451.3 (2015), pp. 3117–3130. DOI: 10.1093/mnras/stv1169. arXiv: 1412.2133 [astro-ph.CO].

[193] Sean Tulin and Hai-Bo Yu. "Dark Matter Self-interactions and Small Scale Structure". In: *Phys. Rept.* 730 (2018), pp. 1–57. DOI: 10.1016/j.physrep.2017.11.004. arXiv: 1705.02358 [hep-ph].

[194] Samuel D. McDermott, Hai-Bo Yu, and Kathryn M. Zurek. "Turning off the Lights: How Dark is Dark Matter?" In: *Phys. Rev. D* 83 (2011), p. 063509. DOI: 10.1103/PhysRevD.83.063509. arXiv: 1011.2907 [hep-ph].

[195] Christian Gross et al. "Dark Matter in the Standard Model?" In: *Phys. Rev. D* 98.6 (2018), p. 063005. DOI: 10.1103/PhysRevD.98.063005. arXiv: 1803.10242 [hep-ph].

[196] K. Azizi, S. S. Agaev, and H. Sundu. "The Scalar Hexaquark *uuddss*: a Candidate to Dark Matter?" In: *J. Phys. G* 47.9 (2020), p. 095001. DOI: 10.1088/1361-6471/ab9a0e. arXiv: 1904.09913 [hep-ph].

[197] Gianfranco Bertone and Tim Tait M. P. "A new era in the search for dark matter". In: *Nature* 562.7725 (2018), pp. 51–56. DOI: 10.1038/s41586-018-0542-z. arXiv: 1810.01668 [astro-ph.CO].

[198] Elisa G. M. Ferreira. "Ultra-light dark matter". In: *Astron. Astrophys. Rev.* 29.1 (2021), p. 7. DOI: 10.1007/s00159-021-00135-6. arXiv: 2005.03254 [astro-ph.CO].

[199] James Alvey et al. "New constraints on the mass of fermionic dark matter from dwarf spheroidal galaxies". In: *Mon. Not. Roy. Astron. Soc.* 501.1 (2021), pp. 1188–1201. DOI: 10.1093/mnras/staa3640. arXiv: 2010.03572 [hep-ph].

[200] S. Tremaine and J. E. Gunn. "Dynamical Role of Light Neutral Leptons in Cosmology". In: *Phys. Rev. Lett.* 42 (1979). Ed. by M. A. Srednicki, pp. 407–410. DOI: 10.1103/PhysRevLett.42.407.

[201] Leszek Roszkowski, Enrico Maria Sessolo, and Sebastian Trojanowski. "WIMP dark matter candidates and searches—current status and future prospects". In: *Rept. Prog. Phys.* 81.6 (2018), p. 066201. DOI: 10.1088/1361-6633/aab913. arXiv: 1707.06277 [hep-ph].

[202] Rabindra N. Mohapatra. "Supersymmetry and R-parity: an Overview". In: *Phys. Scripta* 90 (2015), p. 088004. DOI: 10.1088/0031-8949/90/8/088004. arXiv: 1503.06478 [hep-ph].

[203] Maxim Perelstein. "Little Higgs models and T parity". In: *Pramana* 67 (2006). Ed. by P. Agrawal and A. M. Srivastava, pp. 813–820. DOI: 10.1007/s12043-006-0094-x. arXiv: hep-ph/0703138.

[204] Hsin-Chia Cheng, Jonathan L. Feng, and Konstantin T. Matchev. "Kaluza-Klein dark matter". In: *Phys. Rev. Lett.* 89 (2002), p. 211301. DOI: 10.1103/PhysRevLett.89.211301. arXiv: hep-ph/0207125.

[205] Masha Baryakhtar, Leslie Rosenberg, and Gray Rybka. "Searching for the QCD Dark Matter Axion". In: (Apr. 2025). arXiv: 2504.10607 [hep-ex].

[206] Yudi Santoso. "The Phenomenology of Gravitino Dark Matter Scenarios in Supergravity Models". In: *7th International Heidelberg Conference on Dark Matter in Astro and Particle Physics*. 2009, pp. 77–86. DOI: 10.1142/9789814293792_0007. arXiv: 0903.2860 [hep-ph].

[207] Wilfried Buchmuller. "Gravitino Dark Matter". In: *AIP Conf. Proc.* 1200.1 (2010). Ed. by George Alverson, Brent Nelson, and Pran Nath, pp. 155–164. DOI: 10.1063/1.3327554. arXiv: 0910.1870 [hep-ph].

[208] A. Boyarsky et al. "Sterile neutrino Dark Matter". In: *Prog. Part. Nucl. Phys.* 104 (2019), pp. 1–45. DOI: 10.1016/j.ppnp.2018.07.004. arXiv: 1807.07938 [hep-ph].

[209] Kalliopi Petraki and Raymond R. Volkas. "Review of asymmetric dark matter". In: *Int. J. Mod. Phys. A* 28 (2013), p. 1330028. DOI: 10.1142/S0217751X13300287. arXiv: 1305.4939 [hep-ph].

[210] Andrew Eberhardt and Elisa G. M. Ferreira. "Ultralight fuzzy dark matter review". In: (July 2025). arXiv: 2507.00705 [astro-ph.CO].

[211] Marco Cirelli, Nicolao Fornengo, and Alessandro Strumia. "Minimal dark matter". In: *Nucl. Phys. B* 753 (2006), pp. 178–194. DOI: 10.1016/j.nuclphysb.2006.07.012. arXiv: hep-ph/0512090.

[212] Steven Weinberg. "Must cosmological perturbations remain non-adiabatic after multi-field inflation?" In: *Phys. Rev. D* 70 (2004), p. 083522. DOI: 10.1103/PhysRevD.70.083522. arXiv: astro-ph/0405397.

[213] Lawrence J. Hall et al. "Freeze-In Production of FIMP Dark Matter". In: *JHEP* 03 (2010), p. 080. DOI: 10.1007/JHEP03(2010)080. arXiv: 0911.1120 [hep-ph].

[214] Kimberly K. Boddy et al. "Minimal dark matter freeze-in with low reheating temperatures and implications for direct detection". In: *Phys. Rev. D* 111.6 (2025), p. 063537. DOI: 10.1103/PhysRevD.111.063537. arXiv: 2405.06226 [hep-ph].

[215] Scott Dodelson and Lawrence M. Widrow. "Sterile-neutrinos as dark matter". In: *Phys. Rev. Lett.* 72 (1994), pp. 17–20. DOI: 10.1103/PhysRevLett.72.17. arXiv: hep-ph/9303287.

[216] Naoya Kitajima and Kazunori Nakayama. "Dark photon dark matter from cosmic strings and gravitational wave background". In: *JHEP* 08 (2023), p. 068. DOI: 10.1007/JHEP08(2023)068. arXiv: 2212.13573 [hep-ph].

[217] Takashi Hiramatsu et al. "Production of dark matter axions from collapse of string-wall systems". In: *Phys. Rev. D* 85 (2012). [Erratum: Phys.Rev.D 86, 089902 (2012)], p. 105020. DOI: 10.1103/PhysRevD.85.105020. arXiv: 1202.5851 [hep-ph].

[218] Olivier Wantz and E. P. S. Shellard. "Axion Cosmology Revisited". In: *Phys. Rev. D* 82 (2010), p. 123508. DOI: 10.1103/PhysRevD.82.123508. arXiv: 0910.1066 [astro-ph.CO].

[219] Joshua N. Benabou et al. "Axion Mass Prediction from Adaptive Mesh Refinement Cosmological Lattice Simulations". In: *Phys. Rev. Lett.* 134.24 (2025), p. 241003. DOI: 10.1103/6v21-d6sj. arXiv: 2412.08699 [hep-ph].

[220] Djuna Croon and David J. Weir. "Gravitational Waves from Phase Transitions". In: *Contemp. Phys.* 65 (2024), p. 75. DOI: 10.1080/00107514.2024.2423496. arXiv: 2410.21509 [hep-ph].

[221] Iason Baldes et al. "Ultrahigh-Energy Particle Collisions and Heavy Dark Matter at Phase Transitions". In: *Phys. Rev. Lett.* 134.6 (2025), p. 061001. DOI: 10.1103/PhysRevLett.134.061001. arXiv: 2306.15555 [hep-ph].

[222] Miguel Vanvlasselaer. "Populating dark sectors with relativistic bubble walls". In: Dec. 2024. arXiv: 2412.05653 [hep-ph].

[223] Martina Cataldi, Kristjan Müürsepp, and Miguel Vanvlasselaer. "When bubbles collide". In: (June 2025). arXiv: 2506.12123 [hep-ph].

[224] Howard Baer et al. "Dark matter production in the early Universe: beyond the thermal WIMP paradigm". In: *Phys. Rept.* 555 (2015), pp. 1–60. DOI: 10.1016/j.physrep.2014.10.002. arXiv: 1407.0017 [hep-ph].

[225] Edward W. Kolb and Michael S. Turner. *The Early Universe*. Vol. 69. Taylor and Francis, May 2019. ISBN: 978-0-429-49286-0, 978-0-201-62674-2. DOI: 10.1201/9780429492860.

[226] Martin J. Klein. "Principle of Detailed Balance". In: *Phys. Rev.* 97 (6 Mar. 1955), pp. 1446–1447. DOI: 10.1103/PhysRev.97.1446. URL: https://link.aps.org/doi/10.1103/PhysRev.97.1446.

[227] Hilary Greaves and Teruji Thomas. "On the CPT theorem". In: *Stud. Hist. Phil. Sci. B* 45 (2014), pp. 46–65. DOI: 10.1016/j.shpsb.2013.10.001. arXiv: 1204.4674 [math-ph].

[228] Ken'ichi Saikawa and Satoshi Shirai. "Precise WIMP Dark Matter Abundance and Standard Model Thermodynamics". In: *JCAP* 08 (2020), p. 011. DOI: 10.1088/1475-7516/2020/08/011. arXiv: 2005.03544 [hep-ph].

[229] Benjamin V. Lehmann et al. "Direct detection of primordial black hole relics as dark matter". In: *JCAP* 10 (2019), p. 046. DOI: 10.1088/1475-7516/2019/10/046. arXiv: 1906.06348 [hep-ph].

[230] *Fundamental Physics at the Intensity Frontier*. May 2012. DOI: 10.2172/1042577. arXiv: 1205.2671 [hep-ex].

[231] G. Krnjaic et al. "A Snowmass Whitepaper: Dark Matter Production at Intensity-Frontier Experiments". In: (July 2022). arXiv: 2207.00597 [hep-ph].

[232] P. Sikivie. "Experimental Tests of the Invisible Axion". In: *Phys. Rev. Lett.* 51 (1983). Ed. by M. A. Srednicki. [Erratum: Phys.Rev.Lett. 52, 695 (1984)], pp. 1415–1417. DOI: 10.1103/PhysRevLett.51.1415.

[233] Hojin Yoon et al. "Axion haloscope using an 18 T high temperature superconducting magnet". In: *Phys. Rev. D* 106.9 (2022), p. 092007. DOI: 10.1103/PhysRevD.106.092007. arXiv: 2206.12271 [hep-ex].

[234] Derek F. Jackson Kimball and Karl van Bibber, eds. *The Search for Ultralight Bosonic Dark Matter*. Springer, 2023. ISBN: 978-3-030-95851-0, 978-3-030-95854-1, 978-3-030-95852-7. DOI: 10.1007/978-3-030-95852-7.

[235] Jennifer M. Gaskins. "A review of indirect searches for particle dark matter". In: *Contemp. Phys.* 57.4 (2016), pp. 496–525. DOI: 10.1080/00107514.2016.1175160. arXiv: 1604.00014 [astro-ph.HE].

[236] Nicole F. Bell et al. "Thermalization and annihilation of dark matter in neutron stars". In: *JCAP* 04 (2024), p. 006. DOI: 10.1088/1475-7516/2024/04/006. arXiv: 2312.11892 [hep-ph].

[237] Mariangela Lisanti. "Lectures on Dark Matter Physics". In: *Theoretical Advanced Study Institute in Elementary Particle Physics: New Frontiers in Fields and Strings*. 2017, pp. 399–446. DOI: 10.1142/9789813149441_0007. arXiv: 1603.03797 [hep-ph].

[238] Torsten Bringmann and Christoph Weniger. "Gamma Ray Signals from Dark Matter: Concepts, Status and Prospects". In: *Phys. Dark Univ.* 1 (2012), pp. 194–217. DOI: 10.1016/j.dark.2012.10.005. arXiv: 1208.5481 [hep-ph].

[239] Stefano Profumo. "Astrophysical Probes of Dark Matter". In: *Theoretical Advanced Study Institute in Elementary Particle Physics: Searching for New Physics at Small and Large Scales*. 2013, pp. 143–189. DOI: 10.1142/9789814525220_0004. arXiv: 1301.0952 [hep-ph].

[240] Dylan Folsom et al. "Dark Matter Velocity Distributions for Direct Detection: Astrophysical Uncertainties are Smaller Than They Appear". In: (May 2025). arXiv: 2505.07924 [hep-ph].

[241] Torsten Bringmann and Maxim Pospelov. "Novel direct detection constraints on light dark matter". In: *Phys. Rev. Lett.* 122.17 (2019), p. 171801. DOI: 10.1103/PhysRevLett.122.171801. arXiv: 1810.10543 [hep-ph].

[242] Gurtina Besla, Annika Peter, and Nicolas Garavito-Camargo. "The highest-speed local dark matter particles come from the Large Magellanic Cloud". In: *JCAP* 11 (2019), p. 013. DOI: 10.1088/1475-7516/2019/11/013. arXiv: 1909.04140 [astro-ph.GA].

[243] Martin C. Smith et al. "The RAVE Survey: Constraining the Local Galactic Escape Speed". In: *Mon. Not. Roy. Astron. Soc.* 379 (2007), pp. 755–772. DOI: 10.1111/j.1365-2966.2007.11964.x. arXiv: astro-ph/0611671.

[244] Jonah Herzog-Arbeitman et al. "Empirical Determination of Dark Matter Velocities using Metal-Poor Stars". In: *Phys. Rev. Lett.* 120.4 (2018), p. 041102. DOI: 10.1103/PhysRevLett.120.041102. arXiv: 1704.04499 [astro-ph.GA].

[245] Elisabetta Baracchini. "Directional dark matter searches". In: *SciPost Phys. Proc.* 12 (2023), p. 002. DOI: 10.21468/SciPostPhysProc.12.002.

[246] Jocelyn Monroe and Peter Fisher. "Neutrino Backgrounds to Dark Matter Searches". In: *Phys. Rev. D* 76 (2007), p. 033007. DOI: 10.1103/PhysRevD.76.033007. arXiv: 0706.3019 [astro-ph].

[247] J. Billard, L. Strigari, and E. Figueroa-Feliciano. "Implication of neutrino backgrounds on the reach of next generation dark matter direct detection experiments". In: *Phys. Rev. D* 89.2 (2014), p. 023524. DOI: 10.1103/PhysRevD.89.023524. arXiv: 1307.5458 [hep-ph].

[248] F. Ruppin et al. "Complementarity of dark matter detectors in light of the neutrino background". In: *Phys. Rev. D* 90.8 (2014), p. 083510. DOI: 10.1103/PhysRevD.90.083510. arXiv: 1408.3581 [hep-ph].

[249] Ciaran A. J. O'Hare. "New Definition of the Neutrino Floor for Direct Dark Matter Searches". In: *Phys. Rev. Lett.* 127.25 (2021), p. 251802. DOI: 10.1103/PhysRevLett.127.251802. arXiv: 2109.03116 [hep-ph].

[250] Roni Harnik, Joachim Kopp, and Pedro A. N. Machado. "Exploring nu Signals in Dark Matter Detectors". In: *JCAP* 07 (2012), p. 026. DOI: 10.1088/1475-7516/2012/07/026. arXiv: 1202.6073 [hep-ph].

[251] Valentina De Romeri, Dimitrios K. Papoulias, and Christoph A. Ternes. "Bounds on new neutrino interactions from the first CEνNS data at direct detection experiments". In: *JCAP* 05 (2025), p. 012. DOI: 10.1088/1475-7516/2025/05/012. arXiv: 2411.11749 [hep-ph].

[252] Pablo Blanco-Mas et al. "Clarity through the neutrino fog: constraining new forces in dark matter detectors". In: *JHEP* 08 (2025), p. 043. DOI: 10.1007/JHEP08(2025)043. arXiv: 2411.14206 [hep-ph].

[253] Gonzalo Herrera. "Probing New Physics from Neutrinos at Dark Matter Direct Detection Experiments". In: *25th International Workshop on Neutrinos from Accelerators*. Jan. 2025. arXiv: 2501.10867 [hep-ph].

[254] Zihao Bo et al. "First Indication of Solar B8 Neutrinos through Coherent Elastic Neutrino-Nucleus Scattering in PandaX-4T". In: *Phys. Rev. Lett.* 133.19 (2024), p. 191001. DOI: 10.1103/PhysRevLett.133.191001. arXiv: 2407.10892 [hep-ex].

[255] Elena Aprile et al. "First Indication of Solar B8 Neutrinos via Coherent Elastic Neutrino-Nucleus Scattering with XENONnT". In: *Phys. Rev. Lett.* 133.19 (2024), p. 191002. DOI: 10.1103/PhysRevLett.133.191002. arXiv: 2408.02877 [nucl-ex].

[256] A. Liam Fitzpatrick et al. "The Effective Field Theory of Dark Matter Direct Detection". In: *JCAP* 02 (2013), p. 004. DOI: 10.1088/1475-7516/2013/02/004. arXiv: 1203.3542 [hep-ph].

[257] Tanner D. Trickle. "Direct Detection of Light Dark Matter with Electrons, Phonons, and Magnons". PhD thesis. Caltech, 2022. DOI: 10.7907/n4j3-1b24.

[258] Tanner Trickle, Zhengkang Zhang, and Kathryn M. Zurek. "Effective field theory of dark matter direct detection with collective excitations". In: *Phys. Rev. D* 105.1 (2022), p. 015001. DOI: 10.1103/PhysRevD.105.015001. arXiv: 2009.13534 [hep-ph].

[259] Riccardo Catena and Nicola A. Spaldin. "Linear response theory for light dark matter-electron scattering in materials". In: *Phys. Rev. Res.* 6.3 (2024), p. 033230. DOI: 10.1103/PhysRevResearch.6.033230. arXiv: 2402.06817 [hep-ph].

[260] Fady Bishara et al. "DirectDM: a tool for dark matter direct detection". In: (Aug. 2017). arXiv: 1708.02678 [hep-ph].

[261] Timon Emken et al. "Direct Detection of Strongly Interacting Sub-GeV Dark Matter via Electron Recoils". In: *JCAP* 09 (2019), p. 070. DOI: 10.1088/1475-7516/2019/09/070. arXiv: 1905.06348 [hep-ph].

[262] Eugenio Del Nobile, Marco Nardecchia, and Paolo Panci. "Millicharge or Decay: A Critical Take on Minimal Dark Matter". In: *JCAP* 04 (2016), p. 048. DOI: 10.1088/1475-7516/2016/04/048. arXiv: 1512.05353 [hep-ph].

[263] N. Fornengo, P. Panci, and M. Regis. "Long-Range Forces in Direct Dark Matter Searches". In: *Phys. Rev. D* 84 (2011), p. 115002. DOI: 10.1103/PhysRevD.84.115002. arXiv: 1108.4661 [hep-ph].

[264] Richard H. Helm. "Inelastic and Elastic Scattering of 187-Mev Electrons from Selected Even-Even Nuclei". In: *Phys. Rev.* 104 (1956), pp. 1466–1475. DOI: 10.1103/PhysRev.104.1466.

[265] Gordan Krnjaic. "Testing Thermal-Relic Dark Matter with a Dark Photon Mediator". In: (May 2025). arXiv: 2505.04626 [hep-ph].

[266] Zuowei Liu et al. "A combined analysis of PandaX, LUX, and XENON1T experiments within the framework of dark matter effective theory". In: *JHEP* 11 (2017), p. 024. DOI: 10.1007/JHEP11(2017)024. arXiv: 1708.04630 [hep-ph].

[267] J. Aalbers et al. "Dark Matter Search Results from 4.2 Tonne-Years of Exposure of the LUX-ZEPLIN (LZ) Experiment". In: (Oct. 2024). arXiv: 2410.17036 [hep-ex].

[268] E. Aprile et al. "Constraining the spin-dependent WIMP-nucleon cross sections with XENON1T". In: *Phys. Rev. Lett.* 122.14 (2019), p. 141301. DOI: 10.1103/PhysRevLett.122.141301. arXiv: 1902.03234 [astro-ph.CO].

[269] Marc Schumann. "Direct Detection of WIMP Dark Matter: Concepts and Status". In: *J. Phys. G* 46.10 (2019), p. 103003. DOI: 10.1088/1361-6471/ab2ea5. arXiv: 1903.03026 [astro-ph.CO].

[270] K. Aggarwal et al. "Probing Benchmark Models of Hidden-Sector Dark Matter with DAMIC-M". In: *Phys. Rev. Lett.* 135.7 (2025), p. 071002. DOI: 10.1103/2tcc-bqck. arXiv: 2503.14617 [hep-ex].

[271] Aram Hayrapetyan et al. "Search for long-lived particles using displaced vertices and missing transverse momentum in proton-proton collisions at s=13 TeV". In: *Phys. Rev. D* 109.11 (2024), p. 112005. DOI: 10.1103/PhysRevD.109.112005. arXiv: 2402.15804 [hep-ex].

[272] Emma Tolley. "Dark Matter searches with Mono-X signatures at the ATLAS experiment". In: *PoS* DIS2016 (2016), p. 107. DOI: 10.22323/1.265.0107.

[273] Yuri Gershtein et al. "Discovering hidden sectors with mono-photon Z'o searches". In: *Phys. Rev. D* 78 (2008), p. 095002. DOI: 10.1103/PhysRevD.78.095002. arXiv: 0809.2849 [hep-ph].

[274] Swasti Belwal, Manuel Drees, and Jong Soo Kim. "Analysis of the Bounds on Dark Matter Models from Monojet Searches at the LHC". In: *Phys. Rev. D* 98.5 (2018), p. 055017. DOI: 10.1103/PhysRevD.98.055017. arXiv: 1709.08545 [hep-ph].

[275] Francesca Acanfora et al. "Fusing photons into nothing, a new search for invisible ALPs and Dark Matter at Belle II". In: *JHEP* 11 (2024), p. 156. DOI: 10.1007/JHEP11(2024)156. arXiv: 2307.06369 [hep-ph].

[276] Kento Asai et al. "Sub-GeV dark matter search at ILC beam dumps". In: *JHEP* 02 (2024), p. 129. DOI: 10.1007/JHEP02(2024)129. arXiv: 2301.03816 [hep-ph].

[277] Kyrylo Bondarenko et al. "Towards the optimal beam dump experiment to search for feebly interacting particles". In: *Eur. Phys. J. C* 83.12 (2023), p. 1126. DOI: 10.1140/epjc/s10052-023-12249-5. arXiv: 2304.02511 [hep-ph].

[278] Gaia Lanfranchi, Maxim Pospelov, and Philip Schuster. "The Search for Feebly Interacting Particles". In: *Ann. Rev. Nucl. Part. Sci.* 71 (2021), pp. 279–313. DOI: 10.1146/annurev-nucl-102419-055056. arXiv: 2011.02157 [hep-ph].

[279] Patrick deNiverville, Maxim Pospelov, and Adam Ritz. "Observing a light dark matter beam with neutrino experiments". In: *Phys. Rev. D* 84 (2011), p. 075020. DOI: 10.1103/PhysRevD.84.075020. arXiv: 1107.4580 [hep-ph].

[280] Asher Berlin et al. "Dark Sectors at the Fermilab SeaQuest Experiment". In: *Phys. Rev. D* 98.3 (2018), p. 035011. DOI: 10.1103/PhysRevD.98.035011. arXiv: 1804.00661 [hep-ph].

[281] Oliver Buchmueller, Caterina Doglioni, and Lian Tao Wang. "Search for dark matter at colliders". In: *Nature Phys.* 13.3 (2017), pp. 217–223. DOI: 10.1038/nphys4054. arXiv: 1912.12739 [hep-ex].

[282] Gino Isidori, Felix Wilsch, and Daniel Wyler. "The standard model effective field theory at work". In: *Rev. Mod. Phys.* 96.1 (2024), p. 015006. DOI: 10.1103/RevModPhys.96.015006. arXiv: 2303.16922 [hep-ph].

[283] Adam Falkowski. "Lectures on SMEFT". In: *Eur. Phys. J. C* 83.7 (2023), p. 656. DOI: 10.1140/epjc/s10052-023-11821-3.

[284] Juan Carlos Criado et al. "A complete effective field theory for dark matter". In: *JHEP* 07 (2021), p. 081. DOI: 10.1007/JHEP07(2021)081. arXiv: 2104.14443 [hep-ph].

[285] Huayang Song, Hao Sun, and Jiang-Hao Yu. "Complete EFT operator bases for dark matter and weakly-interacting light particle". In: *JHEP* 05 (2024), p. 103. DOI: 10.1007/JHEP05(2024)103. arXiv: 2306.05999 [hep-ph].

[286] Jin-Han Liang et al. "Dark sector effective field theory". In: *JHEP* 12 (2023), p. 172. DOI: 10.1007/JHEP12(2023)172. arXiv: 2309.12166 [hep-ph].

[287] Sweta Baradia et al. "Search for Dark Matter in association with a Higgs boson at the LHC: A model independent study". In: (Sept. 2024). arXiv: 2409.17803 [hep-ph].

[288] Jason Aebischer, Andrzej J. Buras, and Jacky Kumar. "SMEFT ATLAS: The Landscape Beyond the Standard Model". In: (July 2025). arXiv: 2507.05926 [hep-ph].

[289] Howard Baer, Eun-Kyung Park, and Xerxes Tata. "Collider, direct and indirect detection of supersymmetric dark matter". In: *New J. Phys.* 11 (2009), p. 105024. DOI: 10.1088/1367-2630/11/10/105024. arXiv: 0903.0555 [hep-ph].

[290] Koji Terashi. "SUSY Dark Matter Searches at LHC and Future Colliders". In: (2019). URL: https://cds.cern.ch/record/2704684.

[291] Sophie Kadan. "Searches for Supersymmetry (SUSY) at the Large Hadron Collider". In: (Apr. 2024). arXiv: 2404.16922 [hep-ex].

[292] Giorgio Arcadi et al. "GUT Models at Current and Future Hadron Colliders and Implications to Dark Matter Searches". In: *Phys. Lett. B* 771 (2017), pp. 508–514. DOI: 10.1016/j.physletb.2017.05.023. arXiv: 1704.02328 [hep-ph].

[293] Djuna Croon et al. "GUT Physics in the era of the LHC". In: *Front. in Phys.* 7 (2019), p. 76. DOI: 10.3389/fphy.2019.00076. arXiv: 1903.04977 [hep-ph].

[294] Jalal Abdallah et al. "Simplified Models for Dark Matter Searches at the LHC". In: *Phys. Dark Univ.* 9-10 (2015), pp. 8–23. DOI: 10.1016/j.dark.2015.08.001. arXiv: 1506.03116 [hep-ph].

[295] Enrico Morgante. "Simplified Dark Matter Models". In: *Adv. High Energy Phys.* 2018 (2018), p. 5012043. DOI: 10.1155/2018/5012043. arXiv: 1804.01245 [hep-ph].

[296] Christopher Chang et al. "Global fits of simplified models for dark matter with GAMBIT: I. Scalar and fermionic models with s-channel vector mediators". In: *Eur. Phys. J. C* 83.3 (2023), p. 249. DOI: 10.1140/epjc/s10052-023-11399-w. arXiv: 2209.13266 [hep-ph].

[297] Christopher Chang et al. "Global fits of simplified models for dark matter with GAMBIT: II. Vector dark matter with an s-channel vector mediator". In: *Eur. Phys. J. C* 83.8 (2023). [Erratum: Eur.Phys.J.C 83, 768 (2023)], p. 692. DOI: 10.1140/epjc/s10052-023-11859-3. arXiv: 2303.08351 [hep-ph].

[298] Lipika Kolay and Soumitra Nandi. "Exploring constraints on Simplified Dark Matter model through flavour and electroweak observables". In: *JHEP* 10 (2024), p. 008. DOI: 10.1007/JHEP10(2024)008. arXiv: 2403.20303 [hep-ph].

[299] Oliver Fischer et al. "Unveiling hidden physics at the LHC". In: *Eur. Phys. J. C* 82.8 (2022), p. 665. DOI: 10.1140/epjc/s10052-022-10541-4. arXiv: 2109.06065 [hep-ph].

[300] Asli Abdullahi et al. "From oversimplified to overlooked: the case for exploring Rich Dark Sectors". In: May 2025. arXiv: 2505.05663 [hep-ph].

[301] Brian Batell et al. "Exploring Dark Sector Portals with High Intensity Experiments". In: *Snowmass 2021*. July 2022. arXiv: 2207.06905 [hep-ph].

[302] Meenakshi Narain et al. "The Future of US Particle Physics - The Snowmass 2021 Energy Frontier Report". In: (Nov. 2022). DOI: 10.2172/1908199. arXiv: 2211.11084 [hep-ex].

[303] M. Benedikt et al. "Future Circular Collider Feasibility Study Report: Volume 1, Physics, Experiments, Detectors". In: (Apr. 2025). DOI: 10.17181/CERN.9DKX.TDH9. arXiv: 2505.00272 [hep-ex].

[304] A. Augusto Alves Jr. et al. "The LHCb Detector at the LHC". In: *JINST* 3 (2008), S08005. DOI: 10.1088/1748-0221/3/08/S08005.

[305] S. Chatrchyan et al. "The CMS Experiment at the CERN LHC". In: *JINST* 3 (2008), S08004. DOI: 10.1088/1748-0221/3/08/S08004.

[306] G. Aad et al. "The ATLAS Experiment at the CERN Large Hadron Collider". In: *JINST* 3 (2008), S08003. DOI: 10.1088/1748-0221/3/08/S08003.

[307] Gianluca Lamanna. "The NA62 experiment at CERN". In: *J. Phys. Conf. Ser.* 335 (2011). Ed. by Antonio Di Domenico et al., p. 012071. DOI: 10.1088/1742-6596/335/1/012071.

[308] Benjamin Banto Oberhauser. "Status and prospects of the NA64 experiment". In: *PoS* DISCRETE2024 (2025), p. 015. DOI: 10.22323/1.481.0015.

[309] C. Ahdida et al. "The SHiP experiment at the proposed CERN SPS Beam Dump Facility". In: *Eur. Phys. J. C* 82.5 (2022), p. 486. DOI: 10.1140/epjc/s10052-022-10346-5. arXiv: 2112.01487 [physics.ins-det].

[310] David DeMille, John M. Doyle, and Alexander O. Sushkov. "Probing the frontiers of particle physics with tabletop-scale experiments". In: *Science* 357.6355 (2017), pp. 990–994. DOI: 10.1126/science.aal3003.

[311] Gudrun Heinrich. "Collider Physics at the Precision Frontier". In: *Phys. Rept.* 922 (2021), pp. 1–69. DOI: 10.1016/j.physrep.2021.03.006. arXiv: 2009.00516 [hep-ph].

[312] Joerg Jaeckel and Andreas Ringwald. "The Low-Energy Frontier of Particle Physics". In: *Ann. Rev. Nucl. Part. Sci.* 60 (2010), pp. 405–437. DOI: 10.1146/annurev.nucl.012809.104433. arXiv: 1002.0329 [hep-ph].

[313] Rouven Essig et al. "Working Group Report: New Light Weakly Coupled Particles". In: *Snowmass 2013: Snowmass on the Mississippi*. Oct. 2013. arXiv: 1311.0029 [hep-ph].

[314] Matthew J. Strassler and Kathryn M. Zurek. "Echoes of a hidden valley at hadron colliders". In: *Phys. Lett. B* 651 (2007), pp. 374–379. DOI: 10.1016/j.physletb.2007.06.055. arXiv: hep-ph/0604261.

[315] Cumrun Vafa. "Swamplandish Unification of the Dark Sector". In: (Feb. 2024). arXiv: 2402.00981 [hep-ph].

[316] Jim Alexander et al. "Dark Sectors 2016 Workshop: Community Report". In: Aug. 2016. arXiv: 1608.08632 [hep-ph].

[317] Martin Bauer, Patrick Foldenauer, and Joerg Jaeckel. "Hunting All the Hidden Photons". In: *JHEP* 07 (2018), p. 094. DOI: 10.1007/JHEP07(2018)094. arXiv: 1803.05466 [hep-ph].

[318] Yu-Dai Tsai et al. "Novel constraints on fifth forces and ultralight dark sector with asteroidal data". In: *JCAP* 04 (2023), p. 031. DOI: 10.1088/1475-7516/2023/04/031. arXiv: 2107.04038 [hep-ph].

[319] Philip Sørensen. *Long-range forces - A theory review*. Slides presented at the workshop entitled "The Low-Energy Frontier of Particle Physics". https://agenda.infn.it/event/44002/contributions/249469/attachments/131340/195771/long_range_force_theory_review.pdf. 2025.

[320] Sofiane M. Boucenna et al. "Non-abelian gauge extensions for B-decay anomalies". In: *Phys. Lett. B* 760 (2016), pp. 214–219. DOI: 10.1016/j.physletb.2016.06.067. arXiv: 1604.03088 [hep-ph].

[321] Qing-Hong Cao, Bin Yan, and Dong-Ming Zhang. "Simple non-Abelian extensions of the standard model gauge group and the diboson excesses at the LHC". In: *Phys. Rev. D* 92.9 (2015), p. 095025. DOI: 10.1103/PhysRevD.92.095025. arXiv: 1507.00268 [hep-ph].

[322] Prateek Agrawal et al. "Feebly-interacting particles: FIPs 2020 workshop report". In: *Eur. Phys. J. C* 81.11 (2021), p. 1015. DOI: 10.1140/epjc/s10052-021-09703-7. arXiv: 2102.12143 [hep-ph].

[323] W. Buchmuller and C. Ludeling. "Field Theory and Standard Model". In: *2005 European School of High-Energy Physics*. Sept. 2006. arXiv: hep-ph/0609174.

[324] Silvia Pascoli et al. "Rich Dark Sectors". Online accessed: 2024-04-16. 2025. URL: https://indico.cern.ch/event/1439855/contributions/6461646/.

[325] Martin Bauer et al. "The Low-Energy Effective Theory of Axions and ALPs". In: *JHEP* 04 (2021), p. 063. DOI: 10.1007/JHEP04(2021)063. arXiv: 2012.12272 [hep-ph].

[326] Laura Lopez-Honorez, Thomas Schwetz, and Jure Zupan. "Higgs portal, fermionic dark matter, and a Standard Model like Higgs at 125 GeV". In: *Phys. Lett. B* 716 (2012), pp. 179–185. DOI: 10.1016/j.physletb.2012.07.017. arXiv: 1203.2064 [hep-ph].

[327] Oleg Lebedev. "On Stability of the Electroweak Vacuum and the Higgs Portal". In: *Eur. Phys. J. C* 72 (2012), p. 2058. DOI: 10.1140/epjc/s10052-012-2058-2. arXiv: 1203.0156 [hep-ph].

[328] Kristjan Kannike. "Vacuum Stability of a General Scalar Potential of a Few Fields". In: *Eur. Phys. J. C* 76.6 (2016). [Erratum: Eur.Phys.J.C 78, 355 (2018)], p. 324. DOI: 10.1140/epjc/s10052-016-4160-3. arXiv: 1603.02680 [hep-ph].

[329] Soo-Min Choi, Yoo-Jin Kang, and Hyun Min Lee. "On thermal production of self-interacting dark matter". In: *JHEP* 12 (2016), p. 099. DOI: 10.1007/JHEP12(2016)099. arXiv: 1610.04748 [hep-ph].

[330] Michael Duerr et al. "How to save the WIMP: global analysis of a dark matter model with two s-channel mediators". In: *JHEP* 09 (2016), p. 042. DOI: 10.1007/JHEP09(2016)042. arXiv: 1606.07609 [hep-ph].

[331] Torben Ferber, Alexander Grohsjean, and Felix Kahlhoefer. "Dark Higgs bosons at colliders". In: *Prog. Part. Nucl. Phys.* 136 (2024), p. 104105. DOI: 10.1016/j.ppnp.2024.104105. arXiv: 2305.16169 [hep-ph].

[332] Bob Holdom. "Two U(1)'s and Epsilon Charge Shifts". In: *Phys. Lett. B* 166 (1986), pp. 196–198. DOI: 10.1016/0370-2693(86)91377-8.

[333] Henri Ruegg and Marti Ruiz-Altaba. "The Stueckelberg field". In: *Int. J. Mod. Phys. A* 19 (2004), pp. 3265–3348. DOI: 10.1142/S0217751X04019755. arXiv: hep-th/0304245.

[334] Jun-Xing Pan et al. "Scrutinizing a massless dark photon: basis independence". In: *Nucl. Phys. B* 953 (2020), p. 114968. DOI: 10.1016/j.nuclphysb.2020.114968. arXiv: 1807.11363 [hep-ph].

[335] Asher Berlin et al. "Millicharged relics reveal massless dark photons". In: *JHEP* 05 (2023), p. 046. DOI: 10.1007/JHEP05(2023)046. arXiv: 2211.05139 [hep-ph].

[336] Maria Archidiacono et al. "Unveiling dark fifth forces with linear cosmology". In: *JCAP* 10 (2022), p. 074. DOI: 10.1088/1475-7516/2022/10/074. arXiv: 2204.08484 [astro-ph.CO].

[337] Zachary Bogorad, Peter W. Graham, and Harikrishnan Ramani. "Constraints on long-ranged interactions between dark matter and the Standard Model". In: *JCAP* 04 (2025), p. 006. DOI: 10.1088/1475-7516/2025/04/006. arXiv: 2410.07324 [hep-ph].

[338] Haipeng An, Mark B. Wise, and Yue Zhang. "Effects of Bound States on Dark Matter Annihilation". In: *Phys. Rev. D* 93.11 (2016), p. 115020. DOI: 10.1103/PhysRevD.93.115020. arXiv: 1604.01776 [hep-ph].

[339] Pyungwon Ko, Toshinori Matsui, and Yi-Lei Tang. "Dark matter bound state formation in fermionic Z_2 DM model with light dark photon and dark Higgs boson". In: *JHEP* 10 (2020), p. 082. DOI: 10.1007/JHEP10(2020)082. arXiv: 1910.04311 [hep-ph].

[340] Tsung-Han Yeh et al. "Probing physics beyond the standard model: limits from BBN and the CMB independently and combined". In: *JCAP* 10 (2022), p. 046. DOI: 10.1088/1475-7516/2022/10/046. arXiv: 2207.13133 [astro-ph.CO].

[341] K. S. Babu, Christopher F. Kolda, and John March-Russell. "Implications of generalized Z - Z-prime mixing". In: *Phys. Rev. D* 57 (1998), pp. 6788–6792. DOI: 10.1103/PhysRevD.57.6788. arXiv: hep-ph/9710441.

[342] Eung Jin Chun, Jong-Chul Park, and Stefano Scopel. "Dark matter and a new gauge boson through kinetic mixing". In: *JHEP* 02 (2011), p. 100. DOI: 10.1007/JHEP02(2011)100. arXiv: 1011.3300 [hep-ph].

[343] Marco Fabbrichesi, Emidio Gabrielli, and Gaia Lanfranchi. "The Dark Photon". In: (May 2020). DOI: 10.1007/978-3-030-62519-1. arXiv: 2005.01515 [hep-ph].

[344] Yu. M. Andreev et al. "Search for Light Dark Matter with NA64 at CERN". In: *Phys. Rev. Lett.* 131.16 (2023), p. 161801. DOI: 10.1103/PhysRevLett.131.161801. arXiv: 2307.02404 [hep-ex].

[345] Enrique Fernández-Martínez et al. "Effective portals to heavy neutral leptons". In: *JHEP* 09 (2023), p. 001. DOI: 10.1007/JHEP09(2023)001. arXiv: 2304.06772 [hep-ph].

[346] Walter Grimus. "Neutrino Physics - Models for Neutrino Masses and Lepton Mixing". In: *PoS P* 2GC (2006). Ed. by Loriano Bonora et al., p. 001. DOI: 10.22323/1.034.0001. arXiv: hep-ph/0612311.

[347] Sofiane M. Boucenna, Stefano Morisi, and José W. F. Valle. "The low-scale approach to neutrino masses". In: *Adv. High Energy Phys.* 2014 (2014), p. 831598. DOI: 10.1155/2014/831598. arXiv: 1404.3751 [hep-ph].

[348] Marco Chianese et al. "Investigating two heavy neutral leptons neutrino seesaw mechanism at SHiP". In: *Int. J. Mod. Phys. A* 34.08 (2019), p. 1950047. DOI: 10.1142/S0217751X19500477. arXiv: 1812.01994 [hep-ph].

[349] Basudeb Dasgupta and Joachim Kopp. "Sterile Neutrinos". In: *Phys. Rept.* 928 (2021), pp. 1–63. DOI: 10.1016/j.physrep.2021.06.002. arXiv: 2106.05913 [hep-ph].

[350] Tracy R. Slatyer. "Indirect dark matter signatures in the cosmic dark ages. I. Generalizing the bound on s-wave dark matter annihilation from Planck results". In: *Phys. Rev. D* 93.2 (2016), p. 023527. DOI: 10.1103/PhysRevD.93.023527. arXiv: 1506.03811 [hep-ph].

[351] Giorgio Arcadi et al. "The waning of the WIMP? A review of models, searches, and constraints". In: *Eur. Phys. J. C* 78.3 (2018), p. 203. DOI: 10.1140/epjc/s10052-018-5662-y. arXiv: 1703.07364 [hep-ph].

[352] Tongyan Lin, Hai-Bo Yu, and Kathryn M. Zurek. "On Symmetric and Asymmetric Light Dark Matter". In: *Phys. Rev. D* 85 (2012), p. 063503. DOI: 10.1103/PhysRevD.85.063503. arXiv: 1111.0293 [hep-ph].

[353] Sean Tulin, Hai-Bo Yu, and Kathryn M. Zurek. "Three Exceptions for Thermal Dark Matter with Enhanced Annihilation to $\gamma\gamma$". In: *Phys. Rev. D* 87.3 (2013), p. 036011. DOI: 10.1103/PhysRevD.87.036011. arXiv: 1208.0009 [hep-ph].

[354] Raffaele Tito D'Agnolo et al. "Exponentially Light Dark Matter from Coannihilation". In: *JHEP* 08 (2018), p. 079. DOI: 10.1007/JHEP08(2018)079. arXiv: 1803.02901 [hep-ph].

[355] Sowmiya Balan et al. "Resonant or asymmetric: the status of sub-GeV dark matter". In: *JCAP* 01 (2025), p. 053. DOI: 10.1088/1475-7516/2025/01/053. arXiv: 2405.17548 [hep-ph].

[356] Céline Boehm et al. "Extended gamma-ray emission from Coy Dark Matter". In: *JCAP* 05 (2014), p. 009. DOI: 10.1088/1475-7516/2014/05/009. arXiv: 1401.6458 [hep-ph].

[357] Karim Ghorbani. "Fermionic dark matter with pseudo-scalar Yukawa interaction". In: *JCAP* 01 (2015), p. 015. DOI: 10.1088/1475-7516/2015/01/015. arXiv: 1408.4929 [hep-ph].

[358] D. S. Akerib et al. "Snowmass2021 Cosmic Frontier Dark Matter Direct Detection to the Neutrino Fog". In: *Snowmass 2021*. Mar. 2022. arXiv: 2203.08084 [hep-ex].

[359] Kim Griest and Marc Kamionkowski. "Unitarity Limits on the Mass and Radius of Dark Matter Particles". In: *Phys. Rev. Lett.* 64 (1990), p. 615. DOI: 10.1103/PhysRevLett.64.615.

[360] Fabrizio Nesti and Paolo Salucci. "The Dark Matter halo of the Milky Way, AD 2013". In: *JCAP* 07 (2013), p. 016. DOI: 10.1088/1475-7516/2013/07/016. arXiv: 1304.5127 [astro-ph.GA].

[361] Amand Faessler et al. "Search for the Cosmic Neutrino Background and KATRIN". In: *Rom. J. Phys.* 58.9-10 (2013). Ed. by L. Bravina, Y. Foka, and S. Kabana, pp. 1221–1231. arXiv: 1304.5632 [nucl-th].

[362] C. Boehm and Pierre Fayet. "Scalar dark matter candidates". In: *Nucl. Phys. B* 683 (2004), pp. 219–263. DOI: 10.1016/j.nuclphysb.2004.01.015. arXiv: hep-ph/0305261.

[363] Elias Bernreuther, Saniya Heeba, and Felix Kahlhoefer. "Resonant sub-GeV Dirac dark matter". In: *JCAP* 03 (2021), p. 040. DOI: 10.1088/1475-7516/2021/03/040. arXiv: 2010.14522 [hep-ph].

[364] C. B. Jackson et al. "Gamma-ray lines and One-Loop Continuum from s-channel Dark Matter Annihilations". In: *JCAP* 07 (2013), p. 021. DOI: 10.1088/1475-7516/2013/07/021. arXiv: 1302.1802 [hep-ph].

[365] C. B. Jackson et al. "Gamma Rays from Top-Mediated Dark Matter Annihilations". In: *JCAP* 07 (2013), p. 006. DOI: 10.1088/1475-7516/2013/07/006. arXiv: 1303.4717 [hep-ph].

[366] Kwei-Chou Yang. "Freeze-out forbidden dark matter in the hidden sector in the mass range from sub-GeV to TeV". In: *JHEP* 11 (2022), p. 083. DOI: 10.1007/JHEP11(2022)083. arXiv: 2209.10827 [hep-ph].

[367] Asher Berlin, Dan Hooper, and Samuel D. McDermott. "Simplified Dark Matter Models for the Galactic Center Gamma-Ray Excess". In: *Phys. Rev. D* 89.11 (2014), p. 115022. DOI: 10.1103/PhysRevD.89.115022. arXiv: 1404.0022 [hep-ph].

[368] Michael L. Graesser, Ian M. Shoemaker, and Luca Vecchi. "Asymmetric WIMP dark matter". In: *JHEP* 10 (2011), p. 110. DOI: 10.1007/JHEP10(2011)110. arXiv: 1103.2771 [hep-ph].

[369] David E. Kaplan, Markus A. Luty, and Kathryn M. Zurek. "Asymmetric Dark Matter". In: *Phys. Rev. D* 79 (2009), p. 115016. DOI: 10.1103/PhysRevD.79.115016. arXiv: 0901.4117 [hep-ph].

[370] Csaba Balazs. "Baryogenesis: A small review of the big picture". In: (Nov. 2014). arXiv: 1411.3398 [hep-ph].

[371] Dietrich Bodeker and Wilfried Buchmuller. "Baryogenesis from the weak scale to the grand unification scale". In: *Rev. Mod. Phys.* 93.3 (2021), p. 035004. DOI: 10.1103/RevModPhys.93.035004. arXiv: 2009.07294 [hep-ph].

[372] Timothy Cohen et al. "Asymmetric Dark Matter from a GeV Hidden Sector". In: *Phys. Rev. D* 82 (2010), p. 056001. DOI: 10.1103/PhysRevD.82.056001. arXiv: 1005.1655 [hep-ph].

[373] Juan Herrero-Garcia, Giacomo Landini, and Drona Vatsyayan. "Asymmetries in extended dark sectors: a cogenesis scenario". In: *JHEP* 05 (2023), p. 049. DOI: 10.1007/JHEP05(2023)049. arXiv: 2301.13238 [hep-ph].

[374] Kathryn M. Zurek. "Asymmetric Dark Matter: Theories, Signatures, and Constraints". In: *Phys. Rept.* 537 (2014), pp. 91–121. DOI: 10.1016/j.physrep.2013.12.001. arXiv: 1308.0338 [hep-ph].

[375] Gael Alguero et al. "Co-scattering in micrOMEGAs: A case study for the singlet-triplet dark matter model". In: *SciPost Phys.* 13 (2022), p. 124. DOI: 10.21468/SciPostPhys.13.6.124. arXiv: 2207.10536 [hep-ph].

[376] Marco Battaglieri et al. "US Cosmic Visions: New Ideas in Dark Matter 2017: Community Report". In: *U.S. Cosmic Visions: New Ideas in Dark Matter*. July 2017. arXiv: 1707.04591 [hep-ph].

[377] M. Battaglieri et al. "Dark matter search in a Beam-Dump eXperiment (BDX) at Jefferson Lab: an update on PR12-16-001". In: (Dec. 2017). arXiv: 1712.01518 [physics.ins-det].

[378] L. Marsicano et al. "Novel Way to Search for Light Dark Matter in Lepton Beam-Dump Experiments". In: *Phys. Rev. Lett.* 121.4 (2018), p. 041802. DOI: 10.1103/PhysRevLett.121.041802. arXiv: 1807.05884 [hep-ex].

[379] Bhaskar Dutta, Wei-Chih Huang, and Jayden L. Newstead. "Probing the Dark Sector with Nuclear Transition Photons". In: *Phys. Rev. Lett.* 131.11 (2023), p. 111801. DOI: 10.1103/PhysRevLett.131.111801. arXiv: 2302.10250 [hep-ph].

[380] Michael De Nuccio. "Searches for light dark sectors at Belle II, Belle, and BaBar". In: *PoS* DISCRETE2022 (2024), p. 008. DOI: 10.22323/1.431.0008.

[381] Yu. M. Andreev et al. "Searching for Light Dark Matter and Dark Sectors with the NA64 experiment at the CERN SPS". In: (May 2025). arXiv: 2505.14291 [hep-ex].

[382] Tanmay Kumar Poddar. "Probing light dark matter particles with astrophysical experiments". In: *PoS* EPS-HEP2021 (2022), p. 057. DOI: 10.22323/1.398.0057. arXiv: 2110.03365 [hep-ph].

[383] Kimberly K. Boddy et al. "Snowmass2021 theory frontier white paper: Astrophysical and cosmological probes of dark matter". In: *JHEAp* 35 (2022), pp. 112–138. DOI: 10.1016/j.jheap.2022.06.005. arXiv: 2203.06380 [hep-ph].

[384] C. J. Horowitz and Gang Li. "The Mu and tau number of supernovae". In: *Phys. Lett. B* 443 (1998), pp. 58–62. DOI: 10.1016/S0370-2693(98)01293-3. arXiv: hep-ph/9809492.

[385] Tsurugi Takata et al. "Progenitor dependence of neutrino-driven supernova explosions with the aid of heavy axionlike particles". In: *Phys. Rev. D* 111.10 (2025), p. 103028. DOI: 10.1103/PhysRevD.111.103028. arXiv: 2503.09005 [astro-ph.HE].

[386] Michael S. Turner, KICP/UChicago, and The Kavli Foundation. "Understanding BBN: the physics and its history". In: (Nov. 2021). arXiv: 2111.14254 [astro-ph.CO].

[387] Paul Frederik Depta et al. "BBN constraints on the annihilation of MeV-scale dark matter". In: *JCAP* 04 (2019), p. 029. DOI: 10.1088/1475-7516/2019/04/029. arXiv: 1901.06944 [hep-ph].

[388] Nashwan Sabti et al. "Refined Bounds on MeV-scale Thermal Dark Sectors from BBN and the CMB". In: *JCAP* 01 (2020), p. 004. DOI: 10.1088/1475-7516/2020/01/004. arXiv: 1910.01649 [hep-ph].

[389] Asher Berlin and Nikita Blinov. "Thermal neutrino portal to sub-MeV dark matter". In: *Phys. Rev. D* 99.9 (2019), p. 095030. DOI: 10.1103/PhysRevD.99.095030. arXiv: 1807.04282 [hep-ph].

[390] Asher Berlin, Nikita Blinov, and Shirley Weishi Li. "Dark Sector Equilibration During Nucleosynthesis". In: *Phys. Rev. D* 100.1 (2019), p. 015038. DOI: 10.1103/PhysRevD.100.015038. arXiv: 1904.04256 [hep-ph].

[391] Benjamin W. Lee and Steven Weinberg. "Cosmological Lower Bound on Heavy Neutrino Masses". In: *Phys. Rev. Lett.* 39 (1977). Ed. by M. A. Srednicki, pp. 165–168. DOI: 10.1103/PhysRevLett.39.165.

[392] Carlos A. Argüelles et al. "Dark matter annihilation to neutrinos". In: *Rev. Mod. Phys.* 93.3 (2021), p. 035007. DOI: 10.1103/RevModPhys.93.035007. arXiv: 1912.09486 [hep-ph].

[393] Murat Abdughani et al. "Neutrinophilic Super-Resonant Dark Matter". In: (May 2025). arXiv: 2505.14491 [hep-ph].

[394] Jared A. Evans, Stefania Gori, and Jessie Shelton. "Looking for the WIMP Next Door". In: *JHEP* 02 (2018), p. 100. DOI: 10.1007/JHEP02(2018)100. arXiv: 1712.03974 [hep-ph].

[395] Xin-Chen Duan, Raymundo Ramos, and Yue-Lin Sming Tsai. "Relic density and temperature evolution of a light dark sector". In: *Phys. Rev. D* 110.6 (2024), p. 063535. DOI: 10.1103/PhysRevD.110.063535. arXiv: 2404.12019 [hep-ph].

[396] Kwei-Chou Yang. "Thermodynamic Evolution of Secluded Vector Dark Matter: Conventional WIMPs and Nonconventional WIMPs". In: *JHEP* 11 (2019), p. 048. DOI: 10.1007/JHEP11(2019)048. arXiv: 1905.09582 [hep-ph].

[397] M. Blennow et al. "Neutrino Portals to Dark Matter". In: *Eur. Phys. J. C* 79.7 (2019), p. 555. DOI: 10.1140/epjc/s10052-019-7060-5. arXiv: 1903.00006 [hep-ph].

[398] Lawrence J. Hall, Takeo Moroi, and Hitoshi Murayama. "Sneutrino cold dark matter with lepton number violation". In: *Phys. Lett. B* 424 (1998), pp. 305–312. DOI: 10.1016/S0370-2693(98)00196-8. arXiv: hep-ph/9712515.

[399] David Tucker-Smith and Neal Weiner. "The Status of inelastic dark matter". In: *Phys. Rev. D* 72 (2005), p. 063509. DOI: 10.1103/PhysRevD.72.063509. arXiv: hep-ph/0402065.

[400] Rouven Essig. "Direct Detection of Non-Chiral Dark Matter". In: *Phys. Rev. D* 78 (2008), p. 015004. DOI: 10.1103/PhysRevD.78.015004. arXiv: 0710.1668 [hep-ph].

[401] Nima Arkani-Hamed and Neal Weiner. "LHC Signals for a SuperUnified Theory of Dark Matter". In: *JHEP* 12 (2008), p. 104. DOI: 10.1088/1126-6708/2008/12/104. arXiv: 0810.0714 [hep-ph].

[402] Clifford Cheung et al. "Kinetic Mixing as the Origin of Light Dark Scales". In: *Phys. Rev. D* 80 (2009), p. 035008. DOI: 10.1103/PhysRevD.80.035008. arXiv: 0902.3246 [hep-ph].

[403] Rebecca Krall and Matthew Reece. "Last Electroweak WIMP Standing: Pseudo-Dirac Higgsino Status and Compact Stars as Future Probes". In: *Chin. Phys. C* 42.4 (2018), p. 043105. DOI: 10.1088/1674-1137/42/4/043105. arXiv: 1705.04843 [hep-ph].

[404] Prudhvi N. Bhattiprolu, Evan Petrosky, and Aaron Pierce. "Singlet-doublet dark matter revisited". In: (May 2025). arXiv: 2505.11607 [hep-ph].

[405] Rahool Kumar Barman et al. "Current status of the light neutralino thermal dark matter in the phenomenological MSSM". In: *Phys. Rev. D* 111.1 (2025), p. 015014. DOI: 10.1103/PhysRevD.111.015014. arXiv: 2402.07991 [hep-ph].

[406] B. Rebel, M. C. Sanchez, and S. Wolbers. "Working Group Report: Computing for the Intensity Frontier". In: *Snowmass 2013: Snowmass on the Mississippi*. Oct. 2013. arXiv: 1310.6964 [hep-ex].

[407] J. L. Hewett et al. "Planning the Future of U.S. Particle Physics (Snowmass 2013): Chapter 2: Intensity Frontier". In: *Snowmass 2013: Snowmass on the Mississippi*. Jan. 2014. arXiv: 1401.6077 [hep-ex].

[408] J. Beacham et al. "Physics Beyond Colliders at CERN: Beyond the Standard Model Working Group Report". In: *J. Phys. G* 47.1 (2020), p. 010501. DOI: 10.1088/1361-6471/ab4cd2. arXiv: 1901.09966 [hep-ex].

[409] Richard Keith Ellis et al. "Physics Briefing Book: Input for the European Strategy for Particle Physics Update 2020". In: (Oct. 2019). arXiv: 1910.11775 [hep-ex].

[410] Sergey Alekhin et al. "A facility to Search for Hidden Particles at the CERN SPS: the SHiP physics case". In: *Rept. Prog. Phys.* 79.12 (2016), p. 124201. DOI: 10.1088/0034-4885/79/12/124201. arXiv: 1504.04855 [hep-ph].

[411] JENNIFER2. *Japan and Europe Network for Neutrino and Intensity Frontier Experimental Research*. http://www.jennifer2-project.eu/. Accessed: 2025-05-23. 2019.

[412] Mikhail Shaposhnikov. *ESPP and intensity frontier of particle physics*. Slide presentation. Accessed: 2025-05-23. 2020. URL: https://indico.global/event/9770/contributions/92916/attachments/42535/80065/ESPP_Intensity.pdf.

[413] R Bernabei et al. "Searching for WIMPs by the annual modulation signature". In: *Phys. Lett. B* 424 (1998), pp. 195–201. DOI: 10.1016/S0370-2693(98)00172-5.

[414] R. Bernabei et al. "Search for WIMP annual modulation signature: Results from DAMA / NaI-3 and DAMA / NaI-4 and the global combined analysis". In: *Phys. Lett. B* 480 (2000), pp. 23–31. DOI: 10.1016/S0370-2693(00)00405-6.

[415] R. Abusaidi et al. "Exclusion limits on the WIMP nucleon cross-section from the cryogenic dark matter search". In: *Phys. Rev. Lett.* 84 (2000), pp. 5699–5703. DOI: 10.1103/PhysRevLett.84.5699. arXiv: astro-ph/0002471.

[416] Piero Ullio, Marc Kamionkowski, and Petr Vogel. "Spin dependent WIMPs in DAMA?" In: *JHEP* 07 (2001), p. 044. DOI: 10.1088/1126-6708/2001/07/044. arXiv: hep-ph/0010036.

[417] Eduard Masso, Subhendra Mohanty, and Soumya Rao. "Dipolar Dark Matter". In: *Phys. Rev. D* 80 (2009), p. 036009. DOI: 10.1103/PhysRevD.80.036009. arXiv: 0906.1979 [hep-ph].

[418] Luc Darmé, Soumya Rao, and Leszek Roszkowski. "Light dark Higgs boson in minimal sub-GeV dark matter scenarios". In: *JHEP* 03 (2018), p. 084. DOI: 10.1007/JHEP03(2018)084. arXiv: 1710.08430 [hep-ph].

[419] Asher Berlin, Gordan Krnjaic, and Elena Pinetti. "Reviving MeV-GeV indirect detection with inelastic dark matter". In: *Phys. Rev. D* 110.3 (2024), p. 035015. DOI: 10.1103/PhysRevD.110.035015. arXiv: 2311.00032 [hep-ph].

[420] Ana Luisa Foguel, Peter Reimitz, and Renata Zukanovich Funchal. "Unlocking the Inelastic Dark Matter Window with Vector Mediators". In: (Oct. 2024). arXiv: 2410.00881 [hep-ph].

[421] I. V. Voronchikhin and D. V. Kirpichnikov. "Examining scalar portal inelastic dark matter with lepton fixed target experiments". In: (May 2025). arXiv: 2505.04290 [hep-ph].

[422] Kai Schmidt-Hoberg and Martin Wolfgang Winkler. "Improved Constraints on Inelastic Dark Matter". In: *JCAP* 09 (2009), p. 010. DOI: 10.1088/1475-7516/2009/09/010. arXiv: 0907.3940 [astro-ph.CO].

[423] J. Angle et al. "Constraints on inelastic dark matter from XENON10". In: *Phys. Rev. D* 80 (2009), p. 115005. DOI: 10.1103/PhysRevD.80.115005. arXiv: 0910.3698 [astro-ph.CO].

[424] Xun Chen et al. "Exploring the dark matter inelastic frontier with 79.6 days of PandaX-II data". In: *Phys. Rev. D* 96.10 (2017), p. 102007. DOI: 10.1103/PhysRevD.96.102007. arXiv: 1708.05825 [hep-ex].

[425] Miriam Olmi. "Exploring the inelastic dark matter with the CRESST experiment". PhD thesis. Altra Universita' o Universita' estera, Gran Sasso, 2020.

[426] N. Carlin et al. "COSINE-100 Full Dataset Challenges the Annual Modulation Signal of DAMA/LIBRA". In: (Sept. 2024). arXiv: 2409.13226 [hep-ex].

[427] Iván Coarasa et al. "ANAIS–112 three years data: a sensitive model independent negative test of the DAMA/LIBRA dark matter signal". In: *Commun. Phys.* 7.1 (2024), p. 345. DOI: 10.1038/s42005-024-01827-y. arXiv: 2404.17348 [astro-ph.IM].

[428] R. Bernabei et al. "The DAMA/LIBRA apparatus". In: *Nucl. Instrum. Meth. A* 592 (2008), pp. 297–315. DOI: 10.1016/j.nima.2008.04.082. arXiv: 0804.2738 [astro-ph].

[429] R. Bernabei et al. "First results from DAMA/LIBRA and the combined results with DAMA/NaI". In: *Eur. Phys. J. C* 56 (2008), pp. 333–355. DOI: 10.1140/epjc/s10052-008-0662-y. arXiv: 0804.2741 [astro-ph].

[430] R. Bernabei et al. "Dark Matter with DAMA/LIBRA and its perspectives". In: *J. Phys. Conf. Ser.* 2586.1 (2023), p. 012096. DOI: 10.1088/1742-6596/2586/1/012096.

[431] N. Carlin et al. "Combined Annual Modulation Dark Matter Search with COSINE-100 and ANAIS-112". In: (Mar. 2025). arXiv: 2503.19559 [astro-ph.IM].

[432] Spencer Chang, Neal Weiner, and Itay Yavin. "Magnetic Inelastic Dark Matter". In: *Phys. Rev. D* 82 (2010), p. 125011. DOI: 10.1103/PhysRevD.82.125011. arXiv: 1007.4200 [hep-ph].

[433] E. Aprile et al. "WIMP Dark Matter Search using a 3.1 tonne × year Exposure of the XENONnT Experiment". In: (Feb. 2025). arXiv: 2502.18005 [hep-ex].

[434] G. Angloher et al. "Results on light dark matter particles with a low-threshold CRESST-II detector". In: *Eur. Phys. J. C* 76.1 (2016), p. 25. DOI: 10.1140/epjc/s10052-016-3877-3. arXiv: 1509.01515 [astro-ph.CO].

[435] Eugene Churazov et al. "Positron annihilation spectrum from the Galactic Center region observed by SPI/INTEGRAL". In: *Mon. Not. Roy. Astron. Soc.* 357 (2005), pp. 1377–1386. DOI: 10.1111/j.1365-2966.2005.08757.x. arXiv: astro-ph/0411351.

[436] Georg Weidenspointner et al. "The sky distribution of positronium annihilation continuum emission measured with spi/integral". In: *Astron. Astrophys.* 450 (2006), p. 1012. DOI: 10.1051/0004-6361:20054046. arXiv: astro-ph/0601673.

[437] Georg Weidenspointner et al. "The sky distribution of 511-keV positron annihilation line emission as measured with INTEGRAL/SPI". In: *ESA Spec. Publ.* 622 (2007). Ed. by A. Parmar and L. Ouwehand, p. 25. arXiv: astro-ph/0702621.

[438] J. Chang et al. "An excess of cosmic ray electrons at energies of 300-800 GeV". In: *Nature* 456 (2008), pp. 362–365. DOI: 10.1038/nature07477.

[439] Oscar Adriani et al. "An anomalous positron abundance in cosmic rays with energies 1.5-100 GeV". In: *Nature* 458 (2009), pp. 607–609. DOI: 10.1038/nature07942. arXiv: 0810.4995 [astro-ph].

[440] Douglas P. Finkbeiner and Neal Weiner. "Exciting Dark Matter and the INTEGRAL/SPI 511 keV signal". In: *Phys. Rev. D* 76 (2007), p. 083519. DOI: 10.1103/PhysRevD.76.083519. arXiv: astro-ph/0702587.

[441] Maxim Pospelov and Adam Ritz. "The galactic 511 keV line from electroweak scale WIMPs". In: *Phys. Lett. B* 651 (2007), pp. 208–215. DOI: 10.1016/j.physletb.2007.06.027. arXiv: hep-ph/0703128.

[442] Alexey Boyarsky et al. "Improved big bang nucleosynthesis constraints on heavy neutral leptons". In: *Phys. Rev. D* 104.2 (2021), p. 023517. DOI: 10.1103/PhysRevD.104.023517. arXiv: 2008.00749 [hep-ph].

[443] Nicolás Bernal, Xiaoyong Chu, and Josef Pradler. "Simply split strongly interacting massive particles". In: *Phys. Rev. D* 95.11 (2017), p. 115023. DOI: 10.1103/PhysRevD.95.115023. arXiv: 1702.04906 [hep-ph].

[444] Haipeng An and Daneng Yang. "Direct detection of freeze-in inelastic dark matter". In: *Phys. Lett. B* 818 (2021), p. 136408. DOI: 10.1016/j.physletb.2021.136408. arXiv: 2006.15672 [hep-ph].

[445] Saniya Heeba, Tongyan Lin, and Katelin Schutz. "Inelastic freeze-in". In: *Phys. Rev. D* 108.9 (2023), p. 095016. DOI: 10.1103/PhysRevD.108.095016. arXiv: 2304.06072 [hep-ph].

[446] Patrick J. Fitzpatrick et al. "New thermal relic targets for inelastic vector-portal dark matter". In: *Phys. Rev. D* 106.8 (2022), p. 083507. DOI: 10.1103/PhysRevD.106.083507. arXiv: 2105.05255 [hep-ph].

[447] Mattias Blennow, Stefan Clementz, and Juan Herrero-Garcia. "Self-interacting inelastic dark matter: A viable solution to the small scale structure problems". In: *JCAP* 03 (2017), p. 048. DOI: 10.1088/1475-7516/2017/03/048. arXiv: 1612.06681 [hep-ph].

[448] Mark Vogelsberger et al. "Evaporating the Milky Way halo and its satellites with inelastic self-interacting dark matter". In: (May 2018). DOI: 10.1093/mnras/stz340. arXiv: 1805.03203 [astro-ph.GA].

[449] Gerardo Alvarez and Hai-Bo Yu. "Astrophysical probes of inelastic dark matter with a light mediator". In: *Phys. Rev. D* 101.4 (2020), p. 043002. DOI: 10.1103/PhysRevD.101.043002. arXiv: 1911.11114 [hep-ph].

[450] Rouven Essig et al. "Constraining Dissipative Dark Matter Self-Interactions". In: *Phys. Rev. Lett.* 123.12 (2019), p. 121102. DOI: 10.1103/PhysRevLett.123.121102. arXiv: 1809.01144 [hep-ph].

[451] Stephanie O'Neil et al. "Endothermic self-interacting dark matter in Milky Way-like dark matter haloes". In: *Mon. Not. Roy. Astron. Soc.* 524.1 (2023), pp. 288–306. DOI: 10.1093/mnras/stad1850. arXiv: 2210.16328 [astro-ph.GA].

[452] Dan Hooper et al. "Inelastic Dark Matter As An Efficient Fuel For Compact Stars". In: *Phys. Rev. D* 81 (2010), p. 103531. DOI: 10.1103/PhysRevD.81.103531. arXiv: 1002.0005 [hep-ph].

[453] Matthew McCullough and Malcolm Fairbairn. "Capture of Inelastic Dark Matter in White Dwarves". In: *Phys. Rev. D* 81 (2010), p. 083520. DOI: 10.1103/PhysRevD.81.083520. arXiv: 1001.2737 [hep-ph].

[454] R. Andrew Gustafson et al. "Cosmic-ray cooling in active galactic nuclei as a new probe of inelastic dark matter". In: *Phys. Rev. D* 111.12 (2025), p. L121303. DOI: 10.1103/5m57-vgt2. arXiv: 2408.08947 [hep-ph].

[455] Javier F. Acevedo et al. "Neutrino and gamma-ray signatures of inelastic dark matter annihilating outside neutron stars". In: *JCAP* 03 (2025), p. 028. DOI: 10.1088/1475-7516/2025/03/028. arXiv: 2404.10039 [hep-ph].

[456] Brian Feldstein, Peter W. Graham, and Surjeet Rajendran. "Luminous Dark Matter". In: *Phys. Rev. D* 82 (2010), p. 075019. DOI: 10.1103/PhysRevD.82.075019. arXiv: 1008.1988 [hep-ph].

[457] Douglas P. Finkbeiner and Neal Weiner. "X-ray line from exciting dark matter". In: *Phys. Rev. D* 94.8 (2016), p. 083002. DOI: 10.1103/PhysRevD.94.083002. arXiv: 1402.6671 [hep-ph].

[458] Joshua Eby et al. "Luminous Signals of Inelastic Dark Matter in Large Detectors". In: *JHEP* 09 (2019), p. 115. DOI: 10.1007/JHEP09(2019)115. arXiv: 1904.09994 [hep-ph].

[459] Timon Emken et al. "Electron recoils from terrestrial upscattering of inelastic dark matter". In: *Phys. Rev. D* 105.5 (2022), p. 055023. DOI: 10.1103/PhysRevD.105.055023. arXiv: 2112.06930 [hep-ph].

[460] Francesco D'Eramo et al. "Dark matter inelastic up-scattering with the interstellar plasma: A new source of x-ray lines, including at 3.5 keV". In: *Phys. Rev. D* 93.10 (2016), p. 103011. DOI: 10.1103/PhysRevD.93.103011. arXiv: 1603.04859 [hep-ph].

[461] Peter W. Graham, Harikrishnan Ramani, and Samuel S. Y. Wong. "Enhancing direct detection of Higgsino dark matter". In: *Phys. Rev. D* 111.5 (2025), p. 055030. DOI: 10.1103/PhysRevD.111.055030. arXiv: 2409.07768 [hep-ph].

[462] Alessandro Davoli et al. "Displaced Vertices from Pseudo-Dirac Dark Matter". In: *JHEP* 11 (2017), p. 025. DOI: 10.1007/JHEP11(2017)025. arXiv: 1706.08985 [hep-ph].

[463] Yu-Dai Tsai, Patrick deNiverville, and Ming Xiong Liu. "Dark Photon and Muon $g-2$ Inspired Inelastic Dark Matter Models at the High-Energy Intensity Frontier". In: *Phys. Rev. Lett.* 126.18 (2021), p. 181801. DOI: 10.1103/PhysRevLett.126.181801. arXiv: 1908.07525 [hep-ph].

[464] Dong Woo Kang, P. Ko, and Chih-Ting Lu. "Exploring properties of long-lived particles in inelastic dark matter models at Belle II". In: *JHEP* 04 (2021), p. 269. DOI: 10.1007/JHEP04(2021)269. arXiv: 2101.02503 [hep-ph].

[465] Joe Davighi, Admir Greljo, and Nudzeim Selimovic. "Topological Portal to the Dark Sector". In: *Phys. Rev. Lett.* 134.11 (2025), p. 111804. DOI: 10.1103/PhysRevLett.134.111804. arXiv: 2401.09528 [hep-ph].

[466] John G. Learned and Sandip Pakvasa. "Detecting tau-neutrino oscillations at PeV energies". In: *Astropart. Phys.* 3 (1995), pp. 267–274. DOI: 10.1016/0927-6505(94)00043-3. arXiv: hep-ph/9405296.

[467] M. G. Aartsen et al. "Search for Astrophysical Tau Neutrinos in Three Years of IceCube Data". In: *Phys. Rev. D* 93.2 (2016), p. 022001. DOI: 10.1103/PhysRevD.93.022001. arXiv: 1509.06212 [astro-ph.HE].

[468] Pilar Coloma et al. "Double-Cascade Events from New Physics in Icecube". In: *Phys. Rev. Lett.* 119.20 (2017), p. 201804. DOI: 10.1103/PhysRevLett.119.201804. arXiv: 1707.08573 [hep-ph].

[469] Brian Batell et al. "Inelastic dark matter at the Fermilab Short Baseline Neutrino Program". In: *Phys. Rev. D* 104.7 (2021), p. 075026. DOI: 10.1103/PhysRevD.104.075026. arXiv: 2106.04584 [hep-ph].

[470] Enrico Bertuzzo, Andre Scaffidi, and Marco Taoso. "Searching for inelastic dark matter with future LHC experiments". In: *JHEP* 08 (2022), p. 100. DOI: 10.1007/JHEP08(2022)100. arXiv: 2201.12253 [hep-ph].

[471] Peter W. Graham et al. "Exothermic Dark Matter". In: *Phys. Rev. D* 82 (2010), p. 063512. DOI: 10.1103/PhysRevD.82.063512. arXiv: 1004.0937 [hep-ph].

[472] Nima Arkani-Hamed et al. "Small neutrino masses from supersymmetry breaking". In: *Phys. Rev. D* 64 (2001), p. 115011. DOI: 10.1103/PhysRevD.64.115011. arXiv: hep-ph/0006312.

[473] Taramati et al. "Singlet-doublet fermionic dark matter in gauge theory of baryons". In: (Aug. 2024). DOI: 10.1007/JHEP01(2025)159. arXiv: 2408.12424 [hep-ph].

[474] Steven Weinberg. "Approximate symmetries and pseudoGoldstone bosons". In: *Phys. Rev. Lett.* 29 (1972), pp. 1698–1701. DOI: 10.1103/PhysRevLett.29.1698.

[475] Daniele S. M. Alves et al. "Composite Inelastic Dark Matter". In: *Phys. Lett. B* 692 (2010), pp. 323–326. DOI: 10.1016/j.physletb.2010.08.006. arXiv: 0903.3945 [hep-ph].

[476] Sudhanwa Patra and Soumya Rao. "A Simple Model for Magnetic Inelastic Dark Matter (MiDM)". In: (Dec. 2011). arXiv: 1112.3454 [hep-ph].

[477] Kyu Jung Bae and Jongkuk Kim. "Axion-Mediated Inelastic Dark Matter". In: (Dec. 2023). arXiv: 2312.11210 [hep-ph].

[478] Anastasiia Filimonova et al. "Inelastic Dirac dark matter". In: *JHEP* 06 (2022), p. 048. DOI: 10.1007/JHEP06(2022)048. arXiv: 2201.08409 [hep-ph].

[479] Asli M. Abdullahi et al. "Semi-Visible Dark Photon Phenomenology at the GeV Scale". In: *Phys. Rev. D* 108.1 (2023), p. 015032. DOI: 10.1103/PhysRevD.108.015032. arXiv: 2302.05410 [hep-ph].

[480] Riccardo Catena and Taylor R. Gray. "Spin-1 thermal targets for dark matter searches at beam dump and fixed target experiments". In: *JCAP* 11 (2023), p. 058. DOI: 10.1088/1475-7516/2023/11/058. arXiv: 2307.02207 [hep-ph].

[481] Patrick deNiverville and Claudia Frugiuele. "Hunting sub-GeV dark matter with the NOνA near detector". In: *Phys. Rev. D* 99 (5 Mar. 2019), p. 051701. DOI: 10.1103/PhysRevD.99.051701. URL: https://link.aps.org/doi/10.1103/PhysRevD.99.051701.

[482] Patrick deNiverville et al. "Light dark matter in neutrino beams: production modelling and scattering signatures at MiniBooNE, T2K and SHiP". In: *Phys. Rev. D* 95.3 (2017), p. 035006. DOI: 10.1103/PhysRevD.95.035006. arXiv: 1609.01770 [hep-ph].

[483] Brian Batell, Rouven Essig, and Ze'ev Surujon. "Strong Constraints on Sub-GeV Dark Sectors from SLAC Beam Dump E137". In: *Phys. Rev. Lett.* 113.17 (2014), p. 171802. DOI: 10.1103/PhysRevLett.113.171802. arXiv: 1406.2698 [hep-ph].

[484] J. de Favereau et al. "DELPHES 3, A modular framework for fast simulation of a generic collider experiment". In: *JHEP* 02 (2014), p. 057. DOI: 10.1007/JHEP02(2014)057. arXiv: 1307.6346 [hep-ex].

[485] Philip Bechtle et al. "A proposal for the Lohengrin experiment to search for dark sector particles at the ELSA Accelerator". In: *Eur. Phys. J. C* 85.5 (2025), p. 600. DOI: 10.1140/epjc/s10052-025-14257-z. arXiv: 2410.10956 [hep-ex].

[486] Brian Batell, Maxim Pospelov, and Adam Ritz. "Exploring Portals to a Hidden Sector Through Fixed Targets". In: *Phys. Rev. D* 80 (2009), p. 095024. DOI: 10.1103/PhysRevD.80.095024. arXiv: 0906.5614 [hep-ph].

[487] A. A. Aguilar-Arevalo et al. "Dark Matter Search in Nucleon, Pion, and Electron Channels from a Proton Beam Dump with MiniBooNE". In: *Phys. Rev. D* 98.11 (2018), p. 112004. DOI: 10.1103/PhysRevD.98.112004. arXiv: 1807.06137 [hep-ex].

[488] J. P. Lees et al. "Search for Invisible Decays of a Dark Photon Produced in e^+e^- Collisions at BaBar". In: *Phys. Rev. Lett.* 119.13 (2017), p. 131804. DOI: 10.1103/PhysRevLett.119.131804. arXiv: 1702.03327 [hep-ex].

[489] D. Akimov et al. "First Probe of Sub-GeV Dark Matter beyond the Cosmological Expectation with the COHERENT CsI Detector at the SNS". In: *Phys. Rev. Lett.* 130.5 (2023), p. 051803. DOI: 10.1103/PhysRevLett.130.051803. arXiv: 2110.11453 [hep-ex].

[490] Rouven Essig et al. "First Direct Detection Limits on sub-GeV Dark Matter from XENON10". In: *Phys. Rev. Lett.* 109 (2012), p. 021301. DOI: 10.1103/PhysRevLett.109.021301. arXiv: 1206.2644 [astro-ph.CO].

[491] Eder Izaguirre et al. "Testing GeV-Scale Dark Matter with Fixed-Target Missing Momentum Experiments". In: *Phys. Rev. D* 91.9 (2015), p. 094026. DOI: 10.1103/PhysRevD.91.094026. arXiv: 1411.1404 [hep-ph].

[492] Eder Izaguirre et al. "Analyzing the Discovery Potential for Light Dark Matter". In: *Phys. Rev. Lett.* 115.25 (2015), p. 251301. DOI: 10.1103/PhysRevLett.115.251301. arXiv: 1505.00011 [hep-ph].

[493] Eder Izaguirre et al. "Testing Light Dark Matter Coannihilation With Fixed-Target Experiments". In: *Phys. Rev. D* 96.5 (2017), p. 055007. DOI: 10.1103/PhysRevD.96.055007. arXiv: 1703.06881 [hep-ph].

[494] Anson Hook, Eder Izaguirre, and Jay G. Wacker. "Model Independent Bounds on Kinetic Mixing". In: *Adv. High Energy Phys.* 2011 (2011), p. 859762. DOI: 10.1155/2011/859762. arXiv: 1006.0973 [hep-ph].

[495] David Curtin et al. "Illuminating Dark Photons with High-Energy Colliders". In: *JHEP* 02 (2015), p. 157. DOI: 10.1007/JHEP02(2015)157. arXiv: 1412.0018 [hep-ph].

[496] Bernard Aubert et al. "Search for Invisible Decays of a Light Scalar in Radiative Transitions $\upsilon_{3S} \to \gamma$ A0". In: *34th International Conference on High Energy Physics*. July 2008. arXiv: 0808.0017 [hep-ex].

[497] Jia Liu, Zhen Liu, and Lian-Tao Wang. "Enhancing Long-Lived Particles Searches at the LHC with Precision Timing Information". In: *Phys. Rev. Lett.* 122.13 (2019), p. 131801. DOI: 10.1103/PhysRevLett.122.131801. arXiv: 1805.05957 [hep-ph].

[498] Roel Aaij et al. "Search for Dark Photons Produced in 13 TeV *pp* Collisions". In: *Phys. Rev. Lett.* 120.6 (2018), p. 061801. DOI: 10.1103/PhysRevLett.120.061801. arXiv: 1710.02867 [hep-ex].

[499] Philip Ilten et al. "Proposed Inclusive Dark Photon Search at LHCb". In: *Phys. Rev. Lett.* 116.25 (2016), p. 251803. DOI: 10.1103/PhysRevLett.116.251803. arXiv: 1603.08926 [hep-ph].

[500] Aaron Pierce et al. "Searching for confining hidden valleys at LHCb, ATLAS, and CMS". In: *Phys. Rev. D* 97.9 (2018), p. 095033. DOI: 10.1103/PhysRevD.97.095033. arXiv: 1708.05389 [hep-ph].

[501] Vladimir V. Gligorov et al. "Searching for Long-lived Particles: A Compact Detector for Exotics at LHCb". In: *Phys. Rev. D* 97.1 (2018), p. 015023. DOI: 10.1103/PhysRevD.97.015023. arXiv: 1708.09395 [hep-ph].

[502] Jonathan L. Feng et al. "ForwArd Search ExpeRiment at the LHC". In: *Phys. Rev. D* 97.3 (2018), p. 035001. DOI: 10.1103/PhysRevD.97.035001. arXiv: 1708.09389 [hep-ph].

[503] John Paul Chou, David Curtin, and H. J. Lubatti. "New Detectors to Explore the Lifetime Frontier". In: *Phys. Lett. B* 767 (2017), pp. 29–36. DOI: 10.1016/j.physletb.2017.01.043. arXiv: 1606.06298 [hep-ph].

[504] Eduardo Cortina Gil et al. "Search for Leptonic Decays of Dark Photons at NA62". In: *Phys. Rev. Lett.* 133.11 (2024), p. 111802. DOI: 10.1103/PhysRevLett.133.111802. arXiv: 2312.12055 [hep-ex].

[505] M. Battaglieri et al. "Dark Matter Search in a Beam-Dump eXperiment (BDX) at Jefferson Lab". In: (July 2016). arXiv: 1607.01390 [hep-ex].

[506] A. A. Aguilar-Arevalo et al. "Dark Matter Search in a Proton Beam Dump with MiniBooNE". In: *Phys. Rev. Lett.* 118.22 (2017), p. 221803. DOI: 10.1103/PhysRevLett.118.221803. arXiv: 1702.02688 [hep-ex].

[507] Martin Bauer et al. "ANUBIS: Proposal to search for long-lived neutral particles in CERN service shafts". In: (Sept. 2019). arXiv: 1909.13022 [physics.ins-det].

[508] S. Cerci et al. "FACET: A new long-lived particle detector in the very forward region of the CMS experiment". In: *JHEP* 06 (2022), p. 110. DOI: 10.1007/JHEP06(2022)110. arXiv: 2201.00019 [hep-ex].

[509] Zihao Bo et al. "Dark Matter Search Results from 1.54 Tonne · Year Exposure of PandaX-4T". In: *Phys. Rev. Lett.* 134.1 (2025), p. 011805. DOI: 10.1103/PhysRevLett.134.011805. arXiv: 2408.00664 [hep-ex].

[510] Hong-Jian He, Yu-Chen Wang, and Jiaming Zheng. "Probing light inelastic dark matter from direct detection". In: *Phys. Dark Univ.* 46 (2024), p. 101670. DOI: 10.1016/j.dark.2024.101670. arXiv: 2403.03128 [hep-ph].

[511] Gonzalo Herrera, Alejandro Ibarra, and Satoshi Shirai. "Enhanced prospects for direct detection of inelastic dark matter from a non-galactic diffuse component". In: *JCAP* 04 (2023), p. 026. DOI: 10.1088/1475-7516/2023/04/026. arXiv: 2301.00870 [hep-ph].

[512] E. Aprile et al. "Light Dark Matter Search with Ionization Signals in XENON1T". In: *Phys. Rev. Lett.* 123.25 (2019), p. 251801. DOI: 10.1103/PhysRevLett.123.251801. arXiv: 1907.11485 [hep-ex].

[513] D. Banerjee et al. "Dark matter search in missing energy events with NA64". In: *Phys. Rev. Lett.* 123.12 (2019), p. 121801. DOI: 10.1103/PhysRevLett.123.121801. arXiv: 1906.00176 [hep-ex].

[514] Torsten Åkesson et al. "Light Dark Matter eXperiment (LDMX)". In: (Aug. 2018). arXiv: 1808.05219 [hep-ex].

[515] Rouven Essig et al. "Constraining Light Dark Matter with Diffuse X-Ray and Gamma-Ray Observations". In: *JHEP* 11 (2013), p. 193. DOI: 10.1007/JHEP11(2013)193. arXiv: 1309.4091 [hep-ph].

[516] Mathieu Boudaud, Julien Lavalle, and Pierre Salati. "Novel cosmic-ray electron and positron constraints on MeV dark matter particles". In: *Phys. Rev. Lett.* 119.2 (2017), p. 021103. DOI: 10.1103/PhysRevLett.119.021103. arXiv: 1612.07698 [astro-ph.HE].

[517] Marco Cirelli et al. "Integral X-ray constraints on sub-GeV Dark Matter". In: *Phys. Rev. D* 103.6 (2021), p. 063022. DOI: 10.1103/PhysRevD.103.063022. arXiv: 2007.11493 [hep-ph].

[518] Marco Cirelli et al. "Putting all the X in one basket: Updated X-ray constraints on sub-GeV Dark Matter". In: *JCAP* 07 (2023), p. 026. DOI: 10.1088/1475-7516/2023/07/026. arXiv: 2303.08854 [hep-ph].

[519] Junsong Cang, Yu Gao, and Yin-Zhe Ma. "Probing dark matter with future CMB measurements". In: *Phys. Rev. D* 102.10 (2020), p. 103005. DOI: 10.1103/PhysRevD.102.103005. arXiv: 2002.03380 [astro-ph.CO].

[520] M. Tavani et al. "Science with e-ASTROGAM: A space mission for MeV–GeV gamma-ray astrophysics". In: *JHEAp* 19 (2018). Ed. by A. De Angelis et al., pp. 1–106. DOI: 10.1016/j.jheap.2018.07.001. arXiv: 1711.01265 [astro-ph.HE].

[521] Regina Caputo et al. "All-sky Medium Energy Gamma-ray Observatory eXplorer mission concept". In: *J. Astron. Telesc. Instrum. Syst.* 8.4 (2022), p. 044003. DOI: 10.1117/1.JATIS.8.4.044003. arXiv: 2208.04990 [astro-ph.IM].

[522] Timur Dzhatdoev and Egor Podlesnyi. "Massive Argon Space Telescope (MAST): A concept of heavy time projection chamber for γ-ray astronomy in the 100 MeV–1 TeV energy range". In: *Astropart. Phys.* 112 (2019), pp. 1–7. DOI: 10.1016/j.astropartphys.2019.04.004. arXiv: 1902.01491 [astro-ph.HE].

[523] Peter Ade et al. "The Simons Observatory: Science goals and forecasts". In: *JCAP* 02 (2019), p. 056. DOI: 10.1088/1475-7516/2019/02/056. arXiv: 1808.07445 [astro-ph.CO].

[524] A. Suzuki et al. "The POLARBEAR-2 and the Simons Array Experiment". In: *J. Low Temp. Phys.* 184.3-4 (2016). Ed. by Philippe Camus, Alexandre Juillard, and Alessandro Monfardini, pp. 805–810. DOI: 10.1007/s10909-015-1425-4. arXiv: 1512.07299 [astro-ph.IM].

[525] Davi B. Costa. "Anomaly-free $U(1)^m$ extensions of the Standard Model". In: *Phys. Rev. D* 102.11 (2020), p. 115006. DOI: 10.1103/PhysRevD.102.115006. arXiv: 2007.08733 [hep-ph].

[526] Junji Hisano et al. "Direct detection of the Wino and Higgsino-like neutralino dark matters at one-loop level". In: *Phys. Rev. D* 71 (2005), p. 015007. DOI: 10.1103/PhysRevD.71.015007. arXiv: hep-ph/0407168.

[527] Natsumi Nagata and Satoshi Shirai. "Higgsino Dark Matter in High-Scale Supersymmetry". In: *JHEP* 01 (2015), p. 029. DOI: 10.1007/JHEP01(2015)029. arXiv: 1410.4549 [hep-ph].

[528] Luc Darmé, Soumya Rao, and Leszek Roszkowski. "Signatures of dark Higgs boson in light fermionic dark matter scenarios". In: *JHEP* 12 (2018), p. 014. DOI: 10.1007/JHEP12(2018)014. arXiv: 1807.10314 [hep-ph].

[529] Jinmian Li, Takaaki Nomura, and Takashi Shimomura. "Inelastic dark matter from dark Higgs boson decays at FASER". In: *JHEP* 09 (2022), p. 140. DOI: 10.1007/JHEP09(2022)140. arXiv: 2112.12432 [hep-ph].

[530] Zhi-zhong Xing and Shun Zhou. *Neutrinos in particle physics, astronomy and cosmology*. Advanced Topics in Science and Technology in China. Springer Berlin, Heidelberg, 2011. ISBN: 978-3-642-17559-6, 978-7-308-08024-8. DOI: 10.1007/978-3-642-17560-2.

[531] G. C. Branco et al. "Theory and phenomenology of two-Higgs-doublet models". In: *Phys. Rept.* 516 (2012), pp. 1–102. DOI: 10.1016/j.physrep.2012.02.002. arXiv: 1106.0034 [hep-ph].

[532] Luca Dieci, Alessandra Papini, and Alessandro Pugliese. "Takagi Factorization of Matrices Depending on Parameters and Locating Degeneracies of Singular Values". In: *SIAM Journal on Matrix Analysis and Applications* 43.3 (July 2022), pp. 1148–1161. ISSN: 1095-7162. DOI: 10.1137/21m1456273. URL: http://dx.doi.org/10.1137/21m1456273.

[533] Ansgar Denner et al. "Feynman rules for fermion number violating interactions". In: *Nucl. Phys. B* 387 (1992), pp. 467–481. DOI: 10.1016/0550-3213(92)90169-C.

[534] Adam Alloul et al. "FeynRules 2.0 - A complete toolbox for tree-level phenomenology". In: *Comput. Phys. Commun.* 185 (2014), pp. 2250–2300. DOI: 10.1016/j.cpc.2014.04.012. arXiv: 1310.1921 [hep-ph].

[535] A. Pukhov. "CalcHEP 2.3: MSSM, structure functions, event generation, batchs, and generation of matrix elements for other packages". In: (Dec. 2004). arXiv: hep-ph/0412191.

[536] Gerard 't Hooft. "Naturalness, chiral symmetry, and spontaneous chiral symmetry breaking". In: *NATO Sci. Ser. B* 59 (1980). Ed. by Gerard 't Hooft et al., pp. 135–157. DOI: 10.1007/978-1-4684-7571-5_9.

[537] Nathaniel Craig. "Naturalness: past, present, and future". In: *Eur. Phys. J. C* 83.9 (2023), p. 825. DOI: 10.1140/epjc/s10052-023-11928-7. arXiv: 2205.05708 [hep-ph].

[538] Alessandro Strumia. "Is nature natural?" In: *Nucl. Phys. B* 1007 (2024), p. 116679. DOI: 10.1016/j.nuclphysb.2024.116679. arXiv: 2409.19296 [hep-ph].

[539] Eduardo Cortina Gil et al. "Search for dark photon decays to $\mu^+\mu^-$ at NA62". In: *JHEP* 09 (2023), p. 035. DOI: 10.1007/JHEP09(2023)035. arXiv: 2303.08666 [hep-ex].

[540] Yu. M. Andreev et al. "Probing Light Dark Matter with positron beams at NA64". In: (Aug. 2023). arXiv: 2308.15612 [hep-ex].

[541] M. Tanabashi et al. "Review of Particle Physics". In: *Phys. Rev. D* 98 (3 Aug. 2018), p. 030001. DOI: 10.1103/PhysRevD.98.030001. URL: https://link.aps.org/doi/10.1103/PhysRevD.98.030001.

[542] Maurice Benayoun, Heath Bland O'Connell, and Anthony Gordon Williams. "Vector meson dominance and the ρ meson". In: *Phys. Rev. D* 59 (1999), p. 074020. DOI: 10.1103/PhysRevD.59.074020. arXiv: hep-ph/9807537.

[543] Kyrylo Bondarenko et al. "Phenomenology of GeV-scale Heavy Neutral Leptons". In: *JHEP* 11 (2018), p. 032. DOI: 10.1007/JHEP11(2018)032. arXiv: 1805.08567 [hep-ph].

[544] J. P. Lees et al. "Precise Measurement of the $e^+e^- \to \pi^+\pi^-(\gamma)$ Cross Section with the Initial-State Radiation Method at BABAR". In: *Phys. Rev. D* 86 (2012), p. 032013. DOI: 10.1103/PhysRevD.86.032013. arXiv: 1205.2228 [hep-ex].

[545] Philip Ilten et al. "Serendipity in dark photon searches". In: *JHEP* 06 (2018), p. 004. DOI: 10.1007/JHEP06(2018)004. arXiv: 1801.04847 [hep-ph].

[546] Maxim Pospelov. "Secluded U(1) below the weak scale". In: *Phys. Rev. D* 80 (2009), p. 095002. DOI: 10.1103/PhysRevD.80.095002. arXiv: 0811.1030 [hep-ph].

[547] G. Belanger et al. "Relic density of neutralino dark matter in the MSSM with CP violation". In: *Phys. Rev. D* 73 (2006), p. 115007. DOI: 10.1103/PhysRevD.73.115007. arXiv: hep-ph/0604150.

[548] Nicole F. Bell, Giorgio Busoni, and Isaac W. Sanderson. "Loop Effects in Direct Detection". In: *JCAP* 08 (2018). [Erratum: JCAP 01, E01 (2019)], p. 017. DOI: 10.1088/1475-7516/2018/08/017. arXiv: 1803.01574 [hep-ph].

[549] Javier Reynoso-Cordova, Nassim Bozorgnia, and Marie-Cécile Piro. "The Large Magellanic Cloud: expanding the low-mass parameter space of dark matter direct detection". In: (Sept. 2024). arXiv: 2409.09119 [hep-ph].

[550] R. Agnese et al. "Projected Sensitivity of the SuperCDMS SNOLAB experiment". In: *Phys. Rev. D* 95.8 (2017), p. 082002. DOI: 10.1103/PhysRevD.95.082002. arXiv: 1610.00006 [physics.ins-det].

[551] Marc Schumann et al. "Dark matter sensitivity of multi-ton liquid xenon detectors". In: *JCAP* 10 (2015), p. 016. DOI: 10.1088/1475-7516/2015/10/016. arXiv: 1506.08309 [physics.ins-det].

[552] C. Antel et al. "Feebly-interacting particles: FIPs 2022 Workshop Report". In: *Eur. Phys. J. C* 83.12 (2023), p. 1122. DOI: 10.1140/epjc/s10052-023-12168-5. arXiv: 2305.01715 [hep-ph].

[553] Sergei Gninenko. *NA64 Status Report 2021*. Tech. rep. Geneva: CERN, 2021. URL: https://cds.cern.ch/record/2767779.

[554] C. Cazzaniga et al. "Probing the explanation of the muon (g-2) anomaly and thermal light dark matter with the semi-visible dark photon channel". In: *Eur. Phys. J. C* 81.10 (2021), p. 959. DOI: 10.1140/epjc/s10052-021-09705-5. arXiv: 2107.02021 [hep-ex].

[555] Sergei Gninenko. *Proposal for an experiment to search for dark sector particles weakly coupled to muon at the SPS*. Tech. rep. Geneva: CERN, 2019. DOI: 10.17181/CERN.LEK5.O4J3. URL: https://cds.cern.ch/record/2653581.

[556] L. B. Auerbach et al. "Measurement of electron - neutrino - electron elastic scattering". In: *Phys. Rev. D* 63 (2001), p. 112001. DOI: 10.1103/PhysRevD.63.112001. arXiv: hep-ex/0101039.

[557] J. D. Bjorken et al. "Search for Neutral Metastable Penetrating Particles Produced in the SLAC Beam Dump". In: *Phys. Rev. D* 38 (1988), p. 3375. DOI: 10.1103/PhysRevD.38.3375.

[558] Song Li et al. "Unraveling dark Higgs mechanism via dark photon production at an e^+ e^- collider". In: (June 2025). arXiv: 2506.20208 [hep-ph].

[559] Eduardo Cortina Gil et al. "The Beam and detector of the NA62 experiment at CERN". In: *JINST* 12.05 (2017), P05025. DOI: 10.1088/1748-0221/12/05/P05025. arXiv: 1703.08501 [physics.ins-det].

[560] Francesco Tenchini. "Recent Results from Belle and Belle II". In: *Springer Proc. Phys.* 292 (2023), pp. 1–10. DOI: 10.1007/978-3-031-30459-0_1. arXiv: 2306.17340 [hep-ex].

[561] A. Celentano and H. Sieber. *Status and plans of the NA64e and NA64mu Experiments*. 2023.

[562] Yeong Gyun Kim, Kang Young Lee, and Seodong Shin. "Singlet fermionic dark matter". In: *JHEP* 05 (2008), p. 100. DOI: 10.1088/1126-6708/2008/05/100. arXiv: 0803.2932 [hep-ph].

[563] Karim Ghorbani and Parsa Hossein Ghorbani. "Leading Loop Effects in Pseudoscalar-Higgs Portal Dark Matter". In: *JHEP* 05 (2019), p. 096. DOI: 10.1007/JHEP05(2019)096. arXiv: 1812.04092 [hep-ph].

[564] Fatih Ertas and Felix Kahlhoefer. "Loop-induced direct detection signatures from CP-violating scalar mediators". In: *JHEP* 06 (2019), p. 052. DOI: 10.1007/JHEP06(2019)052. arXiv: 1902.11070 [hep-ph].

[565] Seungwon Baek, P. Ko, and Jinmian Li. "Minimal renormalizable simplified dark matter model with a pseudoscalar mediator". In: *Phys. Rev. D* 95.7 (2017), p. 075011. DOI: 10.1103/PhysRevD.95.075011. arXiv: 1701.04131 [hep-ph].

[566] Dan Hooper et al. "Gamma-Rays and Gravitational Waves from Inelastic Higgs Portal Dark Matter". In: (July 2025). arXiv: 2507.22975 [hep-ph].

[567] William J. Marciano, Cen Zhang, and Scott Willenbrock. "Higgs Decay to Two Photons". In: *Phys. Rev. D* 85 (2012), p. 013002. DOI: 10.1103/PhysRevD.85.013002. arXiv: 1109.5304 [hep-ph].

[568] Martin Wolfgang Winkler. "Decay and detection of a light scalar boson mixing with the Higgs boson". In: *Phys. Rev. D* 99.1 (2019), p. 015018. DOI: 10.1103/PhysRevD.99.015018. arXiv: 1809.01876 [hep-ph].

[569] M. Spira et al. "Higgs boson production at the LHC". In: *Nucl. Phys. B* 453 (1995), pp. 17–82. DOI: 10.1016/0550-3213(95)00379-7. arXiv: hep-ph/9504378.

[570] Maksym Ovchynnikov, Michael A. Schmidt, and Thomas Schwetz. "Complementarity of $B \to K^{(*)}\mu\bar{\mu}$ and $B \to K^{(*)} + \text{inv}$ for searches of GeV-scale Higgs-like scalars". In: *Eur. Phys. J. C* 83.9 (2023), p. 791. DOI: 10.1140/epjc/s10052-023-11975-0. arXiv: 2306.09508 [hep-ph].

[571] Iryna Boiarska et al. "Phenomenology of GeV-scale scalar portal". In: *JHEP* 11 (2019), p. 162. DOI: 10.1007/JHEP11(2019)162. arXiv: 1904.10447 [hep-ph].

[572] Sin Kyu Kang and Jubin Park. "Unitarity Constraints in the standard model with a singlet scalar field". In: *JHEP* 04 (2015), p. 009. DOI: 10.1007/JHEP04(2015)009. arXiv: 1306.6713 [hep-ph].

[573] Armen Tumasyan et al. "A portrait of the Higgs boson by the CMS experiment ten years after the discovery." In: *Nature* 607.7917 (2022). [Erratum: Nature 623, (2023)], pp. 60–68. DOI: 10.1038/s41586-022-04892-x. arXiv: 2207.00043 [hep-ex].

[574] Georges Aad et al. "A detailed map of Higgs boson interactions by the ATLAS experiment ten years after the discovery". In: *Nature* 607.7917 (2022). [Erratum: Nature 612, E24 (2022)], pp. 52–59. DOI: 10.1038/s41586-022-04893-w. arXiv: 2207.00092 [hep-ex].

[575] Antonio Boveia et al. "Recommendations on presenting LHC searches for missing transverse energy signals using simplified s-channel models of dark matter". In: *Phys. Dark Univ.* 27 (2020). Ed. by Oliver Buchmueller et al., p. 100365. DOI: 10.1016/j.dark.2019.100365. arXiv: 1603.04156 [hep-ex].

[576] Prudhvi N. Bhattiprolu and James D. Wells. "Depleted Higgs boson: Searches for universal coupling suppression, invisible decays, and mixed-in scalars". In: *Phys. Rev. D* 107.5 (2023), p. 055022. DOI: 10.1103/PhysRevD.107.055022. arXiv: 2204.03435 [hep-ph].

[577] D. de Florian et al. "Handbook of LHC Higgs Cross Sections: 4. Deciphering the Nature of the Higgs Sector". In: *CERN Yellow Rep. Monogr.* 2 (2017), pp. 1–869. DOI: 10.23731/CYRM-2017-002. arXiv: 1610.07922 [hep-ph].

[578] Morad Aaboud et al. "Combination of searches for heavy resonances decaying into bosonic and leptonic final states using 36 fb^{-1} of proton-proton collision data at $\sqrt{s} = 13$ TeV with the ATLAS detector". In: *Phys. Rev. D* 98.5 (2018), p. 052008. DOI: 10.1103/PhysRevD.98.052008. arXiv: 1808.02380 [hep-ex].

[579] Albert M Sirunyan et al. "Search for a new scalar resonance decaying to a pair of Z bosons in proton-proton collisions at $\sqrt{s} = 13$ TeV". In: *JHEP* 06 (2018). [Erratum: JHEP 03, 128 (2019)], p. 127. DOI: 10.1007/JHEP06(2018)127. arXiv: 1804.01939 [hep-ex].

[580] R. Barate et al. "Search for the standard model Higgs boson at LEP". In: *Phys. Lett. B* 565 (2003), pp. 61–75. DOI: 10.1016/S0370-2693(03)00614-2. arXiv: hep-ex/0306033.

[581] Felix Kahlhoefer et al. "Implications of unitarity and gauge invariance for simplified dark matter models". In: *JHEP* 02 (2016), p. 016. DOI: 10.1007/JHEP02(2016)016. arXiv: 1510.02110 [hep-ph].

[582] Brian Batell, Maxim Pospelov, and Adam Ritz. "Probing a Secluded U(1) at B-factories". In: *Phys. Rev. D* 79 (2009), p. 115008. DOI: 10.1103/PhysRevD.79.115008. arXiv: 0903.0363 [hep-ph].

[583] A. Anastasi et al. "Search for dark Higgsstrahlung in $e^+e^- \to \mu^+\mu^-$ and missing energy events with the KLOE experiment". In: *Phys. Lett. B* 747 (2015), pp. 365–372. DOI: 10.1016/j.physletb.2015.06.015. arXiv: 1501.06795 [hep-ex].

[584] F. Abudinén et al. "Search for a Dark Photon and an Invisible Dark Higgs Boson in μ+μ- and Missing Energy Final States with the Belle II Experiment". In: *Phys. Rev. Lett.* 130.7 (2023), p. 071804. DOI: 10.1103/PhysRevLett.130.071804. arXiv: 2207.00509 [hep-ex].

[585] J. P. Lees et al. "Search for Low-Mass Dark-Sector Higgs Bosons". In: *Phys. Rev. Lett.* 108 (2012), p. 211801. DOI: 10.1103/PhysRevLett.108.211801. arXiv: 1202.1313 [hep-ex].

[586] Igal Jaegle. "Search for the 'Dark Photon' and the 'Dark Higgs' at Belle". In: *Nucl. Phys. B Proc. Suppl.* 234 (2013). Ed. by Stephan Narison, pp. 33–36. DOI: 10.1016/j.nuclphysbps.2012.11.008. arXiv: 1211.1403 [hep-ex].

[587] I. Jaegle. "Search for the dark photon and the dark Higgs boson at Belle". In: *Phys. Rev. Lett.* 114.21 (2015), p. 211801. DOI: 10.1103/PhysRevLett.114.211801. arXiv: 1502.00084 [hep-ex].

[588] Kingman Cheung et al. "Probing dark photons from a light scalar at Belle II". In: *JHEP* 05 (2024), p. 094. DOI: 10.1007/JHEP05(2024)094. arXiv: 2401.03168 [hep-ph].

[589] Henso Abreu et al. "The FASER detector". In: *JINST* 19.05 (2024), P05066. DOI: 10.1088/1748-0221/19/05/P05066. arXiv: 2207.11427 [physics.ins-det].

[590] Haipeng An, Mark B. Wise, and Yue Zhang. "Strong CMB Constraint On P-Wave Annihilating Dark Matter". In: *Phys. Lett. B* 773 (2017), pp. 121–124. DOI: 10.1016/j.physletb.2017.08.010. arXiv: 1606.02305 [hep-ph].

[591] M. Gockeler et al. "Is there a Landau pole problem in QED?" In: *Phys. Rev. Lett.* 80 (1998), pp. 4119–4122. DOI: 10.1103/PhysRevLett.80.4119. arXiv: hep-th/9712244.

[592] Anastasiia Filimonova, Ruth Schäfer, and Susanne Westhoff. "Probing dark sectors with long-lived particles at BELLE II". In: *Phys. Rev. D* 101.9 (2020), p. 095006. DOI: 10.1103/PhysRevD.101.095006. arXiv: 1911.03490 [hep-ph].

[593] Natalia Borodatchenkova, Debajyoti Choudhury, and Manuel Drees. "Probing MeV dark matter at low-energy e+e- colliders". In: *Phys. Rev. Lett.* 96 (2006), p. 141802. DOI: 10.1103/PhysRevLett.96.141802. arXiv: hep-ph/0510147.

[594] Graham D. Kribs, David McKeen, and Nirmal Raj. "Breaking up the Proton: An Affair with Dark Forces". In: *Phys. Rev. Lett.* 126.1 (2021), p. 011801. DOI: 10.1103/PhysRevLett.126.011801. arXiv: 2007.15655 [hep-ph].

[595] Patrick J. Blackstone et al. "Hadronic Decays of a Higgs-mixed Scalar". In: (July 2024). arXiv: 2407.13587 [hep-ph].

[596] Torsten Bringmann et al. "Strong constraints on self-interacting dark matter with light mediators". In: *Phys. Rev. Lett.* 118.14 (2017), p. 141802. DOI: 10.1103/PhysRevLett.118.141802. arXiv: 1612.00845 [hep-ph].

[597] Felix Kahlhoefer, Kai Schmidt-Hoberg, and Sebastian Wild. "Dark matter self-interactions from a general spin-0 mediator". In: *JCAP* 08 (2017), p. 003. DOI: 10.1088/1475-7516/2017/08/003. arXiv: 1704.02149 [hep-ph].

[598] E. Aprile et al. "First Dark Matter Search with Nuclear Recoils from the XENONnT Experiment". In: *Phys. Rev. Lett.* 131.4 (2023), p. 041003. DOI: 10.1103/PhysRevLett.131.041003. arXiv: 2303.14729 [hep-ex].

[599] Paul Frederik Depta, Marco Hufnagel, and Kai Schmidt-Hoberg. "Updated BBN constraints on electromagnetic decays of MeV-scale particles". In: *JCAP* 04 (2021), p. 011. DOI: 10.1088/1475-7516/2021/04/011. arXiv: 2011.06519 [hep-ph].

[600] Masahiro Kawasaki et al. "Revisiting Big-Bang Nucleosynthesis Constraints on Long-Lived Decaying Particles". In: *Phys. Rev. D* 97.2 (2018), p. 023502. DOI: 10.1103/PhysRevD.97.023502. arXiv: 1709.01211 [hep-ph].

[601] G. G. Raffelt. *Stars as laboratories for fundamental physics: The astrophysics of neutrinos, axions, and other weakly interacting particles*. May 1996. ISBN: 978-0-226-70272-8.

[602] Edward Hardy and Robert Lasenby. "Stellar cooling bounds on new light particles: plasma mixing effects". In: *JHEP* 02 (2017), p. 033. DOI: 10.1007/JHEP02(2017)033. arXiv: 1611.05852 [hep-ph].

[603] P. S. Bhupal Dev, Rabindra N. Mohapatra, and Yongchao Zhang. "Revisiting supernova constraints on a light CP-even scalar". In: *JCAP* 08 (2020). [Erratum: JCAP 11, E01 (2020)], p. 003. DOI: 10.1088/1475-7516/2020/08/003. arXiv: 2005.00490 [hep-ph].

[604] Gonzalo Herrera and Kohta Murase. "Probing light dark matter through cosmic-ray cooling in active galactic nuclei". In: *Phys. Rev. D* 110.1 (2024), p. L011701. DOI: 10.1103/PhysRevD.110.L011701. arXiv: 2307.09460 [hep-ph].

[605] Dmitry Gorbunov, Igor Krasnov, and Sergey Suvorov. "Constraints on light scalars from PS191 results". In: *Phys. Lett. B* 820 (2021), p. 136524. DOI: 10.1016/j.physletb.2021.136524. arXiv: 2105.11102 [hep-ph].

[606] Eduardo Cortina Gil et al. "Search for π^0 decays to invisible particles". In: *JHEP* 02 (2021), p. 201. DOI: 10.1007/JHEP02(2021)201. arXiv: 2010.07644 [hep-ex].

[607] Eduardo Cortina Gil et al. "Measurement of the very rare $K^+ \to \pi^+ \nu\bar{\nu}$ decay". In: *JHEP* 06 (2021), p. 093. DOI: 10.1007/JHEP06(2021)093. arXiv: 2103.15389 [hep-ex].

[608] F. Bergsma et al. "Search for Axion Like Particle Production in 400-GeV Proton - Copper Interactions". In: *Phys. Lett. B* 157 (1985), pp. 458–462. DOI: 10.1016/0370-2693(85)90400-9.

[609] P. Abratenko et al. "Search for a Higgs Portal Scalar Decaying to Electron-Positron Pairs in the MicroBooNE Detector". In: *Phys. Rev. Lett.* 127.15 (2021), p. 151803. DOI: 10.1103/PhysRevLett.127.151803. arXiv: 2106.00568 [hep-ex].

[610] P. Abratenko et al. "Search for long-lived heavy neutral leptons and Higgs portal scalars decaying in the MicroBooNE detector". In: *Phys. Rev. D* 106.9 (2022), p. 092006. DOI: 10.1103/PhysRevD.106.092006. arXiv: 2207.03840 [hep-ex].

[611] I. Adachi et al. "Search for a long-lived spin-0 mediator in b→s transitions at the Belle II experiment". In: *Phys. Rev. D* 108.11 (2023), p. L111104. DOI: 10.1103/PhysRevD.108.L111104. arXiv: 2306.02830 [hep-ex].

[612] J. P. Lees et al. "Search for Long-Lived Particles in e^+e^- Collisions". In: *Phys. Rev. Lett.* 114.17 (2015), p. 171801. DOI: 10.1103/PhysRevLett.114.171801. arXiv: 1502.02580 [hep-ex].

[613] Roel Aaij et al. "Search for hidden-sector bosons in $B^0 \to K^{*0}\mu^+\mu^-$ decays". In: *Phys. Rev. Lett.* 115.16 (2015), p. 161802. DOI: 10.1103/PhysRevLett.115.161802. arXiv: 1508.04094 [hep-ex].

[614] R. Aaij et al. "Search for long-lived scalar particles in $B^+ \to K^+\chi(\mu^+\mu^-)$ decays". In: *Phys. Rev. D* 95.7 (2017), p. 071101. DOI: 10.1103/PhysRevD.95.071101. arXiv: 1612.07818 [hep-ex].

[615] J. Blumlein et al. "Limits on neutral light scalar and pseudoscalar particles in a proton beam dump experiment". In: *Z. Phys. C* 51 (1991), pp. 341–350. DOI: 10.1007/BF01548556.

[616] F. Bergsma et al. "A Search for Decays of Heavy Neutrinos in the Mass Range 0.5-GeV to 2.8-GeV". In: *Phys. Lett. B* 166 (1986), pp. 473–478. DOI: 10.1016/0370-2693(86)91601-1.

[617] Philip Harris, Philip Schuster, and Jure Zupan. "Snowmass White Paper: New flavors and rich structures in dark sectors". In: *Snowmass 2021*. July 2022. arXiv: 2207.08990 [hep-ph].

[618] Takehiko Asaka and Mikhail Shaposhnikov. "The νMSM, dark matter and baryon asymmetry of the universe". In: *Phys. Lett. B* 620 (2005), pp. 17–26. DOI: 10.1016/j.physletb.2005.06.020. arXiv: hep-ph/0505013.

[619] Martin Bauer, Matthias Neubert, and Andrea Thamm. "Collider Probes of Axion-Like Particles". In: *JHEP* 12 (2017), p. 044. DOI: 10.1007/JHEP12(2017)044. arXiv: 1708.00443 [hep-ph].

[620] Daniel Aloni, Yotam Soreq, and Mike Williams. "Coupling QCD-Scale Axionlike Particles to Gluons". In: *Phys. Rev. Lett.* 123.3 (2019), p. 031803. DOI: 10.1103/PhysRevLett.123.031803. arXiv: 1811.03474 [hep-ph].

[621] Martin Bauer et al. "Flavor probes of axion-like particles". In: *JHEP* 09 (2022), p. 056. DOI: 10.1007/JHEP09(2022)056. arXiv: 2110.10698 [hep-ph].

[622] Giovani Dalla Valle Garcia et al. "Phenomenology of axionlike particles with universal fermion couplings revisited". In: *Phys. Rev. D* 109.5 (2024), p. 055042. DOI: 10.1103/PhysRevD.109.055042. arXiv: 2310.03524 [hep-ph].

[623] Maksym Ovchynnikov and Andrii Zaporozhchenko. "ALPs coupled to gluons in the GeV mass range – data-driven and consistent". In: (Jan. 2025). arXiv: 2501.04525 [hep-ph].

[624] Yehor Kyselov and Maksym Ovchynnikov. "Searches for long-lived dark photons at proton accelerator experiments". In: *Phys. Rev. D* 111.1 (2025), p. 015030. DOI: 10.1103/PhysRevD.111.015030. arXiv: 2409.11096 [hep-ph].

[625] Tao Han et al. "Phenomenology of hidden valleys at hadron colliders". In: *JHEP* 07 (2008), p. 008. DOI: 10.1088/1126-6708/2008/07/008. arXiv: 0712.2041 [hep-ph].

[626] Nathaniel Craig et al. "Naturalness in the Dark at the LHC". In: *JHEP* 07 (2015), p. 105. DOI: 10.1007/JHEP07(2015)105. arXiv: 1501.05310 [hep-ph].

[627] I. Yu. Kobzarev, L. B. Okun, and I. Ya. Pomeranchuk. "On the possibility of experimental observation of mirror particles". In: *Sov. J. Nucl. Phys.* 3.6 (1966), pp. 837–841.

[628] Robert Foot, H. Lew, and R. R. Volkas. "A Model with fundamental improper space-time symmetries". In: *Phys. Lett. B* 272 (1991), pp. 67–70. DOI: 10.1016/0370-2693(91)91013-L.

[629] Z. G. Berezhiani, A. D. Dolgov, and R. N. Mohapatra. "Asymmetric inflationary reheating and the nature of mirror universe". In: *Phys. Lett. B* 375 (1996), pp. 26–36. DOI: 10.1016/0370-2693(96)00219-5. arXiv: hep-ph/9511221.

[630] Z. Chacko, Hock-Seng Goh, and Roni Harnik. "The Twin Higgs: Natural electroweak breaking from mirror symmetry". In: *Phys. Rev. Lett.* 96 (2006), p. 231802. DOI: 10.1103/PhysRevLett.96.231802. arXiv: hep-ph/0506256.

[631] Akitaka Ariga et al. "FASER: ForwArd Search ExpeRiment at the LHC". In: (Jan. 2019). arXiv: 1901.04468 [hep-ex].

[632] G. Acampora et al. "SND@LHC: the scattering and neutrino detector at the LHC". In: *JINST* 19.05 (2024), P05067. DOI: 10.1088/1748-0221/19/05/P05067. arXiv: 2210.02784 [hep-ex].

[633] O Aberle et al. *BDF/SHiP at the ECN3 high-intensity beam facility*. Tech. rep. Geneva: CERN, 2022. URL: http://cds.cern.ch/record/2839677.

[634] B. Acharya et al. "MoEDAL-MAPP, an LHC Dedicated Detector Search Facility". In: *Snowmass 2021*. Sept. 2022. arXiv: 2209.03988 [hep-ph].

[635] Aram Apyan et al. "DarkQuest: A dark sector upgrade to SpinQuest at the 120 GeV Fermilab Main Injector". In: *Snowmass 2021*. Mar. 2022. arXiv: 2203.08322 [hep-ex].

[636] Babak Abi et al. "Deep Underground Neutrino Experiment (DUNE), Far Detector Technical Design Report, Volume I Introduction to DUNE". In: *JINST* 15.08 (2020), T08008. DOI: 10.1088/1748-0221/15/08/T08008. arXiv: 2002.02967 [physics.ins-det].

[637] Cristiano Alpigiani et al. "Recent Progress and Next Steps for the MATHUSLA LLP Detector". In: *2022 Snowmass Summer Study*. Mar. 2022. arXiv: 2203.08126 [hep-ex].

[638] Giulio Aielli et al. "Expression of interest for the CODEX-b detector". In: *Eur. Phys. J. C* 80.12 (2020), p. 1177. DOI: 10.1140/epjc/s10052-020-08711-3. arXiv: 1911.00481 [hep-ex].

[639] Jeremi Niedziela. "SHIFT@LHC: Searches for new physics with shifted interaction on a fixed target at the Large Hadron Collider". In: *JHEP* 24 (2020), p. 204. DOI: 10.1007/JHEP10(2024)204. arXiv: 2406.08557 [hep-ph].

[640] Jonathan L. Feng et al. "The Forward Physics Facility at the High-Luminosity LHC". In: *J. Phys. G* 50.3 (2023), p. 030501. DOI: 10.1088/1361-6471/ac865e. arXiv: 2203.05090 [hep-ex].

[641] B. Hacisahinoglu et al. "PREFACE: A search for long-lived particles at the Large Hadron Collider". In: (Feb. 2025). arXiv: 2502.14598 [hep-ex].

[642] Volodymyr Gorkavenko et al. "LHCb potential to discover long-lived new physics particles with lifetimes above 100 ps". In: *Eur. Phys. J. C* 84.6 (2024), p. 608. DOI: 10.1140/epjc/s10052-024-12906-3. arXiv: 2312.14016 [hep-ph].

[643] V. Kholoimov et al. "A Downstream and vertexing algorithm for Long Lived Particles (LLP) selection at the first High-level trigger (HLT1) of LHCb". In: (Mar. 2025). arXiv: 2503.13092 [hep-ex].

[644] Jean-Loup Tastet, Oleg Ruchayskiy, and Inar Timiryasov. "Reinterpreting the ATLAS bounds on heavy neutral leptons in a realistic neutrino oscillation model". In: *JHEP* 12 (2021), p. 182. DOI: 10.1007/JHEP12(2021)182. arXiv: 2107.12980 [hep-ph].

[645] Oleksii Mikulenko et al. "New physics at the Intensity Frontier: how much can we learn and how?" In: (Dec. 2023). arXiv: 2312.00659 [hep-ph].

[646] Oleksii Mikulenko et al. "Unveiling new physics with discoveries at Intensity Frontier". In: (Dec. 2023). arXiv: 2312.05163 [hep-ph].

[647] Kierthika Chathirathas et al. "Finding excesses in model parameter space". In: *Eur. Phys. J. C* 85.2 (2025), p. 149. DOI: 10.1140/epjc/s10052-025-13795-w. arXiv: 2407.20329 [hep-ph].

[648] Oleksii Mikulenko. "Quasi-Dirac Heavy Neutral Leptons in the Left-Right Symmetric Model". In: (June 2024). arXiv: 2406.13850 [hep-ph].

[649] Qing-Hong Cao, Kun Cheng, and Yandong Liu. "Distinguishing Dirac from Majorana Heavy Neutrino at Future Lepton Colliders". In: *Phys. Rev. Lett.* 134.2 (2025), p. 021801. DOI: 10.1103/PhysRevLett.134.021801. arXiv: 2403.06561 [hep-ph].

[650] Alexander Monin, Alexey Boyarsky, and Oleg Ruchayskiy. "Hadronic decays of a light Higgs-like scalar". In: *Phys. Rev. D* 99.1 (2019), p. 015019. DOI: 10.1103/PhysRevD.99.015019. arXiv: 1806.07759 [hep-ph].

[651] Serguei Chatrchyan et al. "Search for a Non-Standard-Model Higgs Boson Decaying to a Pair of New Light Bosons in Four-Muon Final States". In: *Phys. Lett. B* 726 (2013), pp. 564–586. DOI: 10.1016/j.physletb.2013.09.009. arXiv: 1210.7619 [hep-ex].

[652] David Curtin et al. "Exotic decays of the 125 GeV Higgs boson". In: *Phys. Rev. D* 90.7 (2014), p. 075004. DOI: 10.1103/PhysRevD.90.075004. arXiv: 1312.4992 [hep-ph].

[653] Xabier Cid Vidal, Yuhsin Tsai, and Jose Zurita. "Exclusive displaced hadronic signatures in the LHC forward region". In: *JHEP* 01 (2020), p. 115. DOI: 10.1007/JHEP01(2020)115. arXiv: 1910.05225 [hep-ph].

[654] Georges Aad et al. "Search for light long-lived neutral particles that decay to collimated pairs of leptons or light hadrons in pp collisions at $\sqrt{s} =$ 13 TeV with the ATLAS detector". In: *JHEP* 06 (2023), p. 153. DOI: 10.1007/JHEP06(2023)153. arXiv: 2206.12181 [hep-ex].

[655] Georges Aad et al. "Search for short- and long-lived axion-like particles in $H \to aa \to 4\gamma$ decays with the ATLAS experiment at the LHC". In: *Eur. Phys. J. C* 84.7 (2024), p. 742. DOI: 10.1140/epjc/s10052-024-12979-0. arXiv: 2312.03306 [hep-ex].

[656] Aram Hayrapetyan et al. "Model-independent search for pair production of new bosons decaying into muons in proton-proton collisions at $\sqrt{s} =$ 13 TeV". In: *JHEP* 12 (2024), p. 172. DOI: 10.1007/JHEP12(2024)172. arXiv: 2407.20425 [hep-ex].

[657] Aram Hayrapetyan et al. "Search for New Resonances Decaying to Pairs of Merged Diphotons in Proton-Proton Collisions at s=13 TeV". In: *Phys. Rev. Lett.* 134.4 (2025), p. 041801. DOI: 10.1103/PhysRevLett.134.041801. arXiv: 2405.00834 [hep-ex].

[658] Aram Hayrapetyan et al. "Search for the decay of the Higgs boson to a pair of light pseudoscalar bosons in the final state with four bottom quarks in proton-proton collisions at $\sqrt{\mathrm{s}} = 13$ TeV". In: *JHEP* 06 (2024), p. 097. DOI: 10.1007/JHEP06(2024)097. arXiv: 2403.10341 [hep-ex].

[659] Mason Acevedo et al. "Multi-track displaced vertices at B-factories". In: *JHEP* 09 (2021), p. 154. DOI: 10.1007/JHEP09(2021)154. arXiv: 2105.12744 [hep-ph].

[660] Iryna Boiarska et al. "Light scalar production from Higgs bosons and FASER 2". In: *JHEP* 05 (2020), p. 049. DOI: 10.1007/JHEP05(2020)049. arXiv: 1908.04635 [hep-ph].

[661] David Curtin and Jaipratap Singh Grewal. "Long Lived Particle Decays in MATHUSLA". In: *Phys. Rev. D* 109.7 (2024), p. 075017. DOI: 10.1103/PhysRevD.109.075017. arXiv: 2308.05860 [hep-ph].

[662] Michael L. Graesser. "Broadening the Higgs boson with right-handed neutrinos and a higher dimension operator at the electroweak scale". In: *Phys. Rev. D* 76 (2007), p. 075006. DOI: 10.1103/PhysRevD.76.075006. arXiv: 0704.0438 [hep-ph].

[663] Michael L. Graesser. "Experimental Constraints on Higgs Boson Decays to TeV-scale Right-Handed Neutrinos". In: (May 2007). arXiv: 0705.2190 [hep-ph].

[664] A. Caputo et al. "The seesaw portal in testable models of neutrino masses". In: *JHEP* 06 (2017), p. 112. DOI: 10.1007/JHEP06(2017)112. arXiv: 1704.08721 [hep-ph].

[665] Jonathan M. Butterworth et al. "Higgs phenomenology as a probe of sterile neutrinos". In: *Phys. Rev. D* 100.11 (2019), p. 115019. DOI: 10.1103/PhysRevD.100.115019. arXiv: 1909.04665 [hep-ph].

[666] Daniele Barducci et al. "The see-saw portal at future Higgs Factories". In: *JHEP* 03 (2021), p. 117. DOI: 10.1007/JHEP03(2021)117. arXiv: 2011.04725 [hep-ph].

[667] Martin Bauer, Guillaume Rostagni, and Jonas Spinner. "Axion-Higgs portal". In: *Phys. Rev. D* 107.1 (2023), p. 015007. DOI: 10.1103/PhysRevD.107.015007. arXiv: 2207.05762 [hep-ph].

[668] Frank Deppisch, Suchita Kulkarni, and Wei Liu. "Heavy neutrino production via Z' at the lifetime frontier". In: *Phys. Rev. D* 100.3 (2019), p. 035005. DOI: 10.1103/PhysRevD.100.035005. arXiv: 1905.11889 [hep-ph].

[669] Asli M. Abdullahi et al. "The present and future status of heavy neutral leptons". In: *J. Phys. G* 50.2 (2023), p. 020501. DOI: 10.1088/1361-6471/ac98f9. arXiv: 2203.08039 [hep-ph].

[670] Pedro Schwaller, Daniel Stolarski, and Andreas Weiler. "Emerging Jets". In: *JHEP* 05 (2015), p. 059. DOI: 10.1007/JHEP05(2015)059. arXiv: 1502.05409 [hep-ph].

[671] Graham D. Kribs and Ethan T. Neil. "Review of strongly-coupled composite dark matter models and lattice simulations". In: *Int. J. Mod. Phys. A* 31.22 (2016), p. 1643004. DOI: 10.1142/S0217751X16430041. arXiv: 1604.04627 [hep-ph].

[672] Elias Bernreuther et al. "Strongly interacting dark sectors in the early Universe and at the LHC through a simplified portal". In: *JHEP* 01 (2020), p. 162. DOI: 10.1007/JHEP01(2020)162. arXiv: 1907.04346 [hep-ph].

[673] Guillaume Albouy et al. "Theory, phenomenology, and experimental avenues for dark showers: a Snowmass 2021 report". In: *Eur. Phys. J. C* 82.12 (2022), p. 1132. DOI: 10.1140/epjc/s10052-022-11048-8. arXiv: 2203.09503 [hep-ph].

[674] Hsin-Chia Cheng, Lingfeng Li, and Ennio Salvioni. "A theory of dark pions". In: *JHEP* 01 (2022), p. 122. DOI: 10.1007/JHEP01(2022)122. arXiv: 2110.10691 [hep-ph].

[675] Hsin-Chia Cheng et al. "Dark showers from Z-dark Z' mixing". In: *JHEP* 04 (2024), p. 081. DOI: 10.1007/JHEP04(2024)081. arXiv: 2401.08785 [hep-ph].

[676] Christian Bierlich et al. "A comprehensive guide to the physics and usage of PYTHIA 8.3". In: *SciPost Phys. Codeb.* 2022 (2022), p. 8. DOI: 10.21468/SciPostPhysCodeb.8. arXiv: 2203.11601 [hep-ph].

[677] Kyrylo Bondarenko et al. "Sensitivity of the intensity frontier experiments for neutrino and scalar portals: analytic estimates". In: *JHEP* 08 (2019), p. 061. DOI: 10.1007/JHEP08(2019)061. arXiv: 1902.06240 [hep-ph].

[678] M. Anelli et al. "A facility to Search for Hidden Particles (SHiP) at the CERN SPS". In: (Apr. 2015). arXiv: 1504.04956 [physics.ins-det].

[679] Akitaka Ariga et al. "Technical Proposal for FASER: ForwArd Search ExpeRiment at the LHC". In: (Dec. 2018). arXiv: 1812.09139 [physics.ins-det].

[680] A. Blondel et al. "Searches for long-lived particles at the future FCC-ee". In: *Front. in Phys.* 10 (2022), p. 967881. DOI: 10.3389/fphy.2022.967881. arXiv: 2203.05502 [hep-ex].

[681] John F. Donoghue, J. Gasser, and H. Leutwyler. "The Decay of a Light Higgs Boson". In: *Nucl. Phys. B* 343 (1990), pp. 341–368. DOI: 10.1016/0550-3213(90)90474-R.

[682] Armen Tumasyan et al. "A search for decays of the Higgs boson to invisible particles in events with a top-antitop quark pair or a vector boson in proton-proton collisions at $\sqrt{s} = 13\,\text{TeV}$". In: *Eur. Phys. J. C* 83.10 (2023), p. 933. DOI: 10.1140/epjc/s10052-023-11952-7. arXiv: 2303.01214 [hep-ex].

[683] Catherine Bernaciak et al. "Spying an invisible Higgs boson". In: *Phys. Rev. D* 91 (2015), p. 035024. DOI: 10.1103/PhysRevD.91.035024. arXiv: 1411.7699 [hep-ph].

[684] Philip Bechtle et al. "Probing the Standard Model with Higgs signal rates from the Tevatron, the LHC and a future ILC". In: *JHEP* 11 (2014), p. 039. DOI: 10.1007/JHEP11(2014)039. arXiv: 1403.1582 [hep-ph].

[685] Frank Wilczek. "Decays of Heavy Vector Mesons Into Higgs Particles". In: *Phys. Rev. Lett.* 39 (1977), p. 1304. DOI: 10.1103/PhysRevLett.39.1304.

[686] R. Albanese et al. "SHiP experiment at the SPS Beam Dump Facility". In: (Apr. 2025). arXiv: 2504.06692 [hep-ex].

[687] LHCb collaboration. "Background study from BuSca: Insights from October 2024 LHCb data". In: (2025). URL: https://cds.cern.ch/record/2923556.

[688] LHCb collaboration. "BuSca: a Buffer Scanner at HLT1 using 2024 LHCb data". In: (2024). URL: https://cds.cern.ch/record/2914494.

[689] Reyes et al. Alemany Fernandez. *Summary Report of the Physics Beyond Colliders Study at CERN*. Tech. rep. Geneva: CERN, 2025. URL: https://cds.cern.ch/record/2927631.

[690] Peter Ballett, Matheus Hostert, and Silvia Pascoli. "Dark Neutrinos and a Three Portal Connection to the Standard Model". In: *Phys. Rev. D* 101.11 (2020), p. 115025. DOI: 10.1103/PhysRevD.101.115025. arXiv: 1903.07589 [hep-ph].

[691] Tarek Ibrahim and Pran Nath. "CP Violation From Standard Model to Strings". In: *Rev. Mod. Phys.* 80 (2008), pp. 577–631. DOI: 10.1103/RevModPhys.80.577. arXiv: 0705.2008 [hep-ph].

[692] N. F. Ramsey. "Time Reversal, Charge Conjugation, Magnetic Pole Conjugation, and Parity". In: *Phys. Rev.* 109.1 (1958), pp. 225–226. DOI: 10.1103/PhysRev.109.225.

[693] J. H. Smith, E. M. Purcell, and N. F. Ramsey. "Experimental limit to the electric dipole moment of the neutron". In: *Phys. Rev.* 108 (1957), pp. 120–122. DOI: 10.1103/PhysRev.108.120.

[694] J. D. Jackson, S. B. Treiman, and H. W. Wyld. "Possible tests of time reversal invariance in Beta decay". In: *Phys. Rev.* 106 (1957), pp. 517–521. DOI: 10.1103/PhysRev.106.517.

[695] J. H. Christenson et al. "Evidence for the 2π Decay of the K_2^0 Meson". In: *Phys. Rev. Lett.* 13 (1964), pp. 138–140. DOI: 10.1103/PhysRevLett.13.138.

[696] A. D. Sakharov. "Violation of CP Invariance, C asymmetry, and baryon asymmetry of the universe". In: *Pisma Zh. Eksp. Teor. Fiz.* 5 (1967), pp. 32–35. DOI: 10.1070/PU1991v034n05ABEH002497.

[697] Luca Dieci, Alessandra Papini, and Alessandro Pugliese. *Takagi factorization of matrices depending on parameters and locating degeneracies of singular values*. 2021. DOI: 10.48550/ARXIV.2110.15918. URL: https://arxiv.org/abs/2110.15918.

[698] S.Y. Choi and H. E. Haber. *The Mathematics of Fermion Mass Diagonalization*. https://scipp.ucsc.edu/~haber/ph218/ch2_short.pdf. Online accessed: 2025-09-08.

[699] Howard E. Haber. "A tale of three diagonalizations". In: *Int. J. Mod. Phys. A* 36.04 (2021), p. 2130003. DOI: 10.1142/S0217751X21300027. arXiv: 2009.03990 [hep-ph].

[700] T. Hahn. "Routines for the diagonalization of complex matrices". In: (July 2006). arXiv: physics/0607103.

[701] Ilian Dobrev, Kirill Melnikov, and Thomas Schwetz. "Neutrino oscillations and scattering theory". In: *JHEP* 07 (2025), p. 035. DOI: 10.1007/JHEP07(2025)035. arXiv: 2504.10600 [hep-ph].

[702] Brian Batell, Jonathan L. Feng, and Sebastian Trojanowski. "Detecting Dark Matter with Far-Forward Emulsion and Liquid Argon Detectors at the LHC". In: *Phys. Rev. D* 103.7 (2021), p. 075023. DOI: 10.1103/PhysRevD.103.075023. arXiv: 2101.10338 [hep-ph].

[703] Brian Batell et al. "Discovering dark matter at the LHC through its nuclear scattering in far-forward emulsion and liquid argon detectors". In: *Phys. Rev. D* 104.3 (2021), p. 035036. DOI: 10.1103/PhysRevD.104.035036. arXiv: 2107.00666 [hep-ph].

[704] S. N. Gninenko et al. "The exact tree-level calculation of the dark photon production in high-energy electron scattering at the CERN SPS". In: *Phys. Lett. B* 782 (2018), pp. 406–411. DOI: 10.1016/j.physletb.2018.05.010. arXiv: 1712.05706 [hep-ph].

[705] Yu. M. Andreev et al. "Improved exclusion limit for light dark matter from e+e- annihilation in NA64". In: *Phys. Rev. D* 104.9 (2021), p. L091701. DOI: 10.1103/PhysRevD.104.L091701. arXiv: 2108.04195 [hep-ex].

[706] J. P. Lees et al. "Time-Integrated Luminosity Recorded by the BABAR Detector at the PEP-II e^+e^- Collider". In: *Nucl. Instrum. Meth. A* 726 (2013), pp. 203–213. DOI: 10.1016/j.nima.2013.04.029. arXiv: 1301.2703 [hep-ex].

[707] Bernard Aubert et al. "The BaBar detector". In: *Nucl. Instrum. Meth. A* 479 (2002), pp. 1–116. DOI: 10.1016/S0168-9002(01)02012-5. arXiv: hep-ex/0105044.

[708] James D. Wells. "Annihilation cross-sections for relic densities in the low velocity limit". In: (Mar. 1994). arXiv: hep-ph/9404219.

[709] Andrea Mitridate and Alessandro Podo. "Bounds on Dark Matter decay from 21 cm line". In: *JCAP* 05 (2018), p. 069. DOI: 10.1088/1475-7516/2018/05/069. arXiv: 1803.11169 [hep-ph].

[710] Guido D'Amico, Paolo Panci, and Alessandro Strumia. "Bounds on Dark Matter annihilations from 21 cm data". In: *Phys. Rev. Lett.* 121.1 (2018), p. 011103. DOI: 10.1103/PhysRevLett.121.011103. arXiv: 1803.03629 [astro-ph.CO].

[711] Tracy R. Slatyer and Chih-Liang Wu. "General Constraints on Dark Matter Decay from the Cosmic Microwave Background". In: *Phys. Rev. D* 95.2 (2017), p. 023010. DOI: 10.1103/PhysRevD.95.023010. arXiv: 1610.06933 [astro-ph.CO].

[712] P. A. R. Ade et al. "Planck 2015 results. XIII. Cosmological parameters". In: *Astron. Astrophys.* 594 (2016), A13. DOI: 10.1051/0004-6361/201525830. arXiv: 1502.01589 [astro-ph.CO].

Appendix A

Mathematical details

This appendix provides a detailed derivation of the dark fermion mass eigenstates in the not-so-inelastic Dark Matter (niDM) model introduced in chapter 3. We explicitly perform the diagonalization of the fermion mass matrix arising after spontaneous symmetry breaking in the dark sector, including the effects of both scalar and vector portal couplings, and clarify the role of the $\mathcal{CP}$-violating phase in determining the physical parameters of the model. In appendix A.2, we also present mathematical details regarding the properties of interaction coefficients for a generic fermionic niDM scenario—such a framework was explored in chapter 7. Furthermore, we include a derivation of oscillations between DM states (analogous to neutrino oscillations), which can arise in generic fermionic niDM models. These oscillations were briefly discussed in the outlook of chapter 8.

A.1 Details on the mass diagonalization

To determine the mass eigenstates of the dark fermions, we rewrite the Lagrangian $\mathcal{L}_\chi$ in eq. (3.20) using only the left-handed fields, χ_L and χ_R^c, in a two-component notation

$$\Psi = \begin{pmatrix} \chi_L \\ \chi_R^c \end{pmatrix} . \tag{A.1}$$

Then, adopting the unitary gauge, where

$$H' = \frac{1}{\sqrt{2}}(h' + w) \qquad \text{and} \qquad H = \frac{1}{\sqrt{2}}(0, h + v)^T , \tag{A.2}$$

the Lagrangian becomes

$$\mathcal{L}_\chi = \Psi^\dagger \gamma^0 (i\partial\!\!\!/ - A\!\!\!/' I_{A'})\Psi + \Psi^T C^{-1}(M + h' I_{h'})\Psi + \text{h.c.} , \tag{A.3}$$

with

$$I_{A'} = e' \begin{pmatrix} 1 & 0 \\ 0 & -1 \end{pmatrix}, \quad M = \begin{pmatrix} y_L w & \frac{m_D}{2} \\ \frac{m_D}{2} & y_R w \end{pmatrix}, \quad I_{h'} = y_L \begin{pmatrix} 1 & 0 \\ 0 & 1 + \delta_y \end{pmatrix} , \tag{A.4}$$

and

$$\delta_y = \frac{y_R - y_L}{y_L}\,. \tag{A.5}$$

According to the Takagi factorization lemma [697–699], any complex symmetric mass matrix M can be diagonalized via a unitary transformation U. Following the conventions in Ref. [700], we define the new field basis:

$$\Psi' = \begin{pmatrix} \psi_1' \\ \psi_2' \end{pmatrix} = U\Psi\,, \tag{A.6}$$

with

$$U = \begin{pmatrix} \cos\theta & e^{i\phi}\sin\theta \\ -e^{-i\phi}\sin\theta & \cos\theta \end{pmatrix}\,, \tag{A.7}$$

where

$$\cos\theta = \frac{1}{\sqrt{1+t^2}}, \qquad t = \frac{w(y_R^2 - y_L^2) + D}{m_d\sqrt{\Delta}}\,, \tag{A.8}$$

and

$$D^2 = w^2(y_R^2 - y_L^2)^2 + m_d^2\Delta, \qquad \Delta = y_L^2 + 2y_L y_R\cos(2\phi_d) + y_R^2\,. \tag{A.9}$$

The phase ϕ is determined via

$$e^{i\phi} = \frac{\kappa}{|\kappa|} \qquad \text{with} \qquad \kappa = y_L e^{i\phi_d} + y_R e^{-i\phi_d}\,, \tag{A.10}$$

which leads to

$$\phi = \begin{cases} \text{sign}[(y_L - y_R)\sin\phi_d]\,\arccos\left(\dfrac{y_L + y_R}{\sqrt{\Delta}}\cos\phi_d\right), & \text{if } (y_L - y_R)\sin\phi_d \neq 0\,, \\ \arccos\left(\dfrac{y_L + y_R}{\sqrt{\Delta}}\cos\phi_d\right), & \text{otherwise.} \end{cases} \tag{A.11}$$

This procedure leads to a diagonal mass matrix $M' = \text{diag}(\sigma_1, \sigma_2)$. However, σ_i may contain imaginary parts given their phases

$$e^{i\gamma_1} = \frac{\sigma_1}{|\sigma_1|} \qquad \text{and} \qquad e^{i\gamma_2} = \frac{\sigma_2}{|\sigma_2|}\,, \tag{A.12}$$

where

$$\sigma_1 = y_L w + \frac{m_d}{2} t\, e^{i(\phi_d - \phi)} = \frac{1}{2}\frac{w(y_L^2 + 2y_L y_R e^{-2i\phi_d} + y_R^2) + D}{y_L + y_R e^{-2i\phi_d}}\,, \tag{A.13}$$

$$\sigma_2 = y_R w - \frac{m_d}{2} t\, e^{i(\phi_d + \phi)} = \frac{1}{2}\frac{w(y_L^2 + 2y_L y_R e^{-2i\phi_d} + y_R^2) - D}{y_L e^{-2i\phi_d} + y_R}\,. \tag{A.14}$$

To obtain positive definite mass eigenvalues, we left-multiply the unitary matrix U by $\mathrm{diag}(e^{i\gamma_1/2}, e^{i\gamma_2/2})$, leading to a new unitary transformation

$$U'' = \begin{pmatrix} e^{i\gamma_1/2} & 0 \\ 0 & e^{i\gamma_2/2} \end{pmatrix} U\,, \tag{A.15}$$

and the fields

$$\Psi'' = \begin{pmatrix} \psi_1 \\ \psi_2 \end{pmatrix} = U''\Psi\,. \tag{A.16}$$

We now define the Majorana mass eigenstates:

$$\chi_1 = \psi_1 + \psi_1^c, \qquad \chi_2 = \psi_2 + \psi_2^c\,, \tag{A.17}$$

and using $P_L\chi_i = \psi_i$, the Lagrangian becomes:

$$\mathcal{L}_\chi = \frac{1}{2}\bar\chi_i(i\partial\!\!\!/ - m_i)\chi_i + \frac{1}{2}e' A'_\mu\,\bar\chi_i(i\alpha_{ij} + \beta_{ij}\gamma^5)\gamma^\mu\chi_j \\ - \frac{1}{2}y_L h'\,\bar\chi_i(\hat\alpha_{ij} + i\hat\beta_{ij}\gamma^5)\chi_j\,, \tag{A.18}$$

where the Majorana fields have masses given by

$$m_1^2 = m_d^2 + 2w^2(y_L^2 + y_R^2) + 2wD, \quad m_2^2 = m_d^2 + 2w^2(y_L^2 + y_R^2) - 2wD\,, \tag{A.19}$$

and the interaction coefficients are the given in tables 3.2 and 3.3. The Majorana fields χ_1 and χ_2 are the physical propagating fields—since they are the fermionic mass eigenstates of $\mathcal{L}_\chi$—corresponding to χ^* and χ in our notation of chapter 3.[1]

To express these results in terms of the physical Majorana masses m_1 and m_2, we must reparameterize m_d and ϕ_d as

$$m_d^2 = \bar m^2 - 2w^2(y_L^2 + y_R^2), \tag{A.20}$$

$$\cos(2\phi_d) = \frac{1}{2w^2 y_L y_R}\left[\frac{1}{4m_d^2}\left(\Delta\bar m^4 - 4w^4(y_R^2 - y_L^2)^2\right) - w^2(y_R^2 + y_L^2)\right] \tag{A.21}$$

$$= \frac{\Delta\bar m^4 + 4w^2(w^2(y_L^4 + 6y_L^2y_R^2 + y_R^4) - \bar m^2(y_L^2 + y_R^2))}{8w^2 y_L y_R(\bar m^2 - 2w^2(y_L^2 + y_R^2))}\,, \tag{A.22}$$

where

$$\bar m^2 = \frac{m_1^2 + m_2^2}{2}, \qquad \Delta\bar m^2 = \frac{m_1^2 - m_2^2}{2}\,.$$

Consistency of this reparameterization imposes:

$$\bar m^2 \geq 2w^2(y_L^2 + y_R^2), \tag{A.23}$$

$$2w(y_L + y_R)\sqrt{\bar m^2 - w^2(y_L + y_R)^2} \geq \Delta\bar m^2 \geq 2w|y_R - y_L|\sqrt{\bar m^2 - w^2(y_R - y_L)^2}\,, \tag{A.24}$$

[1] A common notation found in the literature is $\chi_1 \equiv \chi$ and $\chi_2 \equiv \chi^*$.

along with the trivial constraint $\bar{m}^2 \geq \Delta\bar{m}^2$.

Finally, since the consistency checks are involved and multiple values of ϕ_d correspond to the same mass spectrum (one in each quadrant), it is practical to treat the $\mathcal{CP}$-violating phase ϕ_d as an input parameter. For instance, one may adopt a small $\phi_d \ll 1$, which allows the two mass m_1 and m_2 to serve as approximate free parameters, since the Majorana masses eq. (A.19) are only quadratic in ϕ_d. Alternatively, specific values such as $\phi_d = \pi/2$ can simplify the diagonalization—as done in chapter 5 where a maximal $\mathcal{CP}$-violating phase was considered. Most often, one simply adopts $\phi_d = 0$.

A.2 Properties of the Interaction Coefficients

In this section, we summarize the bilinear identities used to derive the symmetry properties of the interaction coefficients appearing in the generic niDM effective Lagrangian introduced in chapter 7.

For two generic fermion fields χ_i and χ_j (either Dirac or Majorana), the following Hermitian conjugation relations hold:

- $(\bar{\chi}_i\chi_j)^\dagger = \bar{\chi}_j\chi_i \;\Rightarrow\; \hat{\alpha}_{ij} = \hat{\alpha}^*_{ji}$;
- $(\bar{\chi}_i\gamma_5\chi_j)^\dagger = -\bar{\chi}_j\gamma_5\chi_i \;\Rightarrow\; \hat{\beta}_{ij} = \hat{\beta}^*_{ji}$;
- $(\bar{\chi}_i\gamma_\mu\chi_j)^\dagger = \bar{\chi}_j\gamma_\mu\chi_i \;\Rightarrow\; \alpha_{ij} = -\alpha^*_{ji}$;
- $(\bar{\chi}_i\gamma_5\gamma_\mu\chi_j)^\dagger = \bar{\chi}_j\gamma_5\gamma_\mu\chi_i \;\Rightarrow\; \beta_{ij} = \beta^*_{ji}$.

In the special case where χ_i and χ_j are Majorana fermions, the bilinears also satisfy transposition symmetry relations:

- $(\bar{\chi}_i\chi_j)^T = \bar{\chi}_j\chi_i \;\Rightarrow\; \hat{\alpha}_{ij} = \hat{\alpha}_{ji}$;
- $(\bar{\chi}_i\gamma_5\chi_j)^T = \bar{\chi}_j\gamma_5\chi_i \;\Rightarrow\; \hat{\beta}_{ij} = \hat{\beta}_{ji}$;
- $(\bar{\chi}_i\gamma_\mu\chi_j)^T = -\bar{\chi}_j\gamma_\mu\chi_i \;\Rightarrow\; \alpha_{ij} = -\alpha_{ji}$;
- $(\bar{\chi}_i\gamma_5\gamma_\mu\chi_j)^T = \bar{\chi}_j\gamma_5\gamma_\mu\chi_i \;\Rightarrow\; \beta_{ij} = \beta_{ji}$.

Combining the Hermiticity and transposition properties, we conclude that all interaction coefficients are real for Majorana fermions.

A.3 Extra: **Oscillating Dark Matter**

Looking at the generic niDM effective Lagrangian introduced in chapter 7, we observe that the dark sector can exhibit a rich flavor structure. This naturally raises the question: could dark matter particles undergo oscillations analogous to those of SM neutrinos? In particular, when the mass splitting between dark matter states is small, why would such oscillations not occur?

Indeed, dark matter may exhibit oscillatory behavior. In this section, we explicitly derive the oscillation probabilities, following the approach of Ref. [701]. As in the case of neutrinos, the oscillation phenomenon arises from quantum interference between amplitudes when the propagating intermediate states are kinematically indistinguishable.

We focus on the case of DM searches via scattering processes at high-energy facilities [702, 703], as these events closely parallel SM neutrino oscillations. In such scenarios, DM particles are produced at high energies without resolving their mass eigenstates. After propagating over a finite distance, they scatter off electrons or nuclei at downstream detectors. Due to the high energies involved and the limited kinematic information typically accessible in these experiments, it is not possible to determine which specific mass eigenstates participated in the scattering process. This lack of resolution enables interference between amplitudes involving different intermediate states—thereby allowing DM oscillations to occur, as we demonstrate below.

We begin with a generic interaction Lagrangian:

$$\mathcal{L}_\chi^I = \frac{1}{2} e' A'^\mu \, \bar{\chi}_i (i\alpha_{ij} + \beta_{ij}\gamma^5)\gamma_\mu \chi_j \,, \tag{A.25}$$

and consider the scattering process illustrated in fig. A.1.

The total amplitude for producing a final dark matter state χ_i which subsequently scatters into χ_j is given by:

$$\mathcal{M}_{ij} = \sum_k \mathcal{M}_{ik}^P \, e^{-i\frac{m_k^2}{2E}L} \, \mathcal{M}_{kj}^S \,, \tag{A.26}$$

where E is the energy of the propagating DM state, L is the propagation distance from the production vertex to the detector, and $\mathcal{M}_{ik}^{P(S)}$ are the production (scattering) amplitudes.

To simplify the analysis, we assume:

- scattering energies well above all relevant masses, $E \gg m_\chi, m_e$;
- a heavy dark photon, $m_{A'} \gg m_\chi$;
- a small mass splitting $\delta \ll m_\chi$.

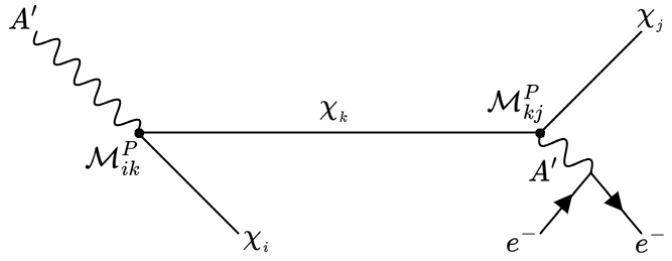

Figure A.1: Schematic Feynman diagram illustrating the production and detection of DM particles at high-energy facilities. The DM mass eigenstates χ_i and χ_k are produced via a dark photon A' decay. The intermediate state χ_k propagates to the detector, where it scatters off an electron (or a nucleus) into χ_j. The full amplitude includes interference between diagrams with both χ and χ^* exchange.

Under these conditions, we may ignore the γ^5-structure differences and define:

$$\mathcal{M}^{P(S)}_{ij} \simeq (i\alpha_{ij} + \beta_{ij})\mathcal{M}^{P(S)} \equiv \kappa_{ij}\,\mathcal{M}^{P(S)}\,, \tag{A.27}$$

where $\kappa_{ij} \in \mathbb{C}$. The diagonal elements are real since $\beta_{ii} \in \mathbb{R}$ and $i\alpha_{ii} \in \mathbb{R}$ (from the coefficients properties of the previous section).

The total amplitude becomes:

$$\begin{aligned}\mathcal{M}_{ij} &= \mathcal{M}^P\mathcal{M}^S \sum_k \kappa_{ik}\kappa_{kj} e^{-i\frac{m_k^2}{2E}L} \\ &= \mathcal{M}^P\mathcal{M}^S e^{-i\frac{m_{\chi^*}^2}{2E}L}\left(\kappa_{i\text{-}}\kappa_{\text{-}j}e^{i\frac{\delta^2 L}{2E}} + \kappa_{i*}\kappa_{*j}\right)\,,\end{aligned} \tag{A.28}$$

where $\delta^2 = m^2_{\chi^*} - m^2_\chi$ and we used a specific two-state system notation for clarity.

The averaged squared amplitude relevant for the cross sections is:

$$\begin{aligned}\overline{|\mathcal{M}_{ij}|^2} &= \overline{|\mathcal{M}^P|^2}\,\overline{|\mathcal{M}^S|^2}\sum_k\sum_{k'} \kappa_{ik}\kappa_{kj}e^{-i\frac{m_k^2}{2E}L}\,\kappa^*_{ik'}\kappa^*_{k'j}e^{i\frac{m_{k'}^2}{2E}L} \\ &= A\left(|\kappa_{i\text{-}}\kappa_{\text{-}j}|^2 + |\kappa_{i*}\kappa_{*j}|^2 + 2\Re\left[\kappa_{i\text{-}}\kappa_{\text{-}j}\kappa^*_{i*}\kappa^*_{*j}e^{i\frac{\delta^2 L}{2E}}\right]\right)\,,\end{aligned} \tag{A.29}$$

with $A = \overline{|\mathcal{M}^P|^2}\,\overline{|\mathcal{M}^S|^2}$.

Since κ is Hermitian (see appendix A.2), we can always rotate away any complex phase via a unitary transformation:

$$\kappa = U\kappa' U^\dagger \quad \text{with} \quad \kappa' \in \mathbb{R}, \quad U = \text{diag}(e^{i\phi}, 1), \quad \tan\phi = \frac{\alpha_{\text{-}*}}{\beta_{\text{-}*}}\,.$$

Assuming $\beta_{\text{-}*} \geq 0$, the rotation angle is uniquely defined.[2]

[2] If $\beta_{\text{-}*} < 0$, the correct angle is adjusted by adding or subtracting π depending on the sign of $\alpha_{\text{-}*}$.

In the rotated (real) basis, the squared amplitudes simplify:

$$\overline{|\mathcal{M}_{--}|^2} = A\left[\kappa_{--}'^4 + \kappa_{-*}'^4 + 2\kappa_{--}'^2\kappa_{-*}'^2\cos\left(\frac{\delta^2 L}{2E}\right)\right], \tag{A.30}$$

$$\overline{|\mathcal{M}_{-*}|^2} = \overline{|\mathcal{M}_{*-}|^2} = A\kappa_{-*}'^2\left[\kappa_{--}'^2 + \kappa_{**}'^2 + 2\kappa_{--}'\kappa_{**}'\cos\left(\frac{\delta^2 L}{2E}\right)\right], \tag{A.31}$$

$$\overline{|\mathcal{M}_{**}|^2} = A\left[\kappa_{**}'^4 + \kappa_{-*}'^4 + 2\kappa_{**}'^2\kappa_{-*}'^2\cos\left(\frac{\delta^2 L}{2E}\right)\right]. \tag{A.32}$$

Summing over all possible final states:

$$\sum_{i,j}\overline{|\mathcal{M}_{ij}|^2} = A\left[\kappa_{--}'^4 + \kappa_{**}'^4 + 2\kappa_{-*}'^2\left(\kappa_{--}'^2 + \kappa_{**}'^2 + (\kappa_{--}' + \kappa_{**}')^2\cos\left(\frac{\delta^2 L}{2E}\right)\right)\right]. \tag{A.33}$$

Alternatively, using implicit equal indices summation:

$$\sum_{i,j}\overline{|\mathcal{M}_{ij}|^2} = A\left[(\kappa_{ik}'\kappa_{ki}')^2 + 2\kappa_{-*}'^2\left(\sum_i \kappa_{ii}'^2 + (\kappa_{ii}')^2\cos\left(\frac{\delta^2 L}{2E}\right)\right)\right]. \tag{A.34}$$

This result explicitly demonstrates that DM oscillatory behavior can be physically realized, as shown by the presence of the interference term proportional to $\cos(\delta^2 L/2E)$ in the total cross section. However, no such behavior arises in two-flavor models where either (i) the off-diagonal coupling κ_{-*}' vanishes—such as in the case of two left-handed chiral fermions with equal charges—or (ii) the diagonal couplings satisfy $\kappa_{--}' = -\kappa_{**}'$, as in the standard niDM scenario (considered in chapter 3) where fermions have opposite charges. In both cases, the oscillation term cancels out in the summed amplitude, and no flavor interference remains.

To allow for observable DM oscillations in a UV-complete niDM framework, one possibility is to introduce at least three chiral fermions in the dark sector—such as neutrinos in the SM. This allows for gauge anomaly cancellation while still maintaining two of the flavors nearly degenerate in mass, permitting coherent flavor transitions over macroscopic distances. Alternatively, one may consider scenarios with Dirac fermions—such as the i2DM model [478]—where oscillations can occur even in two-flavor systems due to the richer structure of the interaction matrix.

Appendix B

FeynRules Implementation

To facilitate the use of various High Energy Physics computational tools, we have developed model files for the `FeynRules` Mathematica® package (version 2.3) [534] describing the *not-so-inelastic Dark Matter* model outlined in chapter 3.

Tables B.1 and B.2 list the fields and parameters used in the most generic model implementation, respectively. We introduced the `FeynRules` flavor-index "`DarkGeneration`", denoted by $d = 1, 2$, to manage interaction coefficients efficiently. Note that $d = 1$ corresponds to the heavier state (i.e., $\chi_1 \equiv \chi^*$) and that "ch" (χ) denotes the vector (χ_1, χ_2). In addition, $A' \equiv Z'$, $H' \equiv S$ and $g_\chi \equiv e'$. External parameters are marked with the symbol ⌜.

Modifications to the base `SM.fr` file are minimal: only lines marked with the comment "`Giovani DVG`" are changed. The standard restrictions remain unaltered—namely, `DiagonalCKM.rst`, `Massless.rst` and `MasslessAllQ.rst`.[1]

Six new files were added to complete the model implementation:
- `pDFDM2M.fr`: defines the dark sector model,
- `DarkPhoton.rst`: places the theory in the dark photon regime by removing Z–Z' mixing,
- `ScalarPortal.rst` and `VectorPortal.rst`: enable or disable the scalar and vector portal interactions independently (by setting the respective mixing, $\theta_{h'h}$ and ϵ, to zero),
- `DecoupleDarkHiggs.rst` and `DecoupleVectorMediator.rst`: sets extremely large masses on the respective mediators, effectively decoupling them from the theory.

[1] Note that `MasslessAllQ.rst` sets all quark Yukawa couplings, masses, and widths to zero, suppressing any tree-level couplings between quarks and the scalar portal.

[2] `MicrOmegas` [375] requires that DM candidates (odd under R-parity, i.e., a new Z_2 symmetry) be named with the "∼" prefix. Thus, χ_i is named "∼ch$i$". All other fields follow their symbolic names.

[3] With decay width defined by `WH1`⌜.

Table B.1: Fields and their masses in the full `FeynRules` implementation. The third row shows the assigned PDG codes.

χ	χ_i	Z'	S	s	$\hat{Z}'$	$s_{Z'}$	$S-w$	A	Z	H_1	H_2
ch	ch$i$[2]	Zp	Sdf	Sd	Zhp	DG0	Sdfnovev	Au	Zu	H1	H2
Mch	Mch$i$				MZp$^{\ulcorner}$	MZp$^{\ulcorner}$				MH1$^{\ulcorner}$[3]	MH2$^{\ulcorner}$
	53+i				53	52				25	51

Table B.2: Parameters defined in the full `FeynRules` implementation.

g_χ	μ_s^2	λ_s	λ_{sh}	m_d	ϕ_d	y_L
gch$^{\ulcorner}$	mussq	ls	lsh	Mdi	phdi	ychL$^{\ulcorner}$
y_R	ϵ	q_ϕ	$\bar{m}^2$	$\Delta\bar{m}^2$	θ_{hs}	w
ychR$^{\ulcorner}$	epsilon$^{\ulcorner}$	P$^{\ulcorner}$	MchBar2$^{\ulcorner}$	DMchBar2$^{\ulcorner}$	thetahs$^{\ulcorner}$	dvev
α_{ij}	β_{ij}	$\hat{\alpha}_{ij}$	$\hat{\beta}_{ij}$	ϵ_Z		$\epsilon_{Z'}$
alphch[i,j]	betach[i,j]	halphch[i,j]	hbetach[i,j]	epsilonZ		epsilonZp
Δ	D	δ_y		θ	ϕ	γ_i
Deltatemp	Dtemp	deltaychRL		thetach	phch	gamch[i]

B.1 Small complex phase

In its most general form, the model features complex mass matrices and phase-dependent interactions due to the $\mathcal{CP}$-violating parameter ϕ_d. Implementing this fully general version in `FeynRules` is highly non-trivial, as many interaction coefficients depend on nontrivial diagonalization procedures and complex phases. In addition, consistency checks must be performed for each choice of input parameters—see appendix A for details.

For this reason, we also provide a simplified implementation valid in the limit $\phi_d \ll 1$, where masses of the physical eigenstates can be approximately defined independently of ϕ_d. In this regime, the interaction coefficients are easier to handle both analytically and numerically. Specifically, the masses `Mch1` and `Mch2` are treated as external parameters, and `phdi` is likewise considered an input (though it must remain small for consistency). Conversely, `ychL` is no longer an external parameter, as it can be expressed in terms of the fermion masses in this limit.

Appendix C

Analytical recasting of beam dump experiments

In this appendix, we revisit the procedure for analytically recasting experimental constraints and estimating the sensitivities of beam dump experiments.

Because dark matter (DM) particles in our model are produced via decays of the mediator, the DM flux can be inferred directly from the number of mediators produced in the experiment. In standard analyses of Majorana DM, one typically considers invisible signatures. In such cases, the number of missing energy events—which can be extracted from exclusion limits in background-free analyses—provides a direct estimate of the number of dark photons produced.

In the case of inelastic DM (iDM) searches, the number of dark photons produced can be estimated using the probability that an excited DM state decays inside the detector volume, denoted by $\mathcal{P}_{\rm dec}$, defined as:

$$\mathcal{P}_{\rm dec} = \exp\left[-\frac{l_{\rm min}}{\tau\langle p\rangle}\right] - \exp\left[-\frac{l_{\rm max}}{\tau\langle p\rangle}\right] , \tag{C.1}$$

where $l_{\rm min/max}$ denote the minimum and maximum distance from the production point to the boundaries of the decay volume, and $\langle p\rangle$ is the average absolute momentum of the decaying particle (i.e., its Lorentz factor times velocity).[1] Since the detection efficiency is the same for niDM and iDM, which share the same decay channels, the number of dark photons producing DM particles that reach the detector can again be estimated using $\mathcal{P}_{\rm dec}$ and the exclusion limits from background-free experiments.

In both scenarios, a straightforward analytical estimate of the number of excited states decaying inside the detector is possible. Corrections may arise from the kinematic distributions of the decay products, finite detector resolution, or geometric effects, but these are expected to lead to second order corrections. This is because (i) niDM and iDM share similar decay phenomenology, and (ii) for invisible searches, even small visible signals are sufficient to veto events.

[1] Typically estimated from the initial beam energy or fitted to data.

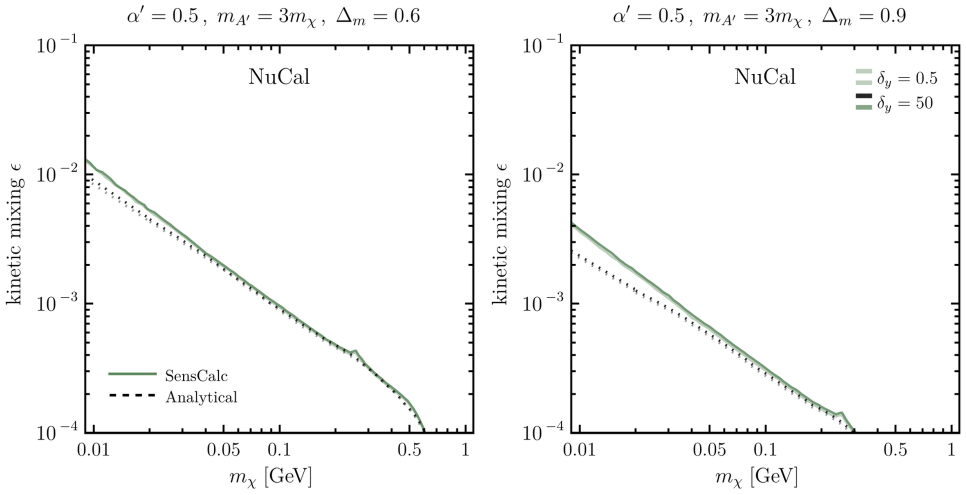

Figure C.1: Comparison between analytical (dashed) and numerical (solid) recasted bounds on the kinetic mixing ϵ from the NuCal beam dump experiment [615]. Each panel shows different relative mass splittings between dark sector fermions, $\Delta_m = (0.6, 0.9)$. The opacity of the curves indicates different values of the left-right Yukawa asymmetry, $\delta_y = (0.5, 50)$.

Corrections due to non-zero backgrounds become relevant only in experiments with significant background levels.

As an illustration, fig. C.1 compares the analytical recasting method applied to the NuCal experiment [615] with the numerical results obtained using the modified `SensCalc` [1] implementation of chapter 4. In the remainder of this appendix, we present in detail the recasting of the missing energy search of NA64, as this data set plays a central role in constraining the niDM model with a vector mediator (see chapter 4).

C.1 Recasting NA64 missing energy searches

The NA64 experiment targets dark photon (A') production followed by invisible decays, as is the case for Majorana Dark Matter (mDM). In our model, however, A' decays into χ and χ^*, and the excited state χ^* may subsequently decay within the detector volume, producing visible signals that may cause the event to be vetoed.

The number of events that pass the NA64 selection criteria for a given set of niDM parameters, $\mathbf{x}_{\text{niDM}} = (m_{A'}, \delta_y, \Delta_m, m_\chi, \alpha', \epsilon)$, can be written as:

$$N_{\text{niDM}}(\mathbf{x}_{\text{niDM}}) = N_{A'}(m_{A'}) - \epsilon^2 \left[\sum_{i=\text{br,an}} f_i(m_{A'})\, g(\mathbf{a}_i, \mathbf{x}_{\text{niDM}}) \right] . \tag{C.2}$$

Here, the first term corresponds to the total number of dark photons, while the second term accounts for vetoed events due to χ^* decays in the detector.

We distinguish between two production channels: production via electron-nucleus bremsstrahlung, $e^- Z \to e^- Z A'$ ($i = \mathrm{br}$), and via resonant annihilation of secondary positrons with atomic electrons, $e^+ e^- \to A'$ ($i = \mathrm{an}$).

The production rates f_i are normalized such that:

$$N_{A'}^{90\%\ \mathrm{exc.}}(m_{A'}) = \epsilon^2_{90\%\ \mathrm{exc.}} \left[f_{\mathrm{br}}(m_{A'}) + f_{\mathrm{an}}(m_{A'}) \right] , \tag{C.3}$$

where $\epsilon_{90\%\ \mathrm{exc.}}$ is the experimental bound reported by NA64 [344, 513] (directly applying to mDM).

The functions g_i give the fraction of events vetoed by NA64 due to χ^* decays in the detector, such that $N_{\mathrm{niDM}} = N_{A'}(m_{A'})$ for $g_i = 0$ and $N_{\mathrm{niDM}} = 0$ for $g_i = 1$. These veto functions depend on the specific experimental conditions of NA64, collectively denoted by $\mathbf{a}_i$.

The veto functions g_i decompose into two terms. The first describes decays of χ^* inside the ECAL, which decrease the total missing energy of the event and may lead to an event being vetoed if $E_{\mathrm{missing}} < 50$ GeV. The second describes decays that would leave a non-zero energy deposit either in the VETO or within the HCAL, both of which cause an event to be vetoed.

A general form for the veto function g can be written as:

$$\begin{aligned} g(\mathbf{a}_i, \mathbf{x}_{\mathrm{niDM}}) = \Omega_i \left(1 - e^{-(L_{\mathrm{ECAL}} - d_i^{\mathrm{low}})/\ell_i^{\mathrm{low}}} \right) \\ + \eta\, e^{-(L_{\mathrm{HCAL}} - d_i^{\mathrm{ave}} - l)/\ell_i^{\mathrm{ave}}} \left(1 - e^{-(L_{\mathrm{HCAL}} + l)/\ell_i^{\mathrm{ave}}} \right) , \end{aligned} \tag{C.4}$$

where

$$\ell_i^j = \frac{\tau_{\chi^*} \sqrt{(E^j_{\chi^*,i})^2 - m^2_{\chi^*}}}{m_{\chi^*}} \tag{C.5}$$

is the decay length of χ^*, which we calculate separately for low-energy dark photons ($j = \mathrm{low}$) and for all dark photons ($j = \mathrm{ave}$).

All parameters appearing in the veto functions g are explained in detail in table C.1.

Finally, we assume that $E^j_{\chi^*,i} = E^j_i/2$, i.e., that the dark photon energy is equally shared between the two daughter particles. This is a reasonable approximation since dark photon energies are typically much larger than the masses of the final-state particles.

With a physical model for the veto functions at NA64, we can benchmark our analytical predictions against those available in the literature for the iDM

[2] This parameter defines an effective ECAL length for low energy dark photon events.

Table C.1: List of parameters used in the veto functions for reinterpreting missing energy bounds from the NA64 experiment [344, 513]. The values in the first row for each parameter correspond to the bremsstrahlung channel ($i = \text{br}$), which is the only one used for the fits. The second row corresponds to the annihilation channel ($i = \text{an}$).

Description	Symbol	Estimated value	Fitted value
Fraction of produced dark photons with low energy ($50\,\text{GeV} \leq E_{A'} \leq 75\,\text{GeV}$)	Ω_{br} Ω_{an}	20% 50%	4% –
Average energy of low energy dark photons producing a signal	$E_{\text{br}}^{\text{low}}$ $E_{\text{an}}^{\text{low}}$	64 GeV Eq. (C.6)	74 GeV –
Low energy dark photon production position plus containment length[2]	$d_{\text{br}}^{\text{low}}$ $d_{\text{an}}^{\text{low}}$	$3X_0$ $d_{\text{br}}^{\text{low}} + 2X_0$	$22X_0$ –
Average energy of dark photons producing a signal	$E_{\text{br}}^{\text{ave}}$ $E_{\text{an}}^{\text{ave}}$	85 GeV Eq. (C.6)	78 GeV –
Average energy dark photon production position	$d_{\text{br}}^{\text{ave}}$ $d_{\text{an}}^{\text{ave}}$	X_0 $d_{\text{br}}^{\text{ave}} + 2X_0$	$11X_0$ –
A' veto efficiency for events leaving hits at VETO + HCAL	η	100%	100%
ECAL length	L_{ECAL}	1 m ($40X_0$)	–
HCAL length	L_{HCAL}	6.5 m	–
Leakage length of showers produced at ECAL leacking energy to VETO + HCAL	l	$5X_0$	$7X_0$

scenario. This comparison allows us to validate our parametrisation and calibrate the various detector-related parameters we introduced. For this validation, we set $f_{\text{an}} = 0$, since the positron annihilation production channel has not been included in previous iDM studies [80, 479].

As a first step, we estimate the parameters $\mathbf{a}_{\text{br}}$ based on available information from NA64 technical reports [553] and prior analyses [704]; these estimates are listed in the third column of table C.1. For the iDM case (i.e., $\delta_y = 0$), our analytical predictions agree with those from Ref. [479] within 14%, with an average deviation of approximately 6%, as shown in fig. C.2.

To further improve this agreement, we perform a fit by varying the $\mathbf{a}_{\text{br}}$ parameters around their estimated values. The best-fit results, shown in the fourth column of table C.1, yield a match to fig. 6 of Ref. [479] with a maximal discrepancy of less than 8% and an average deviation below 2%. Interestingly, the fit reveals that $\Omega_{\text{br}} \ll 1$, indicating that χ^* particles originating from low-energy

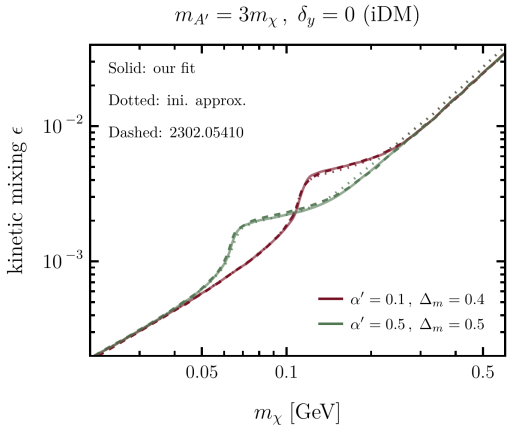

Figure C.2: Comparison of exclusion limits on iDM from the NA64 experiment with 2.84×10^{11} EoT, as obtained in this work (dotted and solid lines) and in Ref. [479] (dashed lines). The dotted curves are based on estimates of the veto function parameters using experimental data, while the solid curves result from fitting these parameters to closely reproduce the bounds from Ref. [479]. Dark photons produced via secondary positron annihilation are not included in the comparison, as they were neglected in the analysis of Ref. [479].

bremsstrahlung dark photons ($E_{A'} \in (50, 75)$ GeV) contribute negligibly to the experimental constraints. We therefore adopt these fitted parameters for our final predictions of bremsstrahlung-induced signals, which dominate over nearly all of the parameter space probed at NA64.

In contrast, no prior studies have analyzed dark photon production from positron annihilation in the context of iDM or niDM [705]. Hence, we cannot benchmark our estimates of $\mathbf{a}_{\rm an}$ against the literature as we did for the bremsstrahlung channel. Nonetheless, we can extract useful information from fig. 1 of Ref. [705] to estimate the average energy of dark photons produced via positron annihilation that are capable of generating missing energy signals.[3] We model the average dark photon energy as

$$E_{\rm an}^{\rm ave}(m_{A'}) = \begin{cases} 50\,\text{GeV}, & m_{A'} < 225\,\text{MeV} \\ 430\,m_{A'} - 47\,\text{GeV}, & m_{A'} \geq 225\,\text{MeV}. \end{cases} \tag{C.6}$$

Finally, we combine both production channels—bremsstrahlung and positron annihilation—to recast NA64 limits on the niDM parameter space using the most recent data release from the collaboration [344].

[3] Since $E_{\rm an}^{\rm ave}$ tends to be small in the relevant parameter region, we approximate $E_{\rm an}^{\rm low} = E_{\rm an}^{\rm ave}$.

Appendix D

Recasting searches at electron–positron colliders

Electron–positron colliders such as PEP-II (BaBar) and SuperKEKB (Belle II) operate at fixed center-of-mass energies $\sqrt{s}$, which provide well-defined event kinematics and a much cleaner background environment compared to hadronic machines. Moreover, because (tree-level) cross sections for electron–positron annihilation can be computed rather straightforwardly, we developed our own dedicated analysis tools in order to maintain full control and understanding of the results.

In this appendix, we describe the two methods employed in this thesis to estimate constraints and sensitivities of searches at this class of colliders. First, we present a fully numerical approach based on Monte Carlo simulations, which we implemented independently. Subsequently, we introduce a semi-analytical approximation, designed to keep closer contact with physical intuition while also providing a reliable cross-check of the simulation results.

D.1 Simulating the collisions

Event generation is performed in the center-of-mass (c.m.) frame by sampling dark photon angles and their corresponding four-momenta according to energy–momentum conservation, based on the analytically computed annihilation cross section $\sigma(e^+e^- \to \gamma A')$—or, more generally, using the relevant cross section for any directly produced particle in the collision. The four-momenta are then boosted to the laboratory frame.

Dark photon decays are subsequently simulated in the A' rest frame, where two-body decays are isotropic. Different dark matter (DM) states are sampled according to the corresponding branching ratios, with kinematics fixed by conservation laws.[1] The final-state momenta are boosted back to the laboratory

[1] Strictly speaking, the process $e^+e^- \to \gamma\chi\chi^*$ should not be factorized into production and

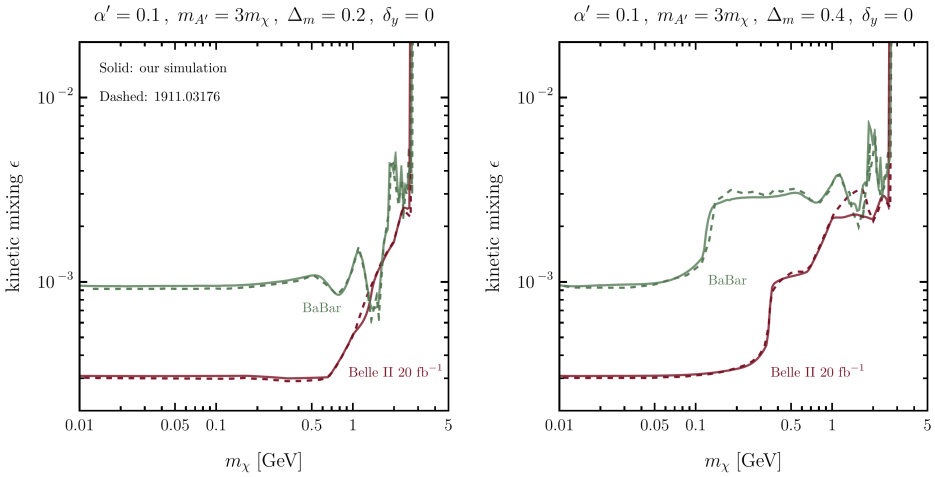

Figure D.1: Comparison of BaBar exclusion limits and Belle II projected sensitivities on iDM from mono-photon searches [91, 488], as obtained in this work (solid lines) and in Ref. [3] (dashed lines).

frame using the A' momenta.

If a χ^* is produced, we sample its lifetime and channel. The decay vertex is then obtained by multiplying the lifetime with the particle momentum. The same procedure is applied to long-lived dark photons or dark Higgs bosons. All (tree-level) cross sections and branching ratios are computed analytically. For the vector portal, we neglect three-body kaon modes and higher-multiplicity decays since they are subdominant in the mass ranges of interest (see chapter 4). For scalar-mediated higher-multiplicity decays, we approximate them as cascades of two-body decays. Mediator decays into SM particles are taken from `SensCalc` [1]. Following Ref. [3], charged pions and kaons are treated as muons in the detector response.

All these steps are implemented in a Mathematica®-based Monte Carlo event generator, available at `/gdvgarcia/niDM/MissingEnergyEEcolliders`. Figure D.1 shows our validation of the simulation against Ref. [3] for missing-energy searches of inelastic DM (iDM), setting $\delta_y = 0$. Details of the cuts and beam conditions used in these analyses are provided in appendix D.3. Validation for displaced-vertex searches is still ongoing; however, for this case we have developed and validated an alternative method, which is discussed in the following section.

decay, for large A' widths—preset in most cases we studied. However, this effect mainly smears the photon and χ^* energies and is negligible within the accuracy goals of this work [3].

D.2 A (semi-)analytical approach

During the development of the Monte Carlo event generator, we realized that in the specific case of two-body decay chains, all relevant distributions can be expressed in analytical form through successive Lorentz boosts. Furthermore, we observed that kinematic cuts on the SM-visible decay products have only a minor impact across most of the parameter space of interest. Consequently, in many cases the only essential ingredients are the decay position of the (semi-)visible particle(s), together with the direction of the associated photon (when present), in order to determine whether the event is observable.

The procedure is straightforward. As an illustrative example, consider the typical displaced-vertex plus high-energy photon signature in standard iDM [3]. Since the visibly decaying excited state is produced via a two-body dark photon decay, the χ^* four-momentum in the A' rest frame can be written as[2]

$$k_*^{(A')} = \left(E_*,\ p_* \cos\theta_*,\ p_* \sin\theta_* \cos\phi_*,\ p_* \sin\theta_* \sin\phi_*\right), \tag{D.1}$$

with

$$E_*^{(A')} = \frac{m_{A'}^2 - m_\chi^2 + m_{\chi^*}^2}{2m_{A'}}, \qquad p_*^{(A')} = \sqrt{\left(E_*^{(A')}\right)^2 - m_{\chi^*}^2}. \tag{D.2}$$

Because of the kinematics of two-body decays, the direction of $k_*^{(A')}$ is uniformly distributed, and hence the angular distributions of $\theta_*^{(A')}$ and $\phi_*^{(A')}$ are immediately known.

A similar expression holds for the dark photon four-momentum $k_{A'}^{(\mathrm{CM})}$ in the c.m. frame of the collision, where the A' energy is

$$E_{A'}^{(\mathrm{CM})} = \frac{E_{\mathrm{CM}}^2 + m_{A'}^2}{2E_{\mathrm{CM}}}, \tag{D.3}$$

with E_{CM} the total c.m. collision energy. The azimuthal distribution $\phi_{A'}^{(\mathrm{CM})}$ is uniform, while the polar angle $\theta_{A'}^{(\mathrm{CM})}$ follows the differential cross section $d\sigma/d\theta_{A'}^{(\mathrm{CM})}$, with total cross section $\sigma \equiv \sigma(e^+e^- \to A'\gamma)$. By kinematic relations, this distribution also fixes the polar angle of the SM photon, $\theta_\gamma^{(\mathrm{CM})}$, since $\theta_\gamma^{(\mathrm{CM})} = \pi - \theta_{A'}^{(\mathrm{CM})}$. Consequently,

$$\frac{d\sigma}{d\theta_\gamma^{(\mathrm{CM})}} = -\frac{d\sigma}{d\theta_{A'}^{(\mathrm{CM})}}. \tag{D.4}$$

Boosting $k_{A'}^{(\mathrm{CM})}$ with the c.m. velocity $\vec{v}_{\mathrm{CM}}$ gives $k_{A'}^{(\mathrm{lab})}$, and similarly for the photon. The excited state momentum $k_*^{(\mathrm{lab})}$ is then obtained by boosting

[2] Strictly speaking, each variable x in the following equations should carry the superscript $x^{(A')}$; we omit this for compactness.

$k_*^{(A')}$ with $k_{A'}^{(\mathrm{lab})}$. These lab-frame momenta directly yield the polar angles $\theta_i^{(\mathrm{lab})}$ relevant for the experimental cuts, while the spatial momentum $\vec{p}_*^{\,(\mathrm{lab})}$ combined with the lifetime τ_* determines the excited state vertex position $\vec{l}_*$.

Since the polar angle is defined relative to $\vec{v}_{\mathrm{CM}}$, the azimuthal angles of the photon and dark photon are unaffected by the boost. We may therefore set them to zero without loss of generality, as they are uniformly distributed and detectors typically cover the full azimuthal range—removing the need for an additional integration.[3] With these simplifications, the detection probability density (suppressing lab-frame superscripts for compactness) can be written as

$$\mathcal{D} \equiv \frac{d\mathcal{P}}{d\theta_\gamma^{(\mathrm{CM})}\, d\theta_*^{(A')}\, d\phi_*^{(A')}} = \frac{1}{\sigma}\frac{d\sigma}{d\theta_\gamma^{(\mathrm{CM})}}\,\Theta(\theta_{\min} \le \theta_* \le \theta_{\max}) \times \frac{1}{4\pi}\,\sin\theta_*^{(A')}\left(e^{-R_{\min}/|l_*^{yz}|} - e^{-R_{\max}/|l_*^{yz}|}\right)\left(1 - e^{-X_{\lim}/l_*^x}\right), \quad \text{(D.5)}$$

where Θ is the step function ($\Theta(C) = 1$ if the condition C holds and 0 otherwise). Here $\theta_{\min(\max)}$ denote the detector's angular acceptance, $R_{\min(\max)}$ the minimum (maximum) transverse displacement $|l_*^{yz}|$, and $X_{\lim}$ the maximal (minimal) allowed longitudinal displacement l_*^x if p_{*x} is positive (negative).

Since all quantities in eq. (D.5) are either fixed cuts or analytical functions of the angles $\theta_\gamma^{(\mathrm{CM})}$, $\theta_*^{(A')}$ and $\phi_*^{(A')}$, the total detection probability is obtained by integration:

$$\mathcal{P} = \int_{\theta_{\min}^{(\mathrm{CM})}}^{\theta_{\max}^{(\mathrm{CM})}} d\theta_\gamma^{(\mathrm{CM})} \int_0^{\pi} d\theta_*^{(A')} \int_0^{2\pi} d\phi_*^{(A')}\,\mathcal{D}\,, \quad \text{(D.6)}$$

where $\theta_{\min\,/\,\max}^{(\mathrm{CM})}$ denotes the boosted detector coverage into the c.m. frame of the collision. In addition, events must satisfy kinematic constraints: since the photon must carry at least a certain minimal energy $E_\gamma^{\min}$, the maximal dark photon mass probed is $m_{A'}^{\max} = E_{\mathrm{CM}} - E_\gamma^{\min}$.

Although the method is in principle fully analytical, in practice the integrations in eq. (D.6) must usually be evaluated numerically. Hence the designation "(semi-)analytical approach." In this way, the expected number of detected events at an electron–positron collider is

$$N = \epsilon\,\mathcal{P} N_{A'} \times \mathrm{Br}(\chi^* \to \text{visible})\,\mathrm{Br}(A' \to \chi^*\chi)\,, \quad \text{(D.7)}$$

where $N_{A'} = \sigma\mathcal{L}$ is the number of produced dark photons, $\mathcal{L}$ is the integrated luminosity, ϵ is the displaced-vertex detection efficiency,[4] $\mathrm{Br}(\chi^* \to \text{visible})$ is

[3] Here we assume the beams propagate along the detector axis, such that the polar angle coincides with the detector coverage. This holds exactly for BaBar and is an excellent approximation for Belle II.

[4] An additional factor accounting for photon detection efficiency can be included in ϵ if applicable.

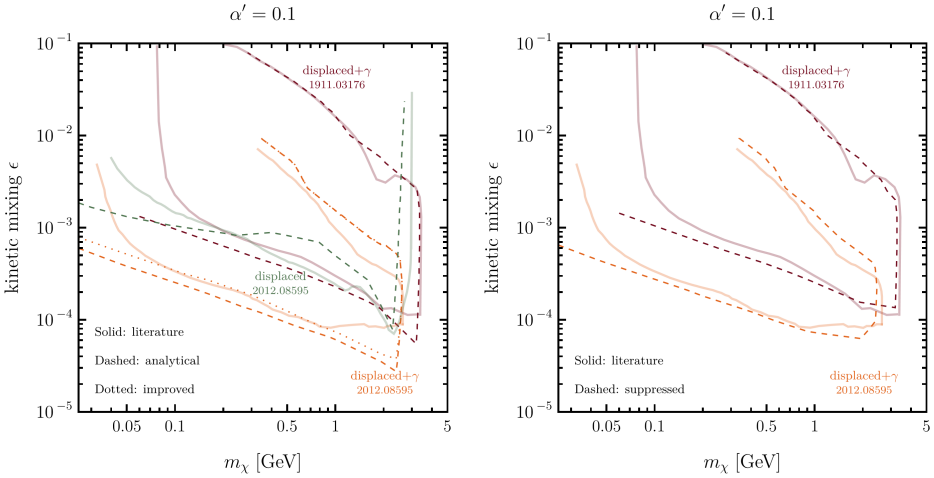

Figure D.2: Validation of the (semi-)analytical approach (dashed) against previous results in the literature (solid) [3, 79]. Estimates are for Belle II sensitivities, though each reference assumes a different integrated luminosity: 20 fb^{-1} for Ref. [3] and 100 fb^{-1} for Ref. [79]. Parameters in Ref. [3]: $m_{A'} = 3m_\chi$, $\Delta_m = 0.4$; in Ref. [79]: $m_{A'} = 4m_\chi$, $m_{h'} = 1$ GeV, $\Delta_m = 1$, $\theta_{h'h} = 10^{-5}$. The labels "displaced+γ" and "displaced" denote, respectively, searches for a displaced vertex accompanied by a high-energy photon, and searches for two vertices with at least one displaced. In the right panel, the sharp kinematic cut in displaced+γ searches, $E_{\rm CM} \geq m_{A'} + E_\gamma^{\rm min}$, has been smoothed. The dotted curve shows an improved analytical treatment, as discussed in the text.

the branching ratio of the excited state into SM-detectable final states, and $\mathrm{Br}(A' \to \chi^*\chi)$ the dark photon branching ratio into $\chi^*\chi$. In standard pseudo-Dirac iDM scenarios with $\epsilon \ll 1$ and $\alpha' \gg \alpha$, one has $\mathrm{Br}(A' \to \chi^*\chi) \simeq 1$ (for no parity breaking, $\delta_y = 0$), and $\mathrm{Br}(\chi^* \to \text{visible}) \approx 1$ when considering only the vector portal and splittings $m_{\chi^*} - m_\chi \lesssim 3$ GeV.

This method is exact in regions where cuts on the visible particles are negligible, which covers a large portion of parameter space. Typically, the visible SM particles from decays have sufficient energy to pass detector thresholds and sufficiently large opening angles, especially for sizeable mass splittings. At low masses ($\lesssim 100$ MeV), however, the large boost reduces the opening angle between decay products, making cuts more relevant. At high masses, the photon energy cut $E_\gamma^{\rm min}$ becomes important, especially near the kinematic endpoint $m_{A'}^{\rm max}$, where the dark photon absorbs nearly all collision energy. To account for this, we introduce a smooth suppression factor $S(m_{A'})$ near threshold, such that the new prediction for the number of detected events is $N' = S(m_{A'})N$. $S(m_{A'})$ is implemented via a sigmoidal interpolation function, interpolating between the regime $m_{A'} \ll m_{A'}^{\rm max}$ (no suppression) and $m_{A'} = m_{A'}^{\rm max}$ (full suppression). The interpolation parameters are tuned using existing results from the literature. We neglect discrepancies at very low mass since our focus lies on $m \gtrsim 100$ MeV, while the

Table D.1: Veto criteria used in the BaBar mono-photon analysis [3]. The variables θ_{lab}, x, and R_{yz} describe the vertex of the visibly decaying particle (typically χ^*) in the laboratory frame: θ_{lab} is the polar angle with respect to the $+x$ direction, x the longitudinal position of the decay, and R_{yz} is the transverse distance from the x axis in the plane perpendicular to it. $E_\gamma^{(\text{CM})}$ and $\theta_\gamma^{(\text{CM})}$ denote, respectively, the photon energy and polar angle in the center-of-mass frame.

Particle Type	Calorimeter / Drift Chamber	Muon System
Electrons	(i) either $E(e^-)$ or $E(e^+) > 150$ MeV (ii) $17^\circ < \theta_{\text{lab}} < 142^\circ$ (iii) -113 cm $< x < 185$ cm (iv) $R_{yz} < 102$ cm	(i) $E(e^+) + E(e^-) > 300$ MeV (ii) $20^\circ < \theta_{\text{lab}} < 150^\circ$ (iii) -223 cm $< x < 297$ cm (iv) $R_{yz} < 243$ cm
Muons	(i) either $p(\mu^-)$ or $p(\mu^+) > 150$ MeV (ii)–(iv) same as electrons	(i) $p(\mu^+) + p(\mu^-) > 300$ MeV (ii)–(iv) same as electrons
Hadrons	Treat as muons	Treat as muons
Photons	$E_\gamma^{(\text{CM})} > 2$ GeV $32.5^\circ < \theta_\gamma^{(\text{CM})} < 99^\circ$	– –

sub-100 MeV region is more appropriately probed by beam-dump experiments.

The semi-analytical approach may be further refined by accounting for the position-dependence of detector efficiencies and by excluding regions where electron final states are removed due to irreducible backgrounds (see table D.4; for details, see Ref. [3]). In practice, such refinements only marginally improve agreement with numerical simulations, while substantially increasing the computation time. Since our baseline implementation already reproduces the literature at the level of accuracy required (relative errors below $\sim 70\%$ for intermediate masses away from thresholds), we adopt this simpler scheme. Near threshold, the interpolation restores comparable accuracy. The validation against earlier studies, including the threshold-suppressed and improved versions, is shown in fig. D.2. The collider setup and selection cuts assumed in these results are detailed in the remainder.

D.3 Set-up and cuts for electron–positron colliders

In this section, we briefly summarize the electron–positron collider experiments considered in this work, namely BaBar and Belle II. We outline their basic properties relevant for our results, together with the selection cuts applied in the analyses of mono-photon and displaced-vertices searches.

BaBar: The BaBar collaboration searched for mono-γ events in a dataset of 53 fb^{-1} [488] collected at the PEP-II asymmetric e^+e^- collider at SLAC. The machine operated at a c.m. energy $\sqrt{s} = 10.58$ GeV, corresponding to the

Table D.2: Veto criteria used in the Belle II mono-photon analysis [3]. Here $\theta_\gamma^{(\mathrm{lab})}$ denotes the polar angle between the $+x$ direction and the photon momentum in the laboratory frame. All remaining variables are defined as in table D.1.

Particle Type	Calorimeter / Drift Chamber	Muon System
Electrons	(i) either $E(e^-)$ or $E(e^+) > 150$ MeV (ii) $17^\circ < \theta_{\mathrm{lab}} < 150^\circ$ (iii) -112 cm $< x < 206$ cm (iv) $R_{yz} < 135$ cm	(i) $E(e^+) + E(e^-) > 300$ MeV (ii) $25^\circ < \theta_{\mathrm{lab}} < 145^\circ$ (iii) -300 cm $< x < 400$ cm (iv) $R_{yz} < 300$ cm
Muons	(i) either $p(\mu^-)$ or $p(\mu^+) > 150$ MeV (ii)–(iv) same as electrons	(i) $p(\mu^+) + p(\mu^-) > 300$ MeV (ii)–(iv) same as electrons
Hadrons	Treat as muons	Treat as muons
Photons	$E_\gamma^{(\mathrm{CM})} > 2$ GeV $\theta_{\mathrm{min}}^{\mathrm{low/high}} < \theta_\gamma^{(\mathrm{lab})} < \theta_{\mathrm{max}}^{\mathrm{low/high}}$	– –

$\Upsilon(4S)$ resonance.[5] The positron beam energy was 3.1 GeV and the electron beam 9.0 GeV, colliding head-on. This configuration implies a boost of the c.m. system along the detector's magnetic field axis of $\beta_x \simeq 0.49$ [707].

Belle II. The potential of Belle II to probe mono-photon signatures, as well as displaced vertices in association with a high-energy photon, was analyzed in Ref. [91]. Their projections were made for an integrated luminosity of 20 fb^{-1} at the SuperKEKB asymmetric e^+e^- collider (KEK), operating at a c.m. energy corresponding to $m_{\Upsilon(4S)}$. The beams consist of 4 GeV positrons and 7 GeV electrons colliding with a crossing angle of 83 mrad. The bisector of this angle aligns with the detector's magnetic field axis, resulting in a c.m. boost of $\vec{\beta} \simeq (0.27, 0.04, 0)$ [91]. Ref. [79] further studied displaced-vertex+γ signatures, as well as di-vertex events with at least one displaced vertex, arising from dark Higgs–strahlung processes $e^+e^- \to A'^* \to A'h'$. These analyses considered larger luminosities of 100 fb^{-1} (already below the data collected by Belle II [82]) and 50 ab^{-1}, which corresponds to the dataset expected by the end of the experiment around 2030.

D.3.1 Missing-energy cuts

A particularly sensitive channel for invisibly decaying dark photons is the mono-photon process

$$e^+e^- \to \gamma A'(\to \chi\chi)\,,$$

[5] Most BaBar data were collected at the $\Upsilon(4S)$ [706], though the analysis in Ref. [488] used mainly data from the $\Upsilon(3S)$ resonance, with non-negligible contributions from the $\Upsilon(2S)$ and off-resonance runs. For the level of accuracy required here, the approximation $\sqrt{s} = 10.58$ GeV is sufficient.

Table D.3: Selection cuts used in the Belle II displaced-vertices analysis [3, 79]. $E_\gamma^{(\mathrm{lab})}$ and $\theta_\gamma^{(\mathrm{lab})}$ denote the photon energy and polar angle in the laboratory frame, respectively. The remaining variables are defined as in table D.1. Photon cuts apply only to displaced+γ searches, while the second-vertex cuts apply exclusively to di-decay searches.

Cut on	**Criteria**
1st Decay Vertex	(i) $0.2\ \mathrm{cm} \leq R_{yz} \leq 60\ \mathrm{cm}$ (ii) $-55\ \mathrm{cm} \leq z \leq 140\ \mathrm{cm}$ (iii) $17^\circ \leq \theta_{\mathrm{lab}} \leq 150^\circ$
Photon	(i) $E_\gamma^{(\mathrm{lab})} > 0.5\ \mathrm{GeV}$ (ii) $17^\circ \leq \theta_\gamma^{(\mathrm{lab})} \leq 150^\circ$
2nd Decay Vertex	(i) $R_{yz} \leq 60\ \mathrm{cm}$ (ii)–(iii) same as first decay vertex

which searches for an energetic photon along an energy unbalance, vetoing any additional visible particles. This search was performed by BaBar [488], currently setting the most stringent bounds on invisible dark photons in the mass range 400 MeV–8 GeV [343, 344]. Belle II is expected to significantly extend these sensitivities [91].

In the context of niDM, these constraints are generally weaker, since dark photons can decay to excited states that in turn decay visibly inside the detector, producing vetoed events.

To reproduce the BaBar single-photon search, we follow the cuts of Ref. [3], summarized in table D.1, which approximate the more sophisticated multivariate BaBar analysis. Similarly, the Belle II cuts from Ref. [3] are adopted, shown in table D.2, as that study explicitly targeted Belle II's mono-γ sensitivity to iDM. In table D.2, the minimum and maximum polar angles for the detected SM photon are defined as

$$\theta_{\mathrm{min}}^{\mathrm{low}} = 5.399^\circ \frac{E_\gamma^{(\mathrm{CM})2}}{\mathrm{GeV}^2} - 58.82^\circ \frac{E_\gamma^{(\mathrm{CM})}}{\mathrm{GeV}} + 195.71^\circ, \tag{D.8}$$

$$\theta_{\mathrm{max}}^{\mathrm{low}} = -7.982^\circ \frac{E_\gamma^{(\mathrm{CM})2}}{\mathrm{GeV}^2} + 87.77^\circ \frac{E_\gamma^{(\mathrm{CM})}}{\mathrm{GeV}} - 120.6^\circ, \tag{D.9}$$

for $m_{A'} < 6$ GeV, and

$$\theta_{\mathrm{min}}^{\mathrm{high}} = 3.3133^\circ \frac{E_\gamma^{(\mathrm{CM})2}}{\mathrm{GeV}^2} - 33.58^\circ \frac{E_\gamma^{(\mathrm{CM})}}{\mathrm{GeV}} + 108.79^\circ, \tag{D.10}$$

$$\theta_{\mathrm{max}}^{\mathrm{high}} = -5.9133^\circ \frac{E_\gamma^{(\mathrm{CM})2}}{\mathrm{GeV}^2} + 54.119^\circ \frac{E_\gamma^{(\mathrm{CM})}}{\mathrm{GeV}} + 13.781^\circ, \tag{D.11}$$

for $m_{A'} \geq 6$ GeV. Here, $E_\gamma^{(\mathrm{CM})}$ denotes the photon energy in the c.m. frame.

Table D.4: Detector regions and corresponding efficiencies in the displaced-vertex analysis. The variable R_{yz} denotes the transverse displacement of the decay vertex from the x axis.

Particle Type	**Inner Region** (100% eff.)	**Outer Region** (30% eff.)
Electrons	0.2 cm $< R_{yz} \leq$ 0.9 cm	17.0 cm $< R_{yz} \leq$ 60.0 cm
Muons/Pions/Kaons	0.2 cm $< R_{yz} \leq$ 17.0 cm	17.0 cm $< R_{yz} \leq$ 60.0 cm

D.3.2 Displaced-vertex cuts

Searches for displaced vertices from long-lived particles are particularly attractive: they are largely free from SM backgrounds, probe complementary regions of parameter space, and can yield valuable information about the dark sector beyond simple exclusion bounds. They are also especially sensitive to scenarios where standard missing-energy searches are suppressed by (semi-)visible dark sector decays. Recently, the Belle II collaboration has performed such searches in the context of pseudo-Dirac iDM with both portals active, setting stringent bounds on the portal couplings to the SM [82].

For our displaced-vertex analysis, we adopt the cuts from Ref. [3], together with those of Ref. [79] for di-decay signatures. These references were designed to study Belle II's sensitivity to iDM in precisely the channels of interest here. The cuts are listed in table D.3, while table D.4 summarizes the additional position-dependent efficiencies used in our improved analysis.

Appendix E

Solving Boltzmann Equations

In this appendix, we provide additional details on the dark matter (DM) freeze-out computation of chapter 5.

We begin with the standard integrated Boltzmann equations for each DM component of not-so-inelastic DM (see chapters 2 and 3). Assuming that Standard Model (SM) particles remain in thermal equilibrium—which is typically valid at the high temperatures relevant to freeze-out—we can write [420]:

$$\begin{aligned}\dot{n}_{\text{-}} + 3Hn_{\text{-}} &= \langle\sigma v\rangle_{\text{--}} \left(n_{\text{-}}^{\text{eq}\,2} - n_{\text{-}}^2\right) + \langle\sigma v\rangle_{\text{-}*} \left(n_{\text{-}}^{\text{eq}} n_*^{\text{eq}} - n_{\text{-}} n_*\right) \\ &\quad + 2\langle\sigma v\rangle_{\chi\chi} \left(n_*^2 - \left(n_{\text{-}} \frac{n_*^{\text{eq}}}{n_{\text{-}}^{\text{eq}}}\right)^2\right) + \left(\langle\sigma v\rangle_{\chi X} n_X^{\text{eq}} + \Gamma_*\right) \left(n_* - n_{\text{-}} \frac{n_*^{\text{eq}}}{n_{\text{-}}^{\text{eq}}}\right) , \end{aligned} \tag{E.1}$$

$$\begin{aligned}\dot{n}_* + 3Hn_* &= \langle\sigma v\rangle_{**} \left(n_*^{\text{eq}\,2} - n_*^2\right) + \langle\sigma v\rangle_{\text{-}*} \left(n_{\text{-}}^{\text{eq}} n_*^{\text{eq}} - n_{\text{-}} n_*\right) \\ &\quad - 2\langle\sigma v\rangle_{\chi\chi} \left(n_*^2 - \left(n_{\text{-}} \frac{n_*^{\text{eq}}}{n_{\text{-}}^{\text{eq}}}\right)^2\right) - \left(\langle\sigma v\rangle_{\chi X} n_X^{\text{eq}} + \Gamma_*\right) \left(n_* - n_{\text{-}} \frac{n_*^{\text{eq}}}{n_{\text{-}}^{\text{eq}}}\right) , \end{aligned} \tag{E.2}$$

where: $n_{\text{-}}$ and n_* are the number densities of the light and excited DM states, χ and χ^*, respectively; n_X is the number density of SM particles or of the pseudoscalar a; H is the Hubble expansion rate; $\langle\sigma v\rangle_{\text{--}}, \langle\sigma v\rangle_{\text{-}*}, \langle\sigma v\rangle_{**}$ refer to the thermally averaged cross sections for DM annihilation into SM final states or mediators ($\chi\chi \to XY$, $\chi\chi^* \to XY$ and $\chi^*\chi^* \to XY$, respectively), while $\langle\sigma v\rangle_{\chi\chi}$ describes excited states annihilation into ground states $\chi^*\chi^* \leftrightarrow \chi\chi$ and $\langle\sigma v\rangle_{\chi X}$ excited state conversion into ground state via scattering off SM particles or mediators $\chi^* X \to \chi X$; Γ_* is the decay rate of the excited state[1]

Assuming the DM particles are non-relativistic and in kinetic equilibrium with the SM thermal bath, we can define the ratio:

$$\xi \equiv \frac{n_*}{n_{\text{-}}} = (1 + \Delta_m)^{3/2} e^{-\Delta_m x} , \qquad \text{with } x \equiv \frac{m_\chi}{T} , \tag{E.3}$$

[1] For completeness, one could also include the processes $\chi\chi \to \chi\chi^*$ and $\chi^*\chi^* \to \chi^*\chi$, which we have omitted for compactness. However, including them does not affect our results, as their contributions also cancel out when computing the Boltzmann equation for $n = n_{\text{-}} + n_*$.

where $\Delta_m \equiv (m_{\chi^*} - m_\chi)/m_\chi$ is the normalized mass splitting.

Summing Eqs. (E.1) and (E.2), we obtain an effective single Boltzmann equation for the total DM abundance $n = n_{\text{-}} + n_*$:

$$\dot{n} + 3Hn = \langle \sigma v \rangle_{\text{eff}} \left(n^{\text{eq}\,2} - n^2 \right) , \tag{E.4}$$

with the effective annihilation cross section given by:

$$\langle \sigma v \rangle_{\text{eff}} = \frac{1}{(1+\xi)^2} \left[\langle \sigma v \rangle_{\text{--}} + 2\xi \langle \sigma v \rangle_{\text{-}*} + \xi^2 \langle \sigma v \rangle_{**} \right] . \tag{E.5}$$

This reduces the problem to that of a single DM species, making the freeze-out dynamics more tractable.

Since in chapter 4 we consider the regime $\Delta_m \ll 1$, we approximate $m_{\chi^*} \approx m_\chi$ when computing thermally averaged cross sections.

To improve computational efficiency, we velocity-expand the annihilation cross sections up to d-wave (i.e., terms up to $\mathcal{O}(v_\chi^4)$), using the formalism of Ref. [708].

We solve the effective Boltzmann equation (E.4) numerically using standard Mathematica®'s differential equation solvers. For comparison and validation, we also employ the analytic freeze-out approximation described in Ref. [135], retaining terms proportional to $1/\Delta_{Y_f}$ as well as velocity terms up to $\mathcal{O}(v_\chi^4)$.

Both methods yield results in excellent agreement with benchmarks in the literature for classical WIMP models [330] and for the standard pseudo-Dirac inelastic DM scenario mediated by a dark photon [3]—see fig. E.1.

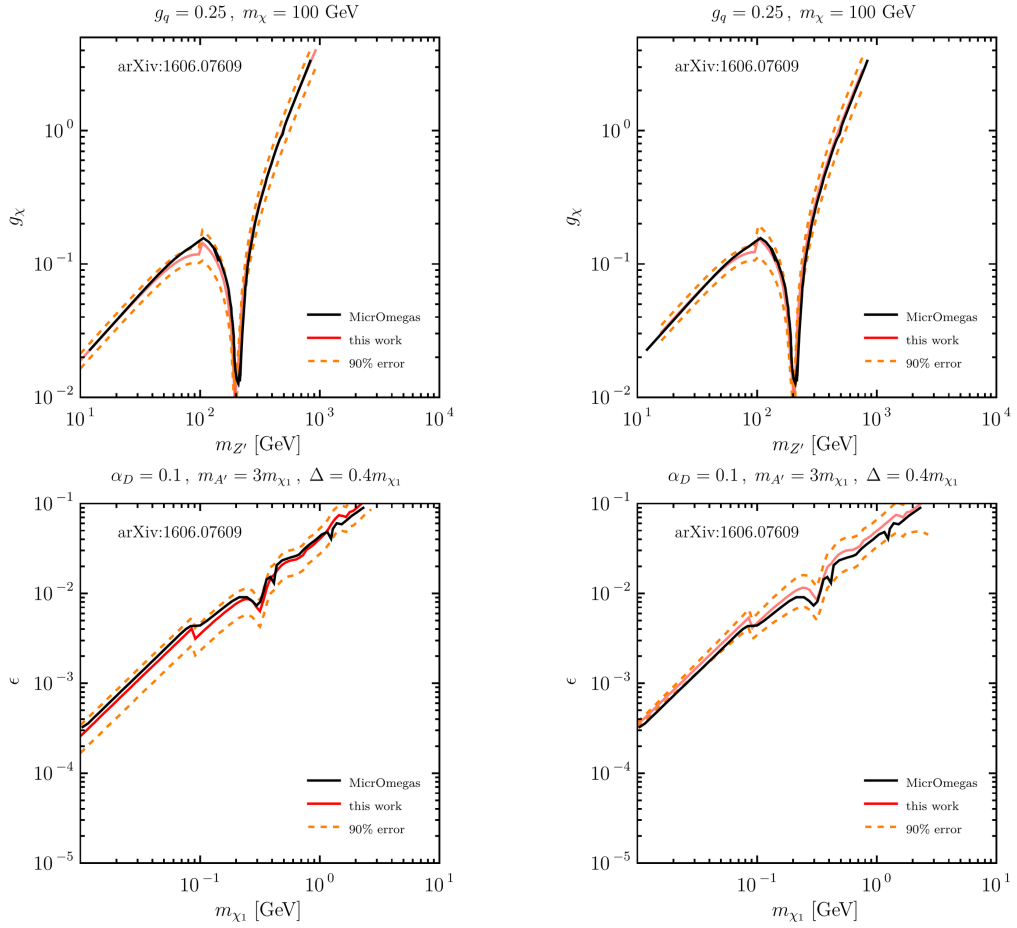

Figure E.1: Validation of our Boltzmann solver for both Majorana DM with a Z' mediator (top) and pseudo-Dirac inelastic DM with a dark photon A' mediator (bottom), compared against the results of Ref. [330] and Ref. [3], respectively. Both references use `MicrOmegas` [375] to compute the DM relic abundance. The left panels show results obtained using the analytical freeze-out approximation, while the right panels display the full numerical solution. Dashed orange lines indicate the estimated 90% uncertainty band around our thermal target line.

Appendix F

Extra: **News from parity in the exothermic limit**

In this appendix, we briefly discuss the important role that parity can play in the limit of small mass splittings, $\delta = m_{\chi^*} - m_\chi < 2m_e$, where the excited state χ^* becomes effectively meta-stable, as it can no longer decay into charged or heavy particles. In this regime, χ^* constitutes a sub-component of the total dark matter (DM) population and can undergo exothermic downscattering in direct detection experiments via the process $\chi^* e^- \to \chi e^-$, releasing its mass excess δ along with part of its kinetic energy. This places the scenario within the broader class of exothermic DM models [471].

Such exothermic signals can lead to strong direct detection constraints even for sub-GeV DM masses [73]. As a result, the relative abundance of excited states, defined as

$$f_* \equiv \frac{n_*}{n_\text{-} + n_*} = \frac{n_*}{n_\text{DM}}\,, \tag{F.1}$$

plays a crucial role in assessing the viability of a given DM model. Here, n_i denotes the number density of the corresponding state. The value of f_* also impacts constraints from indirect detection, including both searches for DM annihilations and DM decays. In our case, decays proceed predominantly via loops into photons, given that decays into neutrinos are highly suppressed by large powers of the ratio $m_{A'}/m_Z$ [75].

We focus here on the vector portal scenario, as studied in chapter 4, now considering small mass splittings. Notably, even though parity breaking leads to suppressed elastic couplings—proportional to the small splitting $\Delta_m \equiv \delta/m_\chi \ll 1$—it can significantly affect f_* due to the exponential Boltzmann suppression of heavier states. For instance, in parity-breaking scenarios, the elastic coupling scales as

$$\alpha'_\text{el} = \cos^2(2\theta)\,\alpha'\,, \qquad \text{with } \cos(2\theta) \propto \Delta_m\,, \tag{F.2}$$

leading to a strong hierarchy, e.g., $\delta = 100$ keV and $m_\chi = 10$ MeV yields $\alpha'_\text{el}/\alpha'_\text{inel} \sim 10^{-5}$. As we show below, the presence of diagonal interactions,

though tiny, can drastically reduce f_*.

Using the full Boltzmann equations from appendix E—including in particular the $\chi^*\chi \to \chi\chi$ process, which is only active in the presence of parity violation—we numerically compute the evolution of f_* until state-changing ($\chi^* \leftrightarrow \chi$) interactions freeze out. We neglect decays of χ^* during this phase and include them later as a multiplicative correction:

$$f_* = f_*^{\text{no decays}} \cdot e^{-t/\tau_*} \,. \tag{F.3}$$

In the numerical evolution, we include the effects of kinetic decoupling, which occurs when downscattering on electrons ($\chi^* e^- \leftrightarrow \chi e^-$) becomes inefficient in exchanging momentum between the dark and visible sectors, following appendix A of Ref. [419]. Additionally, we account for the reheating (or delayed cooling) of the dark sector caused by the conversion of mass-splitting energy into kinetic energy as χ^* transitions to χTo our knowledge, this effect is considered here for the first time in the context of inelastic DM.

Figure F.1 illustrates how parity breaking can significantly reduce the abundance of excited states f_*. This suppression can enable large regions of parameter space to evade stringent constraints from both direct and indirect detection, which typically rule out exothermic sub-GeV scenarios. In particular, our model can bypass much of the parameter space that would otherwise be excluded by decaying DM searches. A comprehensive treatment of all relevant constraints is currently in progress. Figure F.1 suggests that parity violation in the dark sector can resurrect previously excluded models, rendering them viable thermal DM candidates—a conclusion that we have already established for scenarios with larger mass splittings.

As an illustration, in fig. F.1, we have included bounds from: NA64 missing energy searches [344]; Big Bang Nucleosynthesis (BBN) constraints on light new particles in equilibrium with the SM [388], which exclude $m_\chi \lesssim 7$ MeV; and decaying DM constraints, based on the loop-induced decay [75]

$$\Gamma_*(\chi^* \to \chi + 3\gamma) \simeq \frac{17\alpha^4\alpha'\epsilon^2\delta^5}{2^7 \cdot 3^6 \cdot 5^3\pi^3 m_{A'}^4} \cdot \frac{\delta^8}{m_e^8} \,, \tag{F.4}$$

with an approximate conservative limit for X-ray and gamma-ray searches of [6]

$$\frac{\tau_*}{f_*(t_{\text{CMB}})} \cdot \frac{m_\chi}{\delta} > 10^{27}\ \text{s} \,, \tag{F.5}$$

where t_{CMB} is the time of recombination. This inequality ensures that residual excited-state decays evade all late-time searches for decaying DM.

A detailed treatment of these constraints — including updated limits from 21 cm line [709, 710] and CMB anisotropies [711, 712] on decaying and annihilating DM, or low-threshold direct detection [73]—will be presented in a forthcoming work.

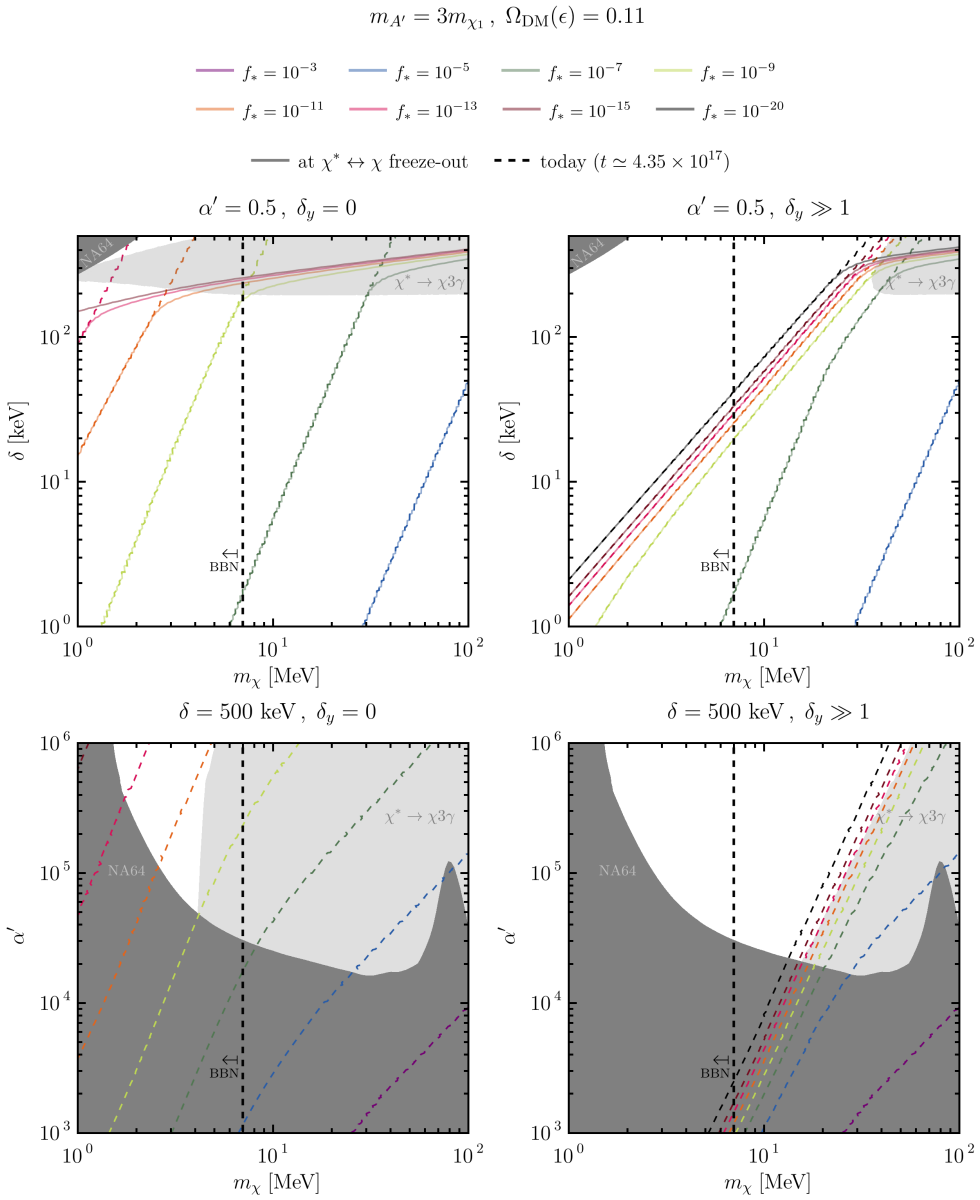

Figure F.1: Relative abundance of excited states $f_* \equiv n_*/n_{\rm DM}$ at the time of excited state freeze-out (solid) and today (dashed), in the (m_χ, δ) plane (top) for fixed dark coupling $\alpha' = 0.5$, and in the (m_χ, α') plane (bottom) for fixed $\delta = 500$ keV. The kinetic mixing ϵ is chosen such that the total relic abundance (from both χ and χ^*) matches the observed DM density. Left panels show the case of parity-conserving inelastic DM ($\delta_y = 0$), while right panels correspond to a large parity-violating scenario ($\delta_y \gg 1$). Gray-shaded regions and areas to the left of the dashed black curves indicate regions excluded by current bounds (see main text).